

SYNTHETIC AND BIOLOGICAL STUDIES OF HEMIKETAL E₂
&
GAINING MOLECULAR INSIGHT ON THE SYNTHESIS OF NANOPARTICLES

By

Danielle Nicole Penk

Dissertation

Submitted to the Faculty of the
Graduate School of Vanderbilt University
in partial fulfillment of the requirements
for the degree of
DOCTOR OF PHILOSOPHY

in

Chemistry

May 12, 2023

Nashville, Tennessee

Approved:

Janet Macdonald, Ph.D.

John McLean, Ph.D.

Nathan Schley, Ph.D.

Claus Schneider, Ph.D.

Steven Townsend, Ph.D.

Copyright © 2022 Danielle Nicole Penk
All Rights Reserved

À la personne qui m'a donné la sagesse tout au long de ma vie.
À la personne qui m'a appris à penser pour les autres avant moi.
À la personne qui m'inspire à me battre sans fin.
À ma mère qui me manque profondément.

Forgiveness does not mean ignoring what has been done or putting a false label on an evil act. It means, rather, that the evil act no longer remains as a barrier to the relationship. Forgiveness is a catalyst creating the atmosphere necessary for a fresh start and a new beginning.

~ Martin Luther King Jr.

ACKNOWLEDGEMENTS

First and foremost, I would like to thank my PI, Dr. Janet Macdonald for her willingness to let me join her lab during the pandemic. Her concern for her graduate students' physical and mental wellbeing is matched by no one at Vanderbilt, yet this is complimented by a desire to do great science. Dr. Janet Macdonald inspired me to do just this: overcome obstacles and stay focused to accomplish great science. I would also like to thank Dr. Gary Sulikowski for his mentorship and guidance while I was in his lab working on the total synthesis of the hemiketals. He has a fountain of knowledge, and I truly enjoyed learning from him. Just as the high pressures and temperatures inside the earth are known to create something as precious as a diamond, so too does Dr. Gary Sulikowski set high expectations of his graduate students in the hopes to create a prized and skillful scientist. He has inspired me to always be a thorough and careful experimentalist. Additionally, I would like to thank my committee members Dr. John McLean, Dr. Nathan Schley, Dr. Steven Townsend, and Dr. Claus Schneider for their guidance and support over the years. I would also like to thank all of my professors who taught me graduate level courses including Dr. Brian Bachmann, Dr. Alissa Hare, Dr. Jeffery Johnston, Dr. Nathan Schley, Dr. Gary Sulikowski, Dr. Steven Townsend, and Dr. Janet Macdonald. I would also like to acknowledge Dr. Adam List. I thoroughly enjoyed working under him and teaching students laboratory techniques. His quirky and dry humor always made me laugh.

Thanks to all of my amazing lab members Madeleine Fort, Christopher Sharp, Nathan Spear, Jeremy Espano, Alexandra Koziel, Andrey Shults, Emma Endres, Peter Edwards, Tony Peng, and last but not least Sarah Simons. I am truly grateful to Maddy, Chris and Nathan who all helped me make a smooth transition from organic total synthesis into the world of nanoparticles. I could always count on Maddy's meows and clever wit to make my day interesting and enjoyable. After my mother passed away in 2020, Chris was very kind and went the extra mile to make sure I was managing alright. This made the lab environment feel very welcoming and safe. I will miss all of Nathan's random Fun Fact Friday's. The philosophical debates and polls that Chris and Nathan would pose I will greatly miss as well. Jeremy's sass and spunkiness always made the lab lively and fun to take part in. I always enjoyed sharing my organic chemistry knowledge with both Lexie and Andrey. Lexie always made the lab environment a warm and

friendly place. I also will miss my desk mate, Andrey, who always had such a calm demeanor. I enjoyed mentoring both Emma and Sarah. Tony and I immediately bonded over our fondness for cats from the first day he joined the lab. While I did not have many interactions with Pete, he was always very respectful and hard-working.

I would like to thank the individuals who helped proofread my thesis: Dr. Jeanette Bertron, Dr. Calvin Larson, Dr. Lianyan Xu, Emma Endres, Cleo Evans, and Chris Sharp.

I would like to acknowledge Biorender for allowing me to create **Figure 1.6** and **Figure 1.7** in Chapter 1 with ease. "Created with Biorender.com"

I had the pleasure of taking and finishing all of my graduate level organic chemistry classes with these individuals: Dr. Joshua Elder, Dr. Calvin Larson, and Dr. Johny Nguyen. Over time we gave ourselves the moniker: The Original Four. I affectionally remember my first year with Cal and Johny at Publicity, one of our favorite restaurants, after one of our Saturday organic exams. I am very honored to be included in Josh and Cleo's wedding as a bridesmaid. Because of our similar interests coming into graduate school, we have all become very close friends. Additionally, I became close friends with Lianyan and enjoyed having our coffee dates. Other individuals I would like to acknowledge are Dr. Katherine Almasy, Dr. Caleb Fast, Dr. Caleb Jones, Dr. Margaret Jones, Dr. Rashanique Quarels, Dr. Bailey Rose, Dr. Carleen Sabusap, Dr. Mark Turlington, Dr. Madison Wright (will miss your meows), Nadjali Chung, Jade Izaguirre, Kelly Richardson, Will & Keelan Weeks.

I would like to thank my family including Janice Penk, Mark Penk, Erica Penk Dr. Walter Penk, and the Ordonez' for their continued support during the time it took me to earn my PhD. I would particularly like to thank my mother. From a very young age my mother instilled in me the highest of excellence, not only in school, but also as a Christian. Despite all of the obstacles faced in graduate school, she inspired me to continue. I would also like to thank my grandfather, Dr. Walter Penk who encouraged and inspired me to also obtain a PhD.

Lastly but certainly not least I would like to thank my husband, Dr. Calvin Larson, who has always believed in my ability as a scientist, despite obstacles faced in our way. He is both a fantastic, intelligent scientist as well as an amazing, supportive, and loving husband.

TABLE OF CONTENTS

	PAGE
DEDICATION	iii
ACKNOWLEDGMENTS	v
LIST OF FIGURES	x
LIST OF SCHEMES	xii
LIST OF TABLES	xiv
LIST OF ABBREVIATIONS	xv
CHAPTER	
1. INTRODUCTION	1
The Discovery of Aspirin	1
Structural and Functional Insights of COX-1 and COX-2	2
The Mechanism of Action of Aspirin	6
The Pharmacological Importance of COX-1 and COX-2 Inhibitors	6
The Inflammatory Response	9
Section Summary	12
Select Total Syntheses of Eicosanoids	12
1969 - Corey's Synthesis of (\pm)-PGF _{2α} and (\pm)-PGE ₂	12
1990 - Wulff's Synthesis of (\pm)-PGE ₂ Methyl Esters	14
1994 - Sato's Synthesis of Enprostil, a 4,5-didehydro PGE ₂ Allene Analog	15
2000 - Fürstner's Synthesis of PGE ₂ -1,15-lactone	16
2003 - Vidari's Synthesis of PGJ ₂	17
2004 - Brummond's Synthesis of 15-deoxy- Δ ^{12,14} -PGJ ₂	19
2018 - Sulikowski's Synthesis of HKE ₂	20

2019 - Stoltz' & Grubbs' Enantioselective Synthesis of 15-deoxy- $\Delta^{12,14}$ -PGJ ₂	21
2019 - Sulikowski's Synthesis of Tricyclic-PGDM Methyl Ester	22
Biosynthetic Pathway of Eicosanoids	24
Biological Roles of Hemiketals in Endothelial Cells	25
Statement of Dissertation	26
References	27
2. PROGRESS TOWARDS A SECOND-GENERATION SYNTHESIS OF HEMIKETAL E ₂	34
Structural Features of HKD ₂ and HKE ₂	34
First Generation Synthesis of HKE ₂	36
Initial Efforts	37
Why β -Elimination is not Observed in the Epimerizations	40
Synthesis of Phosphonate Ester for Horner-Wadsworth-Emmons Reaction	41
Carbonylative Cross Couplings	43
Third Synthetic Approach	45
Optimization of Vasella-Fragmentation-Cyclization	46
Proposed Mechanism of Vasella-Fragmentation-Cyclization	48
Strategy to Access the 1,2-Dicarbonyl Intermediate	49
Davis' Oxaziridine	50
Riley Oxidation	50
Methoxyallene as an Acyl Anion Equivalent	52
The Butadiene Method	55
Umpolung Dithiane Approach	56
Current Route	59
Future Directions	59
References	61

General Experimental Section	66
Compound Preparation: Chemical Synthesis	67
Appendix 1 Relevant Spectral Data for Chapter 2	72
3. GAINING MOLECULAR INSIGHT ON THE SYNTHESIS OF NANOPARTICLES	99
On the Comparison of How Organic and Nanomaterial Chemists Understand Catalysis	99
Enantioselective Catalysis: from the Perspective of Organic Chemists	100
Catalysis: from the Perspective of Nanomaterial Chemists	102
Collaborations between Organic and Nanomaterial Chemists	106
References	107
4. DEPENDANCE OF TRANSITION METAL TELLURIDE PHASES ON METAL PRECURSOR REACTIVITY AND MECHANISTIC IMPLICATIONS	109
Abstract	109
Introduction	109
Experimental Section	113
<i>Materials</i>	113
<i>Synthesis of Transition Metal Telluride (No Ligand)</i>	113
<i>Synthesis of Transition Metal Telluride (with Octadecylamine)</i>	114
<i>Synthesis of Palladium Trifluoromethanesulfonate Pd(OTf)₂</i>	114
<i>Characterization</i>	114
Results and Discussion	115
Conclusion	123
References	125
Appendix 2 Relevant Data for Chapter 4	130

LIST OF FIGURES

FIGURE	PAGE
1.1. Structure of Aspirin (aka Acetylsalicylic acid)	1
1.2. Structure of Ovine Cyclooxygenase-1 (oCOX-1)	2
1.3. Arachidonic Acid (grey) Bound in the Hydrophobic Channel of oCOX-1	3
1.4. Residues in the Heme Binding Region	3
1.5. Structures of Non-steroidal Anti-inflammatory Drugs	8
1.6. Cellular Response to Pathogens Entering a Wound	10
1.7. Generic Cell Converting Arachidonic Acid into Various Eicosanoids to Aid in the Inflammatory Response	11
1.8. Early Studies Demonstrating the Biological Roles of the Hemiketals	25
2.1. Natural Products Containing Keto-hemiketal Groups	35
2.2. π_{C-C} Donation into σ^*_{C-S} Prevents Ease of Deprotonation of 2.101	58
A.2.1. 1H NMR (400 MHz, $CDCl_3$) of 2.54	73
A.2.2. ^{13}C NMR (100 MHz, $CDCl_3$) of 2.54	74
A.2.3. DEPT-135 (100 MHz, $CDCl_3$) of 2.54	75
A.2.4. 1H NMR (400 MHz, $CDCl_3$) of 2.115	76
A.2.5. ^{13}C NMR (100 MHz, $CDCl_3$) of 2.115	77
A.2.6. DEPT-135 (100 MHz, $CDCl_3$) of 2.115	78
A.2.7. IR of 2.115	79
A.2.8. 1H NMR (400 MHz, $CDCl_3$) of 2.62	80
A.2.9. ^{13}C NMR (100 MHz, $CDCl_3$) of 2.62	81
A.2.10. DEPT-135 (100 MHz, $CDCl_3$) of 2.62	82
A.2.11. IR of 2.62	83
A.2.12. 1H NMR (400 MHz, $CDCl_3$) of 2.63	84

A.2.13. ¹ H NMR (400 MHz, CDCl ₃) of 2.64	85
A.2.14. ¹³ C NMR (150 MHz, CDCl ₃) of 2.64	86
A.2.15. DEPT-135 (150 MHz, CDCl ₃) of 2.64	87
A.2.16. IR of 2.64	88
A.2.17. ¹ H NMR (400 MHz, CDCl ₃) of 2.86	89
A.2.18. ¹³ C NMR (100 MHz, CDCl ₃) of 2.86	90
A.2.19. DEPT-135 (100 MHz, CDCl ₃) of 2.86	91
A.2.20. IR of 2.86	92
A.2.21. ¹ H NMR (600 MHz, CDCl ₃) of 2.88	93
A.2.22. ¹³ C NMR (150 MHz, CDCl ₃) of 2.88	94
A.2.23. DEPT-135 (150 MHz, CDCl ₃) of 2.88	95
A.2.24. ¹ H NMR (600 MHz, CDCl ₃) of 2.87 and 2.88	96
A.2.25. ¹³ C NMR (150 MHz, CDCl ₃) of 2.87 and 2.88	97
A.2.26. DEPT-135 (150 MHz, CDCl ₃) of 2.87 and 2.88	98
3.1. Key transition state to explain selectivity for the Midland reduction	100
3.2. Sterics associated with terraces and steps	102
3.3. Transition states calculated using the Horiuti-Polanyi Mechanism	104
3.4. Comparison of catalytic activities for Pt tetrahedral, Pt nanospheres, and Pt/C	105
4.1. XRD of the products of iron, cobalt and nickel salts with didodecyl ditelluride	117
4.2. XRD of the products of ruthenium, palladium, and platinum with didodecyl ditelluride	121
4.3. Representative TEM images	123
A.4.1. XRD of commercially available Fe(OTf) ₂ , Co(OTf) ₂ , and Ni(OTf) ₂ in an air-free sample holder	131
A.4.2. XRD for experiments with FeBr ₂ and FeI ₂ with and without the presence of octadecylamine	131
A.4.3. XRD patterns referenced in Figure 4.1 & Figure 4.2	132
A.4.4. XRD of commercially available ruthenium precursors and their corresponding literature patterns ...	133

LIST OF SCHEMES

SCHEME	PAGE
1.1. Reaction Mechanism of the COX Enzymes at the Peroxidase and Cyclooxygenase Active Sites	4
1.2. Aspirin Treatment of Enzymes COX-1 and COX-2	6
1.3. Corey's Synthesis of (\pm)-PGF _{2α} and (\pm)-PGE ₂	14
1.4. Wulff's Synthesis of (\pm)-PGE ₂ Methyl Esters	15
1.5. Sato's Synthesis of Enprostil, a 4,5-didehydro PGE ₂ Allene Analog	16
1.6. Fürstner's Synthesis of PGE ₂ -1,15-lactone	17
1.7. Vidari's Synthesis of PGJ ₂	18
1.8. Brummond's Synthesis of 15-deoxy- $\Delta^{12,14}$ -PGJ ₂	19
1.9. Sulikowski's Synthesis of HKE ₂	20
1.10. Stoltz' & Grubbs' Enantioselective Synthesis of 15-deoxy- $\Delta^{12,14}$ -PGJ ₂	21
1.11. Sulikowski's Synthesis of Tricyclic-PGDM Methyl Ester	23
1.12. Biosynthetic Pathway of Arachidonic Acid Metabolites	24
2.1. Structural Characteristics of HKD ₂ and HKE ₂	34
2.2. The Sulikowski Lab's Divergent Synthetic Strategy	36
2.3. Epimerization Strategy	37
2.4. First Route towards HKD ₂ and HKE ₂	37
2.5. Orthogonality prevents β -Elimination	40
2.6. Carbonylative Coupling Retrosynthetic Analysis	43
2.7. Hydroformylation and Carbonylative Cross Couplings	44
2.8. Retrosynthetic Analysis starting from D or L-gluconolactones	45
2.9. Mechanism of Vasella-Fragmentation-Cyclization	48
2.10. Current Route to Weinreb amide 2.64	49

2.11. Nucleophilic Addition Strategy	49
2.12. Proposed Mechanism of the Formation of Furan 2.72	51
2.13. Other SeO ₂ Attempts	51
2.14. New Strategy with Methoxyallene	52
2.15. Synthesis of Methoxyallene and MOM allene	53
2.16. Butadiene Strategy	55
2.17. Umpolung Dithiane Approach	56
2.18. Synthesis of Dithiane 2.101	57
2.19. Current Route with Methoxyallene	59
2.20. Future Directions towards HKE ₂	60
2.21. Alternative Route towards HKE ₂	60
3.1. Mechanism of the CBS reduction	100
3.2. Jeffery Johnston's (<i>S,S</i>)- 3 •HNTf ₂ catalyst	101
4.1. The reaction of various metal precursors with didodecyl ditelluride gives Tellurium or Transition Metal Tellurides	112

LIST OF TABLES

TABLE	PAGE
2.1. Optimization of Oxidation Conditions	38
2.2. Epimerization Conditions	39
2.3. Optimization of Claisen-like Condensation	42
2.4. Optimization of Vasella-Fragmentation-Cyclization	47
2.5. Davis' Oxaziridine Attempts	50
2.6. Initial SeO ₂ Attempts	50
2.7. Other SeO ₂ Attempts with Ketals 2.80	52
2.8. Nucleophilic Additions with Methoxyallene 2.83 and MOM allene 2.91	54
2.9. Nucleophilic Additions	54
2.10. Dithiane Deprotonations	57
3.1. Turn over frequencies based on pyrrole, pyrrolidine, and <i>n</i> -butylamine conversions	103
4.1. Summary of Phases (no ligand)	116
4.2. Summary of Phases (with Octadecylamine)	120
A.4.1. Stoichiometry of the nanocrystalline products as determined by EDS (no ligand)	134
A.4.2. Stoichiometry of the nanocrystalline products as determined by EDS (without Octadecylamine)	134

LIST OF ABBREVIATIONS

2,2,6,6-Tetramethylpiperidine 1-oxyl	TEMPO
(<i>S</i>)-binaphthyllithium aluminum hydride	(<i>S</i>)-BINAL-H
(<i>S,S</i>)-(+)- <i>N,N'</i> -Bis(3,5-di- <i>tert</i> -butylsalicylidene)-1,2-cyclohexanediaminocobalt(II)	Jacobsen's (<i>S,S</i>)-cat
1,2-dichloroethane	DCE
1,8-Diazabicyclo[5.4.0]undec-7-ene	DBU
2,3-Dichloro-5,6-dicyano-1,4-benzoquinone	DDQ
2-Iodoxybenzoic acid	IBX
3,4-Dihydropyran	DHP
4-Dimethylaminopyridine	DMAP
4-methylmorpholine 4-oxide	NMO
5-lipoxygenase	5-LOX
5 <i>S</i> -hydroperoxyeicosatetraenoic acid	5 <i>S</i> -HPETE
5 <i>S</i> -hydroxyeicosatetraenoic acid	5 <i>S</i> -HETE
acetic acid	AcOH
acetic anhydride	Ac ₂ O
acetone	(CH ₃) ₂ CO
acetonitrile	CH ₃ CN
allylmagnesium bromide	allylMgBr
angstrom	Å
aqueous	aq
Azobisisobutyronitrile	AIBN
barium hydroxide octahydrate	Ba(OH) ₂ ·8H ₂ O
based on recovered starting material	BRSM
benzene	PhH
benzyltrimethylammonium fluoride	BTAF
Bis(cyclopentadienyl)zirconium(IV) chloride hydride	HZrCp ₂ Cl
Bis(cyclopentadienyl)zirconium(IV) dichloride	Cp ₂ ZrCl ₂
bis(trimethyltin)	(SnMe ₃) ₂
Bis(triphenylphosphine)palladium(II) dichloride	PdCl ₂ (PPh ₃) ₂
Boron tribromide	BBr ₃

Boron trifluoride etherate	BF ₃ ·OEt ₂
carbon dioxide	CO ₂
carbon monoxide	CO
Carbon-13 Nuclear Magnetic Resonance	¹³ C NMR
Cerium(III) trichloride	CeCl ₃
Chloromethyl methyl ether	MeOCH ₂ Cl
chlorotriethylsilane	TESCl
chromic acid	H ₂ CrO ₄
chromium hexacarbonyl	Cr(CO) ₆
chromium trioxide	CrO ₃
copper(I) iodide	CuI
Copper(II) tetrafluoroborate	Cu(BF ₄) ₂
cyclooxygenase-1	COX-1
cyclooxygenase-2	COX-2
cytosolic phospholipidase A ₂	cPLA ₂
doublet	d
doublet of doublets	dd
doublet of doublet of doublets	ddd
degrees Celcius	°C
delta	Δ
Dess–Martin Periodinane	DMP
Deuterated chloroform	CDCl ₃
Deuterated methanol	CD ₃ OD
Deuterium oxide	D ₂ O
diazomethane	CH ₂ N ₂
dibutyl ether	nBu ₂ O
dichloromethane	CH ₂ Cl ₂
diethyl azodicarboxylate	DEAD
diethyl ether	Et ₂ O
diethylamine	Et ₂ NH
Diisobutylaluminium hydride	DIBAL-H
dimethoxyethane	DME
dimethyl methyl phosphonate	DMMP

dimethyl sulfide	Me ₂ S
dimethyl sulfoxide	DMSO
dimethyl zinc	Zn(CH ₃) ₂
dimethyl dioxirane	DMDO
dimethylformamide	DMF
diphenyl dichlorosilane	Ph ₂ SiCl ₂
directed ortho metalation	DoM
Distortionless Enhancement by Polarization Transfer	DEPT
doublet of triplets	dt
equivalents	equiv
ethanol	EtOH
ethyl acetate	EtOAc
ethyl aluminum dichloride	EtAlCl ₂
Formaldehyde	CH ₂ O
gold(I) chloride	AuCl
grams	g
hemiketal D ₂	HKD ₂
hemiketal E ₂	HKE ₂
hertz	Hz
hexamethylphosphoramide	HMPA
hours	h
hydrobromic acid	HBr
hydrochloric acid	HCl
hydrofluoric acid	HF
hydrogen fluoride pyridine	HF·Py
Hydrogen fluoride triethylamine	HF·NEt ₃
hydrogen peroxide	H ₂ O ₂
imidazole	Im
leukotriene A ₄	LTA ₄
ligand	L _n
lipase <i>Pseudomonas</i> sp	lipase PS
lithium aluminum hydride	LAH
lithium diisopropylamine	LDA

lithium(I) chloride	LiCl
multiplet	m
magnesium sulfate	MgSO ₄
manganese(IV) oxide	MnO ₂
megahertz	MHz
<i>meta</i> -Chloroperoxybenzoic acid	<i>m</i> CPBA
methanesulfonyl chloride	MsCl
methanol	CH ₃ OH
methoxymethyl	MOM
methyl <i>tert</i> -butyl ether	MTBE
microwave	mw
milligrams	mg
milliliters	mL
millimoles	mmol
minutes	min
molecular sieves	MS
moles	mol
molybdenum hexacarbonyl	Mo(CO) ₆
<i>N,N'</i> -Diisopropylcarbodiimide	DIC
<i>n</i> -butyllithium	<i>n</i> -BuLi
N-Chlorosuccinimide	NCS
N-Methylpyrrolidone	NMP
non-steroidal anti-inflammatory drugs	NSAIDs
normal	N
Ovine Cyclooxygenase-1	oCOX-1
Oxalyl chloride	(COCl) ₂
ozone	O ₃
palladium(II) acetate	Pd(OAc) ₂
Palladium(II)bis(triphenylphosphine) dichloride	PdCl ₂ [P(C ₆ H ₅) ₃] ₂
Potassium bis(trimethylsilyl)amide	KHMDS
potassium bromide	KBr
potassium carbonate	K ₂ CO ₃
potassium fluoride	KF

potassium hydroxide	KOH
potassium <i>tert</i> -butoxide	<i>t</i> BuOK
potassium triiodide	KI ₃
prostacyclin I ₂	PGI ₂
prostaglandin D ₂	PGD ₂
prostaglandin D ₂ metabolite	PGDM
prostaglandin E ₂	PDE ₂
prostaglandin F _{2α}	PGF _{2α}
prostaglandin H ₂	PGH ₂
prostaglandin J ₂	PGJ ₂
Proton Nuclear Magnetic Resonance	¹ H NMR
protoporphyrin ix	PPIX
<i>p</i> -Toluenesulfonic acid	PTSA
pyridine	Py
Pyridinium chlorochromate	PCC
Pyridinium <i>p</i> -toluenesulfonate	PPTS
quartet	q
reactive oxygen species	ROS
room temperature	rt
selenium dioxide	SeO ₂
silver(I) carbonate	Ag ₂ CO ₃
singlet	s
sodium acetate	NaOAc
sodium bicarbonate	NaHCO ₃
Sodium bis(trimethylsilyl)amide	NaHMDS
sodium borohydride	NaBH ₄
sodium hydride	NaH
sodium hydroxide	NaOH
Sodium hypochlorite	NaOCl
sodium iodide	NaI
sodium sulfate	Na ₂ SO ₄
Sulfur trioxide-pyridine	SO ₃ ·Py
sulfuric acid	H ₂ SO ₄

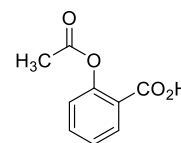
triplet	t
<i>tert</i> -Butyl hydroperoxide	TBHP
<i>tert</i> -Butylamine borane	<i>t</i> -BuNH ₂ ·BH ₃
<i>tert</i> -Butyldimethylsilyl chloride	TBSCl
<i>tert</i> -Butyldimethylsilyl trifluoromethanesulfonate	TBSOTf
<i>tert</i> -butyllithium	<i>t</i> -BuLi
Tetrabutylammonium chloride	nBu ₄ NCl
tetrahydrofuran	THF
Tetrakis(triphenylphosphine)palladium(0)	Pd(PPh ₃) ₄
tetramethylethylenediamine	TMEDA
Tetra- <i>n</i> -butylammonium fluoride	Bu ₄ NF
Tetrapropylammonium perruthenate	TPAP
thromboxane A ₂	TxA ₂
Titanium tetrachloride	TiCl ₄
toluene	tol
Tributylphosphine	PBu ₃
tributyltin hydride	Bu ₃ SnH
triethylamine	Et ₃ N
trifluoroacetic acid	TFA
trimethyl aluminum	Al(CH ₃) ₃
trimethylsilylacetylene	HCCTMS
Trimethylsilyldiazomethane	TMSCHN ₂
triphenyl phosphine	Ph ₃ P
triphenyltin chloride	Ph ₃ SnCl
Tris(dibenzylideneacetone)dipalladium(0)	Pd ₂ dba ₃
water	H ₂ O
zinc	Zn
zinc borohydride	Zn(BH ₄) ₂

CHAPTER 1

INTRODUCTION

The Discovery of Aspirin

Traditional herbal medicine has been used for several thousand years to treat various maladies. For example, qinghaosu, or artemisinin, was known to treat malaria in China more than 1000 years ago.¹ A common method to reduce fever, even before this time, was with the use of willow tree bark or leaves. Unbeknownst to the people of that age, the key component of the willow tree would become an important precursor of a commonly used drug throughout the world several thousand years later. This well-known drug is now known as aspirin (**1.1**) (**Figure 1.1**). A brief timeline towards the discovery of aspirin will be highlighted, and then a discussion of its inhibition of the enzymes cyclooxygenase-1 (COX-1) and cyclooxygenase-2 (COX-2) will ensue.



Aspirin (1.1)

Figure 1.1. Structure of Aspirin (aka Acetylsalicylic acid).

As mentioned previously, ancient civilizations knew of the medicinal benefits of the willow tree. Assyrians (4000 BC) used the extract of willow leaves for uncomfortable musculoskeletal joint pain conditions. Five hundred years later, the Sumerians (3500 BC) described the use of willow tree leaves to treat various ailments. More than two thousand years later, Egyptians (1300 BC) utilized its leaves for general pain, joint pain, and for reducing inflammation associated with wounds. All the aforementioned civilizations knew of the willow tree's ability as an antipyretic medicine. This knowledge was passed on from civilization to civilization and continued into the Grecian age where Hippocrates (400 BC) used it to treat fever as well as reduce pain for mothers in childbirth.² For many centuries, few advancements with the willow tree had progressed, but in 1763 Edward Stone, an Oxfordshire reverend, investigated the use of willow powder to treat ague, or a fever caused from malaria.³ The willow tree powder was prepared by allowing the bark to dry outside a baker's oven for three months, and then, it was pounded and sifted into a powder. The active ingredient of willow tree powder, salicin, was not determined until 1828 when Johann Buchner, professor of pharmacology at the University of Munich, extracted and purified it into yellow crystals. Ten years later, Raffaele Piria, an Italian chemist, resolved the chemical structure of salicin and then oxidized salicyl alcohol to salicylic acid. In 1876 Thomas MacLagan, a Scottish physician, administered the first clinical trial of salicin; however, despite its antipyretic effects, salicin was not accepted as a drug due to problems with gastritis. Roughly two decades later in the late 1890's Arthur Eichengrün, Felix Hoffmann, and Heinrich Dreser worked in a pharmaceutical division at the German dye manufacturer, Bayer. They desired to find an alternative to salicin without the gastritic side effects.⁴ Indeed, they

discovered acetylsalicylic acid, or aspirin. By the time the worldwide outbreak of influenza in 1918 came around, aspirin was widely accepted to treat fever. By 1971 John Vane, a British pharmacologist, demonstrated that aspirin and other anti-inflammatory drugs inhibited the production of prostaglandins.⁵ Five years later aspirin was shown to inhibit cyclooxygenase.⁴ At this point in time, the mechanism of action of how aspirin and other non-steroidal anti-inflammatory drugs (NSAIDs) inhibited the cyclooxygenase enzymes was not known. Before a dialog of this topic, an introduction of the COX enzymes is necessary.

Structural and Functional Insights of COX-1 and COX-2

Since the late 1980's, the enzymes COX-1 and COX-2 have been well known for the established transformation of arachidonic acid towards prostaglandin H₂ (PGH₂) which is then converted into various eicosanoids: prostaglandins, prostacyclin and thromboxanes.⁶ Each eicosanoid plays a specific physiological role in the inflammatory response which will be elaborated in more detail in a later section, but before this, an understanding of how compounds are transformed by the COX enzymes is necessary.

Since the discovery that anti-inflammatory drugs inhibit prostaglandin production in 1971, significant insights regarding the structure and function of the COX enzymes have been established. The genetic arrangement of the COX enzymes is highly conserved in all species of vertebrates including murine organisms.^{7,8} In all of these organisms, the 3D structures of both COX-1 and COX-2 are virtually superimposable; they contain 576 and 581 amino acids, respectively.⁹ The COX enzymes exist as homodimers with a C₂ axis of symmetry and reside in the endoplasmic reticulum and the nuclear envelope.¹⁰ COX-1 is found in most tissues and responsible for basal functions of gastric mucosa, kidney function and platelet aggregation.¹¹ In contrast, COX-2 is constitutively expressed in brain and kidney tissues. COX-2 was originally believed to only be induced during inflammation

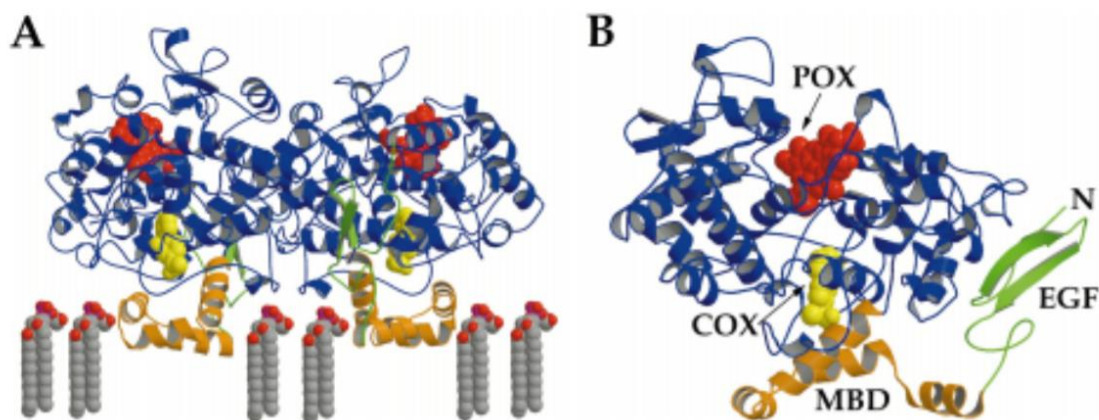


Figure 1.2. Structure of Ovine Cyclooxygenase-1 (oCOX-1) (A) Ribbon diagram of the COX-1 homodimer bound with flurbiprofen bound (yellow). Key structural features of the enzymes are labeled accordingly: epidermal growth factor domain (green), membrane binding domain (gold), catalytic domain (blue), heme (red). (B) Ribbon drawing of COX-1 monomer with flurbiprofen bound (yellow). Reproduced with permission from the Annual Review of Biochemistry, Volume 69 © 2000 by Annual Reviews, <http://www.annualreviews.org>.

when activated by cytokines, mitogens, endotoxins, and tumor promoters; however, it is clear it also plays physiological roles within its expressed tissues in addition to cardiovascular systems.¹² Within both COX enzymes, each subunit of the dimers contains three structural domains: an epidermal growth factor domain (residues 34-72), a membrane binding domain (residues 73-116), and a large catalytic domain (residues 117-586),

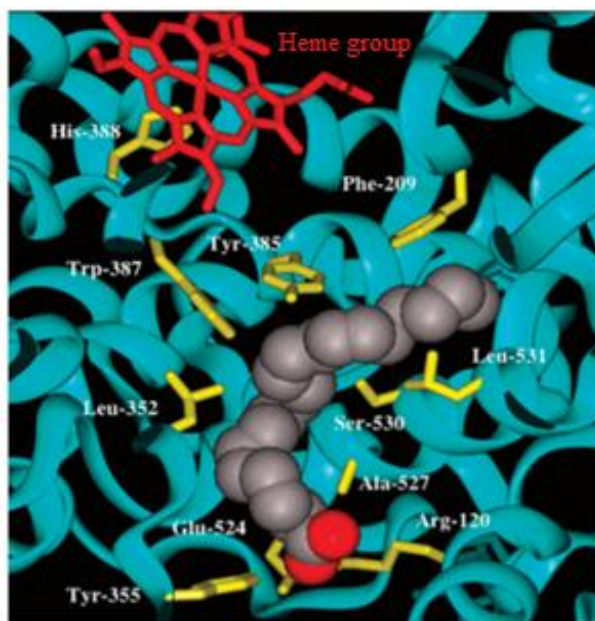


Figure 1.3. Arachidonic Acid (grey) Bound in the Hydrophobic Channel of α COX-1. Oxygens within arachidonic acid (red). Key residues (yellow). Reprinted with permission from Blobaum, A.; Marnett, L. *J. Med. Chem.* **2007**, *50*, 1425–1441.

Further permissions related to this material excerpted should be directed to the American Chemical Society. <https://pubs.acs.org/doi/10.1021/jm0613166>.

proper protein folding and maintaining their native conformations.^{18,19}

Unlike the other three helices, Helix D protrudes into the catalytic domain.

The globular catalytic domain contains two active sites which are interdependent on each other, namely the cyclooxygenase and peroxidase active sites; the peroxidase and heme-binding active sites are one in the same. First, the cyclooxygenase active site will be discussed. The cyclooxygenase active site of COX-2 is significantly larger than in COX-1 which may allow for a larger variety of substrates to be oxidized. In both enzymes this site contains a long, hydrophobic channel, which Marnett coined “the lobby” (**Figure 1.3**).²⁰ This region is where substrates or inhibitors bind to the COX enzymes. The bottom of the channel

containing two active sites (**Figure 1.2**).¹³

Of the three domains, the least is known about the epidermal growth factor and membrane binding domains. From what is known, the epidermal growth factor domain is located near the dimer interface. Studies have shown a direct correlation between the epidermal growth factor domain and stimulation of COX-2 in several cancers.^{14,15,16} Currently, researchers are studying how the inhibition of the epidermal growth factor domain can become a viable option in treating various cancers. The membrane binding domain contains four α -helices (A-D). Mutagenesis of α -helices (A-C) reveals the hydrophobic and aromatic residues within the helices create an interface with the lipid bilayer and, by extension, facilitate in protein folding. Additionally, the residues encircle a pocket, believed to facilitate entry of polyunsaturated fatty acids within the cyclooxygenase active site.¹⁷ In both the COX-1 and COX-2 enzymes, N-glycosylated Asn residues are important for

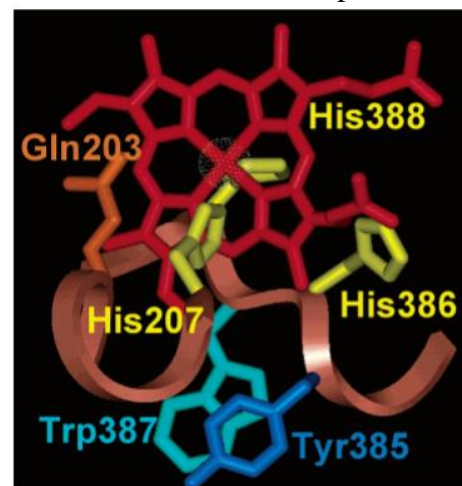
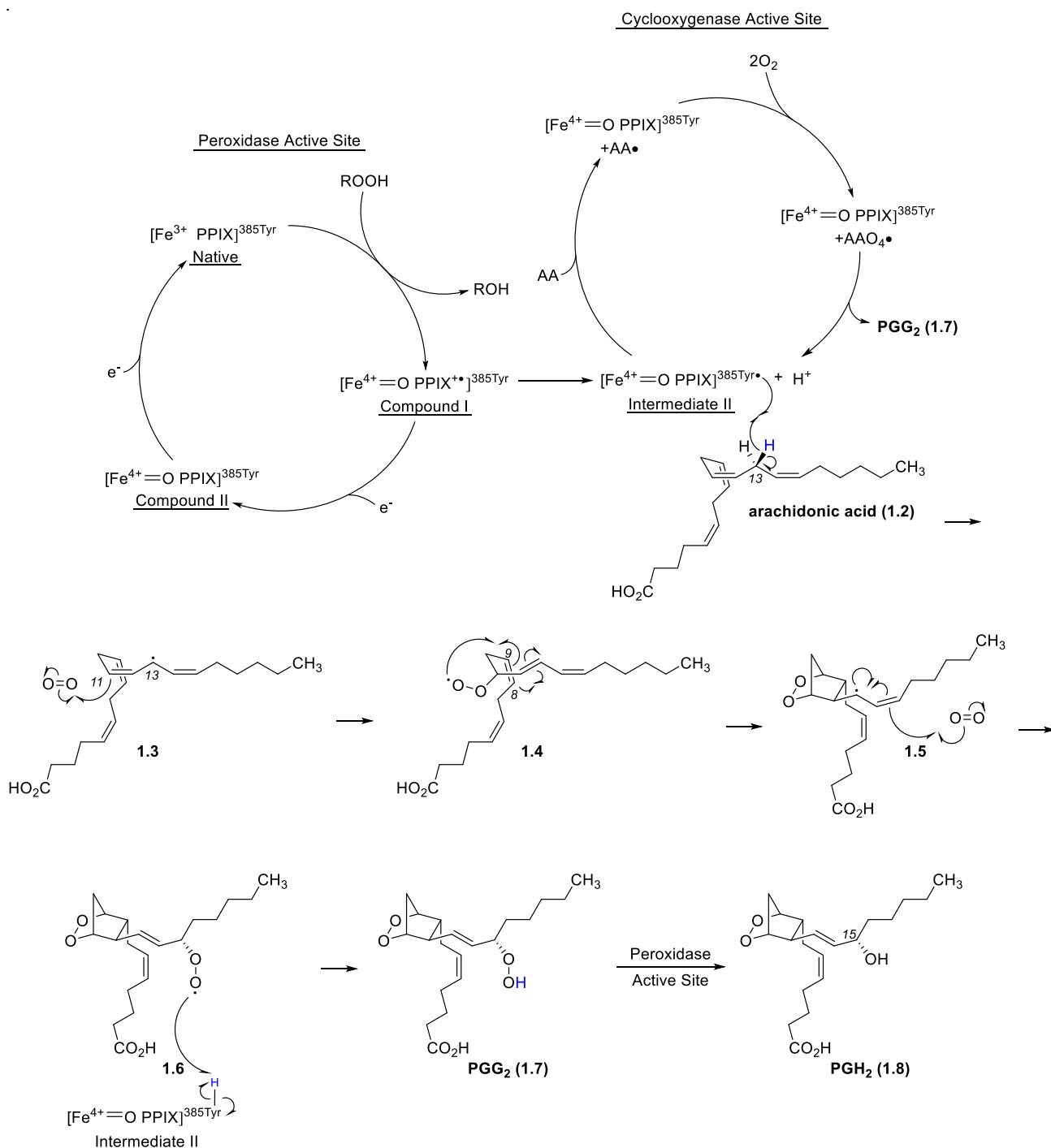


Figure 1.4. Residues in the Heme Binding Region. Reprinted with permission from Rouzer, C.; Marnett, L. *Chem. Rev.* **2003**, *103*, 2239–2304. Copyright 2020 American Chemical Society.

narrows, and this constricted region is where the carboxylate of a substrate binds. Arg120 and Glu524 are charged residues that play a major role in binding carboxylic acid-containing substrates or inhibitors.²¹ The bottom portion of the lobby opens and closes to allow for substrates or inhibitors to enter the cyclooxygenase active site. It is believed that the motion of Helix D destabilizes hydrogen bonding of the constricted residues, thereby facilitating the opening and closing of the bottom of the lobby.

Function of the cyclooxygenase active site relies on the peroxidase active site to perform properly. It requires the heme group in the bottom shallow cleft of the peroxidase active site to undergo oxidation (**Figure**



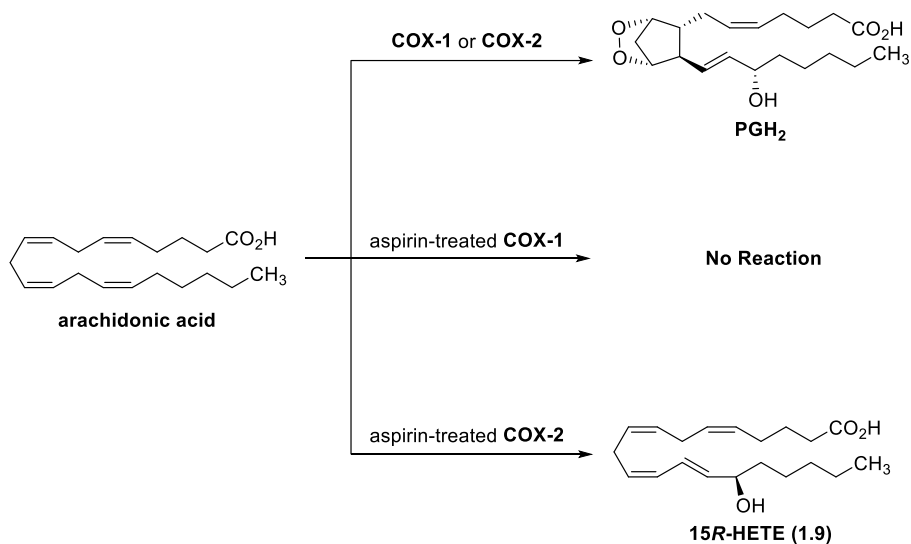
Scheme 1.1. Reaction Mechanism of the COX Enzymes at the Peroxidase and Cyclooxygenase Active Sites.

1.4).²² Activation of the peroxidase active site begins with an organic hydroperoxide reacting with the native [Fe³⁺ protoporphyrin (PPIX)]^{385Tyr} resting state, which results in Compound I and an alcohol byproduct. Compound I undergoes an intramolecular single electron reduction by the nearby Tyr385 to form Intermediate II. The electron transfer occurs from the Tyr385 to the proximal heme ligand His388 then back to the heme group. Alternatively, Compound I can undergo a one electron reduction by an electron donor to yield Compound II. Because the NMR spectrum of Intermediate II and Compound II are identical, electron paramagnetic resonance (EPR) spectroscopy is necessary to elucidate the difference between the two. When a polyunsaturated fatty acid, like arachidonic acid (**1.2**), docks into the cyclooxygenase active site, the Tyr385 radical of Intermediate II can abstract the 13-pro-*S* hydrogen of arachidonic acid, cyclize to form an endoperoxide, which ultimately results in the formation of PGG₂ (**1.7**) (**Scheme 1.1**).²⁰ The initiation of the peroxidase active site with the hydroperoxide is essential for the function of the cyclooxygenase active site; without a source of hydroperoxide, its function stops abruptly.²¹ Once the Tyr385 radical is generated in the peroxidase active site, if a substrate is already present in the docking site of the cyclooxygenase active site, the process becomes autocatalytic until radical induced inactivation occurs.

Other residues important in the catalytic domain include Tyr384 and Gly533. These residues help lock C13 of arachidonic acid into place for the 13-pro-*S* hydrogen abstraction which occurs during the transformation of arachidonic acid to PGH₂ (**1.8**). When arachidonic acid docks into the cyclooxygenase active site, the 385Tyr radical from Intermediate II removes its 13-pro-*S* hydrogen. The resulting pentadienyl radical captures a molecule of oxygen at C11. Next, an impending 5-*exo-trig* cyclization ensues onto C9, and the resulting radical on C8 undergoes another 5-*exo-trig* cyclization to afford the bicyclic peroxide. Residues that help promote the cyclization of the endoperoxide include Val349, Trp387, and Leu534 which also play an important role in the docking arachidonic acid.²³ Following the cyclization, the allylic radical traps a second molecule of oxygen, and the 385Tyr from Intermediate II offers the hydrogen it had originally abstracted from arachidonic acid to ultimately form PGG₂. Recollect the peroxidase and cyclooxygenase active sites within the COX enzymes are interdependent. After the conversion of arachidonic acid to PGG₂ within the cyclooxygenase active site, the peroxidase active site can then reduce PGG₂ to PGH₂. The COX enzymes are not only capable of transforming arachidonic acid, but also other polyunsaturated fatty acids. The importance of this radical cascade is demonstrated by the fact that the COX enzymes are molecular targets of NSAIDs. In order to elucidate the mechanism of action of how NSAIDs like aspirin inhibit COX enzymes, an experiment in which each enzyme was treated with aspirin was constructed.²⁴

The Mechanism of Action of Aspirin

Under normal conditions both COX enzymes can transform arachidonic acid into PGH₂. However, despite the structural similarities of the COX enzymes, when treated with aspirin, they produce different outcomes. Aspirin-treated COX-1 results in complete inhibition of activity. Whereas, when COX-2 is treated with aspirin, it produces 15*R*-hydroxyeicosatetraenoic acid (**1.9**, 15*R*-HETE),^{25,26} the opposite stereochemistry expected at this carbon when compared to PGH₂ (**Scheme 1.2**). In recent years, it has been shown that transformation of arachidonic acid by aspirin acetylated COX-2 also forms 15*R*-HETE.²⁷ Mutation of Ser530 to alanine prevents aspirin's inhibiting effects in COX-2, and peptide analysis reveals aspirin acetylates Ser530.²⁸ Because both COX-1 and COX-2 share the residue Ser530, it was determined that aspirin inhibits both enzymes in the same fashion, but the formation of 15*R*-HETE with aspirin-treated COX-2 was unresolved. The answer lies in the larger side pocket of COX-2.²⁹ When aspirin acetylates Ser530 in COX-2, the result is two-fold. First, arachidonic acid can still bind because the pocket is simply larger than in COX-1. Second, the positioning of the acetyl group on Ser530 alters the conformation of arachidonic acid and therefore, changes the stereochemical outcome of the position oxidized by altering the approach of the second molecule of oxygen to the opposite side.^{30,31} Thus, the larger pocket in COX-2 explains why 15*R*-HETE forms, and additionally why no reaction occurs in COX-1. Extensive site-mutagenesis studies were required to elucidate



other residues' roles in the COX enzymes but will not be discussed herein; for more details, papers by Marnett and Gierse can provide more information.^{32,33}

The Pharmacological Importance of COX-1 and COX-2 Inhibitors

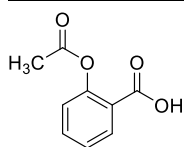
The effectiveness of NSAIDs to reduce pain, fever, or inflammation is useful in a number of clinical disorders including osteoarthritis, rheumatoid arthritis, ankylosing spondylitis, gout, dysmenorrhea, dental pain, and headache.^{34,35} There are several chemical motifs of NSAIDs including acetylated salicylates (aspirin **1.1**), nonacetylated salicylates (salsalate **1.10**), propionic acids (naproxen **1.11** and ibuprofen **1.12**), phenylacetic acids

(diclofenac **1.13**), enolic acids (meloxicam **1.14**), fenamic acids (meclofenamic acid **1.15**), naphthylalanine (nabumetone **1.16**), selective COX-1 inhibitors (Mofezolac **1.18**), and selective COX-2 inhibitors (etoricoxib **1.22** and celecoxib **1.25**) as shown in (**Figure 1.5**). A plethora of other classes of NSAIDs exist but will not be discussed here.^{36,37} As can be implied with the vast variety of structures presented, these drugs will have different effects on *how* the COX enzymes are inhibited and, by extension, result in diverse side effects in different patients.

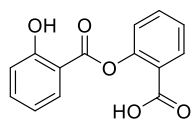
Most NSAIDs, like aspirin and ibuprofen, are nonspecific and inhibit both the COX enzymes; in contrast, coxibs, like celecoxib and rofecoxib, more specifically inhibit COX-2.³⁸ Aspirin is unique because it is the only clinically-used, nonselective NSAID that irreversibly inactivates the COX enzymes through time dependent, covalent modification; all others do so in a noncovalent fashion. Intricate kinetic studies comparing other drugs' inhibition have been conducted but will not be discussed herein; instead, the reader can source a paper by Marnett for more details.¹²

Overall, NSAIDs are considered to be safe, over-the-counter drugs, but gastrointestinal toxicity is experienced by those who take NSAIDs chronically, particularly the elderly.^{39,40} As the population continues to age, it is believed that the daily use of NSAIDs will increase, along with its side effects. Ulcerogenic side effects are attributed to COX-1 inhibition which prevents prostaglandin formation, and these protect the gastric mucosa.⁴¹ Interestingly, low dose aspirin preferentially inhibits COX-1 by reducing platelet thromboxane synthesis and thrombosis in blood platelets. High dose aspirin, on the other hand, can cause gastrointestinal bleeding. Patients with a history of gastrointestinal problems or diseases that impair platelet activities can be sensitive to NSAIDs.⁴² Because several NSAIDs are nonselective and target COX-1, it was believed developing COX-2 inhibitors would solve the gastrointestinal problems. Indeed, coxibs avoid problems with gastritis; however, the tradeoff is that a subset of users experience cardiovascular problems.^{43,44} A risk-benefit analysis is necessary to determine which medications are the best for certain individuals who are susceptible to the negative side effects associated with certain NSAIDs. Other potential drugs may be developed to target the COX enzymes without these side effects.

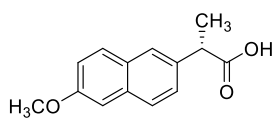
(a) Nonselective NSAIDs



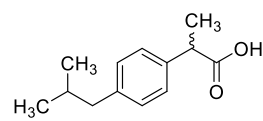
Aspirin (1.1)



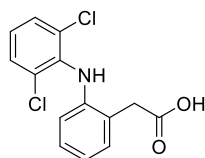
Salsalate (1.10)



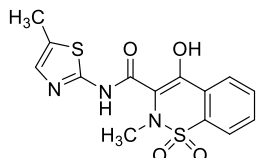
Naproxen (1.11)



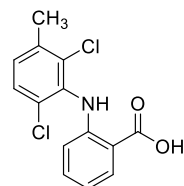
Ibuprofen (1.12)



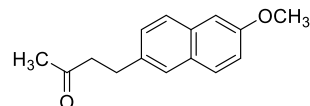
Diclofenac (1.13)



Meloxicam (1.14)

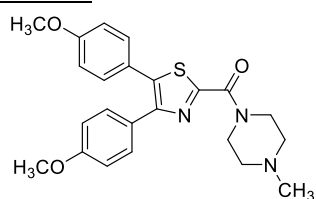


Meclofenamic acid (1.15)

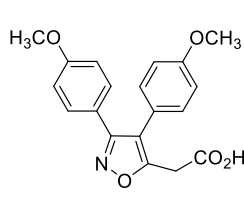


Nabumetone (1.16)

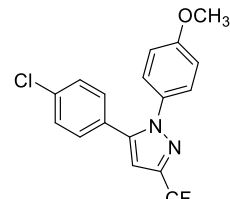
(b) COX-1 Inhibitors



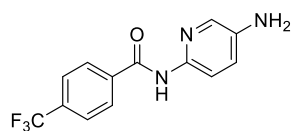
FR122047 (1.17)



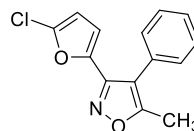
Mofezolac (1.18)



SC-560 (1.19)

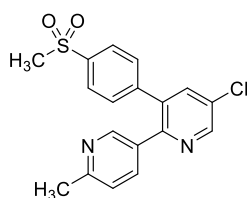


TFAP (1.20)

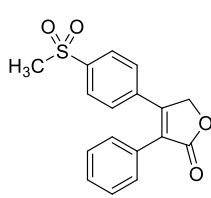


P6 (1.21)

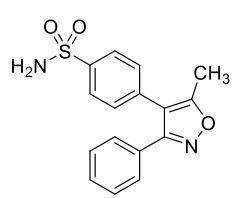
(c) COX-2 Inhibitors



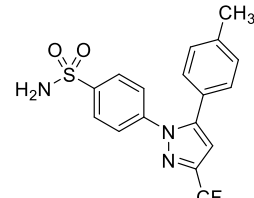
Etoricoxib (1.22)



Rofecoxib (1.23)



Valdecoxib (1.24)



Celecoxib (1.25)

Figure 1.5. Structures of Non-steroidal Anti-inflammatory Drugs (a) Nonselective NSAIDs, (b) COX-1 Inhibitors, (c) COX-2 Inhibitors. Taken from Perrone and coworkers³⁶.

The Inflammatory Response

The inflammatory response is the body's protective, coordinative action against four main pathogens: viruses, bacteria, fungi and parasites. The three overall goals of inflammation are delivering leukocytes, or white blood cells, manipulating blood flow, and initiating repair at the infection site. The first line of defense against these pathogens is anatomic barriers which include skin, oral mucosa, respiratory epithelium and the intestines. The second is a compilation of various chemical and enzymatic systems to protect against antimicrobial breaches. The third defense is innate immune cells including macrophages, granulocytes, and natural killer cells. Finally, if a pathogen overcomes all of these barriers, the adaptive immune response recruits B cells, antibodies, and T cells for aid.⁴⁵ To demonstrate the role eicosanoids and other lipid mediators play in the inflammatory response, the body's response to tissue damage will be discussed.

There are four main changes that occur within blood vessels once the body recognizes that pathogens have entered through a wound. First, local blood vessels near the infection site increase their vascular diameter. This expansion of the local blood vessels is what is responsible for the heat and redness associated with wounds. Increased blood flow also allows white blood cells to access the wound site and eliminate the pathogens more quickly. The second change allows leukocytes, like neutrophils, to adhere to endothelial cells,⁴⁶ or the inner lining of blood vessels (**Figure 1.6**). This allows the leukocytes to squeeze between the endothelial cells into the infection site, a process known as extravasation. All the above-mentioned changes are initiated by nearby macrophages which come into contact with the invading pathogens first. The macrophages release cytokines, chemokines and lipid mediators, each of which have unique receptors (**Figure 1.7**).⁴⁷ The first responders to these signals are neutrophils. Next, the endothelial barrier becomes more permeable to allow more blood cells to enter the infected tissue which results in swelling and pain. Once neutrophils have entered the infection site, both the nearby macrophages and incoming neutrophils partake in phagocytosis, or the process by which foreign matter is digested. Finally, clotting of the wound prevents more pathogens from entering.⁴⁸

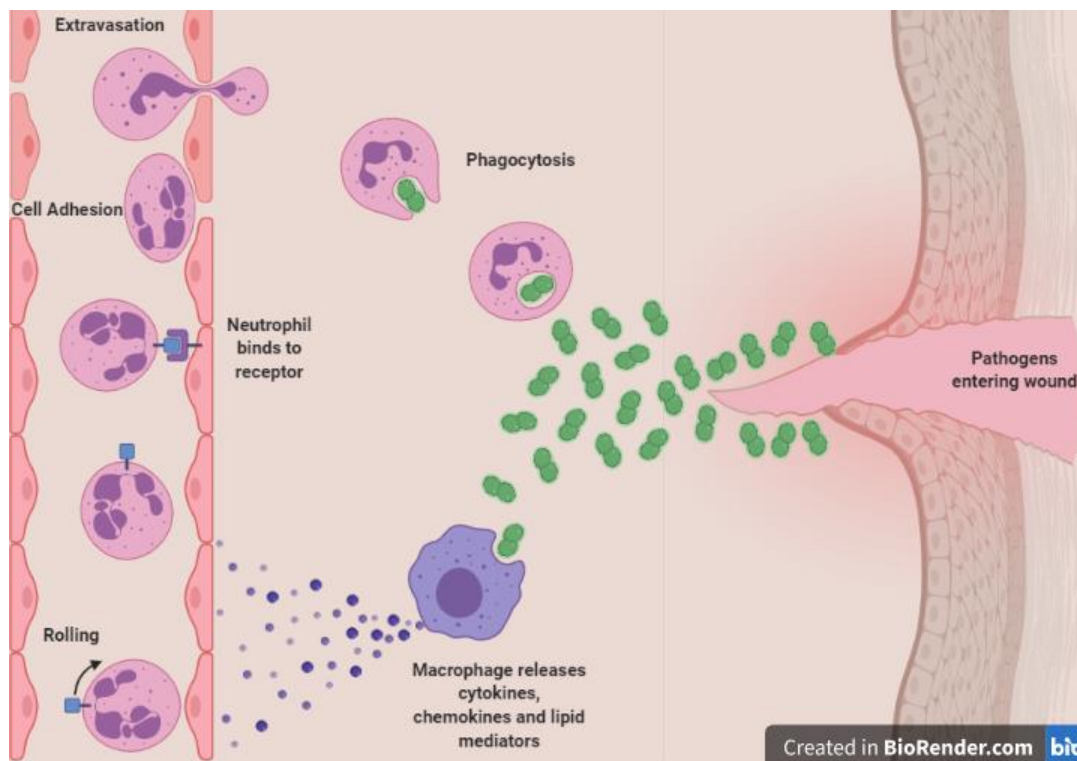
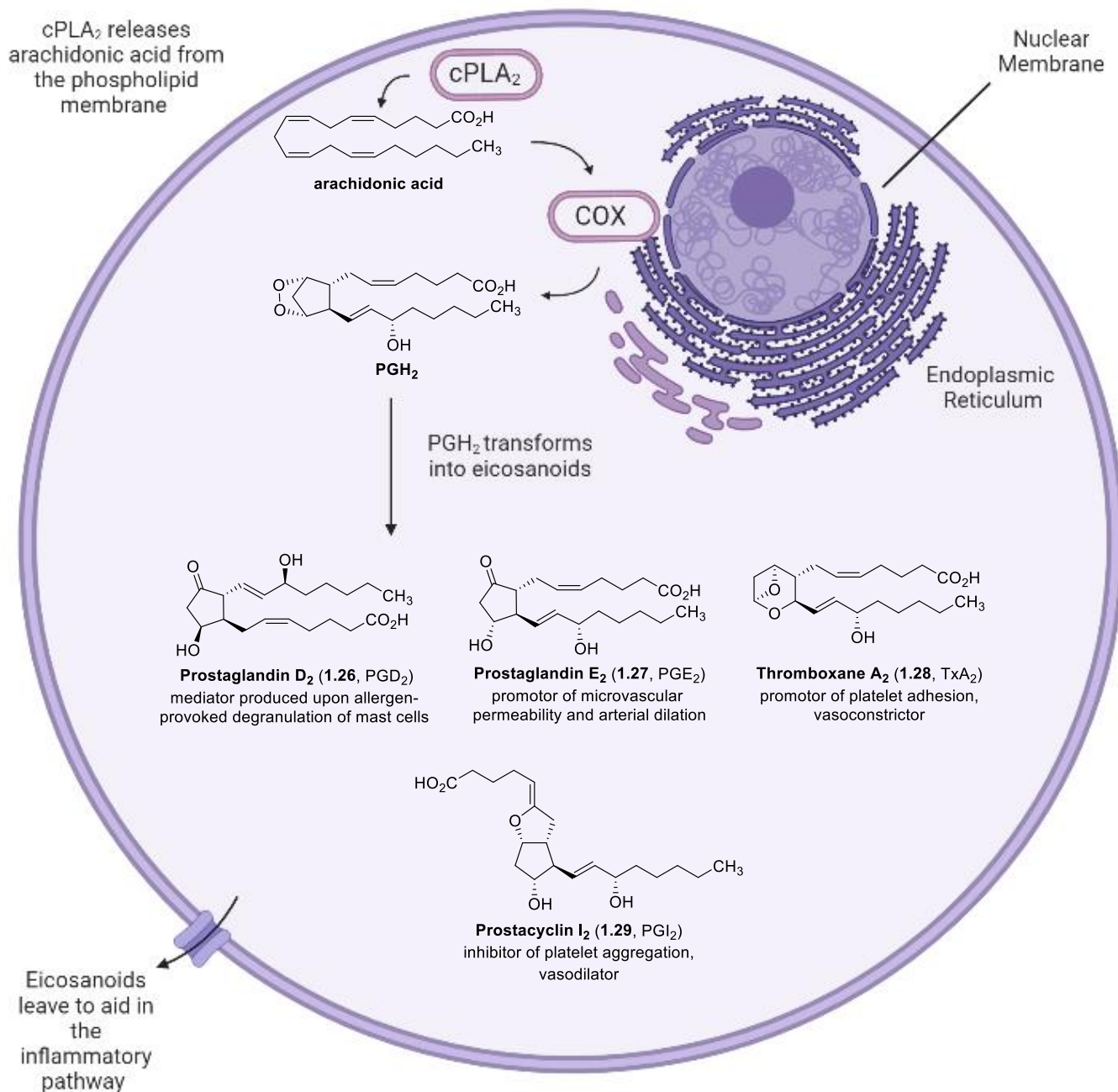


Figure 1.6. Cellular Response to Pathogens Entering a Wound.

The lipid mediators that macrophages release provide signals and facilitate specific actions in explicit tissues and cell types. Eicosanoids are a multitude of lipid mediators that are synthesized from arachidonic acid; it is stored as the esterified form and when arachidonic acid is needed, it is then released by group IV calcium-dependent cytosolic phospholipase A₂ (cPLA₂) from the phospholipid membrane.^{49,50,51} Upon mechanical trauma, cPLA₂ translocates to the nuclear membrane, golgi apparatus, and endoplasmic reticulum where the COX enzymes reside.⁵² Then the COX enzymes produce PGH₂; PGH₂ is then transformed into various arachidonic metabolites including prostaglandin D₂ (**1.26**, PGD₂), prostaglandin E₂ (**1.27**, PGE₂), thromboxane A₂ (**1.28**, TxA₂) and prostacyclin I₂ (**1.29**, PGI₂) (**Figure 1.7**). Prostaglandin D₂ responds to stimuli associated with asthma and allergic rhinitis; in addition, it has potential to exhibit anti-tumorigenic activity in cancer cells.⁶ One of the most abundant prostaglandins produced within the body, prostaglandin E₂, has been shown to augment arterial dilation and increase microvascular permeability. Furthermore, PGE₂ has promoted colorectal adenoma growth.⁵³ Thromboxane A₂, with a half-life of only 30 seconds, has been shown to partake in platelet aggregation and smooth muscle contraction. TxA₂ also plays a major role in angiogenesis and tumorigenesis.⁶ Prostacyclin I₂ is a vasodilator and inhibitor of platelet aggregation.⁵⁴ Each of these arachidonic acid metabolites plays a unique role in the inflammatory response and has specific receptors to regulate their corresponding physiological functions; however, a complete list will not be provided herein; instead, the reader can source a review by Dennis for more information.⁵⁵ While these metabolites can be beneficial to induce inflammation in the innate response, if inflammation, like tissue malfunction, persists this can lead to chronic inflammation and lead to various diseases including obesity, type 2 diabetes, atherosclerosis, asthma, and neurodegenerative diseases.^{56,57}



Created in [BioRender.com](https://www.biorender.com)

Figure 1.7. Generic Cell Converting Arachidonic Acid into Various Eicosanoids to Aid in the Inflammatory Response.

Section Summary

The goals of Chapters 1 & 2 are to establish the importance of arachidonic acid derivatives produced by the COX enzymes and introduce total syntheses to access these compounds. The previous sections demonstrated the complexity and significance of understanding how the enzymes COX-1 and COX-2 interact with polyunsaturated fatty acids and COX inhibitors. It allows one to appreciate the complexity of only two of the 5,000 enzymes discovered within the human body to date.⁵⁸ This section also highlighted how arachidonic acid transformed by the COX enzymes function in the human body during the inflammatory response at a molecular level. While researchers know the structures of these eicosanoids, they do not necessarily have methods to make enough material to conduct studies that specifically investigate their roles and interactions in the human body. The next section will provide an analysis of various total syntheses of COX eicosanoids and then discuss the biosynthetic pathway of certain classes of arachidonic acid metabolites.

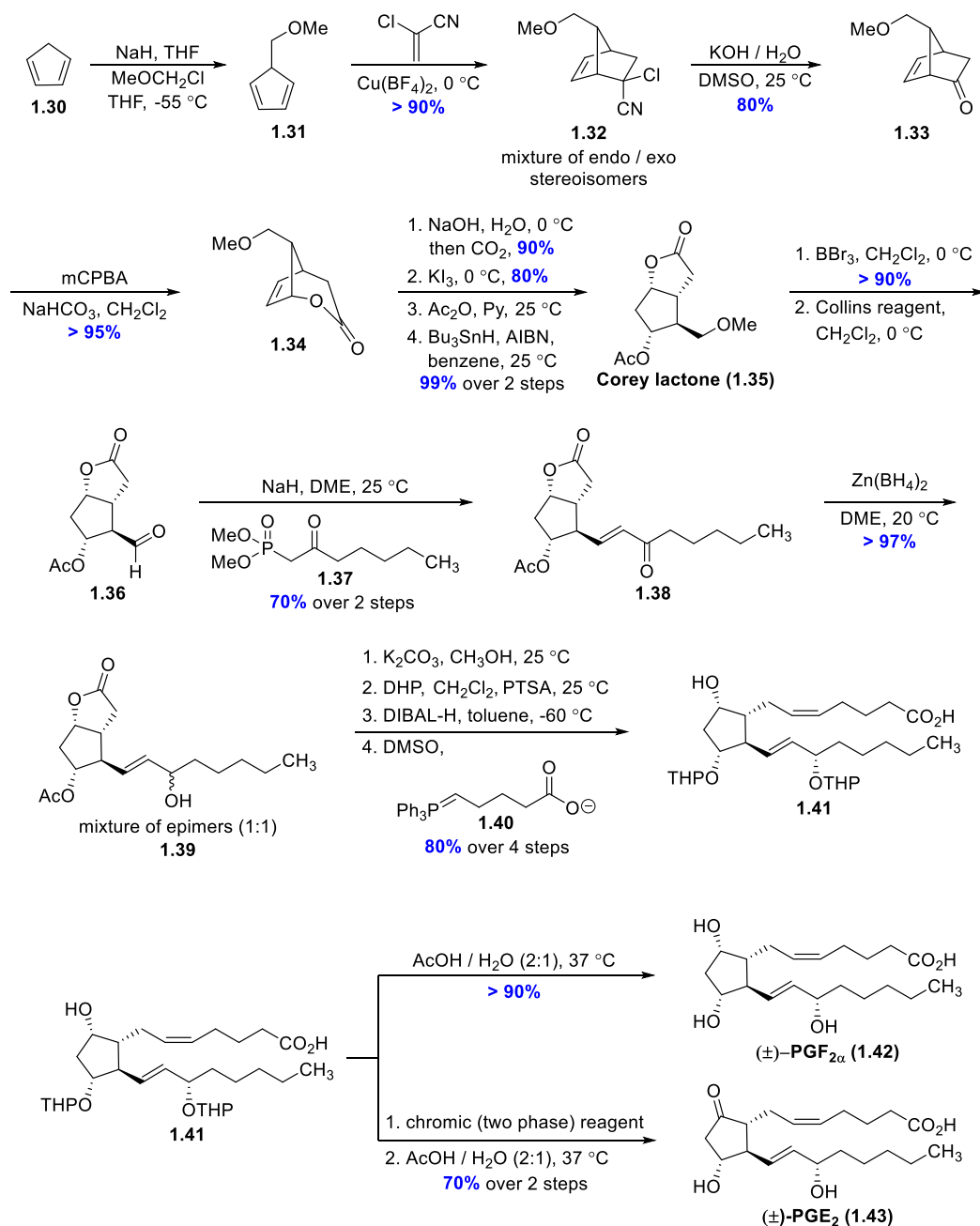
Select Total Syntheses of Eicosanoids

In this section, nine syntheses of various COX eicosanoids have been chosen to demonstrate multiple messages. While older syntheses may not be valued by modern organic chemists and perhaps, even regarded as inferior by some individuals because syntheses of certain molecules were racemic or contain 1:1 mixtures of diastereomers, it is important to appreciate the knowledge of the past. If not for these initial syntheses, the advances of modern organic chemistry would not be seen today. In this section the routes towards various eicosanoids range from the year 1969 to 2019 and proceed in order from oldest to newest. Observing how the field of organic chemistry has maneuvered over those 50 years is fascinating. Secondly, the syntheses of this section provide a variety of unique methods to construct eicosanoids using interesting, classic reactions of organic chemistry. Thirdly, another goal is to allow the reader to appreciate the vast amount of COX eicosanoids that exist and emphasize the need to study these compounds.

1969 - Corey's Synthesis of (±)-PGF_{2α} and (±)-PGE₂

The first synthesis which will be discussed is Corey's synthesis of (±)-PGF_{2α} (**1.42**) or (±)-PGE₂ (**1.43**) (**Scheme 1.3**).⁵⁹ Commencement of the addition of cyclopentadienyl sodium to a slight excess of chloromethyl methyl ether furnished cyclopentadiene **1.31** which was subjected to Diels-Alder reaction with 2-chloroacrylonitrile in the presence of cupric fluoroborate as a catalyst. The resulting product **1.32** contained an inconsequential mixture of endo and exo stereoisomers. Hydrolysis of **1.32** with KOH in DMSO converged to

anti-bicyclic ketone **1.33**. Subsequent Bayer-Villiger oxidation provided lactone **1.34**. A four-step transformation towards the Corey lactone (**1.35**) involved saponification, followed by immediate iodolactonization with KI_3 , acetyl protection and deiodination with tributyltin hydride. Next, demethylation with BBr_3 , followed by oxidation with Collins' reagent provided aldehyde **1.36**.⁶⁰ This aldehyde was treated with the sodium salt of phosphonate **1.37** to give enone **1.38**. Reduction of enone **1.38** with zinc borohydride provided a 1:1 mixture of epimers **1.39**. These epimers can be separated by thin-layer column chromatography. Fortuitously, the undesired 15β -epimer can be oxidized to enone **1.38** with manganese dioxide to be recycled. After a replacement of protecting groups, DIBAL-H reduction of the lactone and Wittig condensation provided cyclopentane **1.41**. Deprotection or oxidation steps from the cyclopentane precursor **1.41** ultimately yielded (\pm) -PGF_{2 α} or (\pm) -PGE₂.

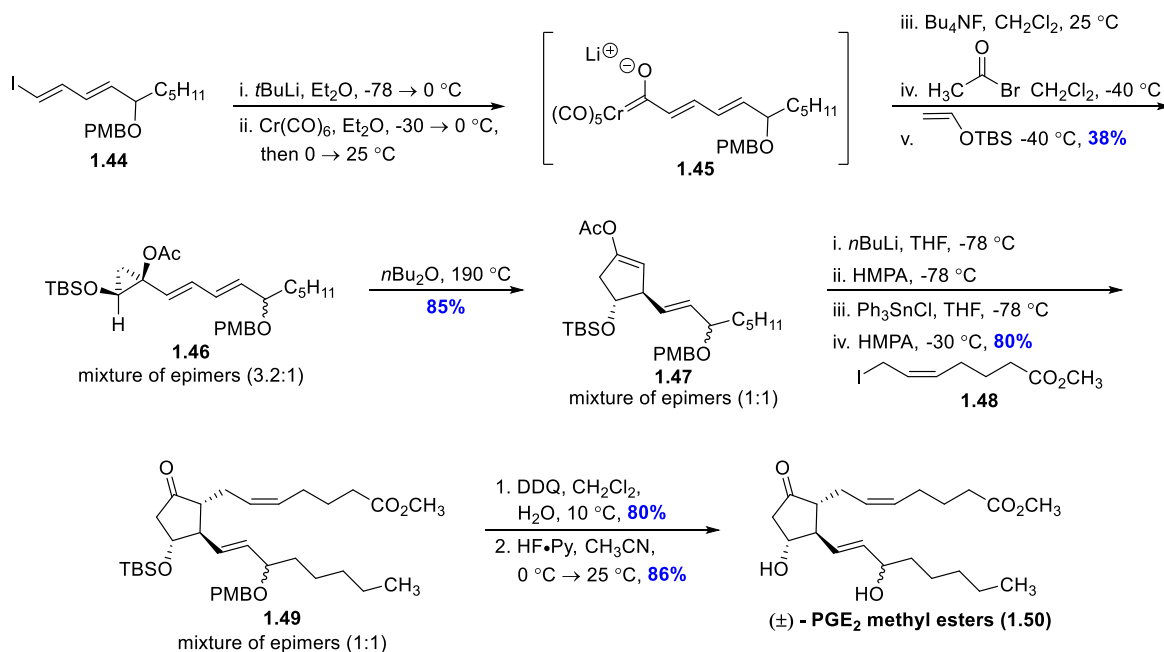


Scheme 1.3. Corey's Synthesis of (±)-PGF_{2α} and (±)-PGE₂.

1990 - Wulff's Synthesis of (±)-PGE₂ Methyl Esters

Wulff's synthesis of the (±)-PGE₂ methyl esters is unique primarily because he utilized a vinyl cyclopropane thermal rearrangement to construct the cyclopentane core of the prostaglandin (**Scheme 1.4**).⁶¹ In this synthesis, carbene **1.45** was prepared from dienyliodide **1.44**.⁶² It was found that treatment with an acyl bromide increased the electrophilic nature of the carbene complex to react with enol ethers. Thus, after removal of lithium salts with tetrabutylammonium, carbene **1.45** was treated with acetyl bromide and then an enol silane to afford the *cis*-dienyl cyclopropane **1.46** in a 3.2:1 ratio of epimers. This mixture of epimers **1.46** is carried forward into the thermal

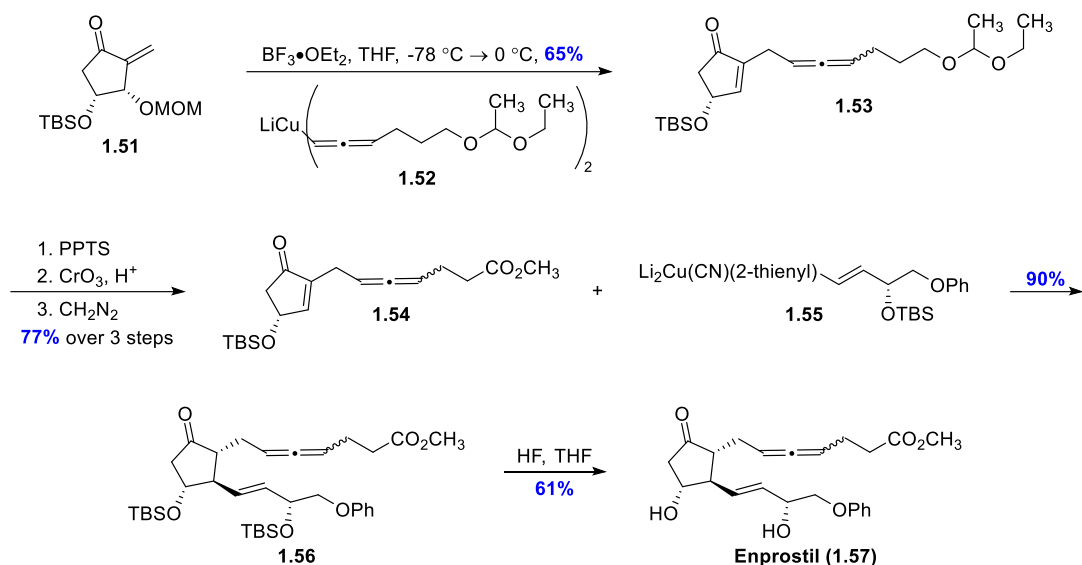
ring expansion at 190 °C to yield cyclopentene **1.47** as a 1:1 mixture of epimers in 85% yield.⁶³ Noyori's method of utilizing triorganotin halides to transmetalate with lithium enolates allows for the installation of side chain **1.48**.⁶⁴ Then, final removal of the *p*-methoxybenzyl and *tert*-butyldimethylsilyl groups affords a racemic mixture of PGE₂ methyl esters.



Scheme 1.4. Wulff's Synthesis of (±)-PGE₂ Methyl Esters.

1994 - Sato's Synthesis of Enprostil, a 4,5-didehydro PGE₂ Allene Analog

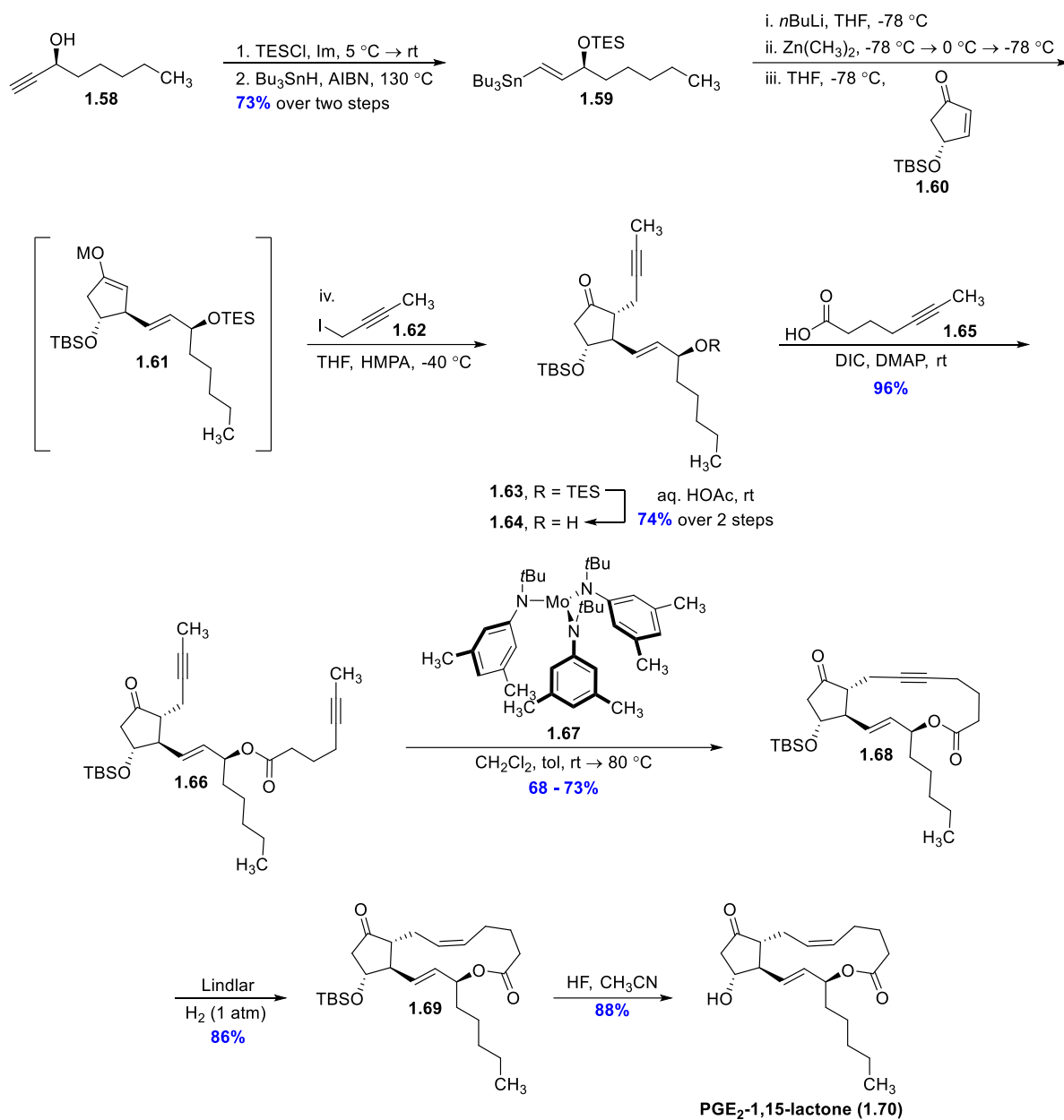
Prostaglandin analogs incorporating allenic groups in place of alkenes into the side-chain have been shown to be therapeutically useful such as the 4,5-didehydro PGE₂ analog, enprostil (**1.57**) (**Scheme 1.5**).⁶⁵ This drug is valuable in preventing and treating gastric and duodenal ulcers which can be caused while taking COX inhibitors. Sato and coworkers establish the synthesis of enprostil *via* a two-component coupling. The synthesis first features an interesting 1,4 addition of optically pure enone **1.51** with cupric allene **1.52** in the presence of BF₃·OEt₂ to afford cyclopentenone **1.53**.^{66,67} After a deprotection-oxidation sequence, the resulting carboxylic acid was treated with diazomethane to give methyl ester **1.54**. Next, a 1,4 addition with Michael acceptor **1.54** and organocuprate **1.55**, made in five steps from commercially available (+)-2,3-*O*-isopropylidene-L-threitol, provided cyclopentanone **1.56** in 90% yield. Final deprotection of the *tert*-butyldimethylsilyl ethers with hydrogen fluoride afforded enprostil as a mixture of isomers in 27% overall yield. Sato's synthesis is important since it established the precedence towards pure enprostil, known to cause even fewer side effects than other prostaglandin derivatives.



Scheme 1.5. Sato's Synthesis of Enprostil, a 4,5-didehydro PGE₂ Allene Analog.

2000 - Fürstner's Synthesis of PGE₂-1,15-lactone

Fürstner and coworkers utilized their alkyne metathesis strategy^{68,69} to synthesize prostaglandin lactone analogues from precursors assembled using a Noyori three-component reaction (**Scheme 1.6**).⁷⁰ Prostaglandin lactones such as PGE₂-1,15-lactone (**70**) have been isolated from mollusks of the *Tethys fimbria* species.⁷¹ These ichthyotoxic compounds are secreted upon mechanical trauma as part of the animal's defense system. The synthesis of PGE₂-1,15-lactone begins by using enantiomerically pure vinylstannane **1.59**, accessed in two steps from commercially available (*S*)-oct-1-yn-3-ol (**1.58**). Transmetalation of **1.59** with *n*-BuLi and *in situ* formation of the dimethylzincate was followed by a conjugate addition onto the Michael acceptor, cyclopentenone **1.60**. Subsequent *in situ* trapping of the resulting zinc enolate **1.61** with 4-iodo-but-2-yne (**1.62**) provided the three-component coupling product **1.63**. After deprotection and esterification steps, the alkyne metathesis precursor **1.66** was accessed. Treatment of alkyne metathesis precursor **1.66** with molybdenum precatalyst **1.67** led to cycloalkyne **1.68** in good yield. Semihydrogenation of the resulting alkyne with Lindlar's catalyst and desilylation with hydrogen fluoride afforded PGE₂-1,15-lactone in 28% overall yield. This very elegant synthesis marks the first pure stereoisomer of a prostaglandin derivative among the syntheses discussed herein.

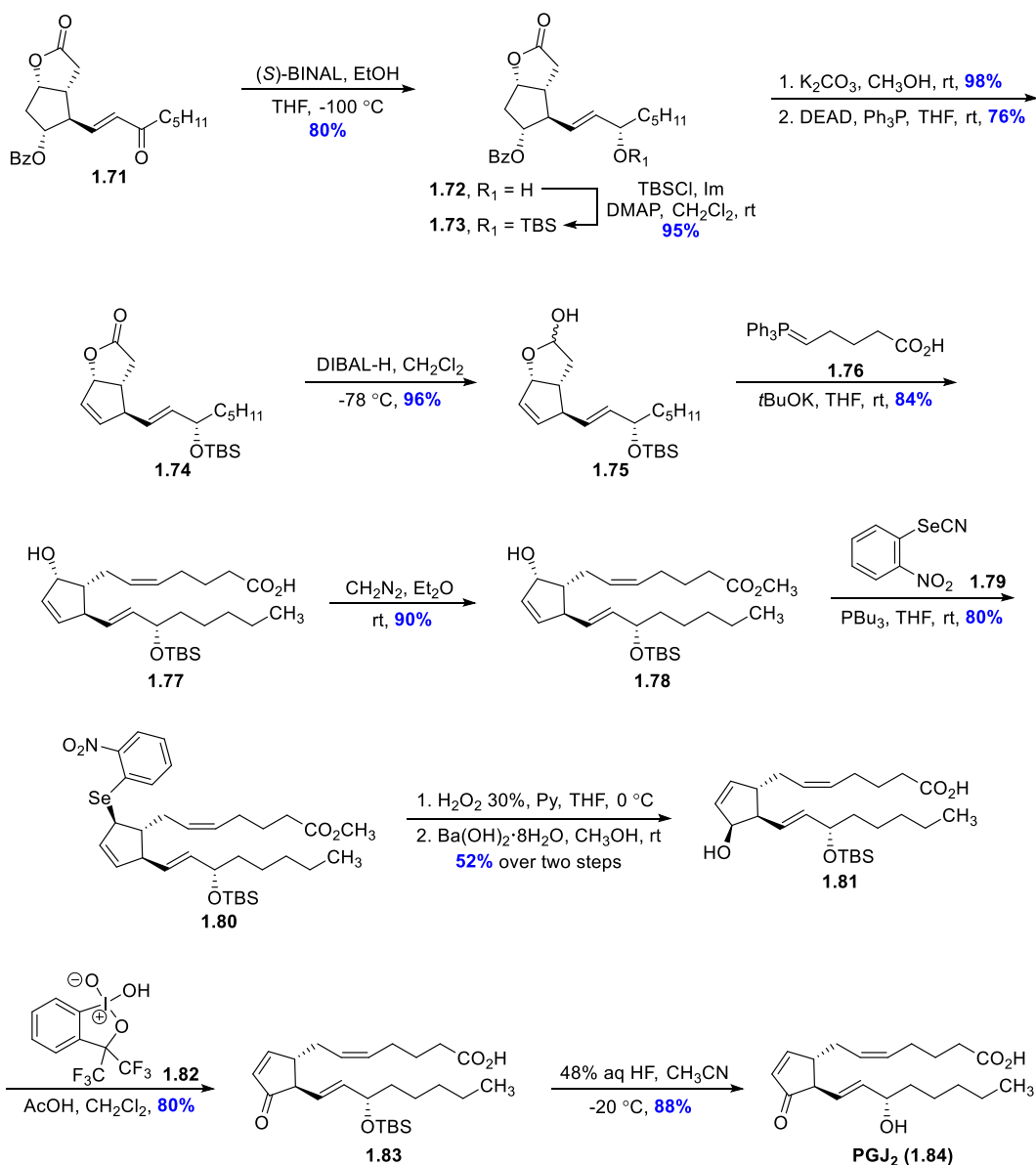


Scheme 1.6. Fürstner's Synthesis of PGE₂-1,15-lactone.

2003 - Vidari's Synthesis of PGJ₂

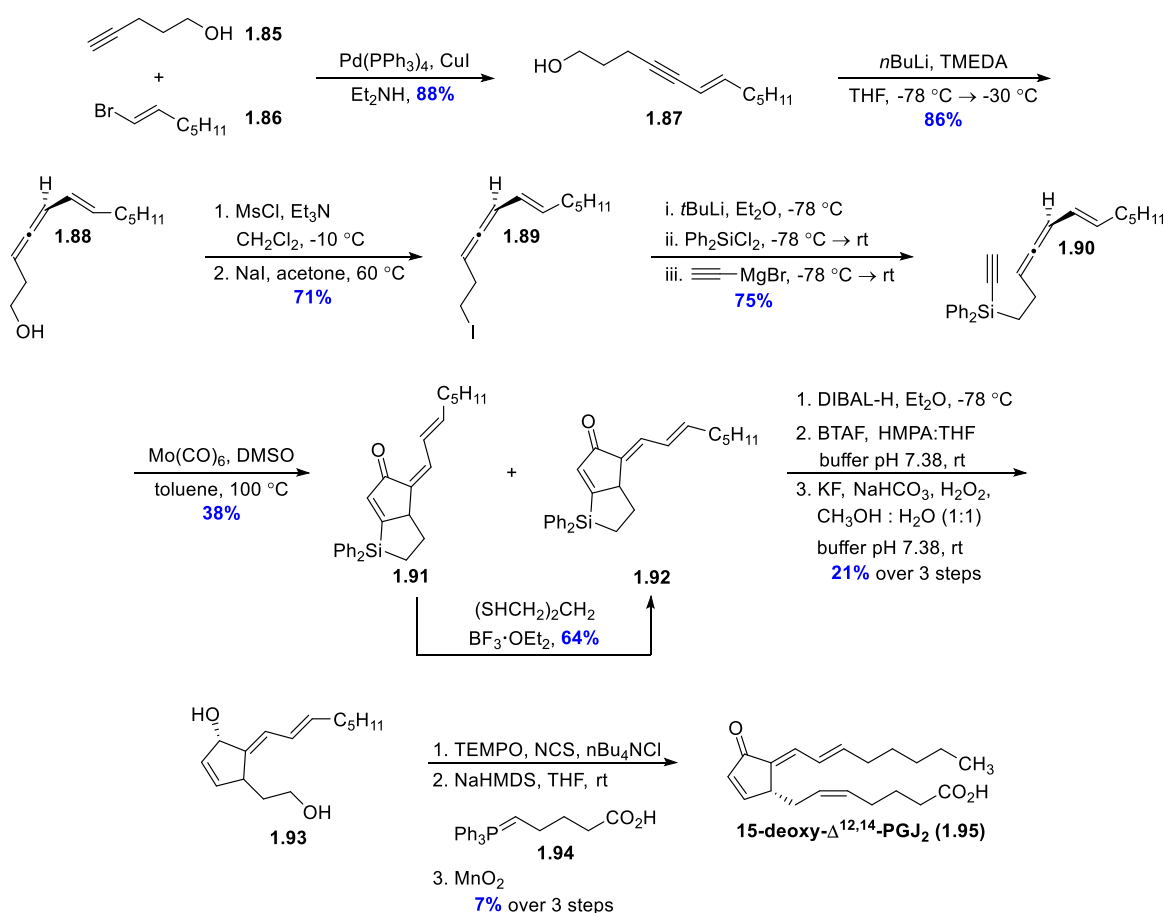
Prostaglandin J₂ and its metabolites have been shown to have anti-neoplastic, anti-inflammatory, and anti-viral effects. Other syntheses of racemic PGJ₂ have been reported by Roberts and Newton; however, Vidari's synthesis is the first enantioselective synthesis of PGJ₂.⁷² The synthesis initiates with known enone **1.71**, which was obtained following Bundy's original protocol (**Scheme 1.7**).⁷³ Noyori reduction of enone **1.71** with (*S*)-BINAL-H,⁷⁴ following an alternation of protecting groups led to a dehydration utilizing diethyl azodicarboxylate (DEAD) and triphenyl phosphine to afford alkene **1.74**.⁷⁵ DIBAL-H reduction and ensuing selective *Z*-olefination

with the non-stabilized Wittig reagent provided olefin **77** in good yield. Treatment of carboxylic acid **1.77** with diazomethane and then conversion to selenide **1.80** proceeded smoothly. Next, oxidation of selenide **1.80** with 30% H₂O₂ allowed the resulting selenoxide intermediate to perform the [2,3] sigmatropic rearrangement to the desired alcohol. Saponification, followed by mild oxidation with hydroxyiodinane oxide **1.82**^{76,77} in AcOH, and desilylation successfully provided PGJ₂ enantioselectively. While this synthesis is quite lengthy, Vidari showcases the first asymmetric synthesis of PGJ₂.



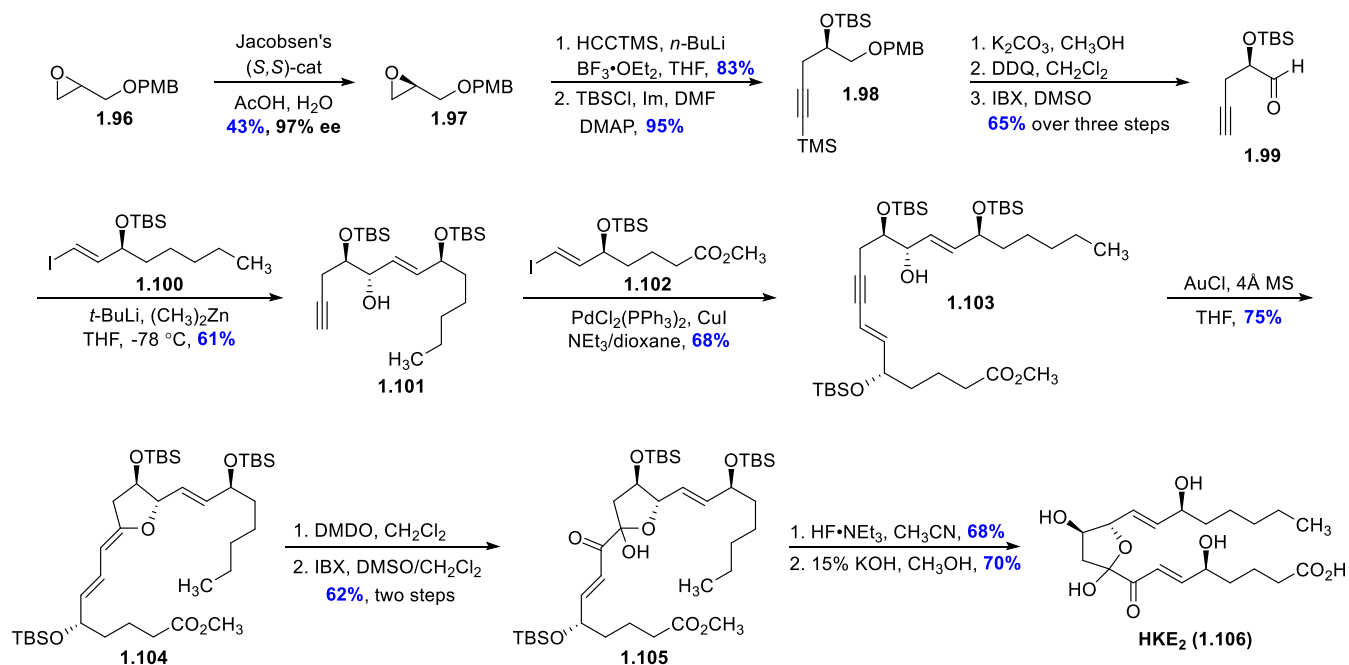
Scheme 1.7. Vidari's Synthesis of PGJ₂.

Brummond's synthesis features an intriguing allenic Pauson-Khand type reaction to establish the carbon framework of the prostaglandin (**Scheme 1.8**).⁷⁸ Initially, a Sonogashira coupling between 4-pentynol (**1.85**) and (*E*)-1-bromo-1-heptene (**1.86**) gives enyne **1.87**. Treatment of enyne **1.87** with *n*-BuLi provides allenol **1.88**.⁷⁹ Then, functional group interconversion, followed by a three-step treatment with *t*-BuLi, diphenyldichlorosilane, and finally ethynylmagnesium bromide provides the alkynyl allene precursor **1.90**. Alkynyl allene **1.90** was subjected to Pauson-Khand conditions to give a 2:1 mixture of enones **1.91** and **1.92**.⁸⁰ A method to catalyze the complete isomerization of enone **1.91** into the desired enone **1.92** was established with boron trifluoride and propanedithiol in 64% yield. With the desired (*E*)-alkylidene cyclopentenone **1.92** in hand, treatment with DIBAL-H, followed by cleavage of the silicon tether with benzyltrimethylammonium fluoride, and subsequent Fleming-Tamao oxidation conditions gave cyclopentene **1.93**.⁸¹ Selective oxidation of the primary alcohol utilizing the TEMPO protocol provided the aldehyde which was immediately reacted under Wittig conditions. Finally, an allylic oxidation with manganese dioxide afforded 15-deoxy- $\Delta^{12,14}$ -PGJ₂. For other syntheses of prostaglandin analogs, the reader is encouraged to peruse this review by Touré and coworkers.⁸²



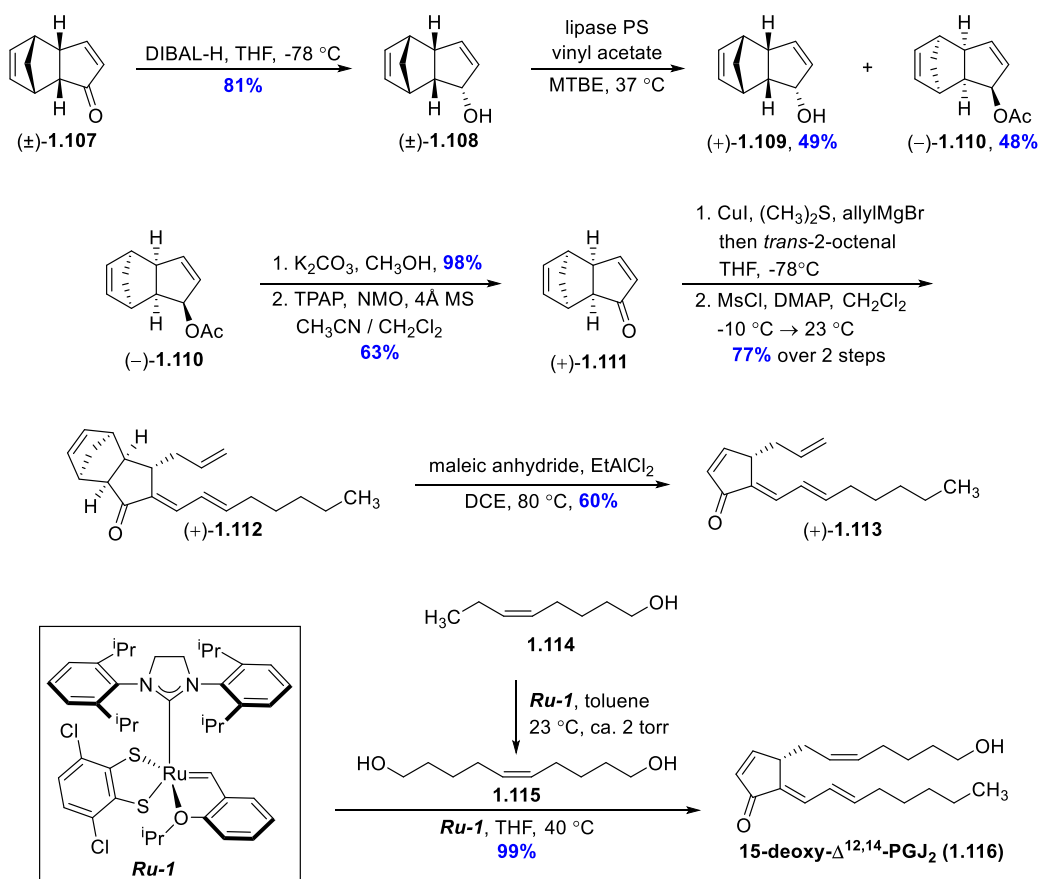
Scheme 1.8. Brummond's Synthesis of 15-deoxy- $\Delta^{12,14}$ -PGJ₂.

Hemiketal E₂ (**1.106**, HKE₂) has been shown to be involved in the inflammatory pathway; more detail about the biological activity of this eicosanoid will be provided after the completion of the total syntheses section on COX metabolites. Sulikowski's synthesis began with a racemic mixture of *p*-methoxybenzyl protected glycidol **1.96** (Scheme 1.9).⁸³ Utilizing Jacobsen's hydrolytic-kinetic resolution,^{84,85} the enantiomerically pure epoxide **1.97** was obtained. After epoxide opening and protection of the secondary alcohol, a three-step deprotection-oxidation sequence yielded aldehyde **1.99**. Then, treatment of vinyl iodide **1.100** with *t*-BuLi, followed by transmetalation with dimethylzinc resulted in a non-basic vinyl zincate which selectively added into the aldehyde in a Felkin-Ahn fashion to yield acetylene **1.101**. Sonogashira coupling between acetylene **1.101** and vinyl iodide **1.102** gave the enyne **1.103**. Then, gold mediated 5-exo-dig ring cyclization yielded furan **1.104**.^{86,87} A two-step oxidation sequence and finally global deprotection afforded the final HKE₂ (**1.106**). The Sulikowski synthesis is groundbreaking because it demonstrates the first pure stereoisomer of HKE₂. Unfortunately, access to the other hemiketal D₂ remains elusive, and further research must be done to synthesize this compound.



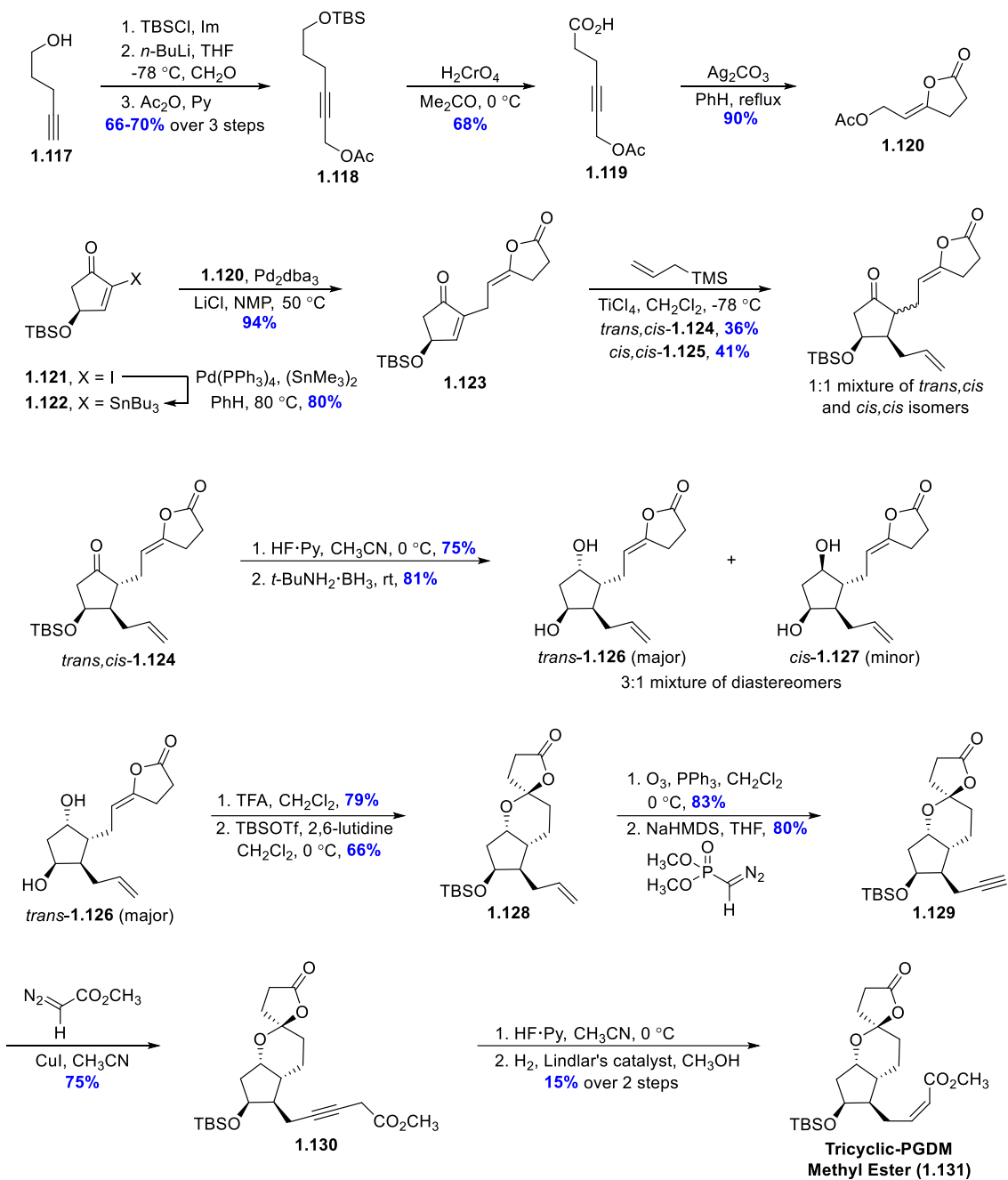
Scheme 1.9. Sulikowski's Synthesis of HKE₂.

Stoltz' and Grubbs' synthesis features a lipase-mediated enzymatic resolution, a clever retro Diels-Alder, and a one pot homodimerization / stereoretentive metathesis.⁸⁸ Initially, racemic *endo*-3-oxodicyclopentadiene (\pm)-**1.107** was treated with DIBAL-H, and the resulting *endo*-alcohol (\pm)-**1.108** was obtained in excellent yield (**Scheme 1.10**). Then kinetic resolution was performed with vinyl acetate in the presence of commercially available lipase PS-on-Celite. *Endo*-acetate ($-$)-**1.110** (48% yield) was separated from *endo*-alcohol ($+$)-**1.109** (49% yield). *Endo*-acetate ($-$)-**1.110** was subjected to deacetylation and Ley-Griffith oxidation conditions to yield ($+$)-**1.111**. A regioselective and stereoselective conjugate addition by diallyl cuprate installed the allyl group and formed an enolate intermediate that was then trapped by the addition of *trans*-2-octenal. The resulting mixture of aldol diastereomers can be converted to the thermodynamically favored *E*-alkenes upon addition of MsCl to afford tricycle ($+$)-**1.112**. From here enone ($+$)-**1.113** can be accessed *via* a Lewis acid catalyzed retro Diels-Alder with EtAlCl₂ and maleic anhydride.⁸⁹ Both enantiomers of **1.113** can be accessed in high enantioselectivity; however, that will not be shown here. Next, the one pot homodimerization of alcohol **1.114** gives diol **1.115** with high *Z*-selectivity in the presence of **Ru-1**.⁹⁰ Final treatment of diol **1.115** with enone ($+$)-**1.113** and **Ru-1** provides 15-deoxy- $\Delta^{12,14}$ -PGJ₂ in 99% yield. This synthesis provides hope that the metathesis approach which will be discussed in more detail in Chapter 2 is indeed feasible.



Scheme 1.10. Stoltz' & Grubbs' Enantioselective Synthesis of 15-deoxy- $\Delta^{12,14}$ -PGJ₂.

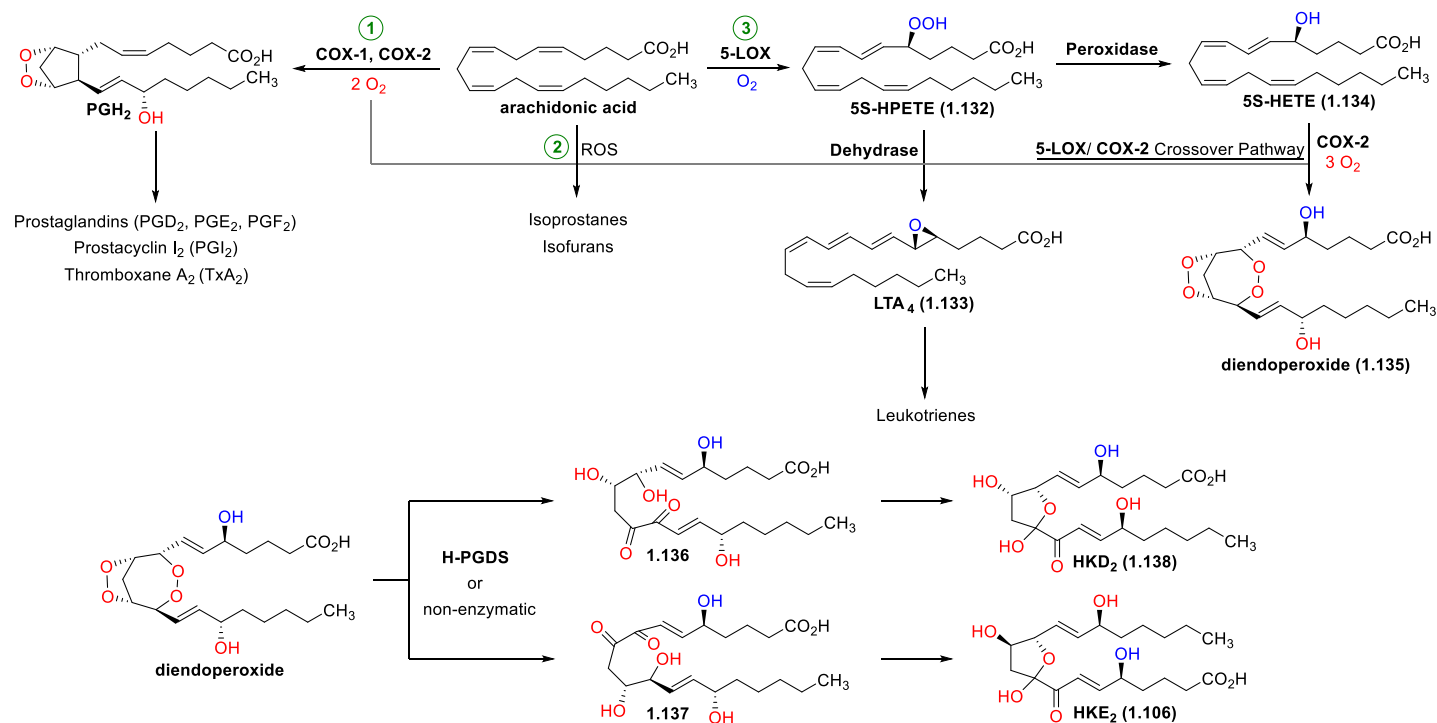
The synthesis of tricyclic-PGDM methyl ester began with a cycloisomerization of alkynyl carboxylic acid **1.119**,⁹¹ which is made from commercially available 4-pentyn-1-ol (**1.117**) in four steps, with silver carbonate to afford allylic acetate **1.120** (Scheme 1.11).⁹² Iodoenone **1.121** was transformed into stannane **1.122** which then underwent a Stille coupling with allylic acetate **1.120**.⁹³ Treatment of the resulting Stille coupling product, enone **1.123**, with titanium tetrachloride and allyltrimethylsilane provided a 1:1 mixture of *trans,cis*-**1.124** and *cis,cis*-**1.125** isomers.⁹⁴ Evidence from careful NMR analysis supported the assignments of both isomers. The isomers were separable by flash column chromatography and the *trans,cis*-**1.124** isomer was carried forward to the tricyclic-PGDM methyl ester. It was found necessary to first remove the bulky *tert*-butyldimethylsilane group and then reduce the resulting ketone with *t*-BuNH₂•BH₃ to allow for an improved 3:1 ratio of diastereomers. The mixture was carried forward (for simplicity only the major *trans*-**1.126** is shown) to form a mixture of spiroacetals (only spiroacetal **1.128** is shown). Ozonolysis, followed by Seyferth-Gilbert conditions of spiroacetal **1.128** afforded alkyne **1.129** in good yield. Copper-catalyzed coupling of alkyne **1.129** with methyl diazomethane gave alkynoate **1.130**.⁹⁵ Final silyl deprotection and semihydrogenation with Lindlar's catalyst provided the tricyclic-PGDM methyl ester (**1.131**). This structurally interesting molecule is significant because its synthesis is the shortest known pathway towards this pure stereoisomer.



Scheme 1.11. Sulikowski's Synthesis of Tricyclic-PGDM Methyl Ester.

Biosynthetic Pathway of Eicosanoids

Although the roles of certain COX eicosanoid byproducts and their syntheses have been established, it is important to address the biosyntheses of other important classes of eicosanoids. Summarized below are three biosynthetic pathways towards various arachidonic acid metabolites (**Scheme 1.12**). The previously mentioned pathway involves the conversion of arachidonic acid to PGH_2 which ultimately transforms into prostaglandins and thromboxanes. The second is a nonenzymatic pathway which utilizes reactive oxygen species (ROS) to provide isoprostanes and isofurans. These nonenzymatic products have important uses as biomarkers of oxidative stress involved in many diseases.^{96,97,98} The third pathway oxidizes arachidonic acid with the enzyme 5-lipoxygenase (5-LOX)^{99,100,101,102} to afford 5*S*-hydroperoxyeicosatetraenoic acid (**1.132**, 5*S*-HPETE). 5*S*-HPETE can dehydrate to give leukotriene A_4 (**1.133**, LTA_4) which eventually forms a series of leukotrienes.^{103,104} Alternatively, the peroxidase enzyme reduces 5*S*-HPETE to afford 5*S*-hydroxyeicosatetraenoic acid (**1.134**, 5*S*-HETE). The most thoroughly studied pathways involve the COX enzymes and 5-LOX. It was an established belief that the biosynthetic pathways toward prostaglandins and leukotrienes acted independently of each other as they diverge after the initial oxidation of arachidonic acid via the enzymes COX-2 and 5-LOX, respectively.⁴⁹ However, Schneider noticed a structural similarity between arachidonic acid and 5*S*-HETE. Upon treatment of these two compounds with COX-2, the results revealed that just as arachidonic acid forms an endoperoxide intermediate PGH_2 , 5*S*-HETE reacts in a similar fashion to form diendoperoxide **1.135**.¹⁰⁵ The identification of



Scheme 1.12. Biosynthetic Pathway of Arachidonic Acid Metabolites. Red oxygens are incorporated from the COX enzymes and blue oxygens from 5-LOX.

this diendoperoxide led to the discovery that a crossover pathway existed between the two enzymes COX-2 and 5-LOX. Subsequent collapse of the diendoperoxide either enzymatically or nonenzymatically yields Hemiketal D₂ (**1.138**, HKD₂) and Hemiketal E₂ (**1.106**, HKE₂). Recently, Schneider and coworkers discovered that the 5-LOX/ COX-2 crossover pathway can also yield 5-hydroxy-prostaglandins.¹⁰⁶ With the biosynthesis established, the next section will encompass what is known about the biological roles of the hemiketals.

Biological Roles of Hemiketals in Endothelial Cells

In 2011, early studies revealed that the hemiketals stimulate tubulogenesis and cell migration in murine pulmonary endothelial cells *in vitro* (**Figure 1.8**).¹⁰⁷ Unpublished results by Schneider demonstrate an increase in angiogenesis *in vivo*. More recently, Schneider and coworkers utilized charge reversal derivatization and liquid chromatography-electrospray ionization-mass spectrometry methods to quantify levels of the hemiketals in human leukocytes stimulated *ex vivo* compared to other 5-LOX and COX-2 metabolites.¹⁰⁸ Furthermore, chemically-synthesized HKE₂ was shown to inhibit platelet aggregation comparable to HKE₂ prepared via enzymatic synthesis.⁸³ A hypothesis exists that the hemiketals may play an important role in tumorigenesis.⁶ When neutrophils, a source of 5S-HETE, interact with macrophages, a source of COX-2, they can synthesize hemiketals from the diendoperoxide as mentioned previously, thereby promoting endothelial cell growth and angiogenesis for tumor cells. Finally, research has also associated COX-2 with a promotion of colorectal cancer by inducing angiogenesis and anti-apoptotic effects.¹² Interest in targeting different domains of COX-2 may lead to potential cancer treatments. Unfortunately, the hemiketals are limited in their availability by enzymatic synthesis which typically only produce microgram amounts.¹⁰⁹ As such, a reproducible and robust total synthesis is needed to produce a substantial amount of material and further elucidate the biological roles of these hemiketals.

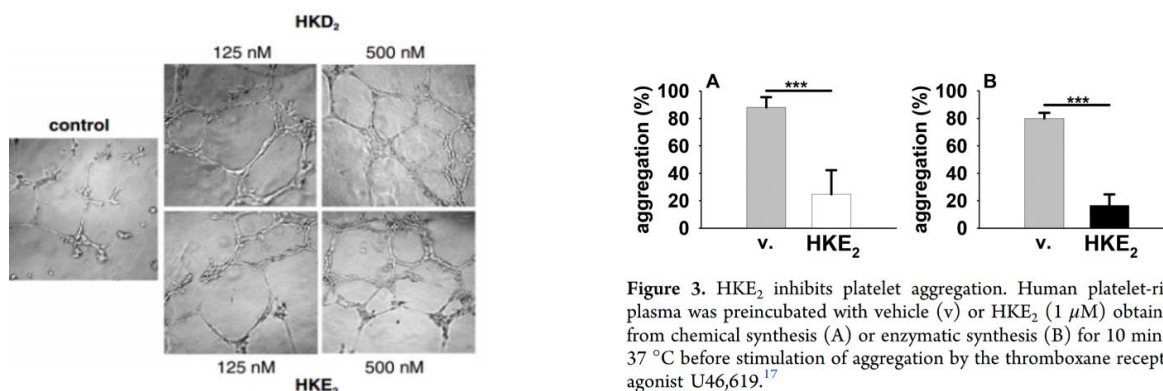


Figure 3. HKE₂ inhibits platelet aggregation. Human platelet-rich plasma was preincubated with vehicle (v) or HKE₂ (1 μ M) obtained from chemical synthesis (A) or enzymatic synthesis (B) for 10 min at 37 °C before stimulation of aggregation by the thromboxane receptor agonist U46,619.¹⁷

Figure 1.8. Early Studies Demonstrating the Biological Roles of the Hemiketals. Left: Treatment of endothelial cells with hemiketal compounds increase of tubulogenesis and ring size formation. Reprinted with permission from Griesser, M.; Suzuki, T.; Tejera, N.; Mont, S.; Boeglin, W. E.; Pozzi, A.; Schneider, C. *PNAS. USA.* **2011**, *108*, 6945–6950. Right: synthesized HKE₂ (A) revealed inhibition of platelet aggregation just like HKE₂ produced from *in vitro* enzymatic synthesis. Reprinted with permission from Boer, R.; Gimenez-Bastida, J. A.; Boutaud, O.; Jana, S.; Schneider, C.; Sulikowski, G. A. *Org. Lett.* **2018**, *20*, 4020–4022. Copyright 2020 American Chemical Society.

Statement of Dissertation

Since the discovery that nonsteroidal anti-inflammatory drugs (NSAIDs) prevent pain, swelling, and inflammation by inhibiting the enzymes cyclooxygenase-1 (COX-1) and cyclooxygenase-2 (COX-2), there has been interest in anti-inflammatory drugs and their mechanisms. Arachidonic acid metabolites play an important role in many inflammatory diseases such as cancer, diabetes, asthma, and multiple sclerosis. Enzymatic metabolic pathways, like the transformation of arachidonic acid to prostaglandins or leukotrienes that utilize the enzymes COX-2 and 5-lipoxygenase (5-LOX) are physiologically relevant. Nonenzymatic pathways also exist, which involve reactive oxygen species (ROS) and ultimately lead to isoprostanes and isofurans. Unfortunately, arachidonic acid metabolites are not readily available. Specifically, newly discovered arachidonic acid metabolites, hemiketals D₂ (HKD₂, **1.138**) and E₂ (HKE₂, **1.106**) are only available in microgram quantities. Thus, in order to further elucidate the biological roles of HKD₂ and HKE₂ in the inflammatory response, a total synthesis is necessary. Understanding their roles could ultimately lead to the improvement of human health in preventing or treating various inflammatory diseases.

References

- (1) Lin, Y. Approaching Traditional Chinese Medicine: Inheritance and Exploration. In *Drug Discovery and Traditional Chinese Medicine: Science, Regulation, and Globalization*; Springer Science + Business Media, LLC: New York, 2001; p 4.
- (2) Mahdi, J. Medicinal Potential of Willow: A Chemical Perspective of Aspirin Discovery. *J. Saudi Chem. Soc.* **2010**, *14*, 317–322.
- (3) Stone, E. XXXII. An Account of the Success of the Bark of the Willow in the Cure of Agues. In a Letter to the Right Honourable George Earl of Macclesfield, President of R. S. from the Rev. Mr. Edward Stone, of Chipping-Norton in Oxfordshire. *Philos. Trans. R. Soc.* **1763**, *53*, 195–200.
- (4) Desborough, M.; Keeling, D. The Aspirin Story – from Willow to Wonder Drug. *Br. J. Haematol.* **2017**, *177*, 674–683.
- (5) Vane, J. Inhibition of Prostaglandin Synthesis as a Mechanism of Action for Aspirin-like Drugs. *Nat New Biol* **1971**, *231*, 232–235.
- (6) Schneider, C.; Pozzi, A. Cyclooxygenases and Lipoxygenases in Cancer. *Cancer Metastasis Rev.* **2011**, *30*, 277–294.
- (7) Chandrasekharan, N.; Simmons, D. The Cyclooxygenases. *Genome Biol* **2004**, *5*, 241.
- (8) Tanabe, T.; Tohnai, N. Cyclooxygenase Isozymes and Their Gene Structures and Expression. *Prostaglandins Other Lipid Mediat* **2002**, *68–69*, 95–114.
- (9) Rouzer, C.; Marnett, L. Cyclooxygenases: Structural and Functional Insights. *J. Lipid Res.* **2009**, *50*, S29–S34.
- (10) Spencer, A.; Woods, J.; Arakawa, T.; Singer, I.; Smith, W. Subcellular Localization of Prostaglandin Endoperoxide H-1 and -2 by Immunoelectron Microscopy. *J. Biol. Chem.* **1998**, *273*, 9886–9893.
- (11) Meek, I.; van der Laar, M.; Vonkeman, H. Non-Steroidal Anti-Inflammatory Drugs: An Overview of Cardiovascular Risks. *Pharmaceuticals (Basel)* **2010**, *3*, 2146–2162.
- (12) Blobaum, A.; Marnett, L. Structural and Functional Basis of Cyclooxygenase Inhibition. *J. Med. Chem.* **2007**, *50*, 1425–1441.
- (13) Picot, D.; Loll, P.; Garavito, R. The X-Ray Crystal Structure of the Membrane Protein Prostaglandin H2 Synthase-1. *Nature* **1994**, *367*, 243–249.
- (14) Astring, A.; Farivar, A.; Iresjö, B.; Svensson, H.; Gustavsson, B.; Lundholm, K. EGF Receptor and COX-1/COX-2 Enzyme Proteins as Related to Corresponding MRNAs in Human per-Operative Biopsies of Colorectal Cancer. *BMC Cancer* **2013**, *13*, 511.
- (15) Kim, Y.; Park, S.; Pyo, H. Cyclooxygenase-2 (COX-2) Negatively Regulates Expression of Epidermal Growth Factor Receptor and Causes Resistance to Gefitinib in COX-2–Overexpressing Cancer Cells. *Mol. Cancer Res.* **2009**, *7*, 1367–1377.

- (16) Hsu, J.; Chang, K.; Chen, S.; Lee, C.; Chang, S.; Cheng, H.; Chang, W.; Chen, B. Epidermal Growth Factor-Induced Cyclooxygenase-2 Enhances Head and Neck Squamous Cell Carcinoma Metastasis through Fibronectin up-Regulation. *Oncotarget* **2015**, *6*, 1723–1739.
- (17) Spencer, A.; Thuresson, E.; Otto, J.; Song, I.; Smith, T.; DeWitt, D.; Garavito, R.; Smith, W. The Membrane Binding Domains of Prostaglandin Endoperoxide H Synthases 1 and 2 MAPPING AND MUTATIONAL ANALYSIS. *J. Biol. Chem.* **1999**, *274*, 32936–32942.
- (18) Otto, J.; DeWitt, D.; Smith, W. N-Glycosylation of Prostaglandin Endoperoxide Synthases-1 and -2 and Their Orientations in the Endoplasmic Reticulum. *J. Biol. Chem.* **1993**, *268*, 18234–18242.
- (19) Mutsaers, J.; Van Halbeek, H.; Kamerling, J.; Vliegenthart, J. Determination of the Structure of the Carbohydrate Chains of Prostaglandin Endoperoxide Synthase from Sheep. *Eur. J. Biochem.* **1985**, *147*, 569–574.
- (20) Rouzer, C.; Marnett, L. Mechanism of Free Radical Oxygenation of Polyunsaturated Fatty Acids by Cyclooxygenases. *Chem. Rev.* **2003**, *103*, 2239–2304.
- (21) Smith, W.; DeWitt, D.; Garavito, R. Cyclooxygenases: Structural, Cellular, and Molecular Biology. *Annu. Rev. Biochem.* **2000**, *69*, 145–182.
- (22) Dietz, R.; Nastainczyk, W.; Ruf, H. Higher Oxidation States of Prostaglandin H Synthase. *Eur. J. Biochem.* **1988**, *171*, 321–328.
- (23) Thuresson, E.; Lakkides, K.; Rieke, C.; Sun, Y.; Wingerd, B.; Micielli, R.; Mulichak, A.; Malkowski, M.; Garavito, R.; Smith, W. Prostaglandin Endoperoxide H Synthase-1 THE FUNCTIONS OF CYCLOOXYGENASE ACTIVE SITE RESIDUES IN THE BINDING, POSITIONING, AND OXYGENATION OF ARACHIDONIC ACID. *J. Biol. Chem.* **2001**, *276*, 10347–10359.
- (24) Holtzman, M.; Turk, J.; Shornick, L. Identification of a Pharmacologically Distinct Prostaglandin H Synthase in Cultured Epithelial Cells. *J. Biol. Chem.* **1992**, *267*, 21438–21445.
- (25) Lecomte, M.; Laneuville, O.; Ji, C.; DeWitt, D.; Smith, W. Acetylation of Human Prostaglandin Endoperoxide Synthase-2 (Cyclooxygenase-2) by Aspirin. *J. Biol. Chem.* **1994**, *269*, 13207–13215.
- (26) Meade, E.; Smith, W.; DeWitt, D. Differential Inhibition of Prostaglandin Endoperoxide Synthase (Cyclooxygenase) Isozymes by Aspirin and Other Non-Steroidal Anti-Inflammatory Drugs. *J. Biol. Chem.* **1993**, *268*, 6610–6614.
- (27) Giménez-Bastida, J.; Boeglin, W.; Boutaud, O.; Malkowski, M.; Schneider, C. Residual Cyclooxygenase Activity of Aspirin-Acetylated COX-2 Forms 15R-Prostaglandins That Inhibit Platelet Aggregation. *FASEB J.* **2019**, *33*, 1033–1041.
- (28) Wennogle, L.; Liang, H.; Quintavalla, J.; Bowen, B.; Wasvary, J.; Miller, D.; Allentoff, A.; Boyer, W.; Kelly, M.; Marshall, P. Comparison of Recombinant Cyclooxygenase-2 to Native Isoforms: Aspirin Labeling of the Active Site. *FEBS Lett.* **1995**, *371*, 315–320.
- (29) Rowlinson, S.; Crews, B.; Goodwin, D.; Schneider, C.; Gierse, J.; Marnett, L. Spatial Requirements for 15-(R)-Hydroxy-5Z,8Z,11Z,13E-Eicosatetraenoic Acid Synthesis within the Cyclooxygenase Active Site of Murine COX-2. *J. Biol. Chem.* **2000**, *275*, 6586–6591.

- (30) Xiao, G.; Tsai, A.; Palmer, G.; Boyar, W.; Marshall, P.; Kulmacz, R. Analysis of Hydroperoxide-Induced Tyrosyl Radicals and Lipoxygenase Activity in Aspirin-Treated Human Prostaglandin H Synthase-2. *Biochemistry* **1997**, *36*, 1836–1845.
- (31) Schneider, C.; Brash, A. Stereospecificity of Hydrogen Abstraction in the Conversion of Arachidonic Acid to 15R-HETE by Aspirin-Treated Cyclooxygenase-2. *J. Biol. Chem.* **2000**, *275*, 4743–4746.
- (32) Kennedy, T.; Smith, C.; Marnett, L. Investigation of the Role of Cysteines in Catalysis by Prostaglandin Endoperoxide Synthase. *J. Biol. Chem.* **1994**, *269*, 27357–27364.
- (33) Gierse, J.; McDonald, J.; Hauser, S.; Rangwala, S.; Koboldt, C.; Seibert, K. A Single Amino Acid Difference between Cyclooxygenase-1 (COX-1) and -2 (COX-2) Reverses the Selectivity of COX-2 Specific Inhibitors. *J. Biol. Chem.* **1996**, *271*, 15810–15814.
- (34) Ong, C.; Lirk, P.; Tan, C.; Seymour, R. An Evidence-Based Update on Nonsteroidal Anti-Inflammatory Drugs. *Clin. Med. Res.* **2007**, *5*, 19–34.
- (35) Díaz-González, F.; Sánchez-Madrid, F. NSAIDs: Learning New Tricks from Old Drugs. *Eur. J. Immunol.* **2015**, *45*, 679–686.
- (36) Perrone, M.; Scilimati, A.; Simone, L.; Vitale, P. Selective COX-1 Inhibition: A Therapeutic Target to Be Reconsidered. *Curr. Med. Chem.* **2010**, *17*, 3769–3805.
- (37) Luong, C.; Miller, A.; Barnett, J.; Chow, J.; Ramesha, C.; Browner, M. Flexibility of the NSAID Binding Site in the Structure of Human Cyclooxygenase-2. *Nature* **1996**, *3*, 927–933.
- (38) Rimon, G.; Sidhu, R.; Lauver, A.; Lee, J.; Sharma, N.; Yuan, C.; Frieler, R.; Trievel, R.; Lucchesi, B.; Smith, W. Coxibs Interfere with the Action of Aspirin by Binding to One Monomer of Cyclooxygenase-1. *PNAS* **2010**, *107*, 28–33.
- (39) Wongrakpanich, S.; Wongrakpanich, A.; Melhado, K.; Rangaswami, J. A Comprehensive Review of Non-Steroidal Anti-Inflammatory Drug Use in The Elderly. *Aging Dis.* **2018**, *9*, 143–150.
- (40) Davis, A.; Robson, J. The Dangers of NSAIDs: Look Both Ways. *Br. J. Gen. Pract.* **2016**, *66*, 172–173.
- (41) Matsui, H.; Shimokawa, O.; Kaneko, T.; Nagano, Y.; Rai, K.; Hyodo, I. The Pathophysiology of Non-Steroidal Anti-Inflammatory Drug (NSAID)-Induced Mucosal Injuries in Stomach and Small Intestine. *J. Clin. Biochem. Nutr.* **2011**, *48*, 107–111.
- (42) Day, R.; Graham, G. Non-Steroidal Anti-Inflammatory Drugs (NSAIDs). *BMJ* **2013**, *346*, 3195.
- (43) Varga, Z.; Sabzwari, S.; Vargova, V. Cardiovascular Risk of Nonsteroidal Anti-Inflammatory Drugs: An Under-Recognized Public Health Issue. *Cureus* **2017**, *9*, 1144.
- (44) Zarghi, A.; Arfaei, S. Selective COX-2 Inhibitors: A Review of Their Structure-Activity Relationships. *Iran J. Pharm. Res.* **2011**, *10*, 655–683.
- (45) Murphy, K.; Weaver, C. Principles of Innate Immunity. In *Janeway's Immunobiology*; Garland Science, Taylor & Francis Group, LLC: New York, 2017; p 5.
- (46) Michiels, C. Endothelial Cell Functions. *J. Cell. Physiol.* **2003**, *196*, 430–443.
- (47) Murphy, K.; Weaver, C. Appendices III - IV. Cytokines, Chemokines and Their Receptors. In *Janeway's Immunobiology*; Garland Science, Taylor & Francis Group, LLC: New York, 2017; pp 811–815.

- (48) Murphy, K.; Weaver, C. Pattern Recognition by Cells of the Innate Immune System. In *Janeway's Immunobiology*; Garland Science, Taylor & Francis Group, LLC: New York, 2017; pp 85–86.
- (49) Funk, C. D. Prostaglandins and Leukotrienes: Advances in Eicosanoid Biology. *Science (1979)* **2001**, *294*, 1871–1875.
- (50) Sun, G.; Chuang, D.; Zong, Y.; Jiang, J.; Lee, J.; Gu, Z.; Simonyi, A. Role of Cytosolic Phospholipase A2 in Oxidative and Inflammatory Signaling Pathways in Different Cell Types in the Central Nervous System. *Mol. Neurobiol.* **2014**, *50*, 6–14.
- (51) Bittova, L.; Sumandea, M.; Cho, W. A Structure-Function Study of the C2 Domain of Cytosolic Phospholipase A2. Identification of Essential Calcium Ligands and Hydrophobic Membrane Binding Residues. *J. Biol. Chem.* **1999**, *274*, 9665–9672.
- (52) Schievella, A.; Regier, M.; Smith, W.; Lin, L. Calcium-Mediated Translocation of Cytosolic Phospholipase A2 to the Nuclear Envelope and Endoplasmic Reticulum. *J. Biol. Chem.* **1995**, *270*, 30749–30754.
- (53) Wang, D.; Wang, H.; Shi, Q.; Katkuri, S.; Walhi, W.; Desvergne, B.; Das, S. Dey, S.; DuBois, R. Prostaglandin E2 Promotes Colorectal Adenoma Growth via Transactivation of the Nuclear Peroxisome Proliferator-Activated Receptor δ . *Cancer Cell* **2004**, *6*, 285–295.
- (54) Ricciotti, E.; FitzGerald, G. Prostaglandins and Inflammation. *Arterioscler. Thromb. Vasc. Biol.* **2011**, *31*, 986–1000.
- (55) Dennis, E. A; Norris, P. C. Eicosanoid Storm in Infection and Inflammation. *Nat Rev Immunol* **2015**, *15*, 511–523.
- (56) Medzhitov, R. Origin and Physiological Roles of Inflammation. *Nature* **2008**, *454*, 428–435.
- (57) Harizi, H.; Corcuff, J. B.; Gualde, N. Arachidonic-Acid-Derived Eicosanoids: Roles in Biology and Immunopathology. *Trends Mol Med* **2008**, *14*, 461–469.
- (58) Robinson, P. Enzymes: Principles and Biotechnological Applications. *Essays Biochem.* **2015**, *59*, 1–41.
- (59) Corey, E.; Weinshenker, N.; Schaaf, T.; Huber, W. Stereo-Controlled Synthesis of D_L-Prostaglandins F₂α and E₂. *J. Am. Chem. Soc.* **1969**, *91*, 5675–5677.
- (60) Collins, J.; Hess, W.; Frank, F. Dipyrindine-Chromium(VI) Oxide Oxidation of Alcohols in Dichloromethane. *Tetrahedron Lett.* **1968**, *9*, 3363–3366.
- (61) Murray, C.; Yang, D.; Wulff, W. Cyclopropanation with Acyloxy Chromium Carbene Complexes. A Synthesis of (+-)-Prostaglandin E₂ Methyl Ester. *J. Am. Chem. Soc.* **1990**, *112*, 5660–5662.
- (62) Casey, C.; Brunsvold, W. Reaction of Metal-Carbene Complexes with Vinylolithium Reagents. *J. Organomet. Chem.* **1974**, *77*, 345–352.
- (63) Salaün, J.; Barnier, J. Spirovetivanes from Silylated 1-Hydroxycyclopropanecarboxaldehyde. *Tetrahedron Lett.* **1984**, *25*, 1273–1276.
- (64) Suzuki, M.; Yanagiasawa, A.; Noyori, R. Prostaglandin Synthesis. 16. The Three-Component Coupling Synthesis of Prostaglandins. *J. Am. Chem. Soc.* **1988**, *110*, 4718–4726.

- (65) Ono, N.; Kawanaka, Y.; Yoshida, Y.; Sato, F. Synthesis of a Key Intermediate for Preparation of 4,5-Didehydro Prostaglandins Containing an Allenyl Side-Chain Group via Two-Component Coupling Process. Synthesis of Enprostil. *J. Chem. Soc., Chem. Commun.* **1994**, 1251–1252.
- (66) Okamoto, S.; Kobayashi, Y.; Kato, H.; Hori, K.; Yakahashi, T.; Tsuji, J.; Sato, F. Prostaglandin Synthesis via Two-Component Coupling. Highly Efficient Synthesis of Chiral Prostaglandin Intermediates 4-Alkoxy-2-Alkyl-2-Cyclopenten-1-One and 4-Alkoxy-3-Alkenyl-2-Methylenecyclopentan-1-One. *J. Org. Chem.* **1988**, *53*, 5590–5592.
- (67) Michelot, D.; Linstrumelle, G. Cuprates Alleniques I : Preparations et Reactions. Synthese Stereoselective de La Pheromone de La Bruche Parasite Du Haricot. *Tetrahedron Lett.* **1976**, *17*, 275–276.
- (68) Fürstner, A.; Davies, P. Alkyne Metathesis. *Chem. Commun.* **2005**, 2307–2320.
- (69) Fürstner, A.; Mathes, C.; Lehmann, C. Mo[N(t-Bu)(Ar)]₃ Complexes As Catalyst Precursors: In Situ Activation and Application to Metathesis Reactions of Alkynes and Diynes. *J. Am. Chem. Soc.* **1999**, *121*, 9453–9454.
- (70) Fürstner, A.; Grela, K.; Mathes, C.; Lehmann, C. Novel and Flexible Entries into Prostaglandins and Analogues Based on Ring Closing Alkyne Metathesis or Alkyne Cross Metathesis. *J. Am. Chem. Soc.* **2000**, *122*, 11799–11805.
- (71) Cimino, G.; Crispino, A.; Marzo, D.; Sodano, G.; Spinella, A.; Villani, G. A Marine Mollusc Provides the First Example of in Vivo Storage of Prostaglandins: Prostaglandin-1,15-Lactones. *Experientia* **1991**, *47*, 56–60.
- (72) Zanoni, G.; Porta, A.; Toma, Q.; Castronovo, F.; Vidari, G. First Enantioselective Total Synthesis of (8S,12R,15S)-Prostaglandin J₂. *J. Org. Chem.* **2003**, *68*, 6437–6439.
- (73) Yankee, E.; Axen, U.; Bundy, G. Total Synthesis of 15-Methylprostaglandins. *J. Am. Chem. Soc.* **1974**, *96*, 5865–5876.
- (74) Noyori, R.; Tomino, I.; Tanimoto, Y.; Nishizawa, M. Asymmetric Synthesis via Axially Dissymmetric Molecules. 6. Rational Designing of Efficient Chiral Reducing Agents. Highly Enantioselective Reduction of Aromatic Ketones by Binaphthol-Modified Lithium Aluminum Hydride Reagents. *J. Am. Chem. Soc.* **1984**, *106*, 6709–6716.
- (75) Dow, R.; Kelly, R.; Schletter, I.; Wierenga, W. A Direct Alcohol for Hydrazine Interchange: Scope and Stereochemistry. *Synth. Commun.* **1981**, *11*, 43–53.
- (76) Dess, D.; Martin, J. A Useful 12-I-5 Triacetoxyperiodinane (the Dess-Martin Periodinane) for the Selective Oxidation of Primary or Secondary Alcohols and a Variety of Related 12-I-5 Species. *J. Am. Chem. Soc.* **1991**, *113*, 7277–7287.
- (77) VanderRoest, J.; Grieco, P. Studies Relating to the Structure of Bruceoside C: Total Synthesis of the Alleged Aglycon of Bruceoside C. *J. Org. Chem.* **1996**, *61*, 5316–5325.
- (78) Brummond, K.; Sill, P.; Chen, H. The First Total Synthesis of 15-Deoxy- Δ ^{12,14}-Prostaglandin J₂ and the Unambiguous Assignment of the C₁₄ Stereochemistry. *Org. Lett.* **2004**, *6*, 149–152.
- (79) Enomoto, M.; Katsuki, T.; Yamaguchi, M. Highly Regioselective Isomerization of Acetylenes to Allenes. *Tetrahedron Lett.* **1986**, *27*, 4599–4600.

- (80) Kent, J.; Wan, H.; Brummond, K. A New Allenic Pauson-Khand Cycloaddition for the Preparation of α -Methylene Cyclopentenones. *Tetrahedron Lett.* **1995**, *36*, 2407–2410.
- (81) Jones, G.; Landais, Y. The Oxidation of the Carbon-Silicon Bond. *Tetrahedron* **1996**, *52*, 7599–7662.
- (82) Touré, B.; Hall, D. Natural Product Synthesis Using Multicomponent Reaction Strategies. *Chem. Rev.* **2009**, *109*, 4439–4486.
- (83) Boer, R.; Gimenez-Bastida, J. A.; Boutaud, O.; Jana, S.; Schneider, C.; Sulikowski, G. A. Total Synthesis and Biological Activity of the Arachidonic Acid Metabolite Hemiketal E2. *Org. Lett.* **2018**, *20*, 4020–4022.
- (84) Furrow, M.; Schaus, S.; Jacobsen, E. Practical Access to Highly Enantioenriched C-3 Building Blocks via Hydrolytic Kinetic Resolution. *J. Org. Chem.* **1998**, *63*, 6776–6777.
- (85) Trygstad, T.; Pang, Y.; Forsyth, C. Versatile Synthesis of the C3–C14 Domain of 7-Deoxyokadaic Acid. *J. Org. Chem.* **2009**, *74*, 910–913.
- (86) Alcaide, B.; Almendros, P.; Alonso, J. Gold Catalyzed Oxycyclizations of Alkynols and Alkyndiols. *Org. Biomol. Chem.* **2011**, *9*, 4405–4416.
- (87) Harkat, H.; Weibel, J.; Pale, P. Synthesis of Functionalized THF and THP through Au-Catalyzed Cyclization of Acetylenic Alcohols. *Tetrahedron Lett.* **2007**, *48*, 1439–1442.
- (88) Li, J.; Stoltz, B.; Grubbs, R. Enantioselective Synthesis of 15-Deoxy- Δ 12,14-Prostaglandin J2. *Org. Lett.* **2019**, *21*, 10139–10142.
- (89) Grieco, P.; Abood, N. Cycloalkenone Synthesis via Lewis Acid-Catalyzed Retro Diels-Alder Reactions of Norbornene Derivatives: Synthesis of 12-Oxophytodienoic Acid (12-OxoPDA). *J. Org. Chem.* **1989**, *54*, 6008–6010.
- (90) Li, J.; Ahmed, T.; Xu, C.; Stoltz, B.; Grubbs, R. Concise Syntheses of Δ 12-Prostaglandin J Natural Products via Stereoretentive Metathesis. *J. Am. Chem. Soc.* **2019**, *141*, 154–158.
- (91) Pale, P.; Chucho, J. Silver Assisted Heterocyclization of Acetylenic Compounds. *Tetrahedron Lett.* **1987**, *28*, 6447–6448.
- (92) Kimbrough, J.; Austin, Z.; Milne, G.; Sulikowski, G. Synthesis of a Human Urinary Metabolite of Prostaglandin D2. *Org. Lett.* **2019**, *21*, 10048–10051.
- (93) Trost, B.; VanVranken, D. Asymmetric Transition Metal-Catalyzed Allylic Alkylations. *Chem. Rev.* **1996**, *96*, 395–422.
- (94) Danheiser, R.; Dixon, B.; Gleason, R. Five-Membered Ring Annulation via Propargyl- and Allylsilanes. *J. Org. Chem.* **1992**, *57*, 6094–6097.
- (95) Suárez, A.; Fu, G. A Straightforward and Mild Synthesis of Functionalized 3-Alkynoates. *Angew. Chem. Int. Ed.* **2004**, *43*, 3580–3582.
- (96) Jahn, U.; Galano, J.; Durand, T. Beyond Prostaglandins—Chemistry and Biology of Cyclic Oxygenated Metabolites Formed by Free-Radical Pathways from Polyunsaturated Fatty Acids. *Angew. Chem. Int. Ed.* **2008**, *47*, 5894–5955.

- (97) Montuschi, P.; Corradi, M.; Ciabattini, G.; Nightingale, J.; Kharitonov, S. A.; Barnes, P. Increased 8-Isoprostane, a Marker of Oxidative Stress, in Exhaled Condensate of Asthma Patients. *J. Am. J. Respir. Crit. Care Med* **1999**, *160*, 216–220.
- (98) Oger, C.; Cuyamendous, C.; de la Torre, A.; Candy, M.; Guy, A.; Bultel-Poncé, V.; Durand, T.; Galano, J. History of Chemical Routes towards Cyclic Non-Enzymatic Oxygenated Metabolites of Polyunsaturated Fatty Acids. *Synthesis (Stuttg)* **2018**, *50*, 3257–3280.
- (99) Newcomer, M.; Brash, A. The Structural Basis for Specificity in Lipoxygenase Catalysis. *Protein Science* **2015**, *24*, 298–309.
- (100) Rådmark, O.; Werz, O.; Steinhilber, D.; Samuelsson, B. 5-Lipoxygenase, a Key Enzyme for Leukotriene Biosynthesis in Health and Disease. *Biochim Biophys Acta* **2015**, *1851*, 331–339.
- (101) Gaffney, B. EPR Spectroscopic Studies of Lipoxygenases. *Chem. Asian J.* **2020**, *15*, 42–50.
- (102) Rådmark, O. Arachidonate 5-Lipoxygenase. *Prostaglandins Other Lipid Mediat* **2002**, *68–69*, 211–234.
- (103) Crooks, S.; Stockley, R. Leukotriene B₄. *Int. J. Biochem. Cell Biol.* **1998**, *30*, 173–178.
- (104) Nicolaou, K.; Ramphal, J.; Petasis, N.; Serhan, C. Lipoxins and Related Eicosanoids: Biosynthesis, Biological Properties, and Chemical Synthesis. *Angew. Chem. Int. Ed. Engl.* **1991**, *30*, 1100–1116.
- (105) Schneider, C.; Boeglin, W.; Yin, H.; Stec, D.; Voehler, M. Convergent Oxygenation of Arachidonic Acid by 5-Lipoxygenase and Cyclooxygenase-2. *J. Am. Chem. Soc.* **2006**, *128*, 720–721.
- (106) Nakashima, F.; Suzuki, T.; Gordon, O.; Golding, D.; Okuno, T.; Giménez-Bastida, J.; Yokomizo, T.; Schneider, C. Biosynthetic Crossover of 5-Lipoxygenase and Cyclooxygenase-2 Yields 5-Hydroxy-PGE₂ and 5-Hydroxy-PGD₂. *J. Am. Chem. Soc. Au* **2021**, *1*, 1380–1388.
- (107) Griesser, M.; Suzuki, T.; Hernandez, N.; Mont, S.; Boeglin, W. E.; Pozzi, A.; Schneider, C. Biosynthesis of Hemiketal Eicosanoids by Cross-over of the 5-Lipoxygenase and Cyclooxygenase-2 Pathways. *PNAS. USA.* **2011**, *108*, 6945–6950.
- (108) Giménez-Bastida, J. A.; Shibata, T.; Uchida, K.; Schneider, C. Roles of 5-Lipoxygenase and Cyclooxygenase-2 in the Biosynthesis of Hemiketals E₂ and D₂ by Activated Human Leukocytes. *FASEB J.* **2017**, *31*, 1867–1878.
- (109) Giménez-Bastida, J.; Suzuki, T.; Sprinkel, K.; Boeglin, W. Biomimetic Synthesis of Hemiketal Eicosanoids for Biological Testing. *Prostaglandins Other Lipid Mediat* **2017**, *132*, 41–46.

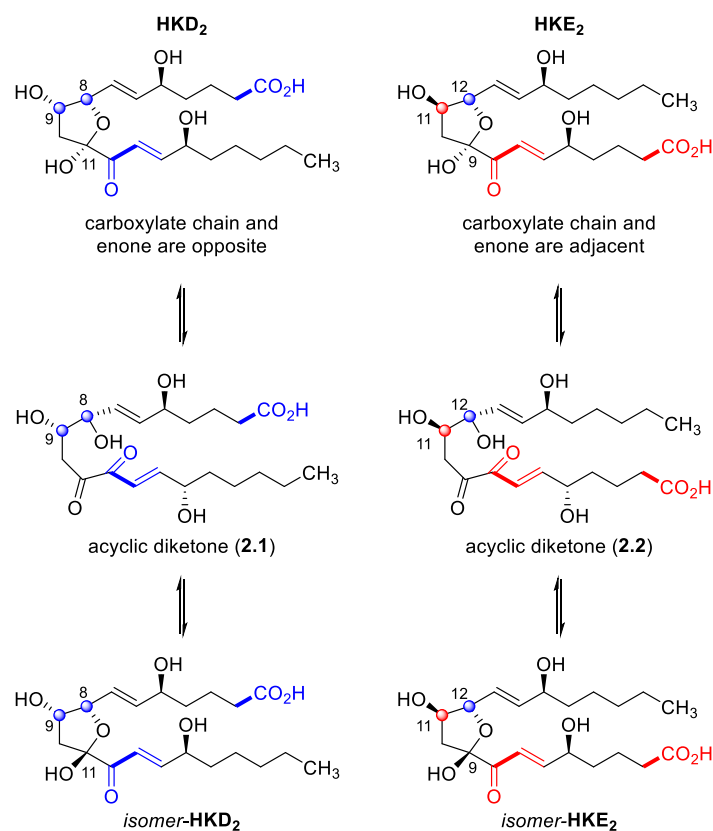
PROGRESS TOWARDS A SECOND-GENERATION SYNTHESIS OF HEMIKETAL E₂Structural Features of HKD₂ and HKE₂

A highly convergent and flexible synthetic route is desirable to access hemiketals D₂ and E₂ for biological study. HKD₂ and HKE₂ have four subtle structural differences. The first distinction to note is the relative stereochemistry of the vicinal stereocenters. In HKD₂, the relative stereochemistry has a *cis* relationship along the C8-C9 bond; whereas, in HKE₂, the vicinal stereocenters at C11-C12 are *trans*. (**Scheme 2.1**).

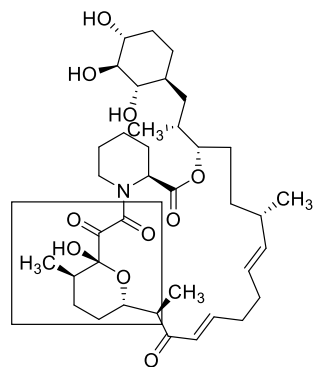
Second, the relative orientation of each side chain differs. Notice that in HKD₂, the carboxylate chain and the enone are on opposite sides (key functional groups highlighted in blue); whereas, in HKE₂ the carboxylate chain and enone are adjacent (key functional groups highlighted in red). It should be noted that the carboxylate chain is designated as

the alpha side chain in the literature, and the hydrocarbon chain is referred to as the omega side chain. Work regarding the syntheses of these side chains can be found in both Dr. Robert Boer and Dr. Alex Allweil's theses.^{1,2} Thirdly, both HKD₂ and HKE₂ are in tautomeric equilibrium. Unpublished results by Schneider demonstrated the isomeric ratios are dependent on different NMR solvents. Because of this phenomenon, for simplicity, no stereocenters will be indicated at C11 in HKD₂ or C9 for HKE₂ for the remainder of the discussion.

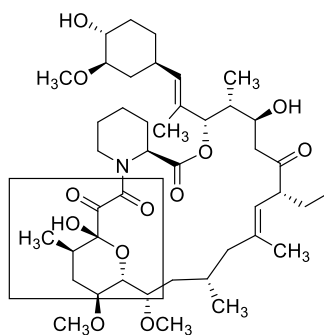
Lastly, probably the most striking feature of these compounds is the keto-hemiketal moiety. For the reader to truly appreciate this structural arrangement of atoms, one must realize the rarity of these functional groups in nature. Antascomycin B (**2.3**),³ FK-506 (**2.4**),⁴ Meridamycin (**2.5**),⁵ Polycavernoside A (**2.6**), Polycavernoside B (**2.7**),^{6,7,8} and Rapamycin (**2.8**)⁹ are the only known natural products to contain keto-hemiketal moieties that are reported in the literature (**Figure 2.1**). Due to the scarcity of these compounds, the Sulikowski laboratory found these hemiketals to be intriguing targets to synthesize.



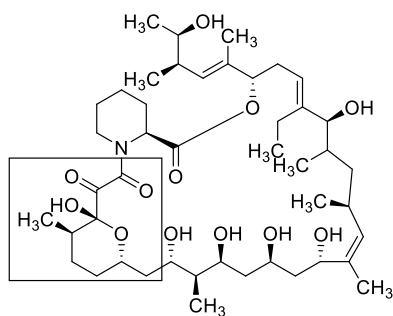
Scheme 2.1. Structural Characteristics of HKD₂ and HKE₂.



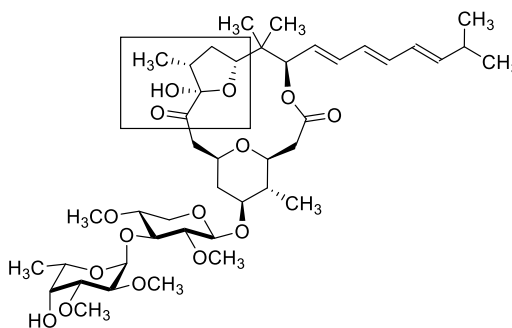
Antascomicin B (2.3)



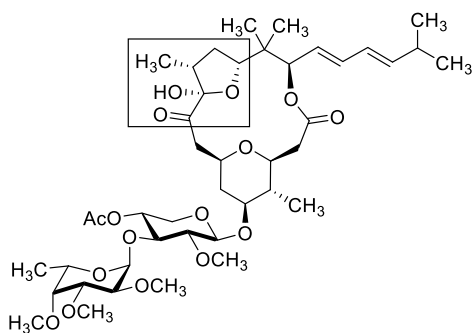
FK-506 (2.4)



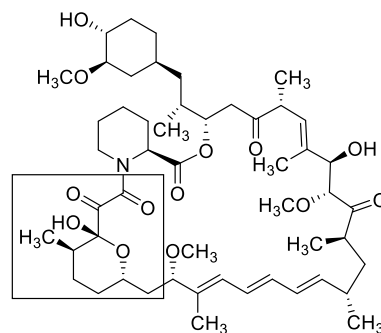
Meridamycin (2.5)



Polycavernoside A (2.6)



Polycavernoside B (2.7)



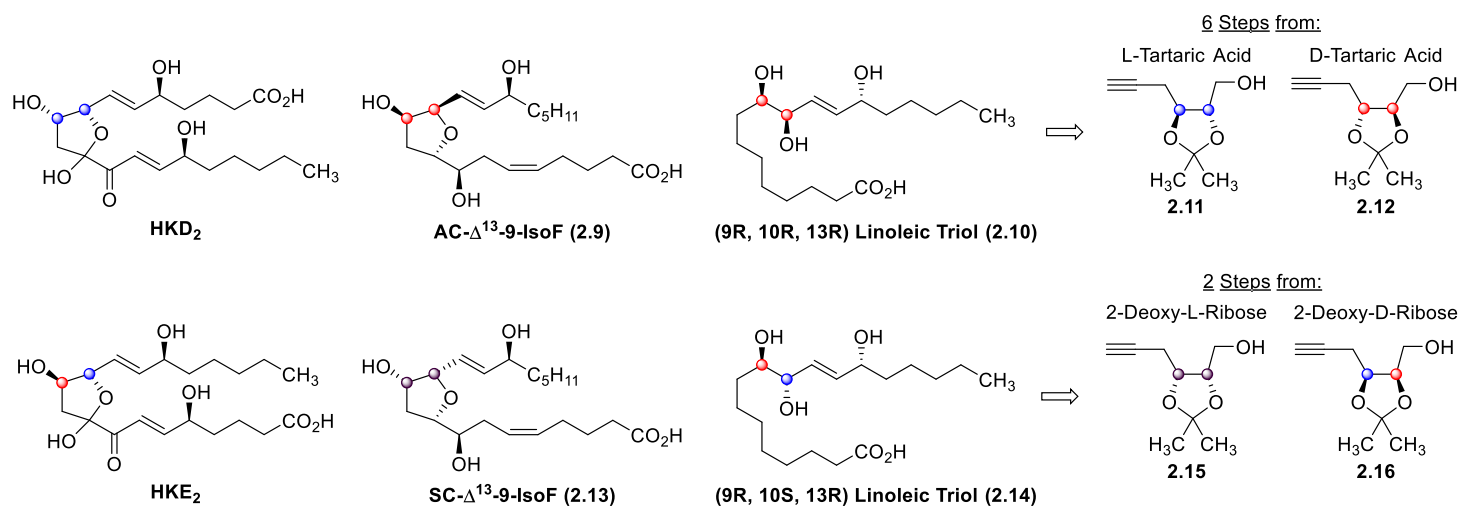
Rapamycin (2.8)

Figure 2.1. Natural Products Containing Keto-hemiketal Groups.

First Generation Synthesis of HKE₂

Sulikowski and coworkers successfully synthesized HKE₂ in 2018, as highlighted in Chapter 1.¹⁰ As with any synthesis, however, there were places to improve the synthetic route. First and foremost, the key gold-mediated cyclization to establish the hemiketal framework was not consistently reproducible and could not be scaled above 50 mg. Secondly, the furan intermediate **1.104** (**Scheme 1.9**) proved unstable with a half-life of only 12 h. Finally, the route proved to be unamenable to HKD₂. Further details regarding why HKD₂ was unsuccessful with this route can be found in Dr. Robert Boer's thesis.¹

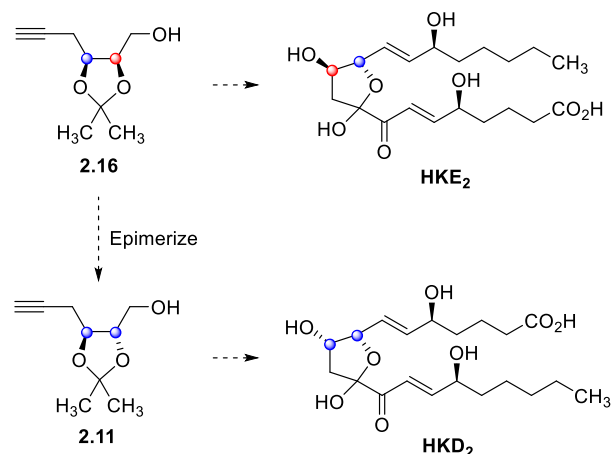
With this unfortunate realization that this method could not be extended to the other hemiketal, a new synthetic route was required to access both hemiketals. Stemming from the need to develop syntheses from common building blocks, the Sulikowski lab actively seeks to use a divergent method to create the hemiketals, isofurans, and linoleic triols all from tartaric acid or ribose sugars (**Scheme 2.2**). For further details regarding the syntheses of hemiketals, the reader should seek Dr. Alex Allweil's thesis dissertation.² Other work relating to isofurans can be found in the thesis dissertations of Dr. Zachary Austin¹¹ and Dr. Calvin Larson.¹² And finally, research highlighting the linoleic triols can be found in Dr. Robert Davis' thesis.¹³ The next sections will relay subsequent, modified routes towards HKD₂ and HKE₂.



Scheme 2.2. The Sulikowski Lab's Divergent Synthetic Strategy.

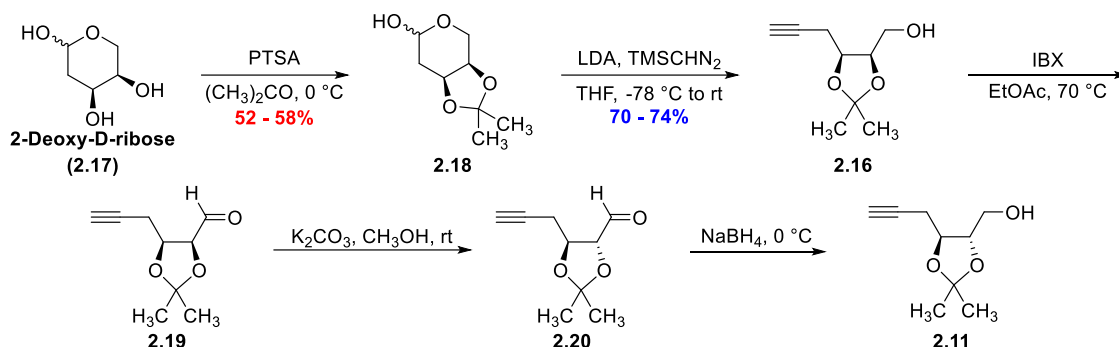
Initial Efforts

The first, modified route towards HKD₂ and HKE₂ employed an epimerization strategy. As shown from **Scheme 2.3**, the vision of this strategy ultimately involved transforming alkynol **2.16** to **2.11** via an epimerization. If successful, this divergent method would allow access to both hemiketals. The details to synthesize intermediates **2.16** and **2.11** are in **Scheme 2.4**. It begins with an acetonide protection of 2-Deoxy-D-ribose, followed by a Colvin rearrangement to obtain alkynol **2.16**. Hereafter, oxidation-epimerization (2 step) or oxidation-epimerization-reduction (3 step) sequences



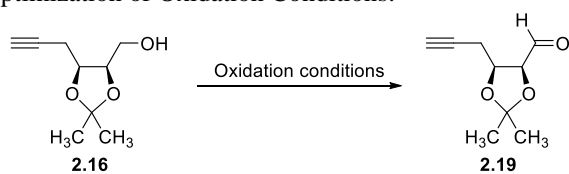
Scheme 2.3. Epimerization Strategy.

were attempted. Unfortunately, this route's oxidation and epimerization steps required significant optimization efforts.



Scheme 2.4. First Route towards HKD₂ and HKE₂.

The first difficulty met was the oxidation to the aldehyde, so a screen of oxidants was conducted to achieve the desired aldehyde in the highest, obtainable yield (**Table 2.1**). Among the oxidation procedures attempted were the classic Swern oxidation (Entry 1),^{14,15,16} Parikh von Doering (Entries 2 – 6),¹⁷ IBX (Entry 7),¹⁸ PCC (Entry 8),¹⁹ DMP (Entry 9),²⁰ and TEMPO (Entries 10 – 11).²¹ This screen revealed that IBX produced the highest yield of aldehyde **2.19**. The second challenge, as illustrated by **Table 2.1**, was that many attempts simply lead to decomposition. Storage of aldehyde **2.19** in benzene at -20 °C was required; otherwise, it would decompose overnight. Because of the propensity of the aldehyde to decompose, once the IBX oxidation was established, aldehyde **2.19** was immediately subjected to epimerization conditions. For this reason, yields in **Table 2.2** are reported either over two or three steps depending on if there was an additional reduction step. After investigating a variety of epimerization procedures,^{22,23} treatment with K₂CO₃ in MeOH provided the most promising results in accordance with the literature.^{24,25}

Table 2.1. Optimization of Oxidation Conditions.

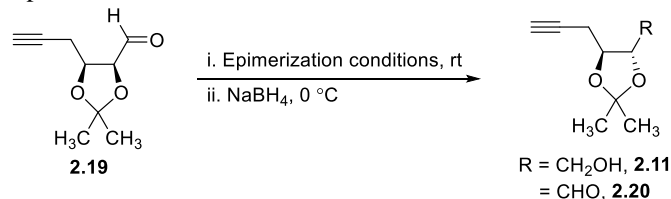
Entry	Oxidation Conditions	Decomposition ^a
1	i. (COCl) ₂ (1.5 eq), CH ₂ Cl ₂ , -78 °C ii. DMSO (2.1 eq), -78 °C, 30 min iii. alkynol (1.0 eq), CH ₂ Cl ₂ , -78 °C, 30 min iv. NEt ₃ (5.0 eq), CH ₂ Cl ₂ , -78 °C for 15 min → 0 °C for 15 min → rt for 45 min	no
2	i. alkynol (1.0 eq), CH ₂ Cl ₂ , 0 °C ii. DMSO (5.0 eq), 0 °C iii. NEt ₃ (4.0 eq), 0 °C iv. SO ₃ • Py (4.0 eq), 0 °C → rt, 2h	yes
3	i. alkynol (1.0 eq), DMSO ii. NEt ₃ (4.0 eq) iii. SO ₃ • Py (2.0 eq), 0 °C, 3.5h	yes
4	i. alkynol (1.0 eq), DMSO-CH ₂ Cl ₂ , 0 °C ii. NEt ₃ (4.0 eq), 0 °C iii. SO ₃ • Py (4.0 eq), 0 °C for 3.5h → rt for 8h	yes
5	i. alkynol (1.0 eq), CH ₂ Cl ₂ , 0 °C ii. DMSO (5.0 eq), 0 °C iii. NEt ₃ (4.0 eq), 0 °C iv. SO ₃ • Py (4.0 eq), 0 °C, 2.5h	yes
6	i. alkynol (1.0 eq), CH ₂ Cl ₂ , 0 °C ii. SO ₃ • Py (5.0 eq), 0 °C iii. NEt ₃ (5.0 eq), 0 °C iv. DMSO, 0 °C, 1h	yes
7	IBX (3.0 eq), EtOAc, 70 °C, 7h	no
8	i. alkynol (1.0 eq), CH ₂ Cl ₂ ii. NaOAc, 0 °C iii. MgSO ₄ , PCC (5.0 eq), 0 °C → rt 8h	no
9	i. DMP (1.5 eq), CH ₂ Cl ₂ , 0 °C 5 min ii. NaHCO ₃ , 0 °C, → rt for 3h	no
10	TEMPO, KBr, aq. NaOCl, pH 9 CH ₂ Cl ₂ , -10 °C, 6h	no rxn
11	TEMPO, KBr, aq. NaOCl, pH 9 CH ₂ Cl ₂ , -10 °C, 24h	no rxn

^a The reaction conditions that were established which did not decompose were immediately carried forward to test epimerization conditions due to the instability of the aldehyde.

Initially, the mixtures of the *trans* and *cis* aldehydes (**2.19** and **2.20**) were separated and purified on NEt₃-buffered silica. However, decomposition was still an issue. To obtain more accurate yields without the threat of decomposition, the aldehydes were reduced with NaBH₄ to the more stable primary alcohols. At first glance, the results of **Table 2.2** appear quite baffling as (Entries 1-3) reveal a preference for the *cis* aldehyde starting material; (Entry 4) shows evidence for the preference of the *trans* aldehyde, while (Entry 5) demonstrates a 1:1 *trans*:*cis* ratio of alcohols. The best postulated hypothesis to explain these results in **Table 2.2** is that the obtained ratios of

trans to *cis* aldehydes or alcohols depends on the state of where the equilibrium lies when the reaction is quenched. Surprisingly, the *cis* aldehyde never fully converts to the *trans* aldehyde. An equilibrium of the diastereomeric aldehydes is obtained, but only during the time the aldehydes remained stable. Unfortunately, there is a time limit. Within two to four hours of the epimerization, the aldehydes begin decomposing depending on the reaction conditions. Longer reaction times did not increase conversion and cooler temperatures would slow the rate of epimerization. We eventually abandoned this route for another as these results were quite bleak, because without full epimerization to the *trans* aldehyde, HKD₂ could never come within our grasp.

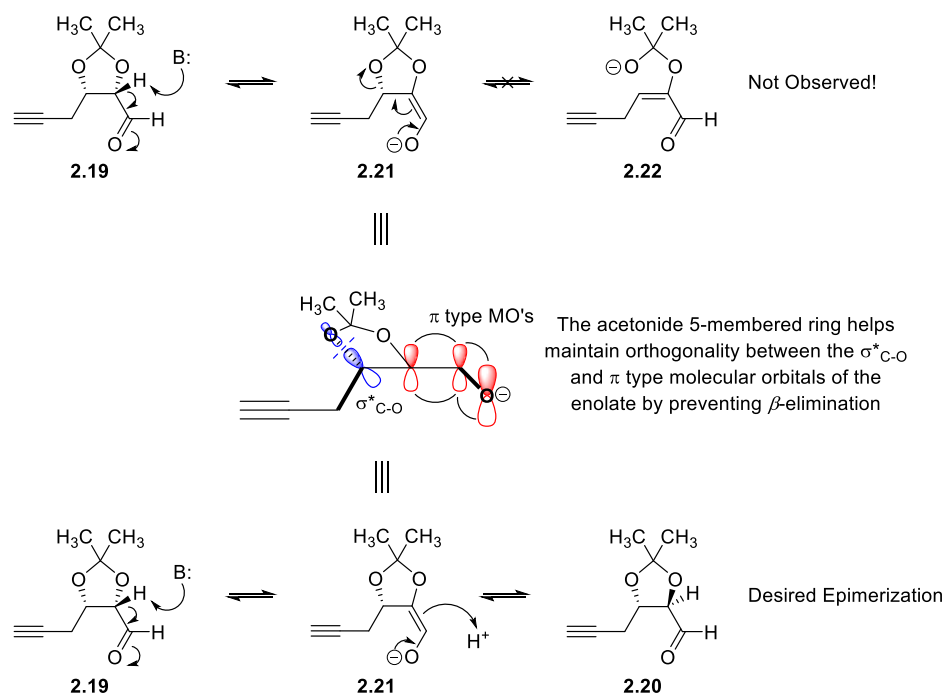
Table 2.2. Epimerization Conditions.



Entry	Epimerization Conditions	NaBH ₄	Results
1	K ₂ CO ₃ (1.0 eq), CH ₃ OH, 4h	no	61% 1:4 <i>trans</i> : <i>cis</i> aldehyde
2	K ₂ CO ₃ (1.0 eq), EtOH, 4 h	no	69%, 1:15 <i>trans</i> : <i>cis</i> aldehyde
3	K ₂ CO ₃ (3.4 eq), CH ₃ OH, 2 h	no	79%, <i>cis</i> aldehyde only
4	K ₂ CO ₃ (3.4 eq), CH ₃ OH, 2.5 h	yes	42%, 5:1 <i>trans</i> : <i>cis</i> alcohols
5	K ₂ CO ₃ (3.4 eq), CH ₃ OH, 3.5 h	yes	28%, 1:1 <i>trans</i> : <i>cis</i> alcohols
6	K ₂ CO ₃ (3.4 eq), CH ₃ OH, 23 h	no	Decomposition
7	NEt ₃ (3.0 eq), CH ₃ OH, 7.5 h	no	Decomposition
8	NEt ₃ (5.0 eq), CH ₃ OH, overnight	yes	Decomposition
9	DBU (1.1 eq), THF, 2 h	yes	Decomposition
10	DBU (3.0 eq), Toluene, overnight	no	Decomposition

Why β -Elimination is not Observed in the Epimerizations

While these epimerizations were not successful, mechanistic understanding of why certain products were not observed is important and interesting to consider (**Scheme 2.5**). In 1990, Masamune and Sharpless published a manuscript on the total synthesis of L-hexoses, explaining why β -elimination products are not observed in a substrate similar to alkyne **2.19**.^{26,27} Analogously, **Scheme 2.5** explains why β -elimination product **2.22** was never observed in these studies. One may recall that in order for an elimination to occur, the orbitals must have a syn periplanar alignment. Because the acetonide helps maintain orthogonality between the enolate and the β -alkoxy substituent, this prevents β -elimination, theoretically allowing the desired epimerization to occur. While the epimerization optimizations were explored, conditions to introduce the alpha side chain were being optimized concomitantly. It was envisioned that if the aldehyde epimerizations proved successful, the subsequent Horner-Wadsworth-Emmons reaction with the necessary phosphonate side chain would need to be established. Thus, the next section discusses paralleled optimization efforts towards the synthesis of the necessary phosphonate side chain.

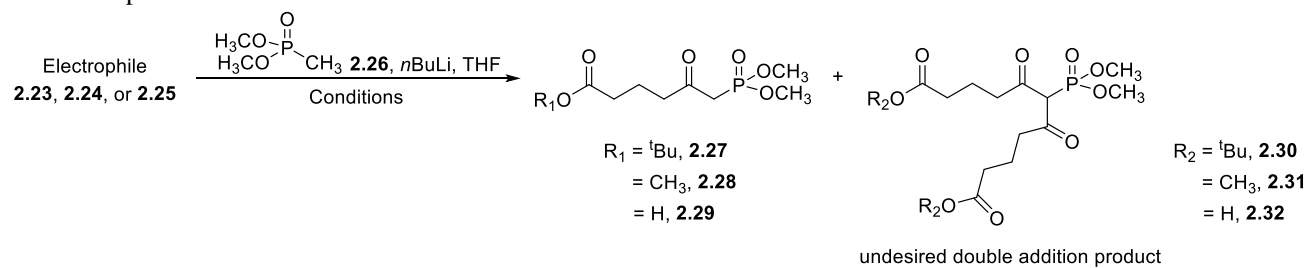


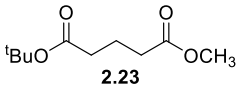
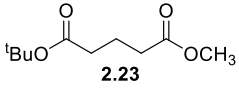
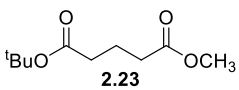
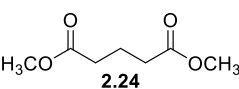
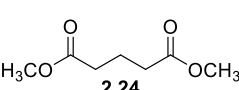
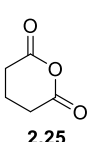
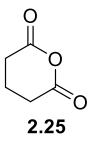
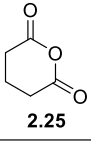
Scheme 2.5. Orthogonality prevents β -Elimination.

Synthesis of Phosphonate Ester for Horner-Wadsworth-Emmons Reaction

To access a phosphonate for a Horner-Wadsworth-Emmons reaction, traditionally, an ester, dimethyl methyl phosphonate (DMMP), and *n*BuLi are used in THF in a Claisen-like reaction.²⁸ Initially, the conditions to access the phosphonate were unsuccessful due to the undesired double-addition products observed (**Table 2.3**). The result of this undesired product is because the desired product is more acidic than the starting material. Fortunately, the double addition problem was resolved after optimizing the solvent use, ester preparation, reaction temperature, and starting electrophile. The first electrophiles attempted were diester **2.23** and dimethyl glutarate **2.24**. Unfortunately, as can be seen (Entries 1-5), minimal product (**2.27**, **2.28**) and/or the presence of double addition side products (**2.30**, **2.31**) were observed. It was found that co-evaporating the dimethyl methyl phosphonate with benzene resulted in lower yields (Entries 1-2). Therefore, an alternate purification technique was utilized. Freshly distilling dimethyl methyl phosphonate before each use was found to improve the yields, albeit the resulting products were still mixtures of the desired and undesired product. Allowing the reaction to stay at cooler temperatures longer was also necessary as shown in Entry 6. Slowly allowing the reaction to warm to temperature rather than immediately taking the reaction out of the -78 °C bath was paramount. Additionally, dilution of the electrophile in THF prevented the undesired double addition product. Most importantly, switching the electrophile to glutaric anhydride **2.25** removed the presence of undesired product **2.32** (Entries 7-8).²⁹ The benefit of using glutaric anhydride **2.25** over the previous two electrophiles allows for the possibility of late-stage esterifications of any variety in case of deprotection problems near the end of the synthesis. Fischer esterification of phosphonate **2.29** with TFA in methanol provided a >95% yield. With the phosphonate ester successfully in hand, mild, Masamune–Roush conditions were attempted,^{30,31} but unfortunately, a complex mixture of products was obtained, so the next ambitious approach was sought.

Table 2.3. Optimization of Claisen-like Condensation.



Entry	Electrophile (1.0 eq)	Electrophile in THF or neat?	Conditions	Results
1	 2.23	THF	DMMP ^a (2.1 eq), <i>n</i> BuLi (2.1 eq) -78 to rt, 1 h 40 min	26 % mixture ^d
2	 2.23	THF	DMMP ^b (2.4 eq), <i>n</i> BuLi (2.4 eq) -78 to rt, overnight	<1 % product
3	 2.23	neat	DMMP ^c (4 eq), <i>n</i> BuLi (4 eq) -78 to rt, 3.5 h	71 % mixture ^d
4	 2.24	neat	DMMP ^c (4 eq), <i>n</i> BuLi (4 eq) -78 to rt, 3.5 h	76 % mixture ^d
5	 2.24	neat	DMMP ^c (4 eq), <i>n</i> BuLi (4 eq) -78 to rt, 4 h	54 % mixture ^d
6	 2.25	THF	DMMP ^c (2 eq), <i>n</i> BuLi (2 eq) 30 min at -78 then rt 3.5 h	8 % product
7	 2.25	THF	DMMP ^c (2 eq), <i>n</i> BuLi (2 eq) -78 to rt, 2 h 40 min	41 % product
8	 2.25	THF	DMMP ^c (2 eq), <i>n</i> BuLi (2 eq) -78 to rt, 3 h	66 % product

^a dried from benzene three times

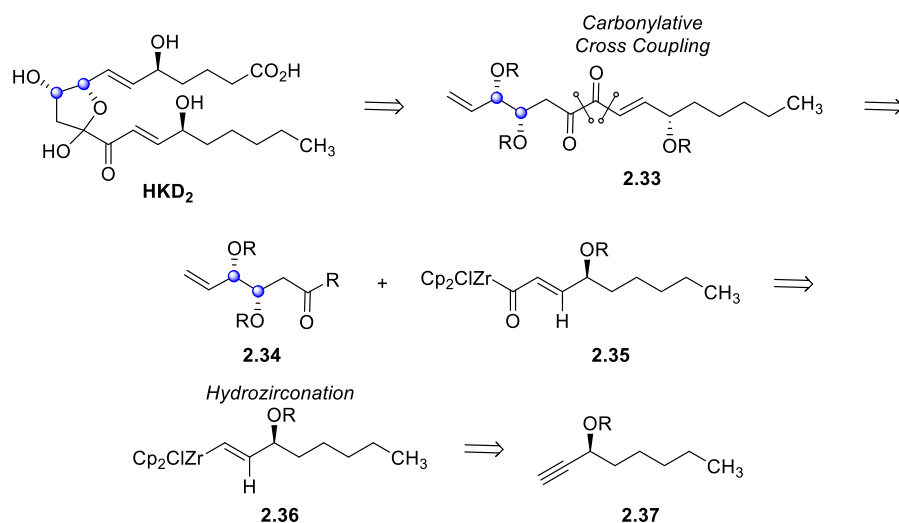
^b dried from benzene three times and vacuum oven dried overnight

^c freshly distilled

^d mixture of phosphonate ester and undesired double addition product

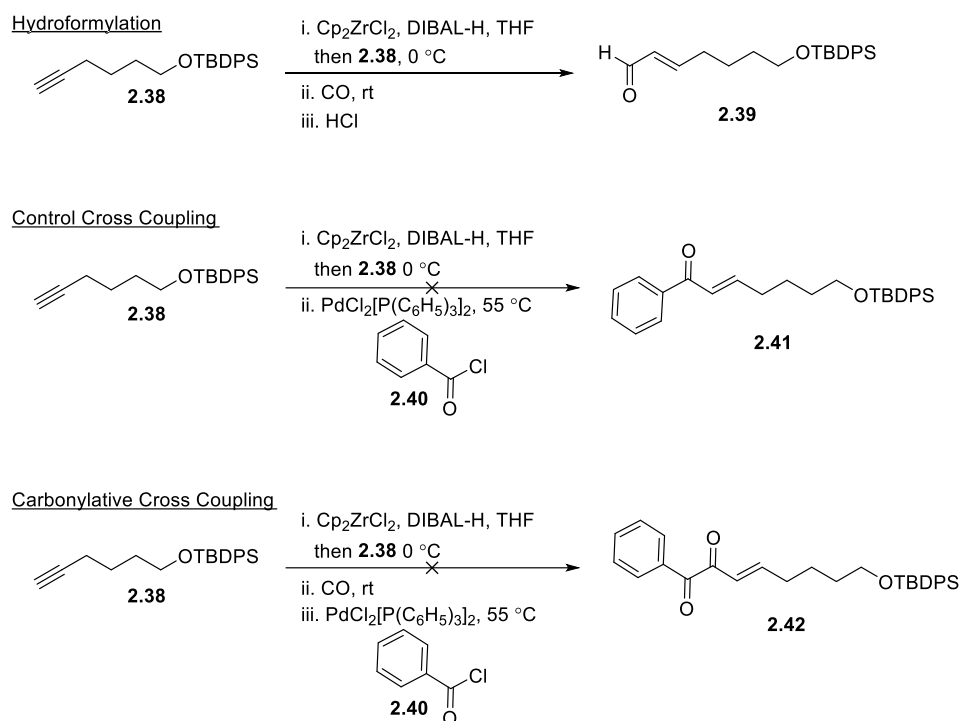
Carbonylative Cross Couplings

The goal behind the next approach involved a high-risk, high-reward carbonylative cross coupling between carbonyl **2.34** and acylzirconocene chloride **2.35** (**Scheme 2.6**). A carbonylative cross coupling is risky because the success depends on overcoming a high energy barrier. It was envisioned that the formation of acylzirconocene chloride **2.35** would precede through a hydrozirconation of alkyne **2.37**. A facile procedure exists to synthesize Schwartz reagent (HZrCp₂Cl) *in situ* with DIBAL-H.³² In the presence of terminal alkynes, Schwartz reagent preferentially performs syn-addition, installing the zirconocene substituent to the less hindered position of the alkyne. One advantage of using acylzirconocene chloride is its ability to act as an acyl anion equivalent. Literature precedence exists for the reaction of acylzirconocene chlorides with α,β -unsaturated ketones,³³ organic halides,³⁴ and imines³⁵ in the presence of palladium catalysts or Lewis acids. Additionally, a variety of palladium-mediated carbonylative couplings have been explored.³⁶ In 2016, the Ready group performed a zirconium-mediated carbonylative cross coupling with aryl Grignard reagents.³⁷ Other groups have also performed transmetalations with zirconocene reagents in various total syntheses.^{38,39,40} Taking advantage of the literature precedence for acylzirconocenes and aryl chlorides as potential coupling partners, a model system was developed to determine if this route could be viable to access HKD₂.



In the chosen model system, Schwartz reagent was added across TBDPS-protected hexynol **2.38** (**Scheme 2.7**). After the successful hydrozirconation, carbon monoxide was bubbled into the solution. To test if the resulting carbonyl was installed, the reaction was quenched with 1M HCl to obtain the corresponding aldehyde **2.39**, based on precedence from the Ready group.³⁷ While full conversion to aldehyde **2.39** was confirmed by crude NMR analysis, this compound was not isolated as the hydroformylation was only a means to determine if the carbonyl installation was successful. The installation proved difficult and inconsistent; furthermore, aldehyde **2.39**,

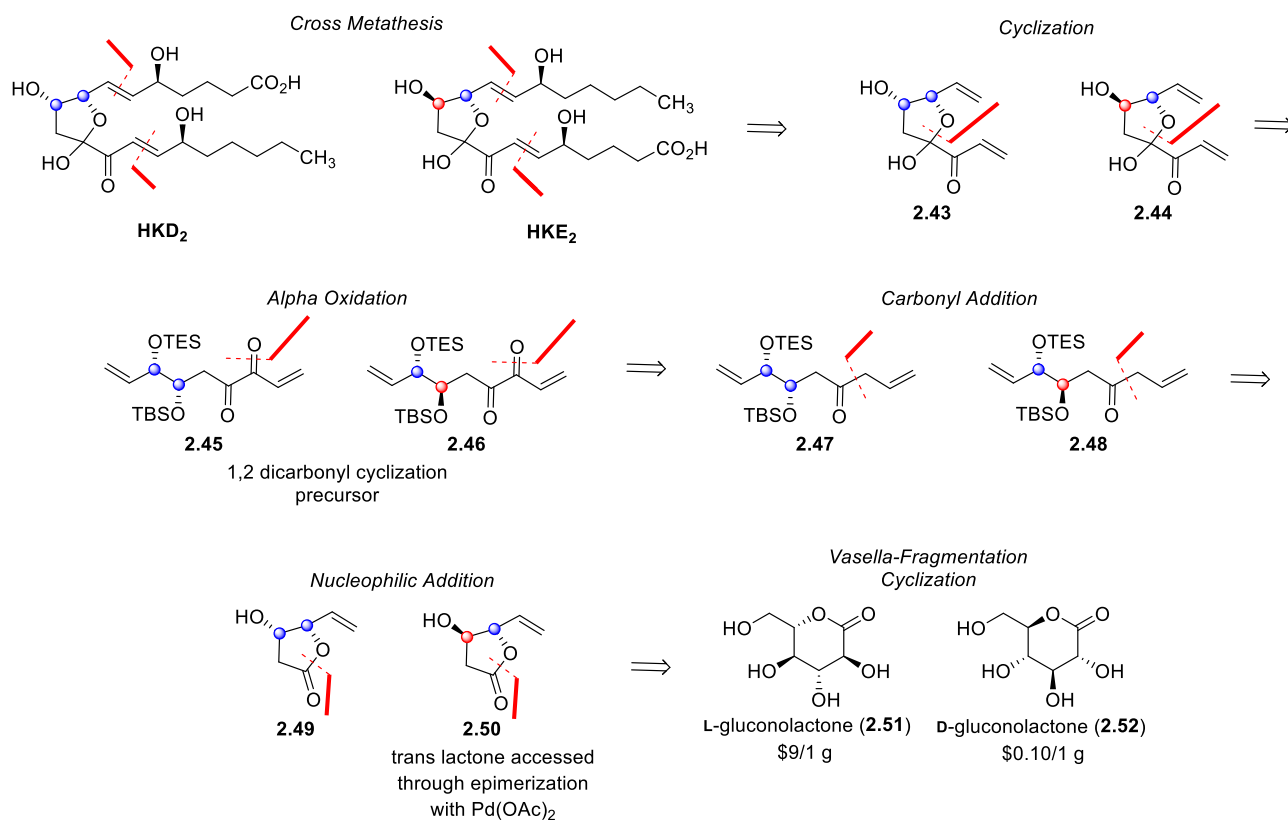
unfortunately, would readily decompose within 30 min. Additionally, a control experiment of a cross coupling between the resulting acylzirconocene from **2.38** and benzoyl chloride **2.40** failed, and only a complex mixture was observed, which illustrates the difficulty of incorporating this carbonyl. Although hydrozirconation, followed by addition of carbon monoxide provided access to the first carbonyl, the subsequent coupling with benzoyl chloride also failed. Without a sure method to access dicarbonyl **2.33**, it was determined that the carbonylative cross-coupling to link both carbonyls would be unlikely to be successful in the real system. Because further optimization of the model system would provide only diminishing returns, this route was abandoned for the next.



Scheme 2.7. Hydroformylation and Carbonylative Cross Couplings.

Third Synthetic Approach

The key intermediate in the newest synthetic approach involves 1,2-dicarbonyl cyclization precursors (**2.45**, **2.46**). Not many general methods exist to synthesize the key 1,2-dicarbonyl intermediate in our synthesis. There are known methods of coupling acid chlorides to acyltributyltins; however, harsh conditions are required and unwanted decarbonylation and butyl transfer side products are observed.⁴¹ A palladium-catalyzed coupling of acylzirconocene chloride with organic halides exists;³⁴ however, this approach is low yielding and requires the use of hazardous carbon monoxide. Still other methods involve oxidizing 1,2-diols to 1,2-dicarbonyls; however, these bonds are known to be sensitive to oxidative cleavage.^{42,43} From a retrosynthetic standpoint, it was imagined

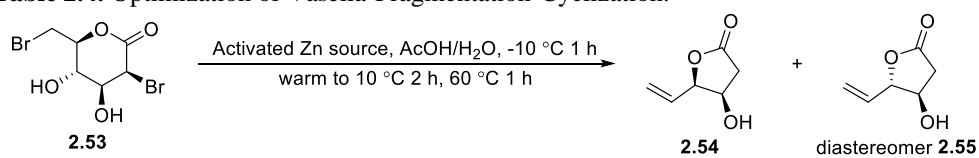


Scheme 2.8. Retrosynthetic Analysis starting from D or L-gluconolactones.

that the two side chains of both hemiketals could be introduced through selective, late-stage olefin cross metatheses, preceded by cyclization. The dicarbonyl-cyclization precursors (**2.45**, **2.46**) could be incorporated through an alpha oxidation, and the allyl handle installed with a Grignard, which would be prefaced by a nucleophilic addition of lactones (**2.49**, **2.50**). This final 3-step transformation of the lactone from D-gluconolactone was inspired by work from Fernandes.⁴⁴ Accessing the relative stereochemistry of both five-membered lactone cores is established in the literature,⁴⁴ starting from D-gluconolactone **2.52** to achieve HKE₂ through a Vasella-fragmentation cyclization. HKD₂ can be accessed analogously from L-gluconolactone **2.51** (Scheme 2.8).

Optimization of Vasella-Fragmentation-Cyclization

The first reaction required towards the synthesis of HKE₂ was a Vasella-fragmentation-cyclization. This transformation of D-gluconolactone to desired lactone **2.50** has an unfortunate history plagued by inefficiency and irreproducibility.^{45,46} In this two-step reaction, D-gluconolactone is first treated with 33% HBr in AcOH to yield dibromosugar **2.53**. It then transforms into the five membered lactone after treatment with zinc and AcOH/H₂O. Unfortunately, numerous attempts to replicate Fernandes' 45% yield only resulted in a 10% yield. Presented in **Table 2.4** are the optimization efforts to access the desired five-membered lactone. Activated zinc was used in all entries following the purification procedure in the Purification of Laboratory Chemicals.⁴⁷ In Entry 1, minimal product **2.54** was observed. It was hypothesized that adding the zinc over multiple portions might improve the yield by increasing the surface area of the zinc. Thus from 3 to 6 additions, (Entry 1 vs. Entry 2) an improvement from 7% to 37% was observed. Reversing the order of addition (Entry 3) and increasing the equivalents of zinc (Entries 4 – 6) have little to no effect on yield. Interestingly, the presence of diastereomer **2.55** was observed in low yield in certain cases (Entry 3 & 7). Altering the form of zinc to course powder showed an improvement to 47% (Entry 9). The last three entries reveal how changing the ratio of acetic acid to water affects the yield. Increasing the solvent to 75% aqueous acetic acid increases slightly to 50% (Entry 12). With the optimized conditions of the Vasella-fragmentation-cyclization in hand, progress towards the total synthesis of HKE₂ could begin.

Table 2.4. Optimization of Vasella-Fragmentation-Cyclization.

Entry	Conditions	Results
1	Zn dust < 10 micron (5.5 eq), AcOH/ H ₂ O (1:1) ^a	7 % product
2	Zn dust < 10 micron (5.5 eq), AcOH/ H ₂ O (1:1) ^b	37 % product
3	Zn dust < 10 micron (5.5 eq), AcOH/ H ₂ O (1:1) ^c	25 % product, 10 % mixture of diastereomers
4	Zn dust < 10 micron (10 eq), AcOH/ H ₂ O (1:1) ^b	33 % product
5	Zn dust < 10 micron (10 eq), AcOH/ H ₂ O (1:1) ^b	39 % product
6	Zn dust < 10 micron (10 eq), AcOH/ H ₂ O (1:1) ^b	42 % product
7	Zn dust < 10 micron (5.5 eq), AcOH/ H ₂ O (1:1) ^{b,d}	39 % product, 6 % mixture of diastereomers
8	Zn dust < 10 micron (5.5 eq), AcOH/ H ₂ O (1:1) ^b	39 % product
9	Zn course powder (5.5 eq), AcOH/ H ₂ O (1:1) ^b	47 % product
10	Zn course powder (5.5 eq), AcOH/ H ₂ O (1:3) ^b	39 % product
11	Zn course powder (5.5 eq), AcOH/ H ₂ O (3:1) ^b	48 % product
12	Zn course powder (5.5 eq), AcOH/ H ₂ O (3:1) ^b	50 % product

^a Zn added to dibromosugar in 3 portions at -10 °C 1 h, rt 3 h, 60 °C 1 h

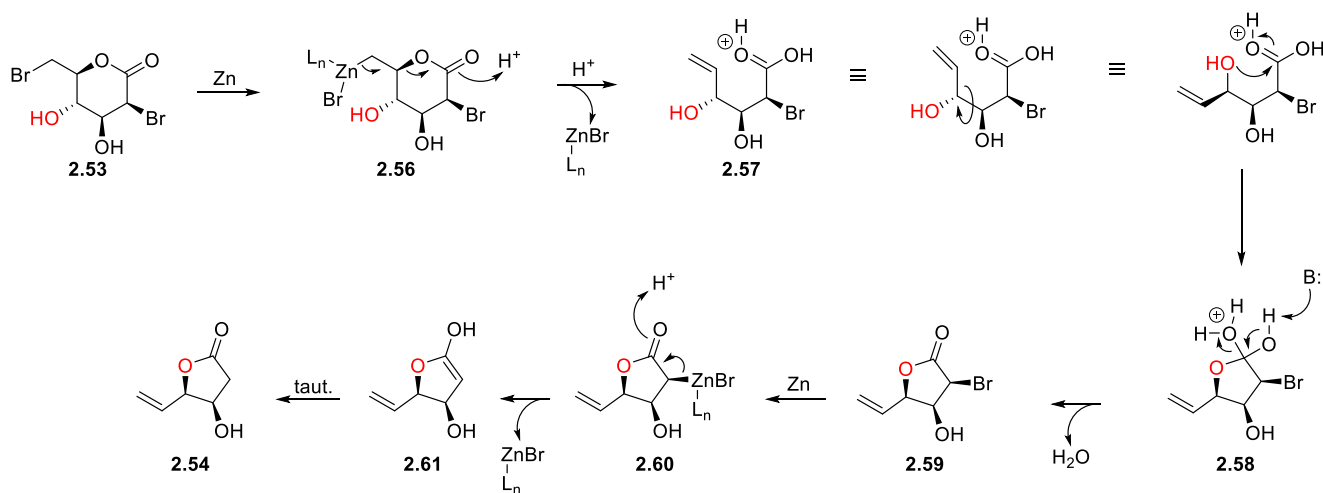
^b Zn added to dibromosugar in 6 portions at -10 °C

^c dibromosugar was added to activated zinc

^d -10 °C, 1 h, 10 °C 2h, rt 1 h, 60 °C 1 h

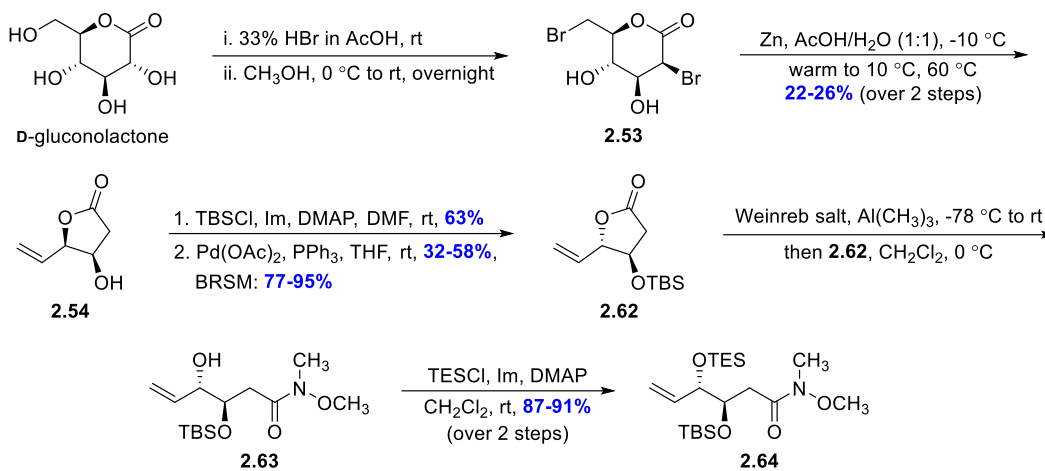
Proposed Mechanism of Vasella-Fragmentation-Cyclization

While the success of the optimization of the Vasella-fragmentation-cyclization is to be celebrated, arguably more important is mechanistic understanding of this intriguing reaction because at first glance this transformation may be difficult to visualize. Mechanistically, it is proposed that this reaction begins with zinc insertion into the dibromosugar **2.53**, followed by fragmentation facilitated by protonation with the acid. An equivalent of zinc bromide, ZnBr-L_n , is eliminated, where L_n represents a bonded-ligand. Then, the alcohol highlighted in red in **2.57**, cyclizes onto the activated carbonyl. After deprotonation, alpha-brominated lactone **2.59** is obtained, followed by another zinc insertion and elimination of zinc bromide. Enol **2.61** then tautomerizes, and the final lactone **2.54** is isolated (**Scheme 2.9**).



Scheme 2.9. Mechanism of Vasella-Fragmentation-Cyclization.

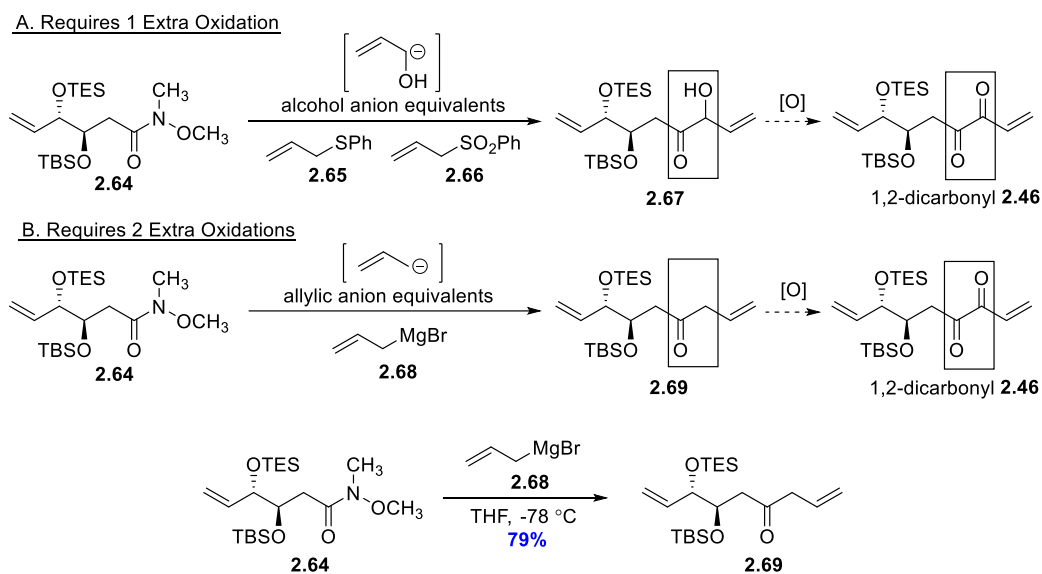
The following route was objectively the most successful one thus far, compared to the previous attempts mentioned (**Scheme 2.10**). In the forward direction, treatment of D-gluconolactone with 33% HBr in AcOH yields dibromosugar **2.53**.⁴⁸ Next, a zinc-mediated Vasella-fragmentation-cyclization sequence afforded five-membered lactone **2.54** in 22-26% yield over two steps.⁴⁴ TBS protection followed by epimerization with $\text{Pd}(\text{OAc})_2$ affords lactone **2.62** which establishes the relative stereochemistry required for HKE₂.⁴⁹ It should be noted that this epimerization step is not needed to access HKD₂ since the stereochemistry is already set. Then, nucleophilic addition with the Weinreb salt and $\text{Al}(\text{CH}_3)_3$, followed by a TES protection yielded Weinreb amide **2.64** in 87-91% yield over two steps (**Scheme 2.10**). The next section will discuss a variety of attempted nucleophilic strategies with Weinreb amide **2.64**.



Scheme 2.10. Current Route to Weinreb amide **2.64**.

Strategy to Access the 1,2-Dicarbonyl Intermediate

This clever strategy is mindful of the oxidation states of both the attacking nucleophile and the resulting product, allowing for the ease of the subsequent oxidation reactions. It was envisioned that dicarbonyl **2.46** could be accessed from Weinreb amide **2.64** via either alcohol anion equivalents with one subsequent oxidation *or* allylic anion equivalents with two following oxidations (**Scheme 2.11**). Routes using alcohol anion equivalents like thiol **2.65** and sulfone **2.66** were largely unsuccessful and will not be discussed further (**Scheme 2.11.A**). However, the route with allylic Grignard **2.68** worked quite well, providing ketone **2.69** in a 79% yield (**Scheme 2.11.B**). Also, because the crude material of this reaction was very clean, the reaction could be carried forward without purification into the next oxidation steps.

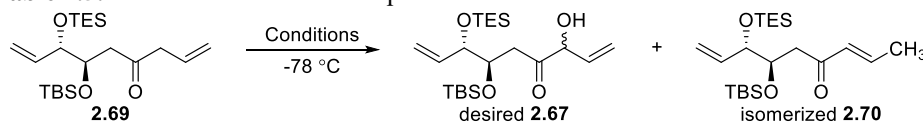


Scheme 2.11. Nucleophilic Addition Strategy.

Davis' Oxaziridine

The success of the alpha oxidation of ketone **2.69** relies upon the difference in acidities of the two different alpha positions. By taking advantage of the more acidic, allylic protons, the regioselective alpha oxidation could occur. Unfortunately, first attempts at alpha oxidation with Davis' oxaziridine^{50,51,52} only provided minimal amounts of desired alpha-hydroxy ketone **2.67** or isomerized enone **2.70** (Table 2.5). Attempts to alter the base, equivalents of oxidant, or the order of addition ultimately did not improve the yield for the desired product. Decomposition pathways towards volatile products may explain why these reactions were low yielding.

Table 2.5. Davis' Oxaziridine Attempts.



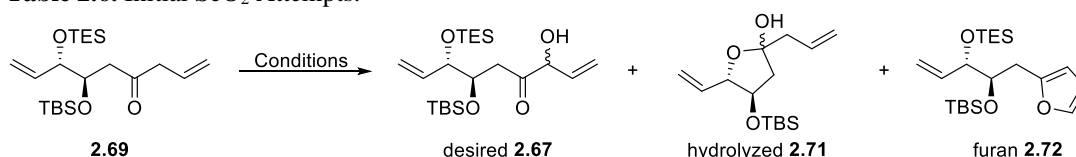
Entry	Base	[O]	Order of Addition	Time	Results
1	NaHMDS (1.0 eq)	1.8 eq	SM \rightarrow B \rightarrow [O] ^a	40 min	6% desired
2	NaHMDS (1.0 eq)	1.0 eq	[O] \rightarrow SM \rightarrow B	20 min	10% isomerized
3	NaHMDS (1.0 eq)	1.7 eq	[O] \rightarrow SM \rightarrow B	20 min	7% isomerized
4	KHMDS (1.2 eq)	2.1 eq	SM \rightarrow B \rightarrow [O]	2 h	2% isomerized
5	KHMDS (1.2 eq)	5.2 eq	SM \rightarrow B \rightarrow [O]	2 h	5% isomerized

^a SM = starting material, B = base, [O] = oxidation with Davis' Oxaziridine.

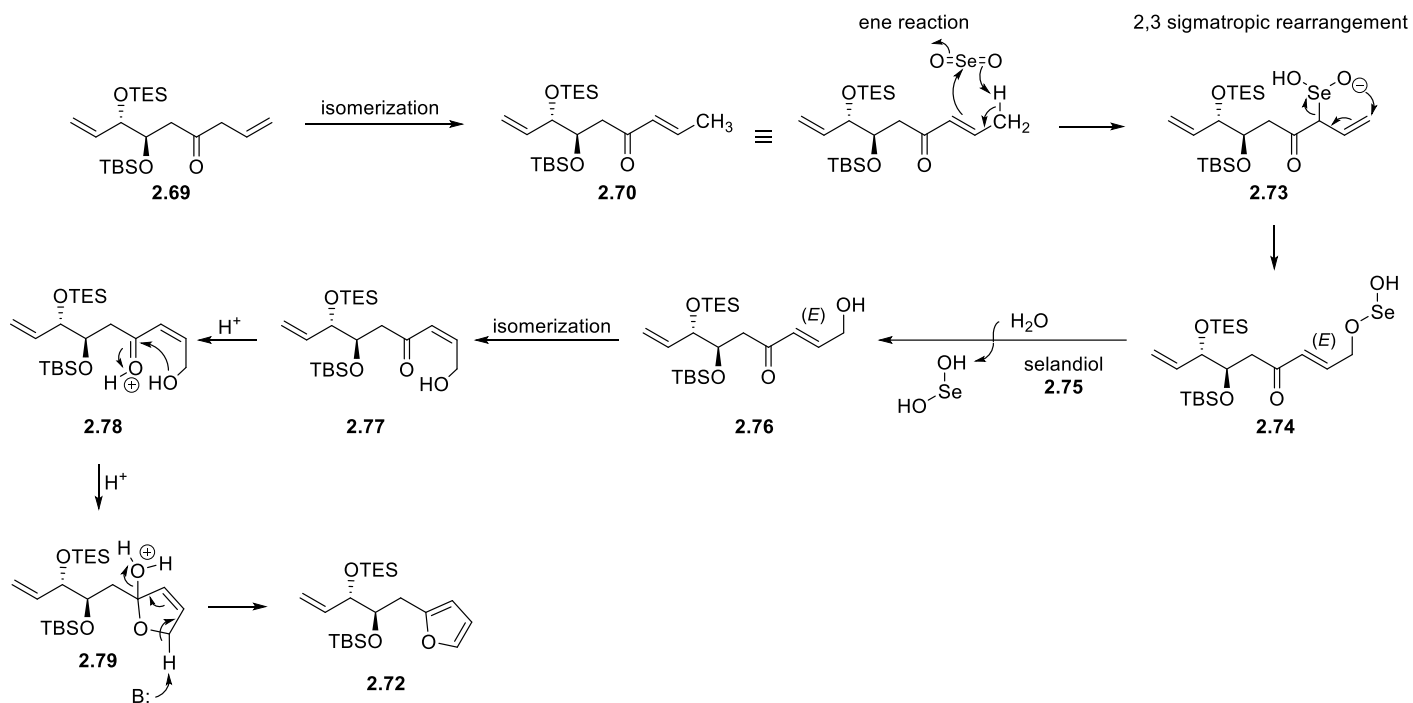
Riley Oxidation

Next, the Riley oxidation with allylic oxidant, selenium dioxide, was attempted.^{53,54,55} Interestingly, upon treatment of ketone **2.69** with SeO_2 , while no desired product was obtained, the formation of furan **2.72**, an isomerization byproduct, was observed (Table 2.6). Understanding of how this furan formed provided insight on how to optimize the route. Scheme 2.12 depicts the proposed mechanism which begins with isomerization of ketone **2.69** to the more thermodynamically stable enone **2.70**. Selenium dioxide performs an ene reaction, followed by a 2,3-sigmatropic rearrangement in an envelope-like transition state to afford allylselenite ester **2.74**, and then hydrolysis provides (*E*)-allylic alcohol **2.76**; isomerization, and finally aromatization provides furan **2.72**.

Table 2.6. Initial SeO_2 Attempts.

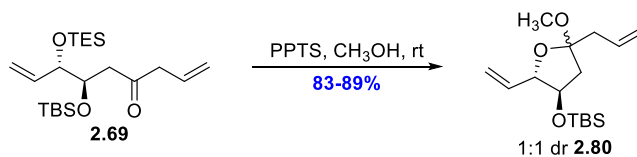


Entry	Conditions	Results
1	SeO_2 (0.5 eq), TBHP (2.2 eq), CH_2Cl_2 , 20 h, rt	15% hydrolyzed
2	SeO_2 (3 eq), dioxane, mw, $110\text{ }^{\circ}\text{C}$, 10 min	10% furan

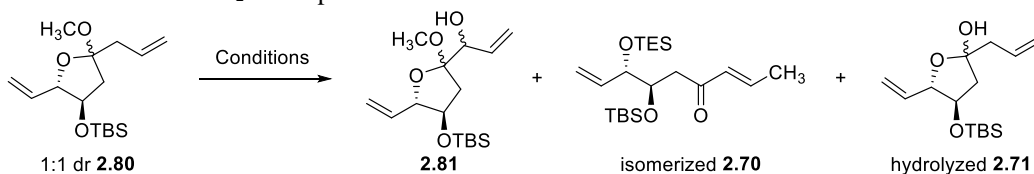


Scheme 2.12. Proposed Mechanism of the Formation of Furan **2.72**.

From this result, it was hypothesized that rather than an oxidation followed by cyclization, reversing these two reactions would possibly prevent the subsequent isomerization. Henceforth, removal of the TES group with PPTS in methanol provided a mixture of ketals **2.80** in 83-89% yield (**Scheme 2.13**).^{56,57} While the removal of the TES group was expected, the installation of the ketals was not. This serendipitous result could later allow for methylated analogs to be used for biological testing. As shown from **Table 2.7**, attempts at allylic oxidation of ketals **2.80** only resulted in hydrolyzed product **2.71** and isomerized enone **2.70**. Unfortunately, it became evident that isomerized enone **2.70** was the more thermodynamically stable product and another strategy was needed. Regrettably, this particular route was bottlenecked by the failed oxidation attempts, but as demonstrated from the success of the Grignard reaction, it is clear that a successful nucleophilic addition *is* possible. Thus, an alternative nucleophile was sought.



Scheme 2.13. Other SeO_2 Attempts.

Table 2.7. Other SeO₂ Attempts with Ketals **2.80**.

Entry	Conditions	Results
1	SeO ₂ (0.5 eq), TBHP (2.2 eq), CH ₂ Cl ₂ , rt, 2.5 h	> 95% hydrolyzed
2	SeO ₂ (3 eq), dioxane, mw, 110 °C, 10 min	3% isomerized
3	SeO ₂ (1 eq), dioxane, 85 °C, 1 h	8% isomerized

Methoxyallene as an Acyl Anion Equivalent

This method installs the 1,2-dicarbonyl as a masked acyl anion equivalent utilizing methoxyallene **2.83**, similar to the previous acyl anion equivalent with acylzirconocene (**Scheme 2.14**).^{58,59} The benefit of this strategic design delivers the nucleophile in the correct oxidation state and provides access to the core of both hemiketals.⁶⁰ Additionally, the methoxy group assists in the selective ortho deprotonation by *n*-butyllithium, leading to an ortho-lithiated species, similar to a Snieckus-directed ortho metalation (DoM).⁶¹ The chosen electrophiles for this reaction were Weinreb amide **2.64** and aldehyde **2.86**. Successful nucleophilic addition into the amide would result with the product in the correct oxidation state due to the Weinreb amide's innate ability to stabilize tetrahedral intermediates. However, if the Weinreb amide fails, the aldehyde would be attempted next since it is more electrophilic. Aldehyde **2.86** can be isolated in 79-83% yield in an LAH reduction of Weinreb amide **2.64**. However, to prevent squandering this precious material, the initial nucleophilic additions with methoxyallene **2.83** were first attempted with benzaldehyde **2.82**. To our delight, α -hydroxy ketone **2.84** was able to be isolated in 40% yield. Now that the proof of concept was successfully achieved with the model system, the real system was attempted next.

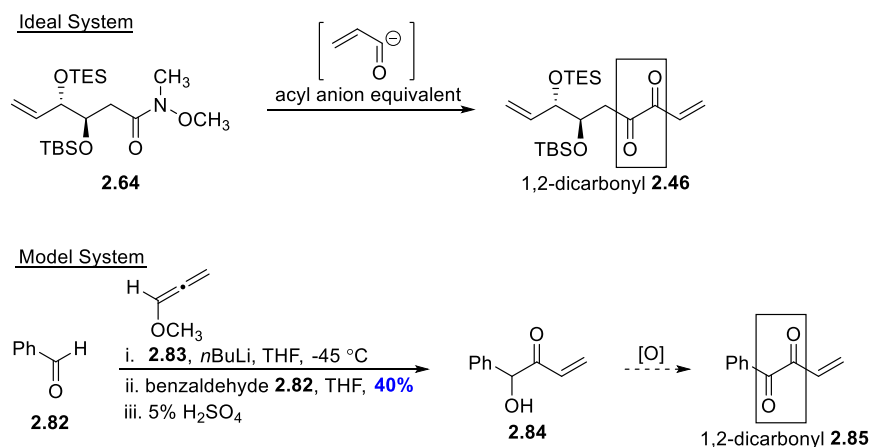
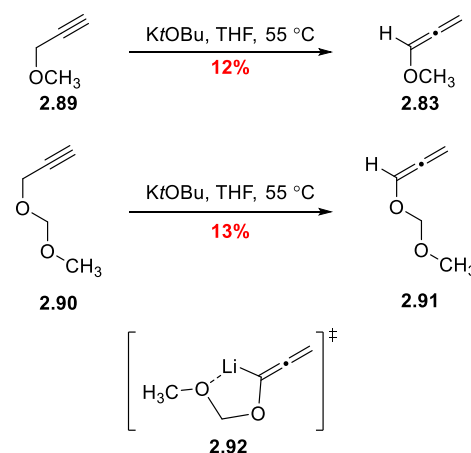
**Scheme 2.14.** New Strategy with Methoxyallene.

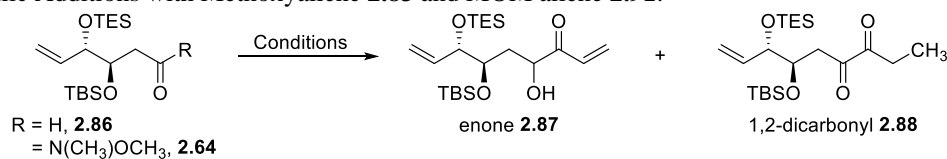
Table 2.8 showcases the massive undertaking of nucleophilic additions attempted with both Weinreb amide **2.64** and aldehyde **2.86**. A variety of parameters were explored including reaction time, temperature for the deprotonation of the allene, acidic workups, additives, equivalents of methoxyallene *etc.* As shown in Entry 1, minimal product was observed under these conditions. Lithium aggregation was believed to be a potential problem; therefore, TMEDA and DBU were added (Entries 2 and 3). Entry 3 was promising because the addition of DBU increased the combined yield of enone **2.87** and 1,2-dicarbonyl **2.88** to 34%. A hypothesis exists that the presence of lithiated-DBU can prevent lithium aggregation due to solvation when treated with LDA or *n*BuLi.⁶² To try and improve upon this yield, Entries 4 – 7 explored how increasing the reaction time or varying temperature and workup affected yield, but no augmentation in product was observed. Entries 6 and 7 were efforts towards achieving transmetalation with Zn(CH₃)₂ and CeCl₃ respectively, but only starting material was observed in both cases.^{63,64} While nucleophilic equivalents were drastically increased to 10 in Entry 8, no improvement in yield was demonstrated. Unfortunately, none of these alterations of the reaction parameters improved the yield other than Entry 3.

The next modification was to constrain the movement of the allene, as it was believed restraining the nucleophile might help guide it to the electrophile more easily; as shown from allene **2.92**, once lithiated, the MOM allene is tethered by an oxygen (Scheme 2.15). Similar to methoxyallene **2.83**, MOM allene **2.91** was synthesized from alkyne **2.90** with potassium *tert*-butoxide in low yields.^{65,66} Regrettably, Entries 9 – 13 in **Table 2.8** demonstrate reactions with both Weinreb amide **2.64** and aldehyde **2.86** were unsuccessful. Even in the presence of DBU (Entries 12 and 13), only provided unreacted starting material.

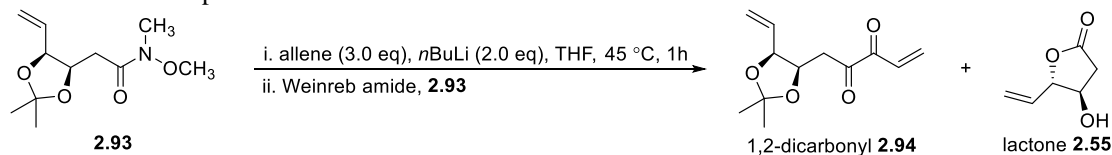
Next, Weinreb amide **2.64** was modified with an acetonide group to give Weinreb amide **2.93**, but these reactions were unsuccessful as well (**Table 2.9**). Both the methoxyallene **2.83** and MOM allene **2.91** were attempted with Weinreb amide **2.93** in Entries 1 and 2, respectively. Only starting material or lactone **2.95** were recovered; lactone **2.95** resulted from the loss of the acetonide protecting group to provide the diol which then cyclized onto the Weinreb amide **2.93**. Thus far the highest yielding conditions are from Entry 3 of **Table 2.8**. Due to the interesting results with TMEDA and DBU, further efforts with other diamine additives will be explored in the future.⁶⁷ The next section will discuss another promising nucleophilic addition approach.



Scheme 2.15. Synthesis of Methoxyallene and MOM allene.

Table 2.8. Nucleophilic Additions with Methoxyallene **2.83** and MOM allene **2.91**.

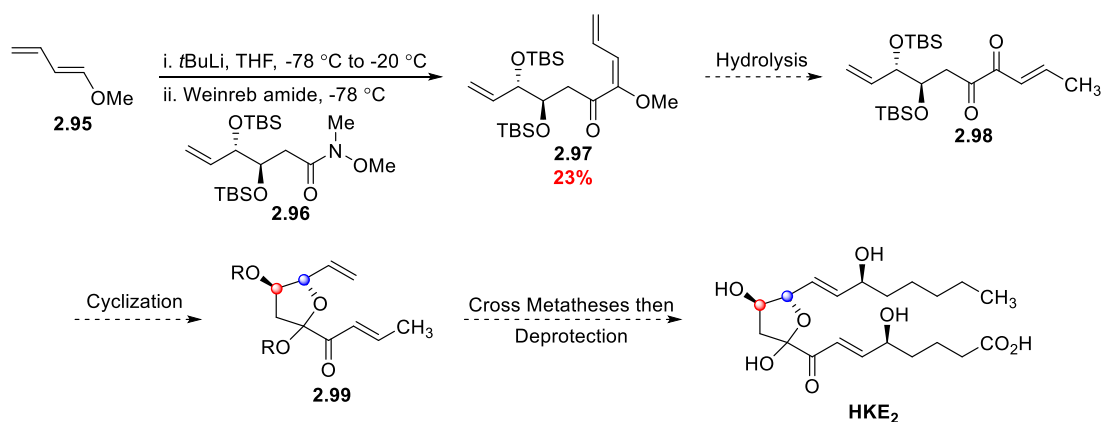
Entry	Conditions	Electrophile (1.0 eq)	Workup	Results
1	methoxyallene (3.0 eq), <i>n</i> BuLi (2.0 eq) THF, -45 °C 2h → 0 °C 3.5h	aldehyde	1N HCl	9.3% SM, 6.9% diketone
2	methoxyallene (3.0 eq), <i>n</i> BuLi (2.0 eq) TMEDA (2.0 eq), THF, -45 °C 1h	aldehyde	1N HCl	34% SM, 12% enone, 2.7% diketone
3	methoxyallene (3.0 eq), <i>n</i> BuLi (2.0 eq) DBU (2.0 eq), THF, -45 °C 1h	aldehyde	1N HCl	4.6% SM, 21% enone/diketone, 13% diketone
4	methoxyallene (3.0 eq), <i>n</i> BuLi (2.0 eq) THF, -45 °C 2h	aldehyde	H ₂ O	45% SM ^a
5	methoxyallene (3.0 eq), <i>n</i> BuLi (2.0 eq) THF, -45 °C 4h	aldehyde	H ₂ O	75% SM
6	methoxyallene (3.0 eq), <i>n</i> BuLi (2.0 eq) Zn(CH ₃) ₂ (2.0 eq), THF, -45 °C 2h → -10 °C 0.67h	aldehyde	H ₂ O then 5% H ₂ SO ₄	56% SM
7	methoxyallene (3.0 eq), <i>n</i> BuLi (2.0 eq) CeCl ₃ (2.0 eq), THF, -45 °C 2h → rt 0.5h	aldehyde	H ₂ O then 5% H ₂ SO ₄	19% SM
8	methoxyallene (10 eq), <i>n</i> BuLi (9.0 eq) THF, -45 °C 1h	aldehyde	H ₂ O then 5% H ₂ SO ₄	3.8% SM, 12% enone/diketone, 13% diketone
9	MOM allene (3.0 eq), <i>n</i> BuLi (2.0 eq) THF, -45 °C 1h	aldehyde	H ₂ O	38% SM
10	MOM allene (3.0 eq), <i>n</i> BuLi (2.0 eq) THF, -45 °C 1h	Weinreb amide	H ₂ O	71% SM
11	methoxyallene (3.0 eq), <i>n</i> BuLi (2.0 eq) DBU (2.0 eq), THF, -45 °C 1h	Weinreb amide	H ₂ O	73% SM
12	MOM allene (3.1 eq), <i>n</i> BuLi (2.0 eq) DBU (2.0 eq), THF, -45 °C 1h	aldehyde	H ₂ O then 5% H ₂ SO ₄	71% SM
13	MOM allene (3.0 eq), <i>n</i> BuLi (2.0 eq) DBU (2.0 eq), THF, -45 °C 1h	Weinreb amide	H ₂ O	71% SM

^a SM = starting material**Table 2.9.** Nucleophilic Additions.

Entry	Conditions	Results
1	methoxyallene	22% SM, 10% lactone
2	MOM allene	6% SM, 31% lactone

The Butadiene Method

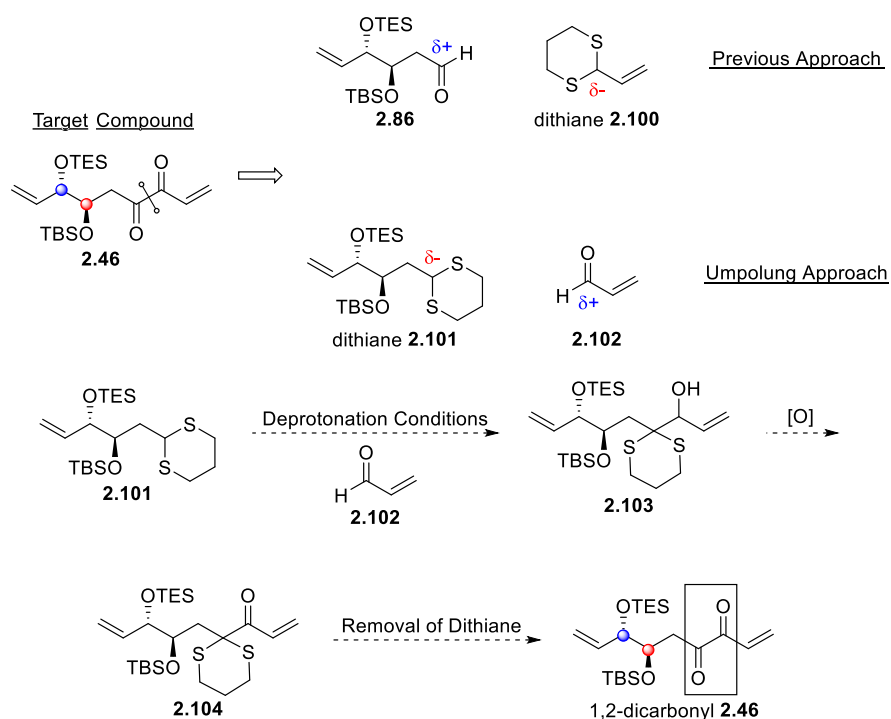
Another acyl anion equivalent very similar to methoxyallene **2.83**, namely methoxybutadiene **2.95**, was attempted. This strategy involved a directed metalation with *tert*-butyllithium,^{68,69} followed by nucleophilic attack into Weinreb amide **2.96** to obtain dicarbonyl precursor **2.97** (Scheme 2.16). With **2.97** already in the correct oxidation state, this would be followed by hydrolysis, protection, cyclization, cross metathesis and deprotection steps to ultimately obtain HKE₂. This reaction to obtain dicarbonyl precursor **2.97** was not pursued further due to its low yield of 23%, but in the future it is worth pursuing because, unlike the nucleophilic attack with methoxyallene **2.83**, only one product is obtained, rather than a mixture of isomers which need to be further oxidized. In 1991, Badanyan and coworkers utilized a similar substrate where the diagnostic vinylic gamma-hydrogen of this structure was confirmed.⁷⁰ Perhaps additives, like TMEDA, DBU, or HMPA, can help improve the yield by breaking up lithium aggregates like shown in the previous section. Concomitantly, while the butadiene nucleophilic additions were explored, conditions to introduce a dithiane were being optimized.



Scheme 2.16. Butadiene Strategy.

Umpolung Dithiane Approach

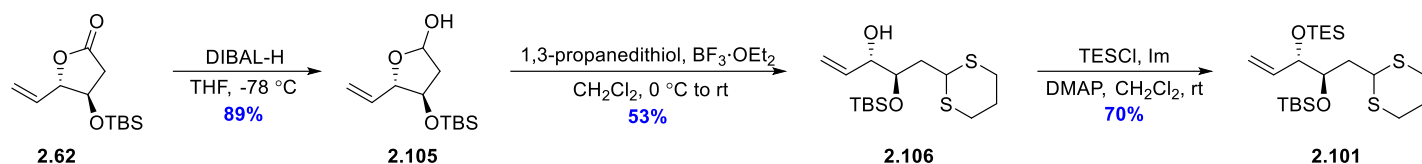
Previous work by Dr. Alex Allweil involved nucleophilic additions with dithianes in which dithiane **2.100** was deprotonated and added into aldehyde **2.86** (**Scheme 2.17**). Unfortunately, despite his extensive optimization efforts, this reaction was unsuccessful. More information can be found in his thesis dissertation regarding this reaction.² Using this work as inspiration, the next idea proposed involved an umpolung approach, where there is a reversal in the polarity of the substrates with dipoles indicated in blue and red. Thus, rather than using aldehyde **2.86** as an electrophile, transforming it into TES-protected dithiane **2.101** to use as a nucleophile under a set of deprotonation conditions was a topic of interest. Then, the corresponding electrophile would be acrolein **2.102** to ultimately access 1,2-dicarbonyl precursor **2.46**.



Scheme 2.17. Umpolung Dithiane Approach.

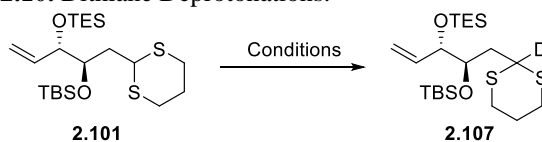
To access TES-protected dithiane **2.101**, epimerized lactone **2.62** (shown previously in **Scheme 2.10**) underwent DIBAL-H reduction to provide lactol **2.105** in an 89% yield (**Scheme 2.18**). This was followed by treatment with 1,3-propanedithiol and $\text{BF}_3 \cdot \text{OEt}_2$ to provide dithiane **2.106** in 53% yield, and finally the TES protection afforded dithiane **2.101** in a 70% yield. Ensuing deprotonations then followed by treatment with either *n*BuLi or *t*BuLi (**Table 2.10**).⁷¹ In all entries, a D_2O quench was conducted to determine if deuterium incorporation was observed, which would indicate the success of the deprotonation, while the absence of deuterium indicates reaction failure. In Entry 1, treatment of dithiane **2.101** with *n*BuLi astonishingly gave 85% of recovered starting material. Due to the overwhelming amount of starting material recovered, next in Entry 2, a more aggressive base *t*BuLi was attempted, but this still resulted in 91% of recovered dithiane **2.101**. Then,

attempts with HMPA and warmer temperatures were tried (Entries 3 – 5). Unfortunately, starting material was obtained again. As a final desperate attempt, deprotonation with *t*BuLi at 0 °C shockingly provided 93% starting material as shown in Entry 6. Next further, attention to the literature was sought to find a possible answer.



Scheme 2.18. Synthesis of Dithiane **2.101**.

Table 2.10. Dithiane Deprotonations.

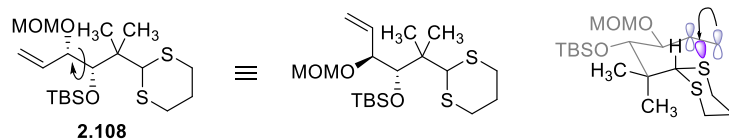


Entry	Conditions (assume D ₂ O quench)	Results
1	dithiane (1.0 eq), <i>n</i> BuLi (1.7 eq) THF, -78 °C 2h	85% SM ^a
2	dithiane (1.0 eq), <i>t</i> BuLi (1.7 eq) THF, -78 °C 2h	91% SM
3	dithiane (1.0 eq), <i>t</i> BuLi (1.7 eq) HMPA (2.5 eq), THF, -78 °C 2h	73% SM
4	dithiane (1.0 eq), <i>n</i> BuLi (1.7 eq) THF, 0 °C 1h	90% SM
5	dithiane (1.0 eq), <i>n</i> BuLi (1.7 eq) HMPA (2.5 eq), THF, 0 °C 1h	77% SM
6	dithiane (1.0 eq), <i>t</i> BuLi (1.7 eq) THF, 0 °C 1h	93% SM

^a SM = starting material

After searching in the literature for divine inspiration to improve the dithiane deprotonation, a helpful review by Dr. Amos Smith was found.⁷² In his review, substrate **2.108** which is quite similar to dithiane **2.101** was highlighted. He explained that the π_{C-C} donation into the σ^*_{C-S} of the dithiane decreases the acidity of the axial hydrogen, and because of this, it results in an overall decrease in the stability of the conjugate base. This is the argument Dr. Amos Smith uses to explain why the deprotonation could not occur in his substrate, and it is hypothesized that therefore dithiane **2.101** is not able to be deprotonated for this reason as well (**Figure 2.2**). It should be noted that the dithiane is shown in a chair-like conformation because the deprotonation preferentially attacks the equatorial hydrogen since it is more acidic than if the hydrogen were in the axial position.^{73,74}

Dr. Amos Smith's substrate



π_{C-C} donation into σ_{C-S}^*
decreases the acidity
of the equatorial H

This work

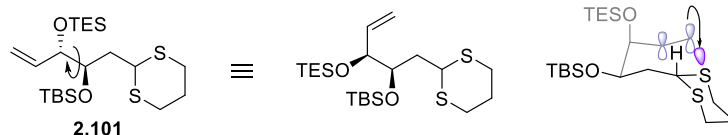
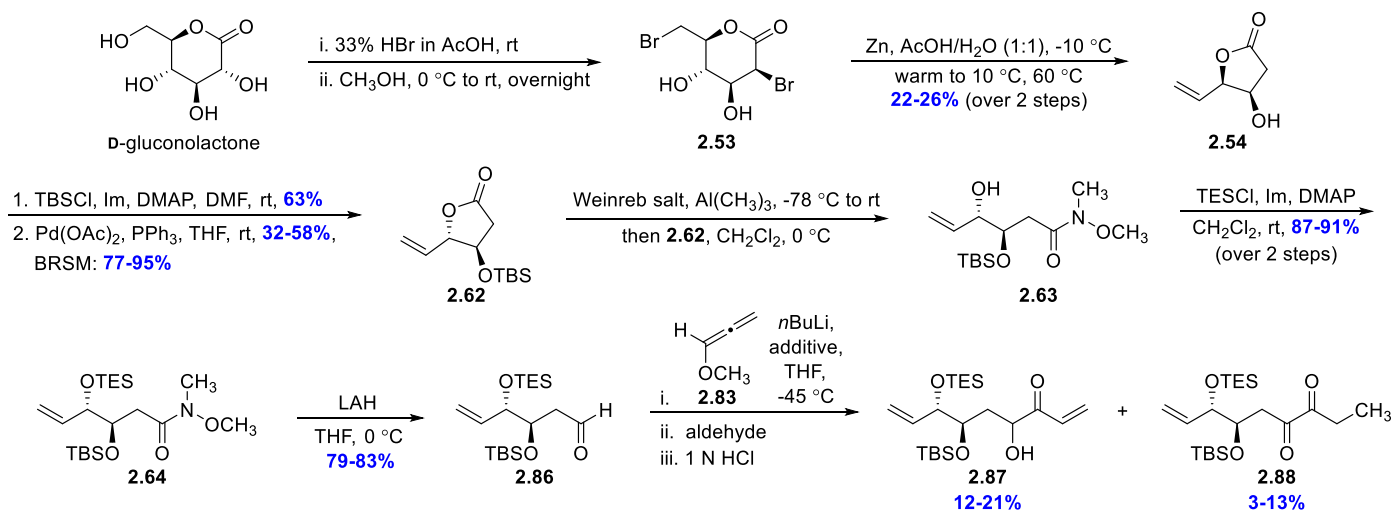


Figure 2.2. π_{C-C} Donation into σ_{C-S}^* Prevents Ease of Deprotonation of **2.101**.

Thus, to summarize the trials of this route towards HKD₂ and HKE₂: major optimizations of the Vasella-fragmentation-cyclization by nuancing the zinc source and adding the zinc over multiple portions significantly improved the yield of lactone **2.54**. The second obstacle was the allylic oxidations with Davis' oxaziridine and SeO₂, after the subsequent nucleophilic addition with allylic Grignard **2.68**. Due to the evidence of the more thermodynamic enone **2.70**, this sequence to access 1,2-dicarbonyl intermediate **2.46** was abandoned for an alternative nucleophilic addition with methoxyallene **2.83**. Extensive optimization efforts to vary reaction time, temperature for the deprotonation of methoxyallene, acidic workups, additives, and equivalents of methoxyallene were conducted. Transmetalation efforts ultimately failed, however, the presence of DBU did considerably increase the yield of the desired isomers (**2.87** & **2.88**). Additionally, nucleophilic addition of methoxybutadiene **2.95** is another nucleophile worth pursuing in the future because only one product **2.97** is obtained, rather than the mixture of isomers (**2.87** & **2.88**). Finally, the routes failed include the oxidation-epimerization sequence which started from 2-Deoxy-D-ribose, carbonylative couplings, and umpolung dithiane approach. The next section summarizes the current route to date after overcoming these challenges.

Current Route

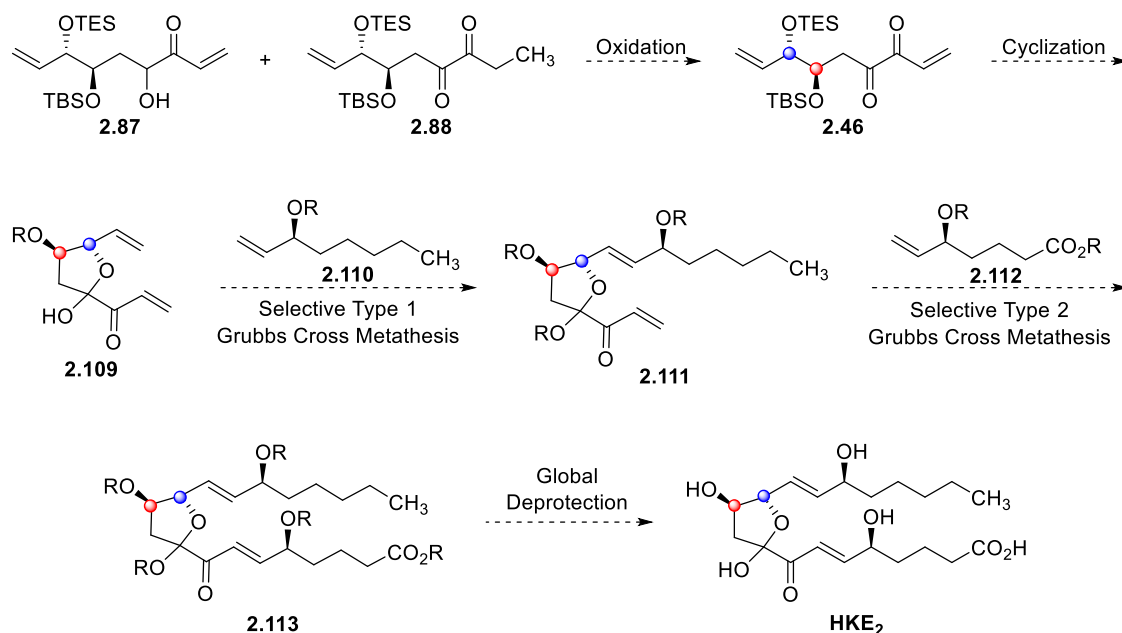


Scheme 2.19. Current Route with Methoxyallene.

In summary, treatment of D-gluconolactone with 33% HBr in AcOH yielded dibromosugar **2.53** (**Scheme 2.19**).⁴⁸ Next, a zinc-mediated Vasella-fragmentation-cyclization sequence afforded five-membered lactone **2.54** in 22-26% yield over two steps.⁴⁴ This is an improvement over previous methods which are lower yielding and require more steps.^{45,46} TBS protection followed by epimerization with Pd(OAc)₂ afforded lactone **2.62** which established the relative stereochemistry required for HKE₂.⁴⁹ Nucleophilic addition with the Weinreb salt and Al(CH₃)₃ followed by TES protection yields Weinreb amide **2.64** in 87-91% yield over 2 steps. Ensuing LAH reduction gave aldehyde **2.86** in 79-83% yield. Next, a nucleophilic addition with methoxyallene **2.83** to establish the 1,2-dicarbonyl framework.⁶⁰ The optimized conditions for the nucleophilic addition between methoxyallene **2.83** and aldehyde **2.86** leveraged the effects of TMEDA and DBU to yield enone **2.87** and its 1,2-dicarbonyl isomer **2.88**.⁷⁵ The benefit of this tactical design delivers the nucleophile in the correct oxidation state.

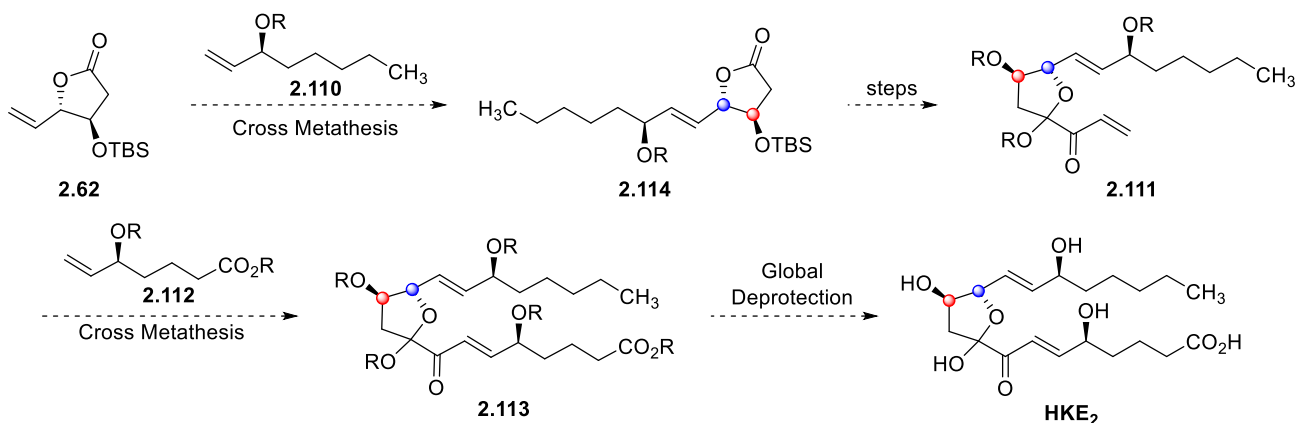
Future Directions

The future hope for this project is to oxidize the mixture of enone **2.87** and 1,2-dicarbonyl **2.88** with mild iodine reagents, alternatives to IBX, to give the desired 1,2-dicarbonyl cyclization precursor **2.46** (**Scheme 2.20**).⁷⁶ However, it should be stated that further investigations of the butadiene nucleophilic addition may provide even higher yields than the current conditions with methoxyallene **2.83**. Next, a selective TES deprotection and ensuing cyclization would provide hemiketal **2.109**. Protection of the hemiketal, followed by subsequent Type I and Type II cross metatheses with Grubbs catalyst,^{77,78} and a final global deprotection would ultimately afford HKE₂.



Scheme 2.20. Future Directions towards HKE₂.

Alternatively, if the Type I and II cross metatheses are nonselective, side chain **2.110** could be installed with a cross metathesis at epimerized lactone **2.62** which may help improve the selectivity (**Scheme 2.21**).⁷⁹ From here the synthesis would proceed as previously stated, and another cross metathesis with ketal **2.111** and side chain **2.112** would ultimately provide access to HKE₂. Once the current route towards HKE₂ has been established, synthesis of HKD₂ would proceed in a similar fashion beginning from L-gluconolactone, previously shown in **Scheme 2.8**.



Scheme 2.21. Alternative Route towards HKE₂.

By enabling access to HKD₂ and HKE₂, further biological studies could be done to probe their roles in the inflammatory pathway, as well as further investigate their effects of angiogenesis and tubulogenesis in murine pulmonary endothelial cells. These studies may help doctors better understand inflammatory diseases and treat patients.

References

- (1) Boer, R. Approaches toward the Chemical Synthesis of Novel Arachidonic Acid Metabolites Hemiketal D2 and Hemiketal E2, Vanderbilt University, 2015.
- (2) Allweil, A. Synthetic Studies on Hemiketal E2 and 5-Hydroxy Prostaglandin E2 Novel Arachidonic Acid Metabolites, Vanderbilt University, 2021.
- (3) Fehr, T.; Sanglier, J.; Schuler, W.; Gschwind, L.; Ponelle, M.; Schilling, W.; Wioland, C. Antascomicins A, B, C, D and E Novel FKBP12 Binding Compounds from a Micromonospora Strain. *J. Antibiot.* **1996**, *49*, 230–233.
- (4) Tanaka, H.; Kuroda, A.; Marusawa, H.; Hatanaka, H.; Kino, T.; Goto, T.; Hashimoto, M.; Tago, T. Structure of FK506, a Novel Immunosuppressant Isolated from Streptomyces. *J. Am. Chem. Soc.* **1987**, *109*, 5031–5033.
- (5) Wu, X.; Wang, L.; Han, Y.; Regan, N.; Li, P.; Villalona, M.; Hu, X.; Briesewitz, R.; Pei, D. Creating Diverse Target-Binding Surfaces on FKBP12: Synthesis and Evaluation of a Rapamycin Analogue Library. *ACS Comb. Sci.* **2011**, 486–495.
- (6) Kasai, Y.; Ito, T.; Sasaki, M. Total Synthesis of (–)-Polycavernoside A: Suzuki–Miyaura Coupling Approach. *Org. Lett.* **2012**, 3186–3189.
- (7) Yotsu-Yamashita, M.; Seki, T.; Paul, V.; Naoki, H.; Yasumoto, T. Four New Analogs of Polycavernoside A. *Tetrahedron Lett.* **1995**, *36*, 5563–5566.
- (8) Yotsu-Yamashita, M.; Haddock, R.; Yasumoto, T. Polycavernoside A: A Novel Glycosidic Macrolide from the Red Alga Polycavernosa Tsudai (Gracilaria Edulis). *J. Am. Chem. Soc.* **1993**, *115*, 1147–1148.
- (9) McAlpine, J.; Swanson, S.; Jackson, M.; Whittern, D. REVISED NMR ASSIGNMENTS FOR RAPAMYCIN. *J. Antibiot.* **1991**, *44*, 688–690.
- (10) Boer, R.; Gimenez-Bastida, J. A.; Boutaud, O.; Jana, S.; Schneider, C.; Sulikowski, G. A. Total Synthesis and Biological Activity of the Arachidonic Acid Metabolite Hemiketal E2. *Org. Lett.* **2018**, *20*, 4020–4022.
- (11) Austin, Z. Total Synthesis of the Delta-13-9-Isosofurans: A Stereodivergent Approach, Vanderbilt University, 2021.
- (12) Larson, C. Stereodivergent Approach to the Total Synthesis of Selected ST and AT Δ 13-9-Isosofurans, Vanderbilt University, 2022.
- (13) Davis, R. Synthesis of Four Diastereomeric Linoleic Triols and Development of a Large Scale Convergent Approach to Apoptolidinone C, Vanderbilt University, 2018.
- (14) Banchet-Cadeddu, A.; Martinez, A.; Guillarme, S.; Parietti, V.; Monneaux, F.; Hénon, E.; Renault, J.; Nuzillard, J.; Haudrechy, A. Use of the NEO Strategy (Nucleophilic Addition/Epoxy Opening) for the Synthesis of a New C-Galactoside Ester Analogue of KRN 7000. *Bioorg. Med. Chem. Lett.* **2011**, *21*, 2510–2514.
- (15) Omura, K.; Swern, D. Oxidation of Alcohols by “Activated” Dimethyl Sulfoxide. a Preparative, Steric and Mechanistic Study. *Tetrahedron* **1978**, *34*, 1651–1660.

- (16) Ireland, R.; Norbeck, D. Application of the Swern Oxidation to the Manipulation of Highly Reactive Carbonyl Compounds. *J. Org. Chem.* **1985**, *50*, 2198–2200.
- (17) Nicolaou, K.; Reddy, K.; Skokotas, G.; Sato, F.; Xiao, X.; Hwang, C. Total Synthesis of Hemibrevetoxin B and (7a.α)-Epi-Hemibrevetoxin B. *J. Am. Chem. Soc.* **1993**, *115*, 3558–3575.
- (18) Jubault, P.; Quirion, J.; Lemonnier, G.; Lion, C. Preparation of Fluorinated Cyclopropane Analogs of Glutamic Acid as MGLuR4 Modulators Useful in the Treatment of Neurological Diseases. WO2011009947, 2011.
- (19) Corey, E.; Suggs, J. Pyridinium Chlorochromate. An Efficient Reagent for Oxidation of Primary and Secondary Alcohols to Carbonyl Compounds. *Tetrahedron Lett.* **1975**, *16*, 2647–2650.
- (20) Chong, K. Studies toward a Unified Synthesis of Apoptolidinone C and Glycosylated Variants, Vanderbilt University, 2017.
- (21) Anelli, P.; Montanari, F.; Quici, S. A GENERAL SYNTHETIC METHOD FOR THE OXIDATION OF PRIMARY ALCOHOLS TO ALDEHYDES: (S)-(+)-2-METHYLBUTANAL. *Org. Syn.* **1990**, *69*, 212.
- (22) Mastalerz, H.; Zhang, G.; Kadow, J.; Fairchild, C.; Long, B.; Vyas, D. Synthesis of 7β-Sulfur Analogues of Paclitaxel Utilizing a Novel Epimerization of the 7α-Thiol Group. *Org. Lett.* **2001**, *3*, 1613–1615.
- (23) Stewart, A.; Meier, K.; Schulz, B.; Steinert, M.; Snider, B. Synthesis and Biological Evaluation of (±)-Dinemasone C and Analogues. *J. Org. Chem.* **2010**, *75*, 6057–6060.
- (24) Lee, A.; Martin, V.; Masamune, S.; Sharpless, B.; Walker, F. Synthesis of Saccharides and Related Polyhydroxylated Natural Products. 3. Efficient Conversion of 2,3-Erythro-Aldoses to 2,3-Threo-Aldoses. *J. Am. Chem. Soc.* **1982**, *104*, 3515–3516.
- (25) Servi, S. 2,2,5-Trimethyl-1,3-Dioxolane-4-Carboxaldehyde as a Chiral Synthon: Synthesis of the Two Enantiomers of Methyl 2,3,6-Trideoxy-α-L-Threo-Hex-2-Enopyranoside, Key Intermediate in the Synthesis of Daunosamine, and of (+)- and (-)-Rhodnose. *J. Org. Chem.* **1985**, *50*, 5865–5867.
- (26) Ko, S.; Lee, A.; Masamune, S.; Reed, L.; Sharpless, K.; Walker, F. Total Synthesis of the L-Hexoses. *Tetrahedron* **1990**, *46*, 245–264.
- (27) Naef, R.; Seebach, D. Direct Diastereoselective Alkylation of Tartaric Acid Through an Enolate. *Angew. Chem. Int. Ed. Engl.* **1981**, *20*, 1030–1031.
- (28) Wenkert, E.; Guo, M.; Lavilla, R.; Porter, B.; Ramachandran, K.; Sheu, J. Polyene Synthesis. Ready Construction of Retinol-Carotene Fragments, (+)-6(E)-LTB₃ Leukotrienes, and Corticocin. *J. Org. Chem.* **1990**, *55*, 6203–6214.
- (29) Sivák, I.; Václav, J.; Berkeš, D.; Kolarovič, A. Straightforward Synthesis of Functionalized (E)-3-Acylacrylic Acids. *Tetrahedron* **2015**, *71*, 8876–8884.
- (30) Blanchette, M.; Choy, W.; Davis, J.; Essinfeld, A.; Masamune, S.; Roush, W.; Sakai, T. Horner-Wadsworth-Emmons Reaction: Use of Lithium Chloride and an Amine for Base-Sensitive Compounds. *Tetrahedron Lett.* **1984**, *25*, 2183–2186.
- (31) Marshall, J.; DuBay, W. Synthesis of the Pseudopterane and Furanocembrane Ring Systems by Intraannular Cyclization of β- and γ-Alkynyl Allylic Alcohols. *J. Org. Chem.* **1994**, *59*, 1703–1708.

- (32) Huang, Z.; Negishi, E. A Convenient and Genuine Equivalent to HZrCp₂Cl Generated in Situ from ZrCp₂Cl₂-DIBAL-H. *Org. Lett.* **2006**, *8*, 3675–3678.
- (33) Hanzawa, Y.; Tabuchi, N.; Taguchi, T. Palladium-Catalyzed Acylation Reactions of Alpha,Beta-Unsaturated Ketones with Acylzirconocene Chloride: Remarkable Control of 1,2- and 1,4-Selectivity by the Catalyt. *Tetrahedron Lett.* **1998**, *39*, 8141–8144.
- (34) Hanzawa, Y.; Tabuchi, N.; Taguchi, T. Palladium-Catalyzed Reactions of Acylzirconocene Chloride with Organic Halides. *Tetrahedron Lett.* **1998**, *39*, 6249–6252.
- (35) Kakuuchi, A.; Taguchi, T.; Hanzawa, Y. Formation of Alpha-Amino Ketones: Addition of Acylzirconocene Chlorides to Imines Catalyzed by Yb(OTf)₃/TMSOTf and Brønsted Acids and Three-Component Reactions of Acylzirconocene Chlorides, Aldehydes, and Amines. *Eur. J. Org. Chem.* **2003**, 116–122.
- (36) Wu, X.; Neumann, H.; Beller, M. Palladium-Catalyzed Carbonylative Coupling Reactions between Ar-X and Carbon Nucleophiles. *Chem. Soc. Rev.* **2011**, *40*, 4986–5009.
- (37) Moss, M.; Han, X.; Ready, J. Zirconocene-Mediated Carbonylative Coupling of Grignard Reagents. *Angew. Chem. Int. Ed.* **2016**, *55*, 10017–10021.
- (38) Hu, T.; Panek, J. Total Synthesis of (-)-Motuporin. *J. Org. Chem.* **1999**, *64*, 3000–3001.
- (39) Ni, Y.; Amarasinghe, K.; Ksebati, B.; Montgomery, J. First Total Synthesis and Stereochemical Definition of Isodomoic Acid G. *Org. Lett.* **2003**, *5*, 3771–3773.
- (40) Dupont, J.; Donato, A. A Concise Synthesis of (S)-(+)-5,6-2H-Pyran-2-One via Hydrozirconation-Carbonylation-Demetallation of O-Benzyl (S)-(-)-4-Pentyn-2-Ol. *Tetrahedron Asymmetry* **1998**, *9*, 949–954.
- (41) Verlhac, J.; Chanson, E.; Jousseau, B.; Quintard, J. A Versatile Access to Unsymmetrical and Symmetrical Alpha-Diketones via Organotin Reagents. *Tetrahedron Lett.* **1985**, *26*, 6075–6078.
- (42) Corey, E.; Kim, C. A Method for the Oxidation of Sec,Tert -1,2-Diols to α -Hydroxy Ketones without Carbon-Carbon Cleavage. *Tetrahedron Lett.* **1974**, *15*, 287–290.
- (43) Grieco, P.; Collins, J.; Moher, E.; Fleck, T.; Gross, R. Synthetic Studies on Quassinoids: Total Synthesis of (-)-Chaparrinone, (-)-Glaucarubolone, and (+)-Glaucarubinone. *J. Am. Chem. Soc.* **1993**, *115*, 6078–6093.
- (44) Fernandes, R.; Kattanguru, P. Step-Economic and Protecting-Group-Free Total Synthesis of (+)-Cardiobutanolide. *Asian J. Org. Chem.* **2013**, *2*, 74–84.
- (45) Krishna, R.; Kumar, E. Olefin Cross-Metathesis Based Approach for the Stereoselective Total Synthesis of (+)-Cardiobutanolide. *Tetrahedron Lett.* **2009**, *50*, 6676–6679.
- (46) Andrey, O.; Sperry, J.; Larsen, U. Brimble, M. An Approach to an Enantioselective Synthesis of Crisamicin A via a Novel Double Hauser–Kraus Annulation Strategy. *Tetrahedron* **2008**, *64*, 3912–3927.
- (47) Armarego, W.; Chai, C. *Purification of Laboratory Chemicals*, 6th ed.; Elsevier Inc., 2009.

- (48) Bock, K.; Lundt, I.; Pedersen, C.; Sonnichsen, R. D-Glycero-D-Gulo-Heptono-1,4-Lactone as a Precursor for the Synthesis of Deoxyheptonolactones and Anhydroheptonolactones. *Carbohydr. Res.* **1988**, *174*, 331–340.
- (49) Ramakrishna, G.; Fernandes, R. Total Synthesis of the Sensitive Triyne Natural Product (4S,5S)-4,8-Dihydroxy-3,4-Dihydrovernoniynone and All of Its Stereoisomers. *Org. Lett.* **2019**, *21*, 5827–5831.
- (50) Yamashita, S.; Iso, K.; Kitajima, K.; Himuro, M.; Hiramata, M. Total Synthesis of Cortistatins A and J. *J. Org. Chem.* **2011**, *76*, 2408–2425.
- (51) Hirai, S.; Utsugi, M.; Iwamoto, M.; Nakada, M. Formal Total Synthesis of (–)-Taxol through Pd-Catalyzed Eight-Membered Carbocyclic Ring Formation. *Chem. Eur. J.* **2015**, *21*, 355–359.
- (52) Towson, J.; Weismiller, M.; Lal, G.; Sheppard, A.; Kumar, A.; Davis, F. (+)-(2R,8aS)-10-(CAMPHORYSULFONYL)OXAZIRIDINE. *Org. Syn.* **1990**, *69*, 158.
- (53) Nakamura, A.; Nakada, M. Allylic Oxidations in Natural Product Synthesis. *Synthesis (Stuttg)* **2013**, *45*, 1421–1451.
- (54) Kozak, J.; Dake, G. Total Synthesis of (+)-Fawcettidine. *Angew. Chem. Int. Ed.* **2008**, *47*, 4221–4223.
- (55) Zou, Y.; Chen, C.; Taylor, C.; Foxman, B.; Snider, B. Formal Synthesis of (±)-Platensimycin. *Org. Lett.* **2007**, *9*, 1825–1828.
- (56) Paterson, I.; Findlay, A.; Florence, G. Total Synthesis and Stereochemical Reassignment of (+)-Dolastatin 19. *Org. Lett.* **2006**, *8*, 2131–2134.
- (57) Paterson, I.; Coster, M.; Chen, D.; Oballa, R.; Wallace, D.; Norcross, R. The Stereocontrolled Total Synthesis of Althohyrtin A/Spongistatin 1: The AB-Spiroacetal Segment. *Org. Biomol. Chem.* **2005**, *3*, 2399–2409.
- (58) Hormuth, S.; Reissig, H. Stereoselective Synthesis of 3(2H)-Dihydrofuranones by Addition of Lithiated Methoxyallene to Chiral Aldehydes. *J. Org. Chem.* **1994**, *59*, 67–73.
- (59) Brasholz, M.; Dugovic, B.; Reissig, H. 3-Alkoxy-2,5-Dihydrofurans by Gold-Catalyzed Allenyl Cyclizations and Their Transformation into 1,4-Dicarbonyl Compounds, Cyclopentenones, and Butenolides. *Synthesis (Stuttg)* **2010**, *22*, 3855–3864.
- (60) Lambert, C.; Schleyer, P.; Wurthwein, E. Experimental and Theoretical Investigations on the Structure and Reactivity of α -Lithiomethoxyallene and Its Grignard Analog. *J. Org. Chem.* **1993**, *58*, 6377–6389.
- (61) Snieckus, V. Directed Ortho Metalation. Tertiary Amide and O-Carbamate Directors in Synthetic Strategies for Polysubstituted Aromatics. *Chem. Rev.* **1990**, *90*, 879–933.
- (62) Pettersen, D.; Amedjkouh, M.; Lill, S.; Ahlberg, P. On the Novel Function of the Additive DBU. Catalytic Deprotonation by a Mixed Dimer of Lithiated DBU and a Chiral Lithium Amide. *J. Chem. Soc., Perkin Trans. 2* **2002**, 1397–1405.
- (63) Imamoto, T.; Kusumoto, T.; Tawarayama, Y.; Sugiura, Y.; Mita, T.; Hatanaka, Y.; Yokoyama, M. Carbon-Carbon Bond-Forming Reactions Using Cerium Metal or Organocerium(III) Reagents. *J. Org. Chem.* **1984**, *49*, 3904–3912.

- (64) Greeves, N.; Lyford, L. Ultrasound Assisted Preparation of Organocerium Reagents. *Tetrahedron Lett.* **1992**, *33*, 4759–4760.
- (65) Takeda, K.; Nakajima, A.; Takeda, M.; Yoshii, E. Discussion Addendum for: [3 + 4] Annulation Using a [Beta-(Trimethylsilyl) Acryloyl]Silane and the Lithium Enolate of an Alpha,Beta-Unsaturated Methyl Ketone: (1R,6S,7S)-4-(Tert-Butyldimethylsiloxy)-6- (Trimethylsilyl)Bicyclo [5.4.0]Undec-4-En-2-One. *Org. Syn.* **1999**, *76*, 199.
- (66) Ricci, A.; Degl'Innocenti, A.; Capperucci, A.; Reginato, G.; Mordini, A. Synthesis and Reactivity of Propenoylstannanes. *Tetrahedron Lett.* **1991**, *32*, 1899–1900.
- (67) Reich, H. Role of Organolithium Aggregates and Mixed Aggregates in Organolithium Mechanisms. *Chem. Rev.* **2013**, *113*, 7130–7178.
- (68) Soderquist, J.; Hassner, A. Sila- and Germacyclopentan-2-Ones from Metallated Enol Ethers. *J. Org. Chem.* **1980**, *45*, 541–543.
- (69) Benbow, J.; McClure, K.; Danishefsky, S. Intramolecular Cycloaddition Reactions of Dienyl Nitroso Compounds: Application to the Synthesis of Mitomycin K. *J. Am. Chem. Soc.* **1993**, *115*, 12305–12314.
- (70) Melikyan, G.; Tosunyan, A.; Babayan, É.; Atanesyan, K.; Badanyan, S. Chemistry and Synthetic Potential of the Reactions of 3-Chloro-1,3-Alkadien-5-Ones with Sodium Methoxide. *J. Org. Chem. USSR (Engl. Transl.)* **1991**, *27* (10), 1802–1807.
- (71) Hu, J.; Jia, Z.; Xu, K.; Ding, H. Total Syntheses of (+)-Stemarin and the Proposed Structures of Stemara-13(14)-En-18-Ol and Stemara-13(14)-En-17-Acetoxy-18-Ol. *Org. Lett.* **2020**, *22*, 1426–1430.
- (72) Smith, A.; Adams, C. Evolution of Dithiane-Based Strategies for the Construction of Architecturally Complex Natural Products. *Acc. Chem. Res.* **2004**, *37*, 365–377.
- (73) Lehn, J.; Wipff, G. Stereoelectronic Properties, Stereospecificity, and Stabilization of Alpha-Oxa and Alpha-Thia Carbanions. *J. Am. Chem. Soc.* **1976**, *98*, 7498–7505.
- (74) Seebach, D.; Gabriel, J.; Hässig, R. Low-Temperature ¹³C-NMR Spectra of ⁶Li- and ¹³C-Labelled Sulfur- and Selenium-Substituted Organolithium Derivatives. *Helv. Chim. Acta* **1984**, *67*, 1083–1099.
- (75) Anderson, K.; Atkinson, S.; Fujiwara, T.; Giles, M.; Matsumoto, T.; Merifield, E.; Singleton, J.; Saito, T.; Sotoguchi, T.; Tornos, J.; Way, E. Routes for the Synthesis of (2S)-2-Methyltetrahydropyran-4-One from Simple Optically Pure Building Blocks. *Org Process Res Dev* **2010**, *14*, 58–71.
- (76) Nicolaou, K.; Montagnon, T.; Baran, P. HIO₃ and I₂O₅: Mild and Selective Alternative Reagents to IBX for the Dehydrogenation of Aldehydes and Ketones. *Angew. Chem. Int. Ed.* **2002**, *41*, 1386–1389.
- (77) Jackson, K.; Henderson, J.; Motoyoshi, H.; Phillips, A. A Total Synthesis of Norhalichondrin B. *Angew. Chem. Int. Ed.* **2009**, *48*, 2346–2350.
- (78) Stewart, I.; Douglas, C.; Grubbs, R. Increased Efficiency in Cross-Metathesis Reactions of Sterically Hindered Olefins. *Org. Lett.* **2008**, *10*, 441–444.
- (79) Chatterjee, A.; Choi, T.; Sanders, D.; Grubbs, R. A General Model for Selectivity in Olefin Cross Metathesis. *J. Am. Chem. Soc.* *2003*, *125*, 11360-11370. **2003**, *125*, 11360–11370.

General Experimental Section

All non-aqueous reactions were performed in flame-dried or oven dried round-bottomed flasks under an atmosphere of argon. Stainless steel syringes or cannula were used to transfer air- and moisture-sensitive liquids. Reaction temperatures were controlled using a thermocouple thermometer and analog hotplate stirrer. Reactions were conducted at room temperature (rt, approximately 23 °C) unless otherwise noted. Flash column chromatography was conducted using silica gel 230-400 mesh. Analytical thin-layer chromatography (TLC) was performed on E. Merck silica gel 60 F254 plates and visualized using UV, and *p*-anisaldehyde stain. Yields were reported as isolated, spectroscopically pure compounds.

Solvents were obtained from an MBraun MB-SPS solvent system. Commercial reagents were used as received unless otherwise noted. Purification of reagents was followed according to the *Purification of Laboratory Chemicals* (2009) or the Encyclopedia of Reagents for Organic Synthesis. The molarity of *n*-butyllithium solutions was determined by titration using diphenylacetic acid as an indicator (average of three determinations).

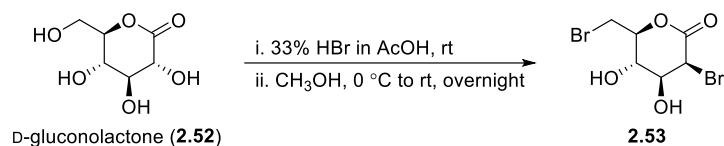
Semi-preparative reverse phase HPLC was conducted on a Waters HPLC system using a Phenomenex Luna 5 μm C18(2) 100A Axia 250 x 10.00 mm column or preparative reverse phase HPLC (Gilson) using a Phenomenex Luna column (100 Å, 50 x 21.20 mm, 5 μm C18) with UV/Vis detection. Infrared spectra were obtained as thin films on NaCl plates using a Thermo Electron IR100 series instrument and are reported in terms of frequency of absorption (cm^{-1}). ^1H NMR spectra were recorded on Bruker 400 or 600 MHz spectrometers and are reported relative to deuterated solvent signals. Data for ^1H NMR spectra are reported as follows: chemical shift (δ ppm), multiplicity (s = singlet, d = doublet, t = triplet, q = quartet, p = pentet, m = multiplet, br = broad, app = apparent), coupling constants (Hz), and integration. ^{13}C NMR spectra were recorded on Bruker 100 or 150 MHz spectrometers and are reported relative to deuterated solvent signals. LC/MS was conducted and recorded on an Agilent Technologies 6130 Quadrupole instrument.

Activation of Zinc. Commercial coarse zinc powder (50.0 g) was stirred in 2% HCl (125 mL) for 1 min, (then the acid was removed by filtration), and washed in a beaker with 2% HCl (125 mL), H_2O (3 x 42 mL), EtOH (2 x 84 mL), and Et_2O (84 mL). (Each wash solution was removed by filtration.) The material was dried under vacuum overnight and used the next day.

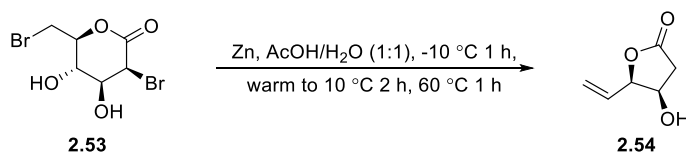
Purification of TMEDA. TMEDA was refluxed over calcium hydride for 2 h and distilled immediately prior to use.

Purification of DBU. DBU was dried over KOH and distilled under vacuum immediately prior to use.

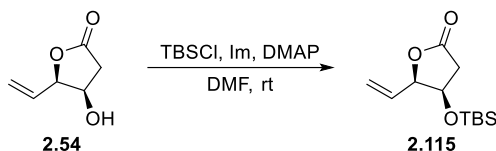
Compound Preparation: Chemical Synthesis



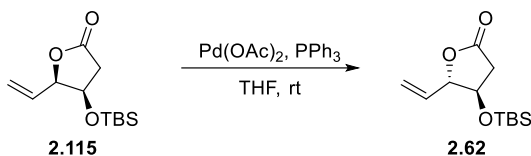
Dibromosugar 2.53 Hydrobromic acid (33% in acetic acid, 240 mL, 1.3 mol) was added to D-glucono-1,5-lactone (**2.52**) (32 g, 180 mmol). The solution was stirred at room temperature for 1 h, cooled to 0 °C, and methanol (960 mL) was added slowly over 5 min. The reaction was allowed to warm to room temperature and maintained overnight. The reaction mixture was concentrated *in vacuo*, and co-concentrated *in vacuo* with water (150 mL). The syrupy residue was dissolved in water (400 mL), and the aqueous solution was extracted with EtOAc (8 x 500 mL), the combined organic extracts were dried (Na₂SO₄), filtered, and concentrated *in vacuo* to afford 54 g of crude **2.53** as a viscous, orange oil.⁴⁸ The crude product **2.53** was carried forward into the next reaction without further purification. ¹H NMR (400 MHz, CD₃OD): δ 5.14 (d, *J* = 4.5 Hz, 1H), 4.52 (dd, *J* = 4.2, 3.0 Hz, 1H), 4.43 (dd, *J* = 9.0, 2.9 Hz, 1H), 4.16 (ddd, *J* = 8.3, 5.3, 2.5 Hz, 1H), 3.77 – 3.70 (m, 1H), 3.64 – 3.55 (m, 1H); ¹³C NMR (100 MHz, CD₃OD): δ 172.9, 82.9, 70.6, 68.1, 49.2, 37.8.



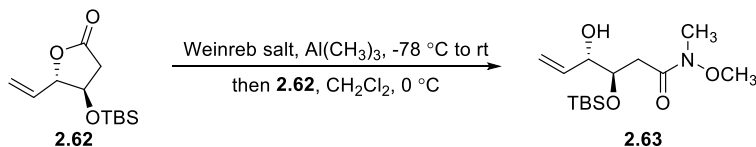
Lactone 2.54 Crude dibromosugar **2.53** (34 g, 110 mmol) was dissolved in 50% aqueous acetic acid (79 mL), cooled to -10 °C, and activated coarse zinc powder⁴⁴ (40 g, 0.61 mol, 5.5 equiv) was added in 6 portions every 10 min. The mixture was allowed to warm to 10 °C over 2 h, heated to 60 °C and maintained for 1 h. The reaction mixture was cooled to room temperature for 30 min, diluted with EtOAc (30 mL), filtered through a plug of Celite and washed with EtOAc (5 x 150 mL). The filtrate was concentrated *in vacuo*, dissolved in EtOAc/toluene (1:1, 150 mL) and concentrated *in vacuo*, the process was repeated twice more. The residue was dissolved in EtOAc (30 mL) and diluted with ice water (30 mL). The aqueous layer was extracted with EtOAc (8 x 100 mL), and the combined organic extracts were dried (MgSO₄), filtered, and concentrated *in vacuo*. The residue was purified by flash column chromatography (gradient 40 to 50% EtOAc/hexanes) to afford 5.2 g (36%) of lactone **2.54** as a yellow oil: *R*_f 0.25 (50% EtOAc/hexanes); ¹H NMR (400 MHz, CDCl₃): δ 5.95 (ddd, *J* = 16.7, 10.6, 6.0 Hz, 1H), 5.61 – 5.51 (m, 2H), 4.95 – 4.90 (m, 1H), 4.57 – 4.52 (m, 1H), 2.81 (dd, *J* = 17.6, 5.5 Hz, 1H), 2.63 (dd, *J* = 17.6, 1.3 Hz, 1H) 1.82 (d, 1H, D₂O exchangeable); ¹³C NMR (100 MHz, CDCl₃): δ 175.2, 130.2, 121.1, 84.4, 69.6, 38.7. Spectral data matched published data.⁴⁴



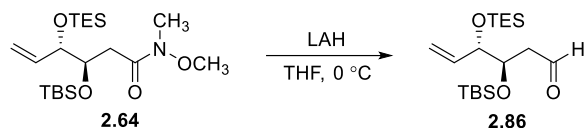
Lactone 2.115 To a solution of lactone **2.54** (4.6 g, 36 mmol, 1 eq) in DMF (36 mL) was added Im (5.4 g, 80 mmol, 2.2 eq), DMAP (0.44 g, 3.6 mmol, 0.10 eq), and TBSCl (6.5 g, 43 mmol, 1.2 eq) respectively. The reaction was allowed to stir overnight at room temperature. The reaction flask was diluted with EtOAc (36 mL), and then quenched with H₂O (36 mL). The aqueous layer was extracted with EtOAc (2 x 80 mL). The combined organic layers were washed with brine (100 mL), dried (MgSO₄), filtered and concentrated *in vacuo*. The crude residue was purified by flash column chromatography (gradient 0 to 20% EtOAc/hexanes) to afford 5.5 g (63%) of the protected lactone **2.115** as a yellow oil: *R_f* 0.30 (20% EtOAc/hexanes); ¹H NMR (400 MHz, CDCl₃): δ 5.98 (ddd, *J* = 17.5, 10.5, 7.2 Hz, 1H), 5.46 – 5.35 (m, 2H), 4.82 – 4.76 (m, 1H), 4.53 – 4.47 (m, 1H), 2.72 (dd, *J* = 17.2, 5.6 Hz, 1H), 2.48 (dd, *J* = 17.4, 2.0 Hz, 1H), 0.88 (s, 9H), 0.061 (s, 3H), 0.056 (s, 3H); ¹³C NMR (100 MHz, CDCl₃): δ 175.3, 132.0, 120.1, 85.6, 70.9, 39.4, 25.8, 18.2, -4.7, -4.8.



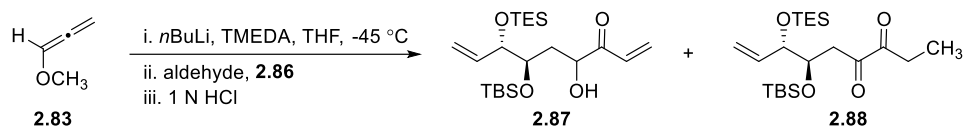
Lactone 2.62 To a solution of lactone **2.115** (5.0 g, 21 mmol) in THF (21 mL) was added PPh₃ (1.1 g, 4.2 mmol, 0.20 equiv) and Pd(OAc)₂ (0.47 g, 2.1 mmol, 0.10 equiv). The reaction was allowed to stir for 6 h at room temperature, filtered through a plug of Celite, and washed with EtOAc (3 x 10 mL). The filtrate was concentrated *in vacuo*, and the residue was purified by flash column chromatography (gradient: 10 to 20% EtOAc/hexanes) to afford 3.0 g (59%) recovered lactone **2.115** as a yellow oil and 1.6 g (32%) of lactone **2.62** as a white solid: *R_f* 0.67 (20% EtOAc/hexanes); ¹H NMR (400 MHz, CDCl₃): δ 5.83 (ddd, *J* = 16.8, 10.7, 5.7 Hz, 1H), 5.41 (d, *J* = 17.2 Hz, 1H), 5.30 (d, *J* = 10.7 Hz, 1H), 4.74 – 4.69 (m, 1H), 4.27 – 4.22 (m, 1H), 2.74 (dd, *J* = 17.4, 6.4 Hz, 1H), 2.43 (dd, *J* = 17.4, 4.2 Hz, 1H), 0.89 (s, 9H), 0.08 (s, 6H); ¹³C NMR (100 MHz, CDCl₃): δ 174.8, 133.1, 118.4, 87.7, 72.8, 37.6, 25.8, 18.1, -4.6, -4.7. Spectral data matched published data.⁴⁹



Weinreb amide 2.63 To a solution of Weinreb salt (2.6 g, 27 mmol, 2.4 eq) in CH₂Cl₂ (27 mL) at -78 °C is added AlMe₃ (13 mL, 27 mmol, 2.4 eq) dropwise. The reaction was allowed to warm to rt for 4 h and 20 min. Then the

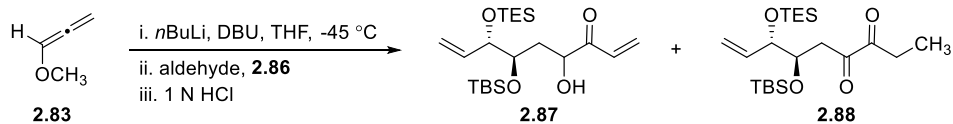


Aldehyde 2.86 To a suspension of LAH (59 mg, 1.6 mmol, 1.3 equiv) in THF (2 mL) at 0 °C was added a solution of Weinreb amide **2.64** (0.50 g, 1.2 mmol) in THF (3 mL). The reaction was stirred at 0 °C for 1 h. The reaction was quenched with saturated aqueous Rochelle salts (5 mL) and stirred for 30 min. The aqueous layer was extracted with EtOAc (3 x 10 mL) and the combined organic layers were dried (MgSO₄), filtered and concentrated *in vacuo*. The crude oil was purified by flash column chromatography (2.5% EtOAc/hexanes) using 1% NEt₃-buffered silica to afford 0.36 g (83%) of aldehyde **2.86** as a clear, yellow oil: *R_f* 0.30 (2.5% EtOAc/hexanes); ¹H NMR (400 MHz, CDCl₃): δ 9.82 (t, *J* = 2.2 Hz, 1H), 5.79 (ddd, *J* = 17.0, 10.3, 6.4 Hz, 1H), 5.26 – 5.14 (m, 2H), 4.11 – 4.03 (m, 2H), 2.61 – 2.43 (m, 2H), 0.94 (t, *J* = 8.0 Hz, 9H), 0.87 (s, 9H), 0.60 (q, *J* = 7.9 Hz, 6H), 0.08 (s, 3H), 0.07 (s, 3H); ¹³C NMR (100 MHz, CDCl₃): δ 201.9, 138.4, 117.1, 78.2, 72.6, 47.4, 26.0, 18.0, 6.9, 5.0, -4.1, -4.7.



Enone 2.87 / 1,2-Dicarbonyl 2.88 To a solution of methoxyallene **2.83** (19 mg, 0.27 mmol, 3.0 equiv) in THF (62 μL) and TMEDA (27 μL, 0.18 mmol, 2.0 equiv) at -45 °C was added *n*BuLi (0.13 mL, 0.18 mmol 2.0 equiv) dropwise. The resulting yellow solution was stirred 20 min. Then, a solution of aldehyde **2.86** (32 mg, 0.089 mmol) in THF (0.25 mL) was added dropwise to the reaction vessel. The reaction was stirred at -45 °C for 1 h. The reaction was quenched with 1N HCl (1 mL). The organic layer was washed with 1N HCl (2 x 2 mL) and the aqueous layer extracted with Et₂O (3 x 5 mL). The combined organic layers were dried (Na₂SO₄), filtered and concentrated *in vacuo*. The crude oil was purified by flash column chromatography (gradient: 0 to 5 % Et₂O/hexanes) with 1% NEt₃-buffered silica to afford 11 mg (34%) of recovered aldehyde **2.86**, 4.5 mg (12%) of enone **2.87**, and 1.0 mg (2.7%) of 1,2-dicarbonyl **2.88**, as clear, yellow oils: **Enone 2.87**: *R_f* 0.29 (10% EtOAc/hexanes); ¹H NMR (600 MHz, CDCl₃): δ 6.48 (dd, *J* = 17.5, 10.5 Hz, 1H), 6.39 (dd, *J* = 17.4, 1.2 Hz, 1H), 5.91 (dd, *J* = 10.5, 1.4 Hz, 1H), 5.86 – 5.76 (m, 1H), 5.18 – 5.10 (m, 2H), 4.56 (ddd, *J* = 7.6, 5.9, 1.9 Hz, 1H), 4.03 – 4.00 (m, 2H), 3.42 (d, 1H, D₂O exchangeable), 1.89 – 1.83 (m, 1H), 1.34 – 1.28 (m, 1H), 0.94 (t, *J* = 8.1 Hz, 9H), 0.93 (s, 9H), 0.60 (q, *J* = 7.7 Hz, 6H), 0.15 (s, 3H), 0.14 (s, 3H); ¹³C NMR (150 MHz, CDCl₃): δ 202.0, 138.0, 131.8, 130.6, 116.5, 78.6, 73.3, 72.0, 38.2, 26.3, 18.5, 7.0, 5.1, -3.6, -4.0. **1,2-Dicarbonyl 2.88**: *R_f* 0.37 (10% EtOAc/hexanes); ¹H NMR (600 MHz, CDCl₃): δ 5.79 (ddd, *J* = 17.2, 10.4, 7.0 Hz, 1H), 5.20 – 5.13 (m, 2H), 4.19 – 4.16 (m, 1H), 3.99 – 3.96 (m, 1H), 2.94 – 2.84 (m, 2H), 2.82 – 2.69 (m, 2H), 1.08 (t, *J* = 7.2 Hz,

3H), 0.93 (t, $J = 8.2$ Hz, 9H), 0.83 (s, 9H), 0.59 (q, $J = 7.9$ Hz, 6H), 0.07 (s, 3H), 0.02 (s, 3H); ^{13}C NMR (150 MHz, CDCl_3): δ 200.1, 198.0, 138.3, 117.1, 78.1, 72.6, 40.7, 29.5, 26.0, 18.2, 7.0, 4.9, -4.0, -4.8.

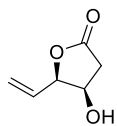


Enone 2.87 / 1,2-Dicarbonyl 2.88 To a solution of methoxyallene **2.83** (20 mg, 0.29 mmol, 3.0 equiv) in THF (62 μL) and DBU (29 μL , 0.19 mmol, 2.0 equiv) at $-45\text{ }^\circ\text{C}$ was added $n\text{BuLi}$ (0.14 mL, 0.19 mmol 2.0 equiv) dropwise. The resulting yellow solution was stirred 20 min. Then, a solution of aldehyde **2.86** (35 mg, 0.097 mmol) in THF (0.25 mL) was added dropwise to the reaction vessel. The reaction was stirred at $-45\text{ }^\circ\text{C}$ for 1 h. The reaction was quenched with 1N HCl (1 mL). The organic layer was washed with 1N HCl (2 x 2 mL) and the aqueous layer extracted with Et_2O (3 x 5 mL). The combined organic layers were dried (Na_2SO_4), filtered and concentrated *in vacuo*. The crude oil was purified by flash column chromatography (gradient: 0 to 5 % Et_2O /hexanes) with 1% NEt_3 -buffered silica to afford 1.8 mg (4.6%) of recovered aldehyde **2.86**, 5.2 mg (13%) of 1,2-dicarbonyl **2.88**, and 8.3 mg (21%) of a mixture of isomers enone **2.87** and 1,2-dicarbonyl **2.88**, as clear, yellow oils: **Enone 2.87**: R_f 0.29 (10% EtOAc /hexanes); ^1H NMR (600 MHz, CDCl_3): δ 6.48 (dd, $J = 17.5, 10.5$ Hz, 1H), 6.39 (dd, $J = 17.4, 1.2$ Hz, 1H), 5.91 (dd, $J = 10.5, 1.4$ Hz, 1H), 5.86 – 5.76 (m, 1H), 5.18 – 5.10 (m, 2H), 4.56 (ddd, $J = 7.6, 5.9, 1.9$ Hz, 1H), 4.03 – 4.00 (m, 2H), 3.42 (d, 1H, D_2O exchangeable), 1.89 – 1.83 (m, 1H), 1.34 – 1.28 (m, 1H), 0.94 (t, $J = 8.1$ Hz, 9H), 0.93 (s, 9H), 0.60 (q, $J = 7.7$ Hz, 6H), 0.15 (s, 3H), 0.14 (s, 3H); ^{13}C NMR (150 MHz, CDCl_3): δ 202.0, 138.0, 131.8, 130.6, 116.5, 78.6, 73.3, 72.0, 38.2, 26.3, 18.5, 7.0, 5.1, -3.6, -4.0. **1,2-Dicarbonyl 2.88**: R_f 0.37 (10% EtOAc /hexanes); ^1H NMR (600 MHz, CDCl_3): δ 5.79 (ddd, $J = 17.2, 10.4, 7.0$ Hz, 1H), 5.20 – 5.13 (m, 2H), 4.19 – 4.16 (m, 1H), 3.99 – 3.96 (m, 1H), 2.94 – 2.84 (m, 2H), 2.82 – 2.69 (m, 2H), 1.08 (t, $J = 7.2$ Hz, 3H), 0.93 (t, $J = 8.2$ Hz, 9H), 0.83 (s, 9H), 0.59 (q, $J = 7.9$ Hz, 6H), 0.07 (s, 3H), 0.02 (s, 3H); ^{13}C NMR (150 MHz, CDCl_3): δ 200.1, 198.0, 138.3, 117.1, 78.1, 72.6, 40.7, 29.5, 26.0, 18.2, 7.0, 4.9, -4.0, -4.8.

Appendix 1

Relevant Spectral Data for Chapter 2

Vasella elimination product



¹H NMR Spectrum of **2.54**

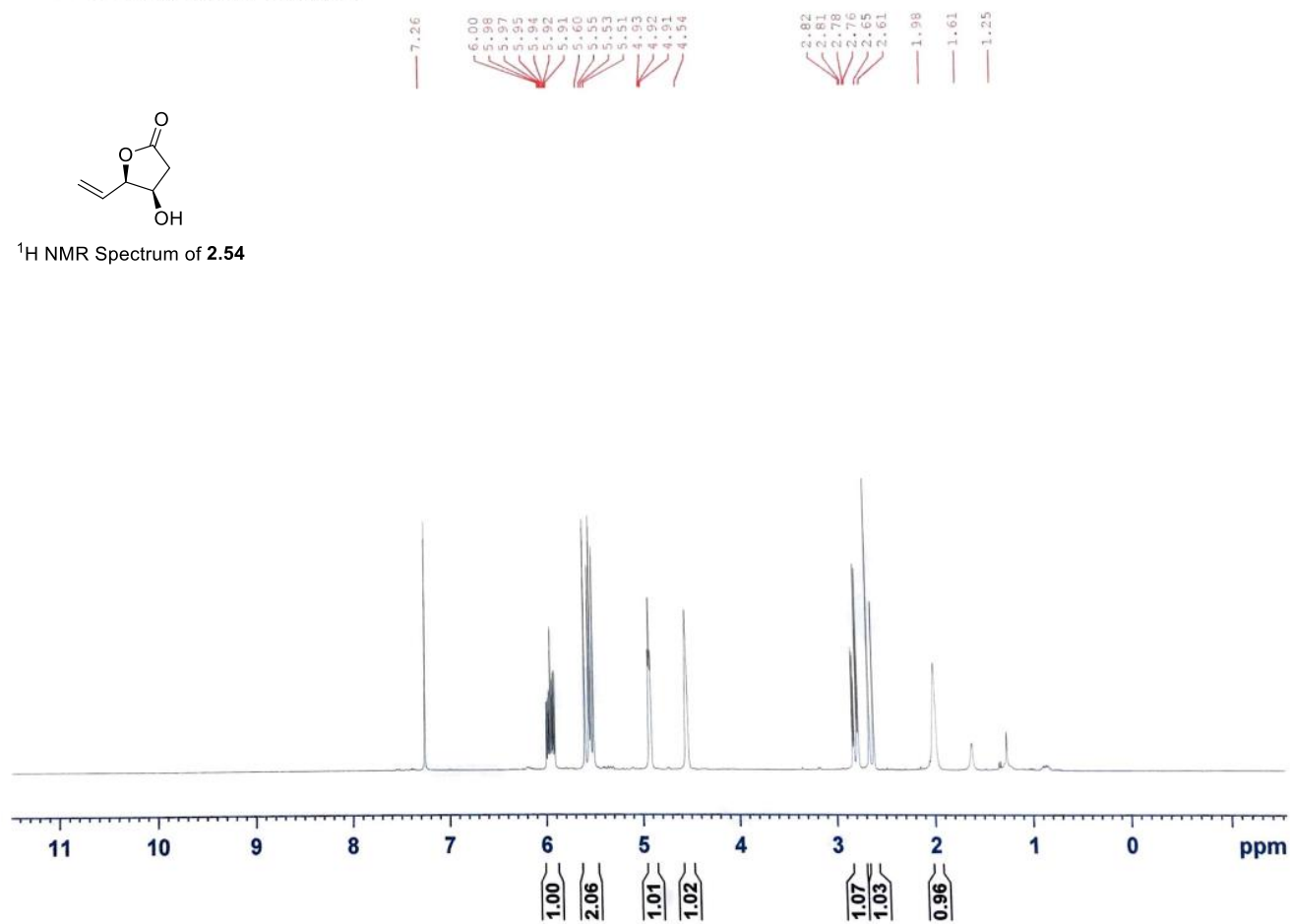


Figure A.2.1. ¹H NMR (400 MHz, CDCl₃) of **2.54**.

Vasella-like Elim

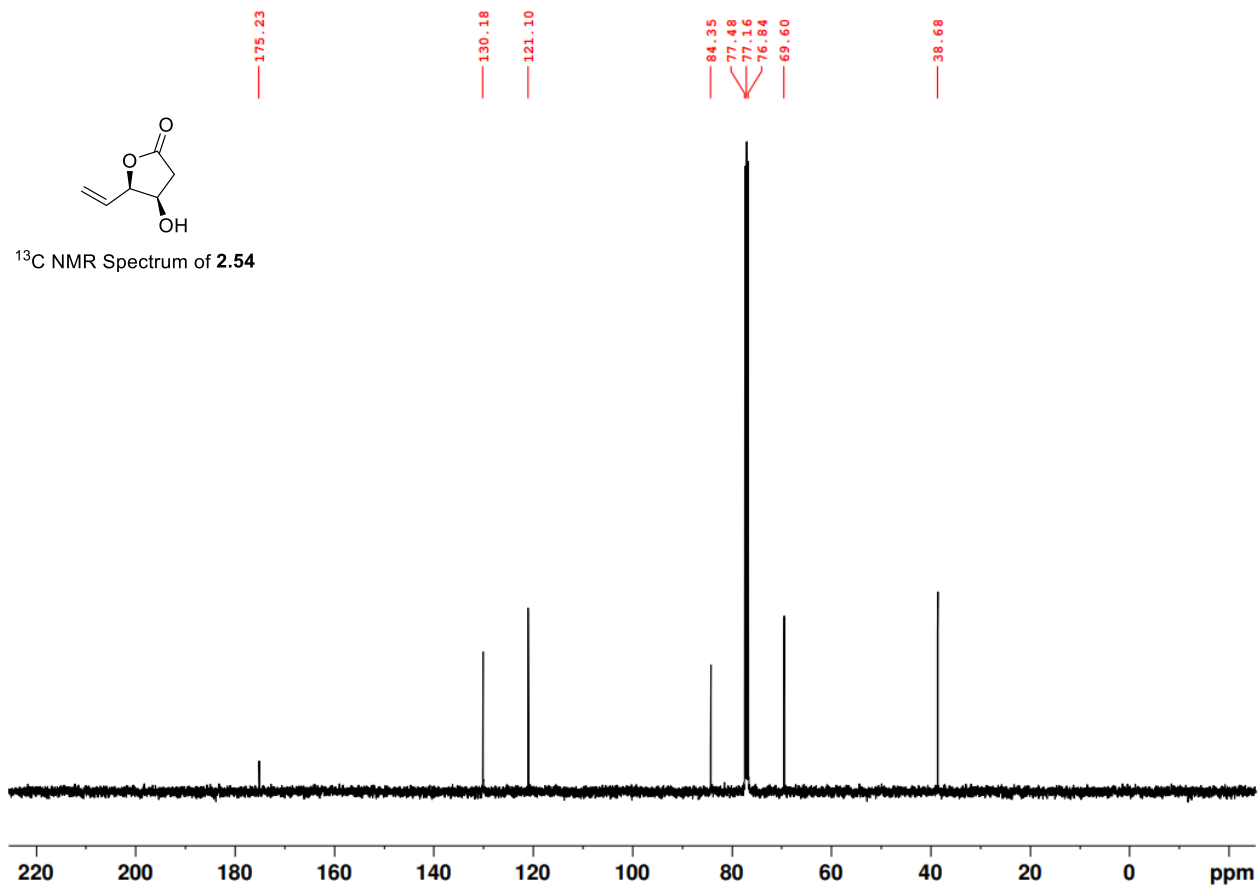


Figure A.2.2. ¹³C NMR (100 MHz, CDCl₃) of 2.54.

Vasella like Elim

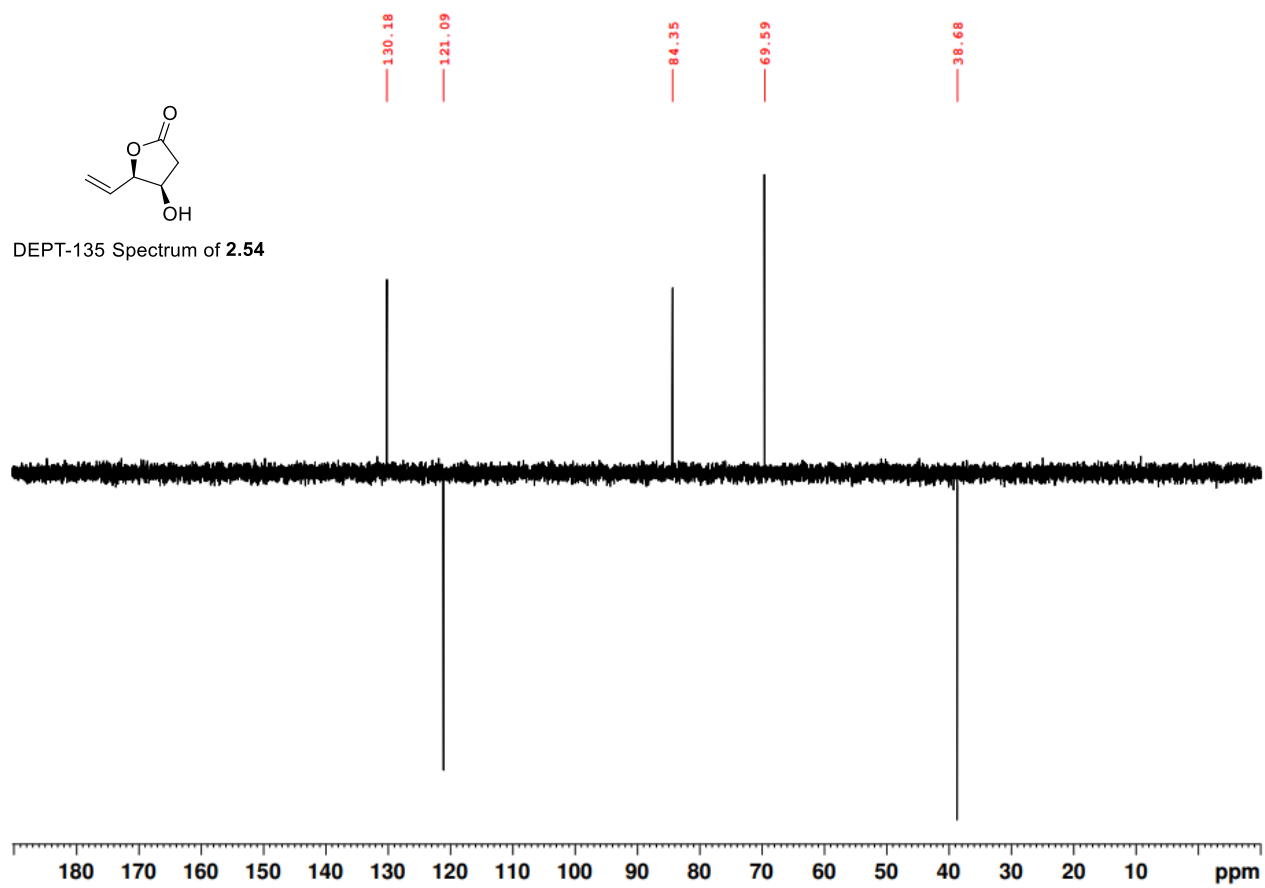
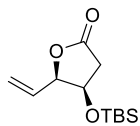


Figure A.2.3. DEPT-135 (100 MHz, CDCl_3) of **2.54**.

TBS lactone



¹H NMR Spectrum of **2.115**

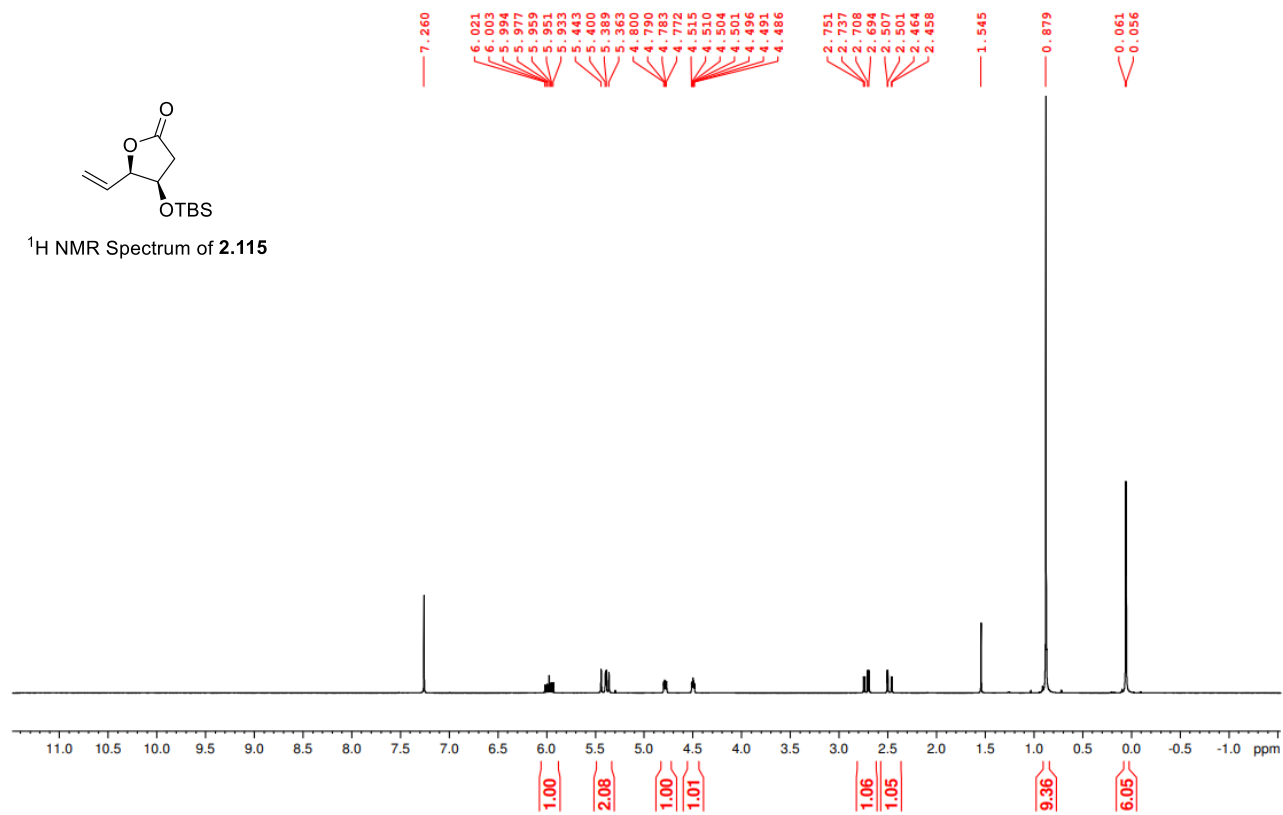


Figure A.2.4. ¹H NMR (400 MHz, CDCl₃) of **2.115**.

TBS lactone

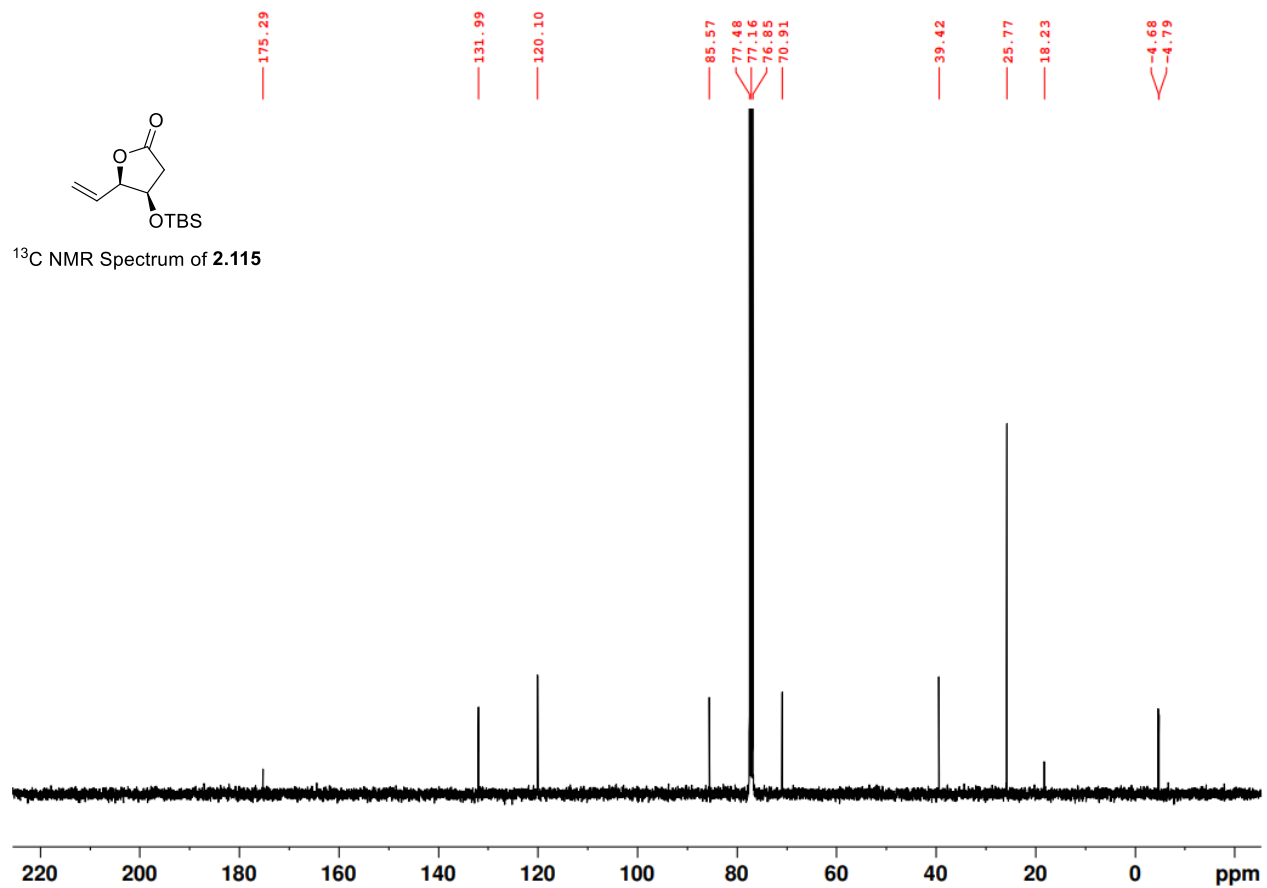
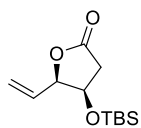


Figure A.2.5. ¹³C NMR (100 MHz, CDCl₃) of 2.115.

TBS lactone



DEPT-135 Spectrum of **2.115**

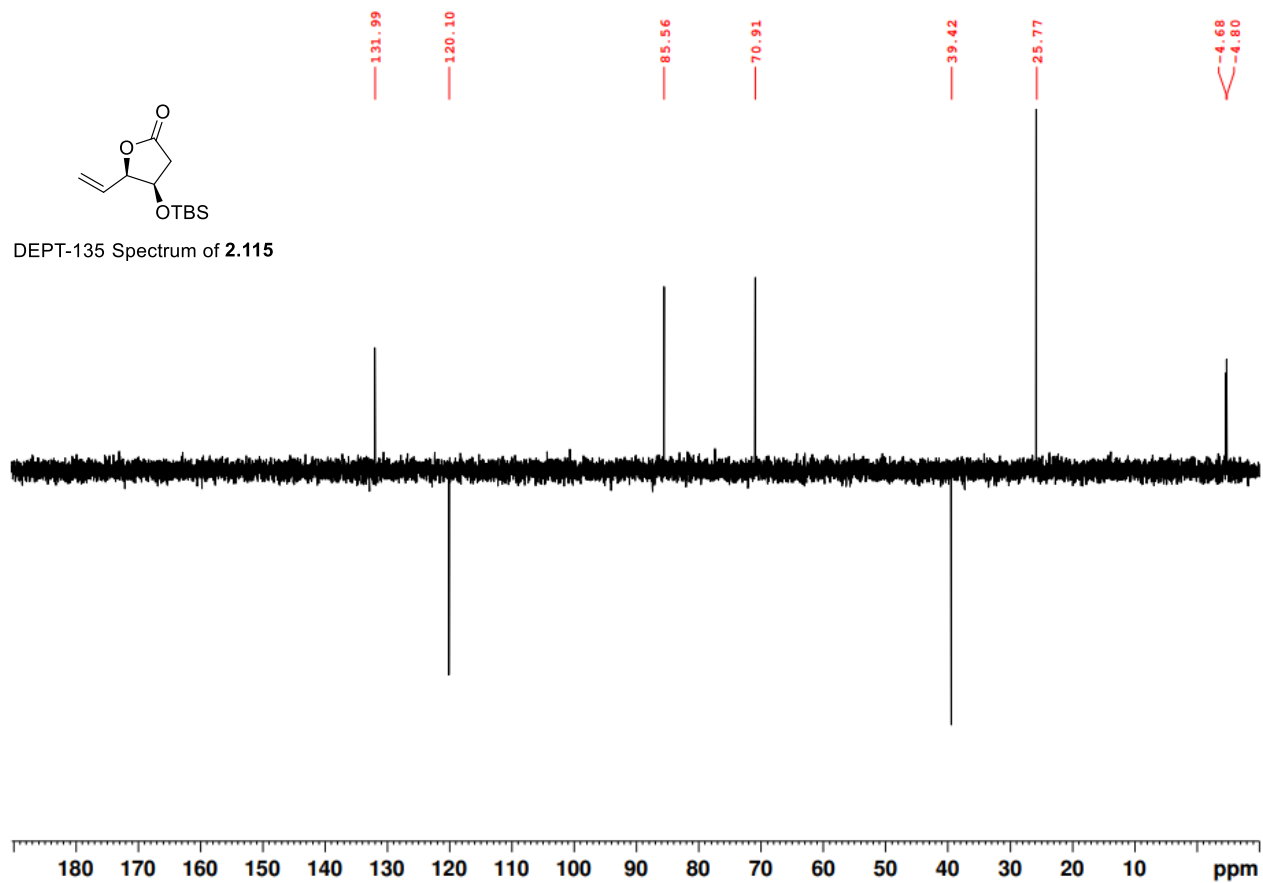


Figure A.2.6. DEPT-135 (100 MHz, CDCl₃) of **2.115**.

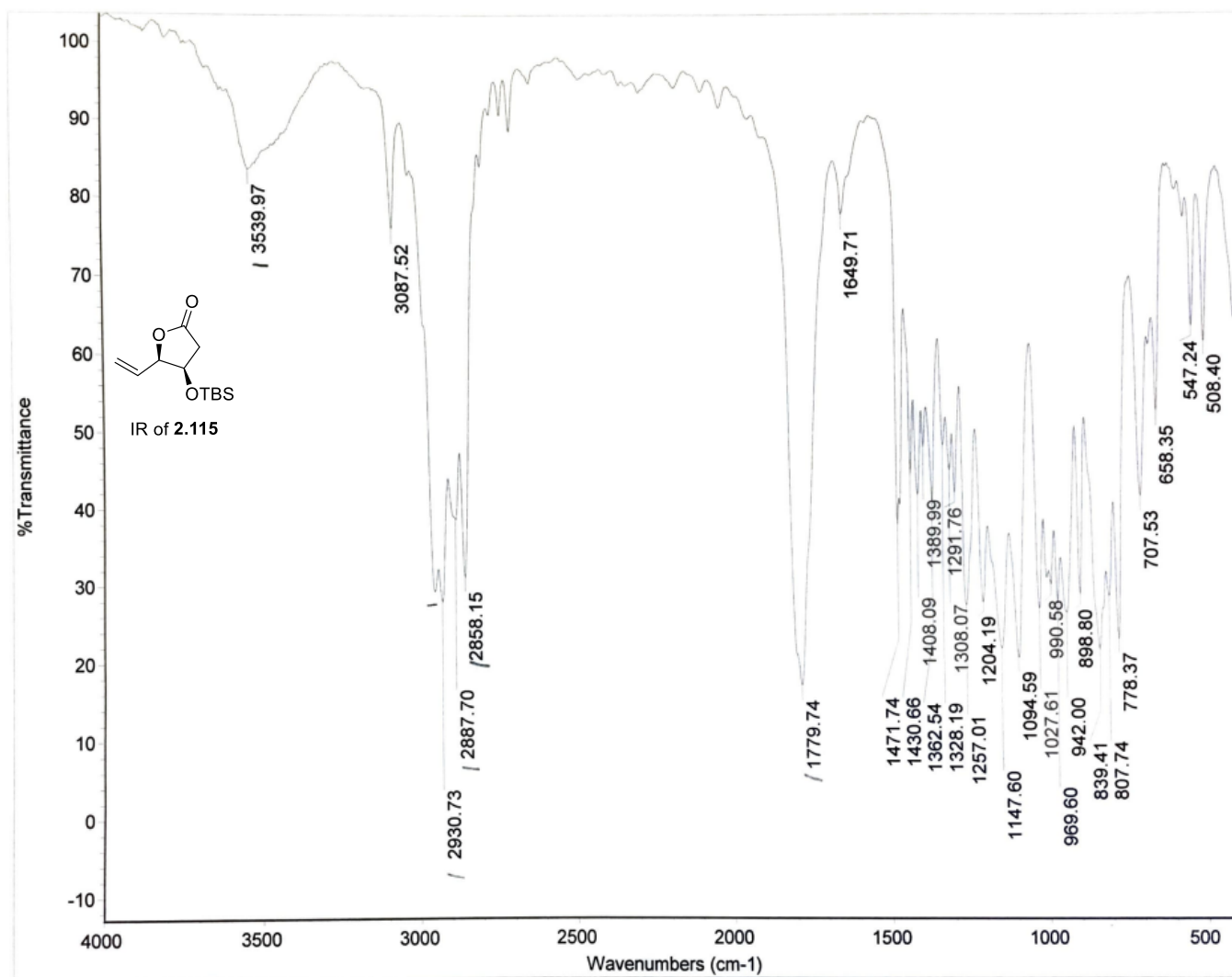


Figure A.2.7. IR of 2.115.

Pd Epimerization

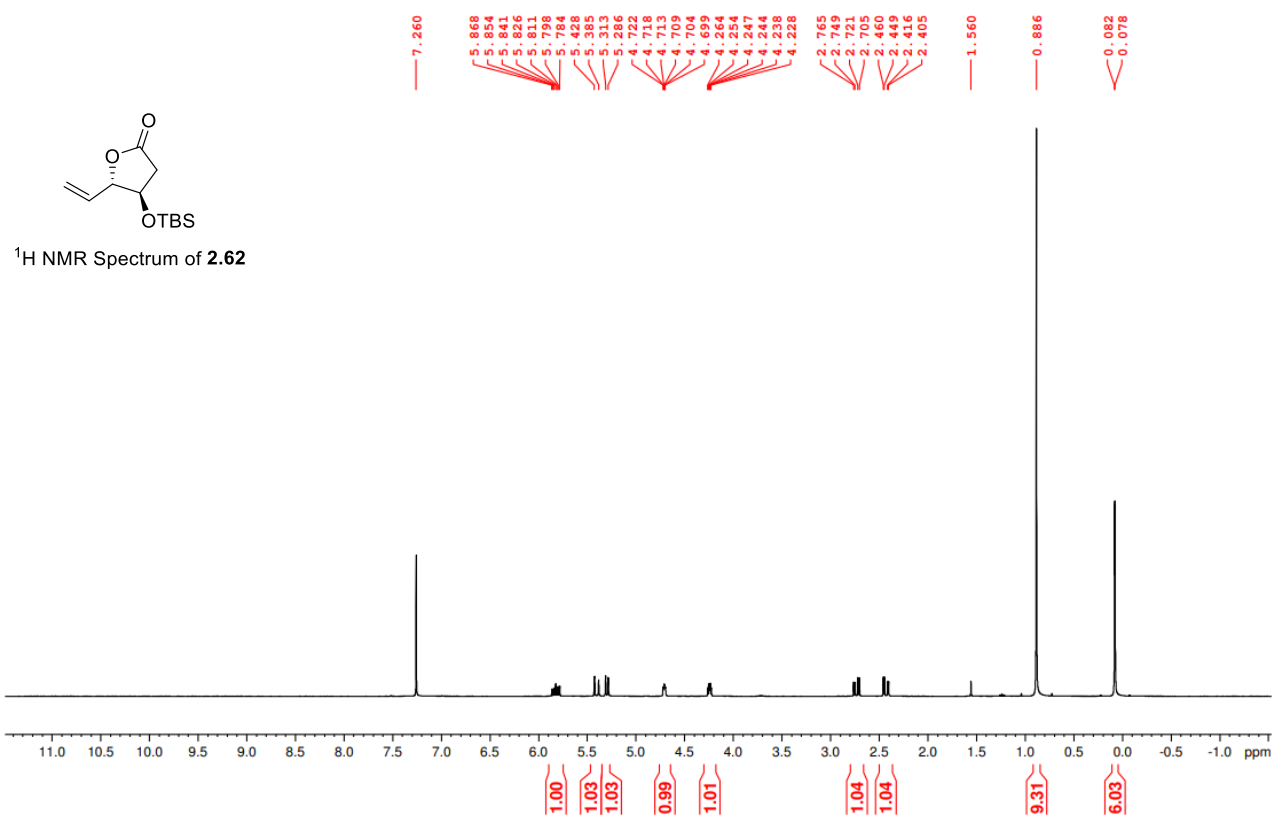


Figure A.2.8. ¹H NMR (400 MHz, CDCl₃) of **2.62**.

Pd Epimerization

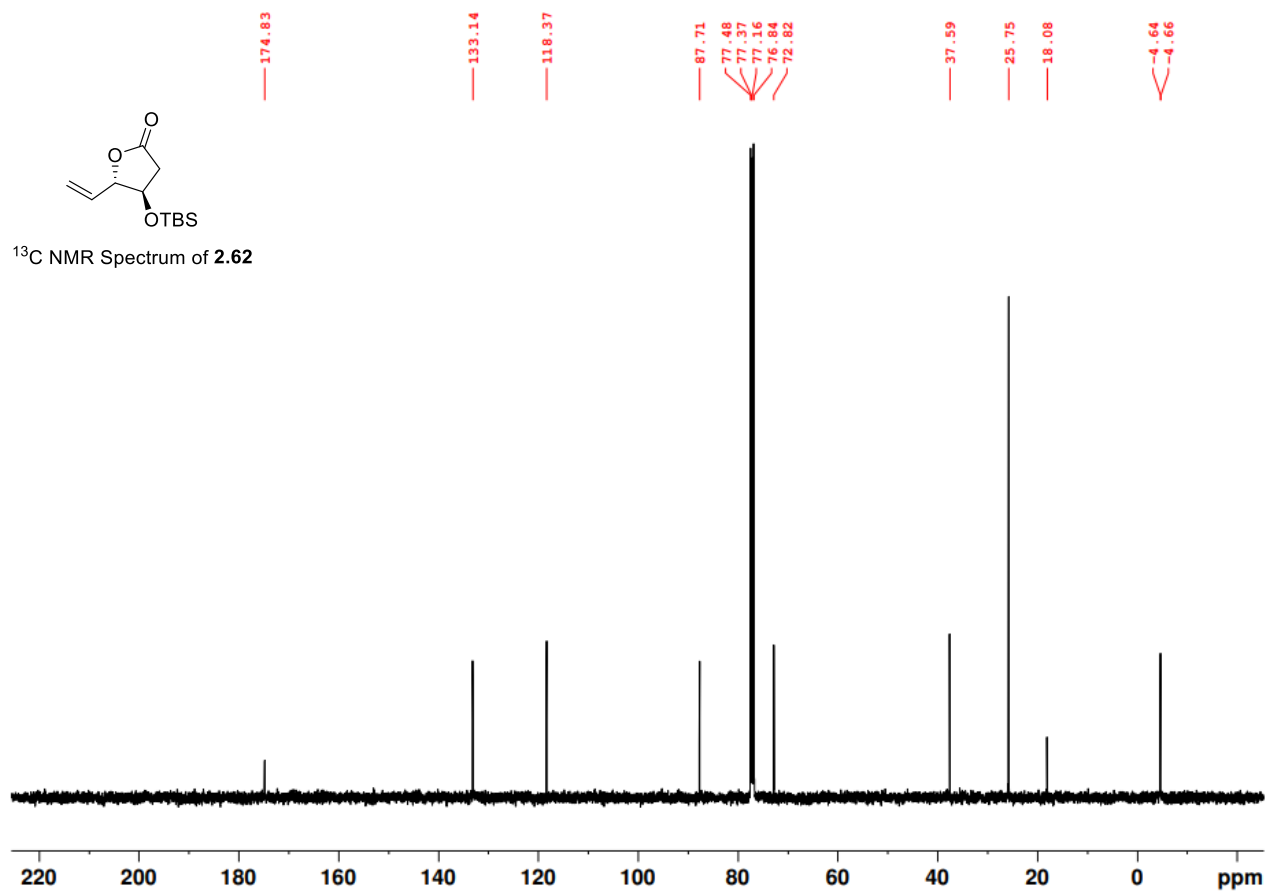


Figure A.2.9. ¹³C NMR (100 MHz, CDCl₃) of 2.62.

Pd Epimerization

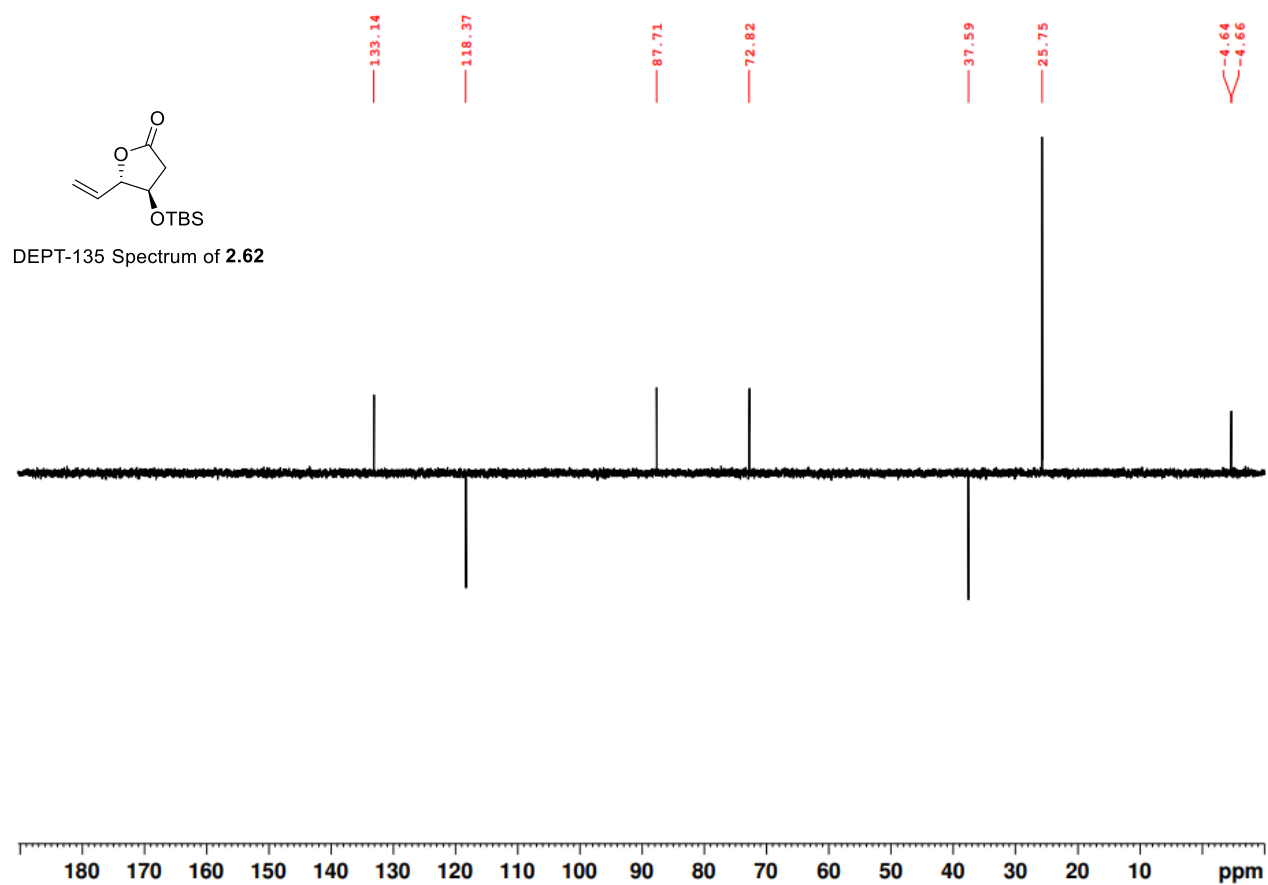


Figure A.2.10. DEPT-135 (100 MHz, CDCl₃) of **2.62**.

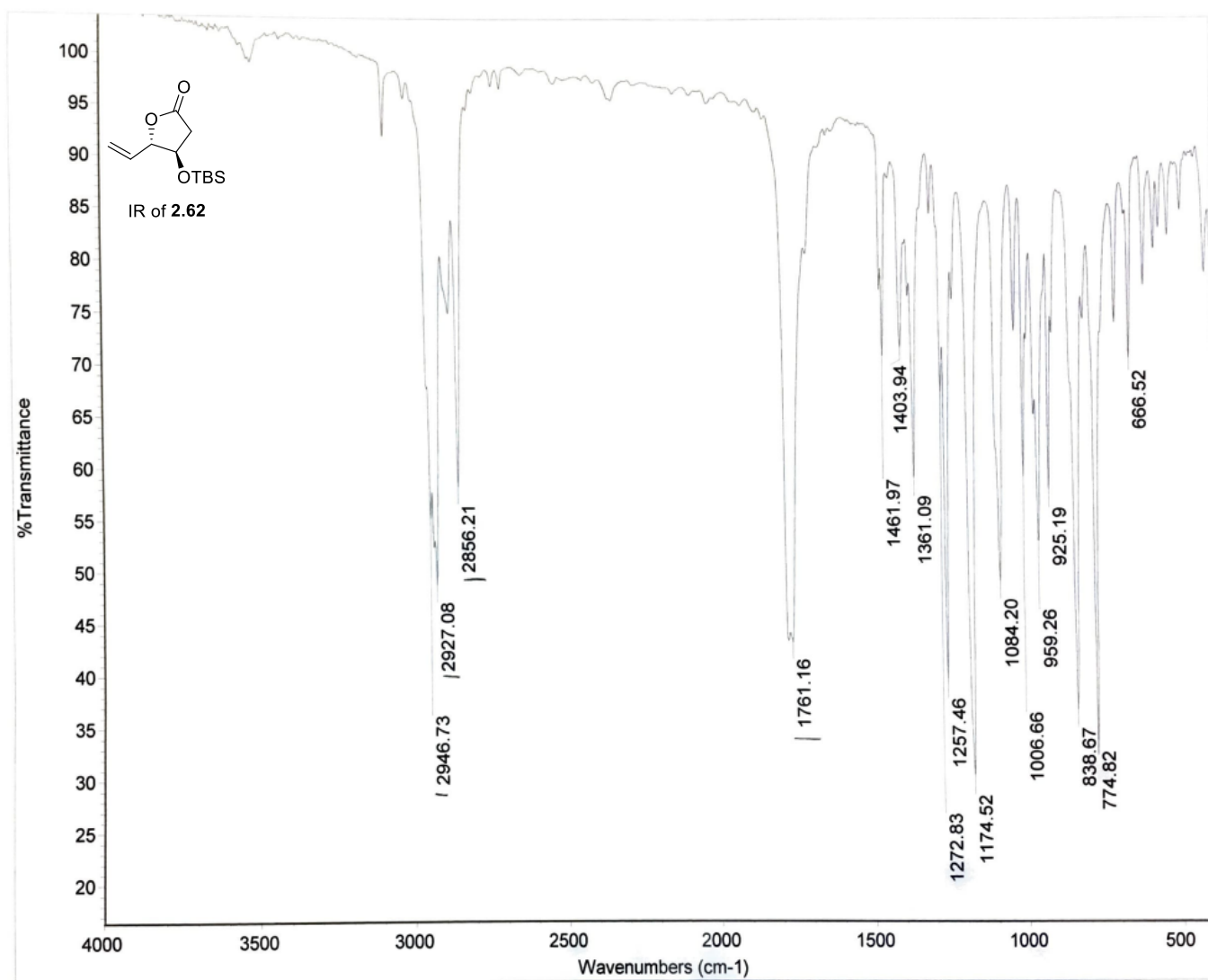
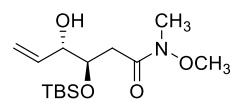


Figure A.2.11. IR of 2.62.

unprotected Weinreb amide



¹H NMR Spectrum of 2.63

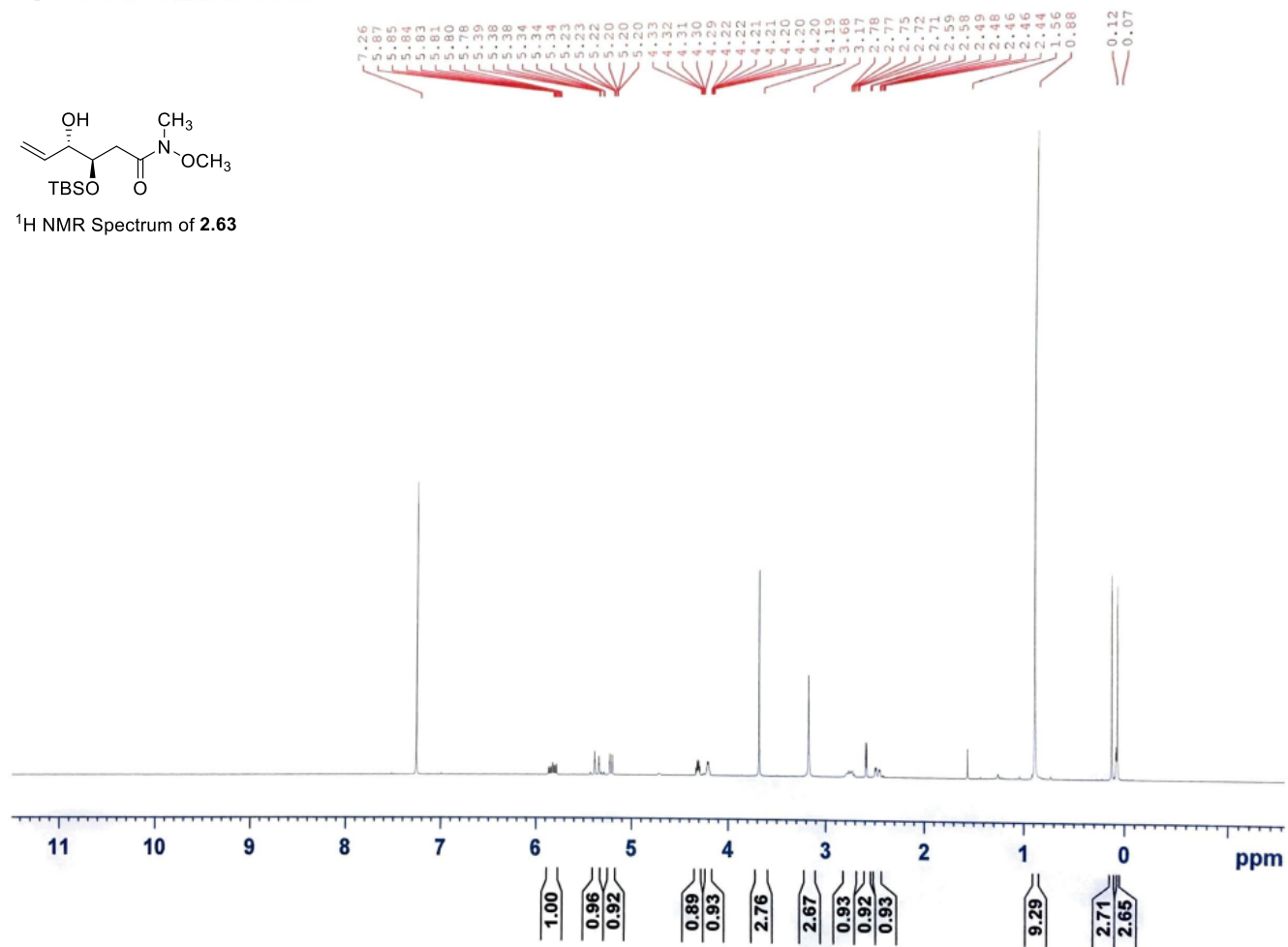


Figure A.2.12. ¹H NMR (400 MHz, CDCl₃) of 2.63.

TES protected Weinreb

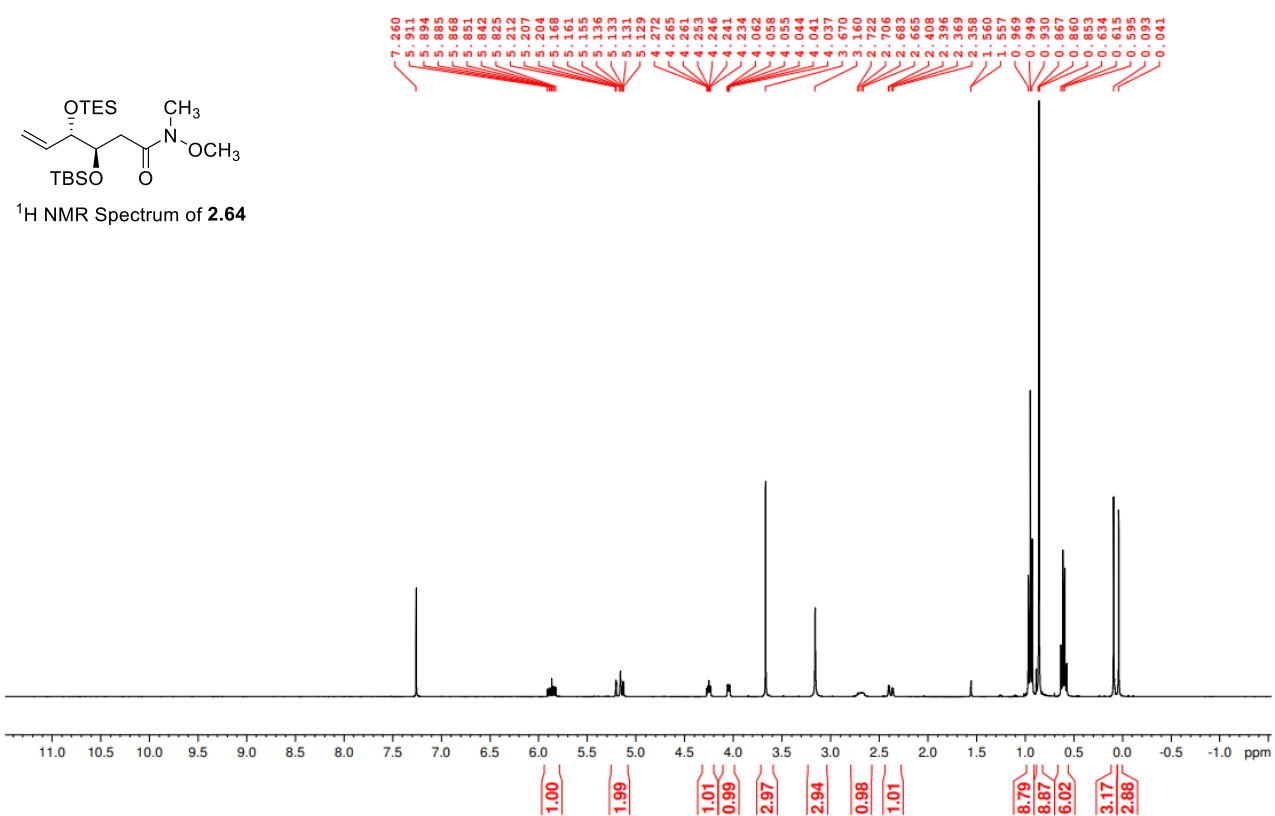
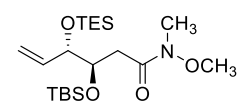


Figure A.2.13. ¹H NMR (400 MHz, CDCl₃) of **2.64**.

TES Protected Weinreb amide



^{13}C NMR Spectrum of **2.64**

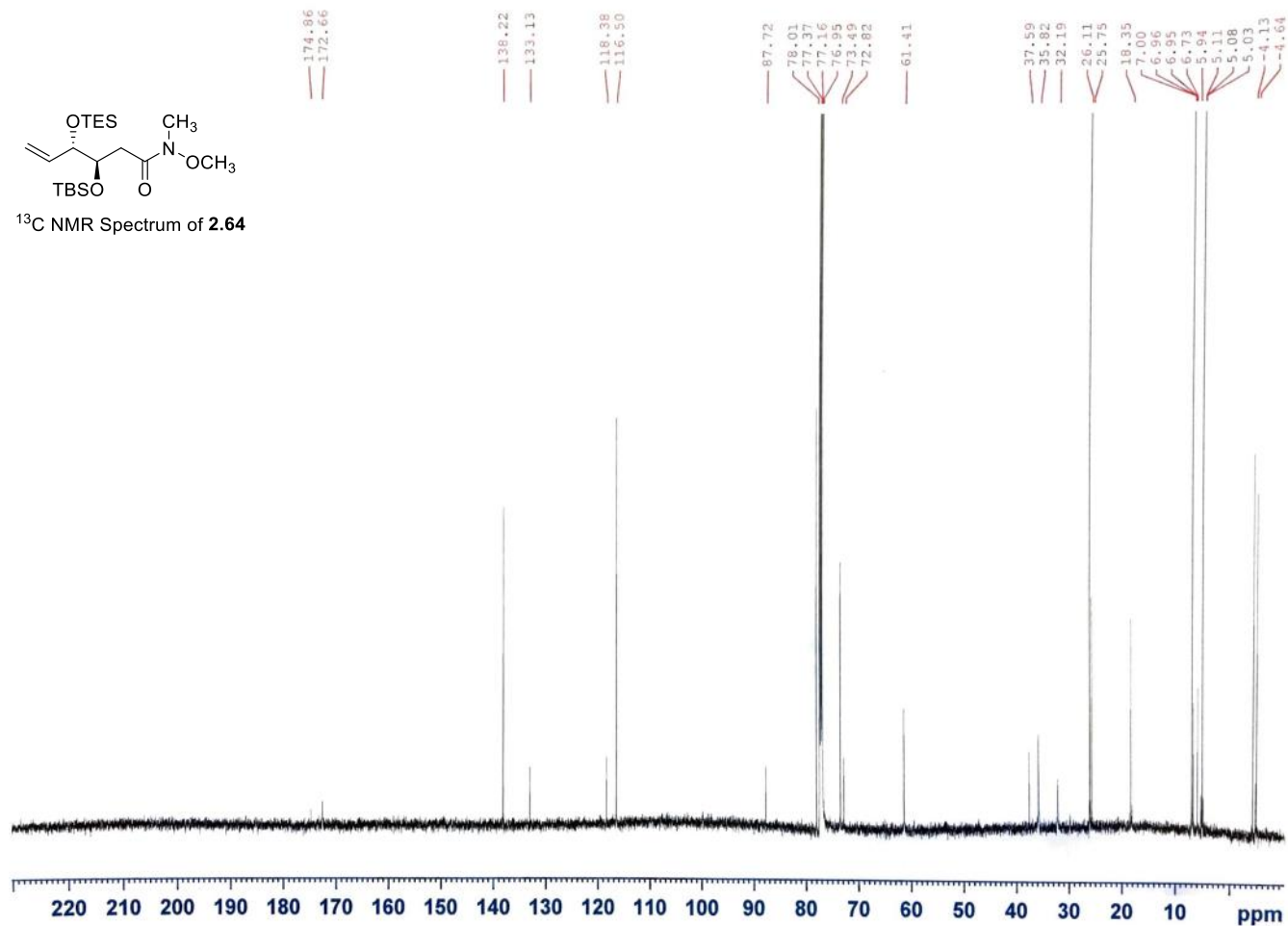


Figure A.2.14. ^{13}C NMR (150 MHz, CDCl_3) of **2.64**.

TES protected Weinreb

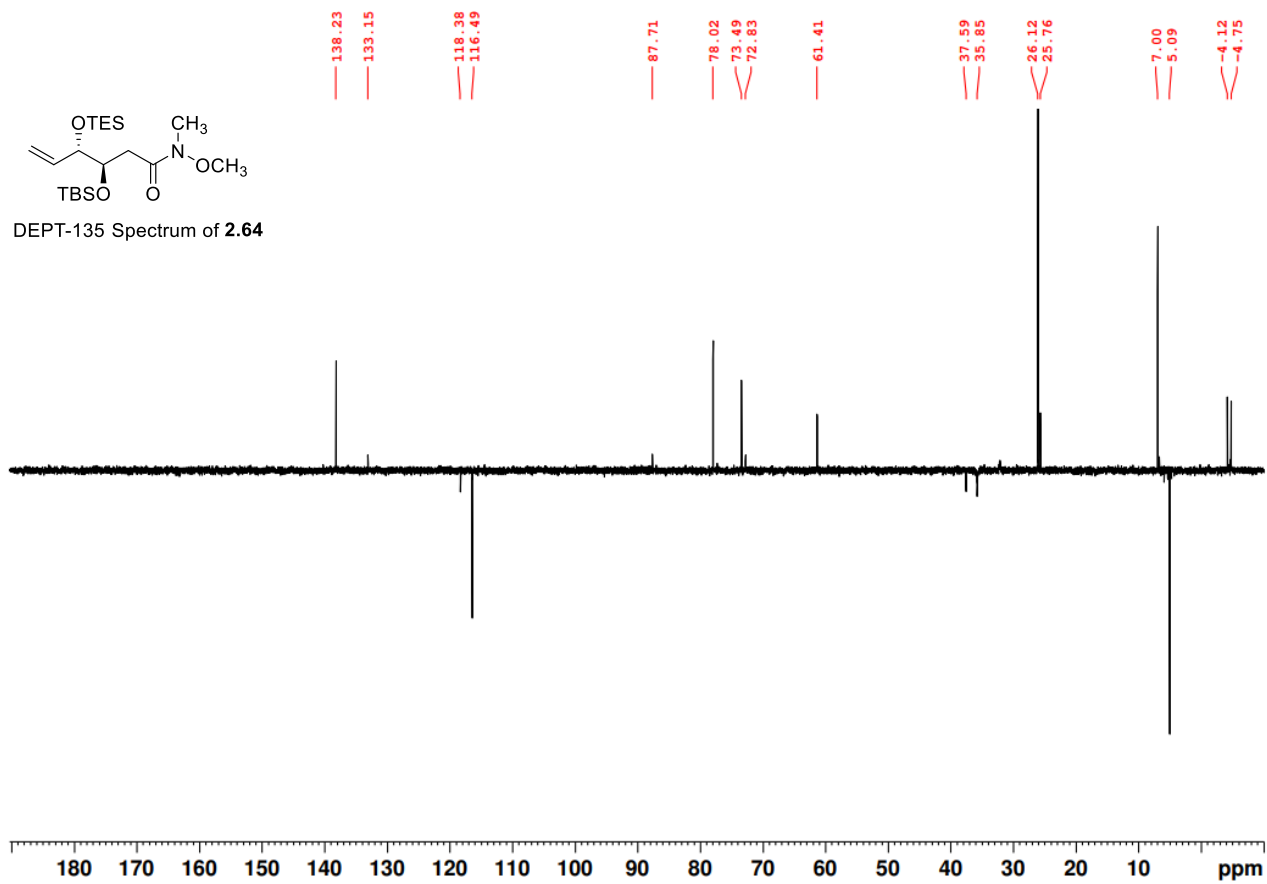


Figure A.2.15. DEPT-135 (150 MHz, CDCl₃) of **2.64**.

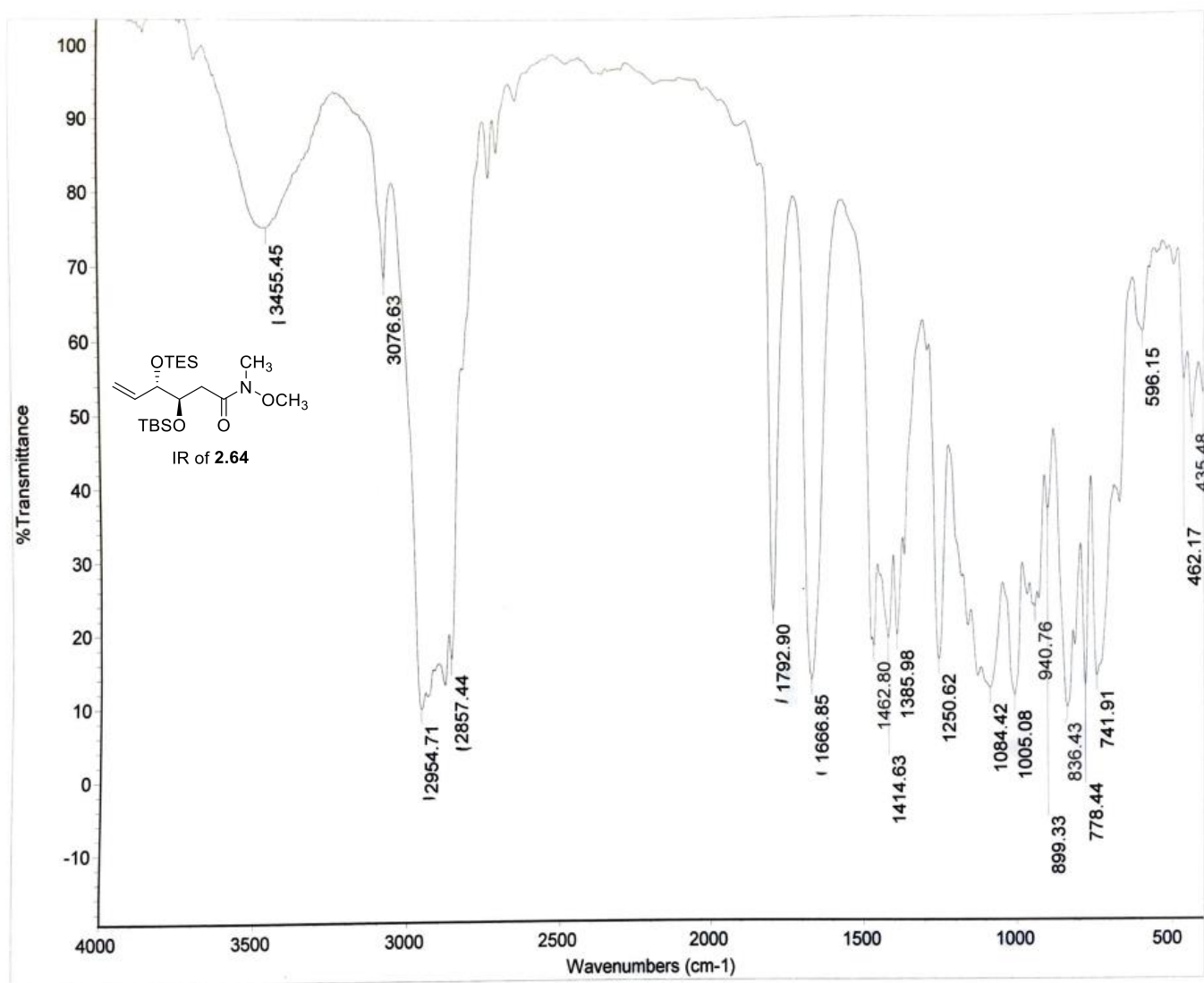
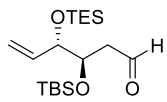


Figure A.2.16. IR of 2.64.

LAH Reduction



¹H NMR Spectrum of **2.86**

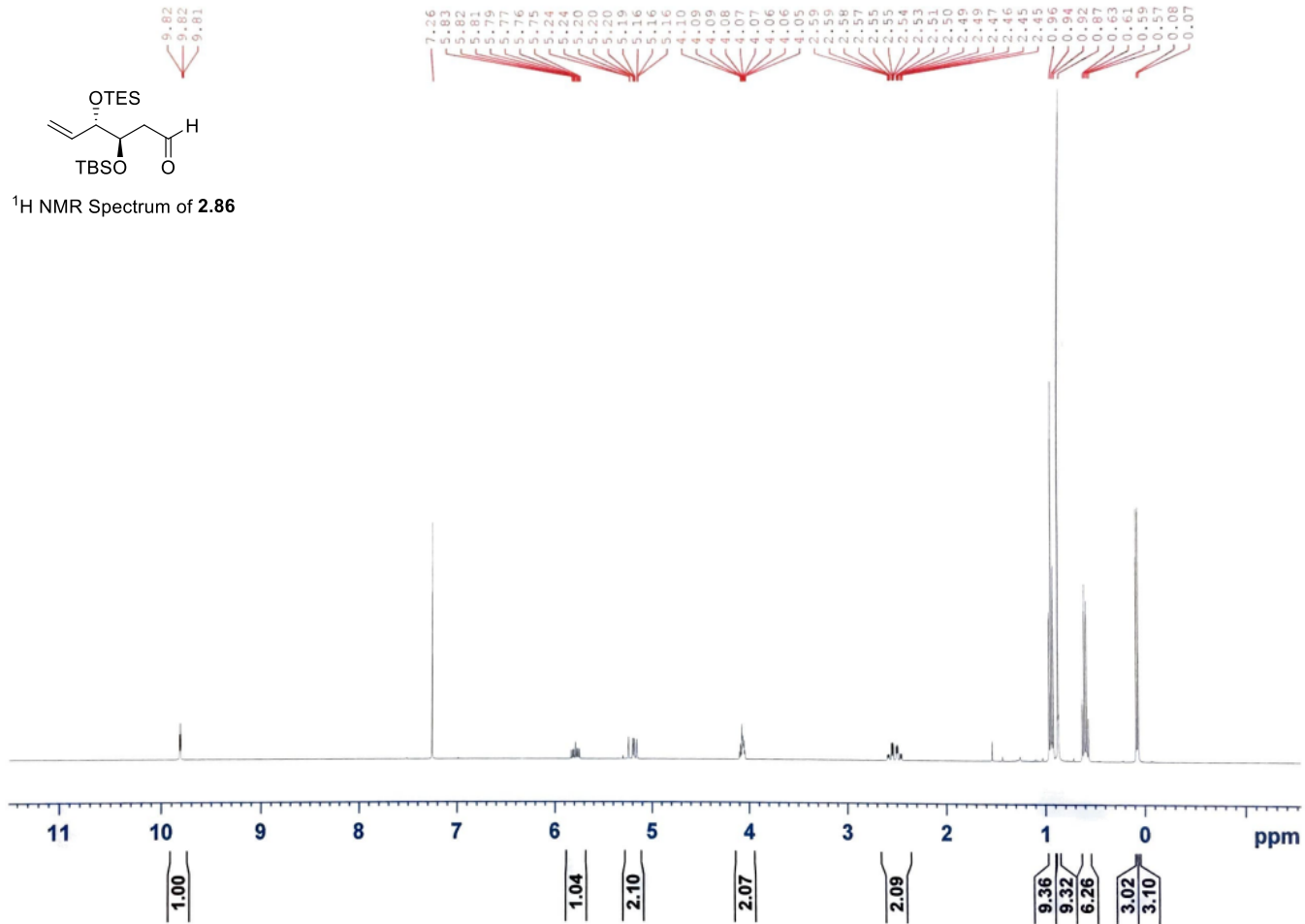
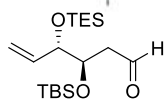


Figure A.2.17. ¹H NMR (400 MHz, CDCl₃) of **2.86**.

LAH Reduction



¹³C NMR Spectrum of **2.86**

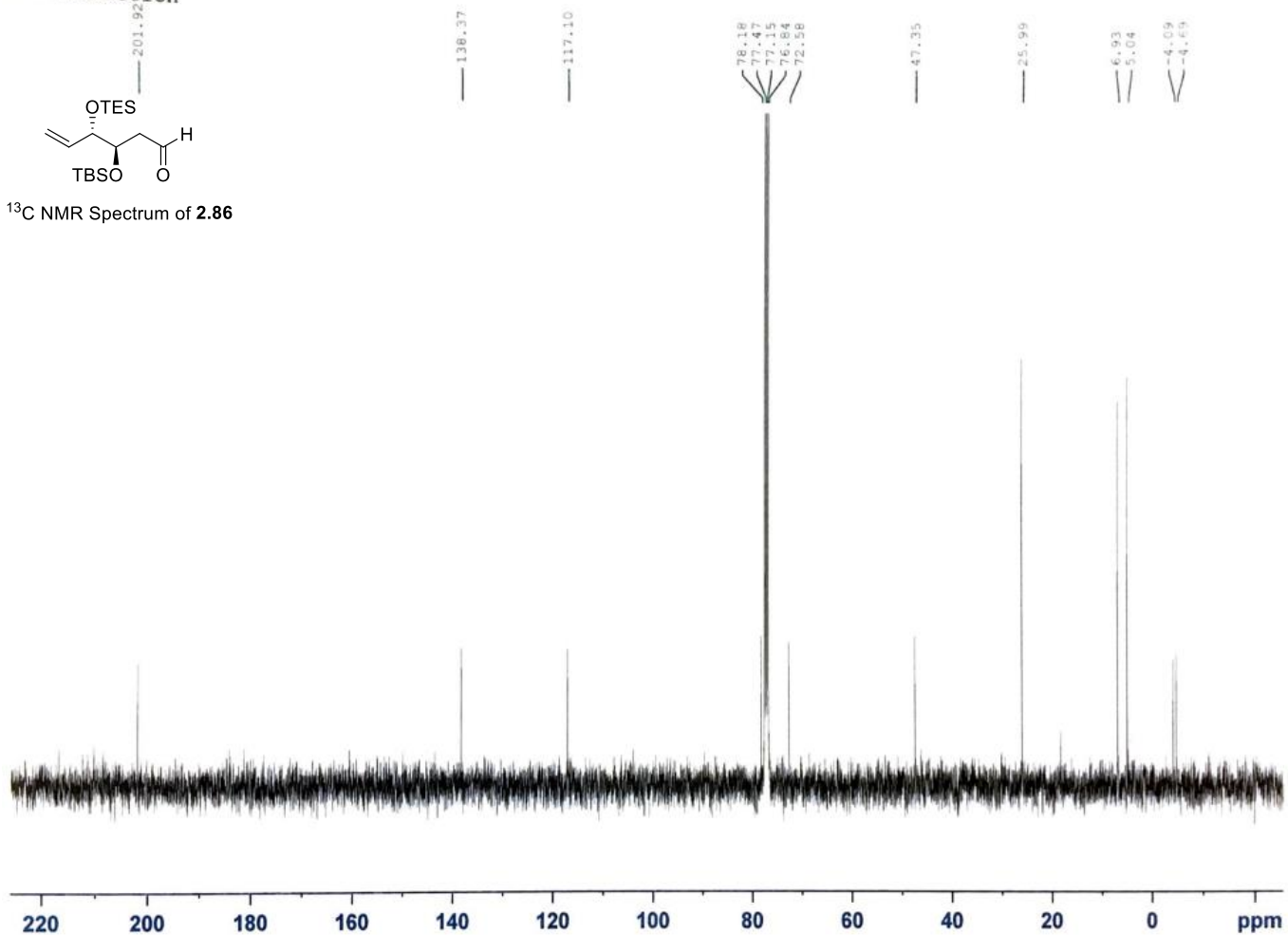
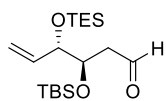


Figure A.2.18. ¹³C NMR (100 MHz, CDCl₃) of **2.86**.

LAH Reduction



DEPT-135 Spectrum of **2.86**

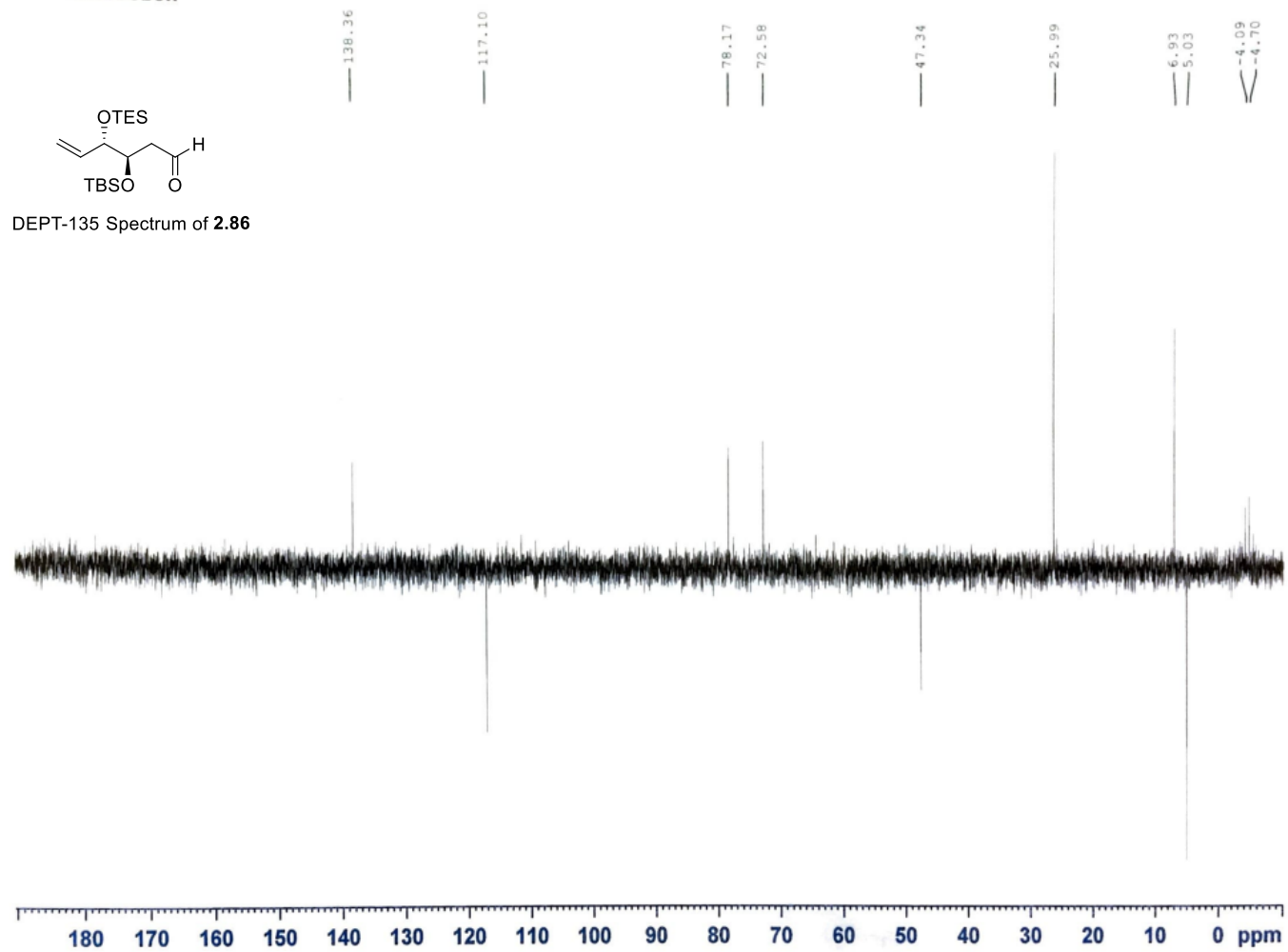


Figure A.2.19. DEPT-135 (100 MHz, CDCl_3) of **2.86**.

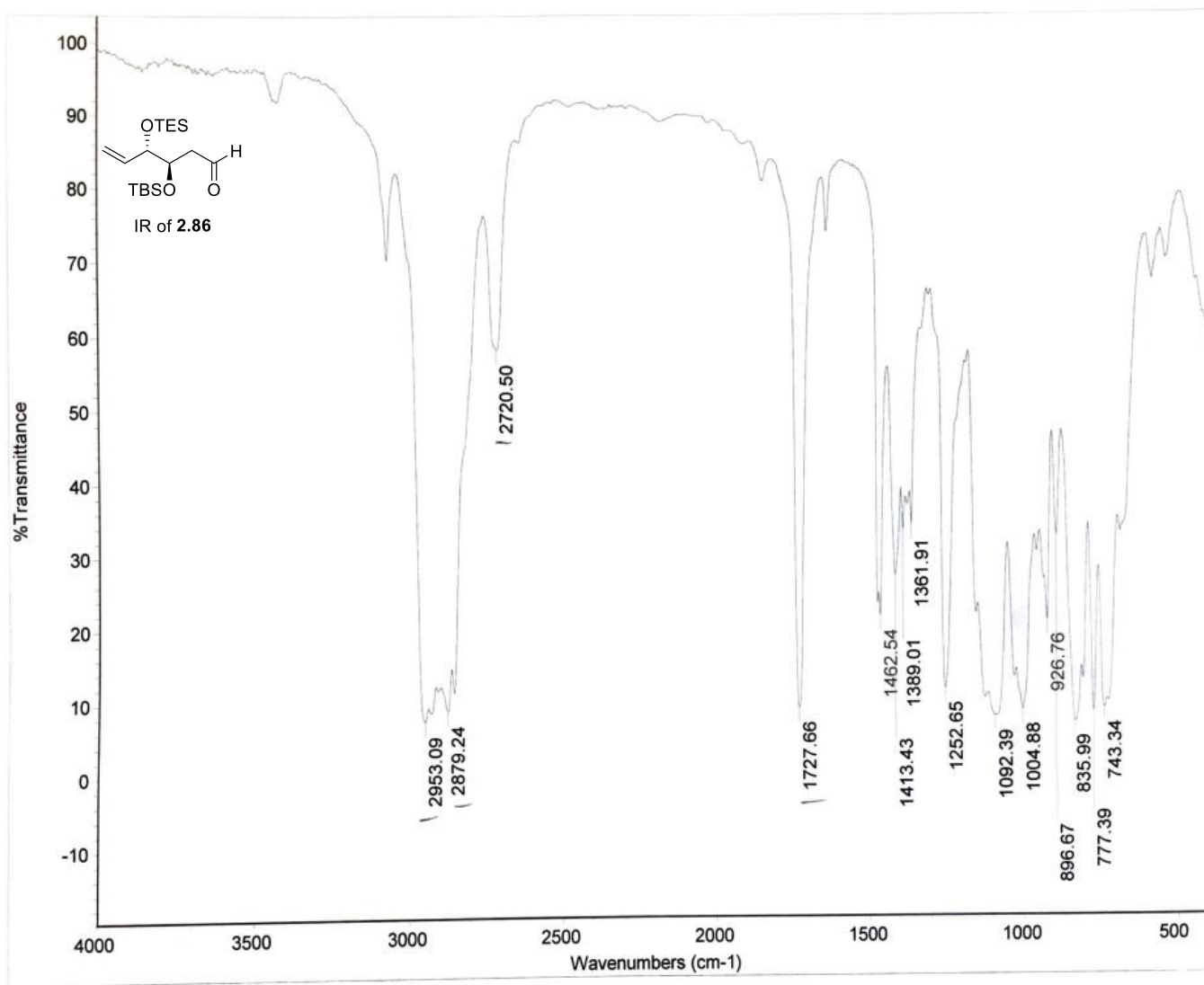


Figure A.2.20. IR of 2.86.

Dicarbonyl

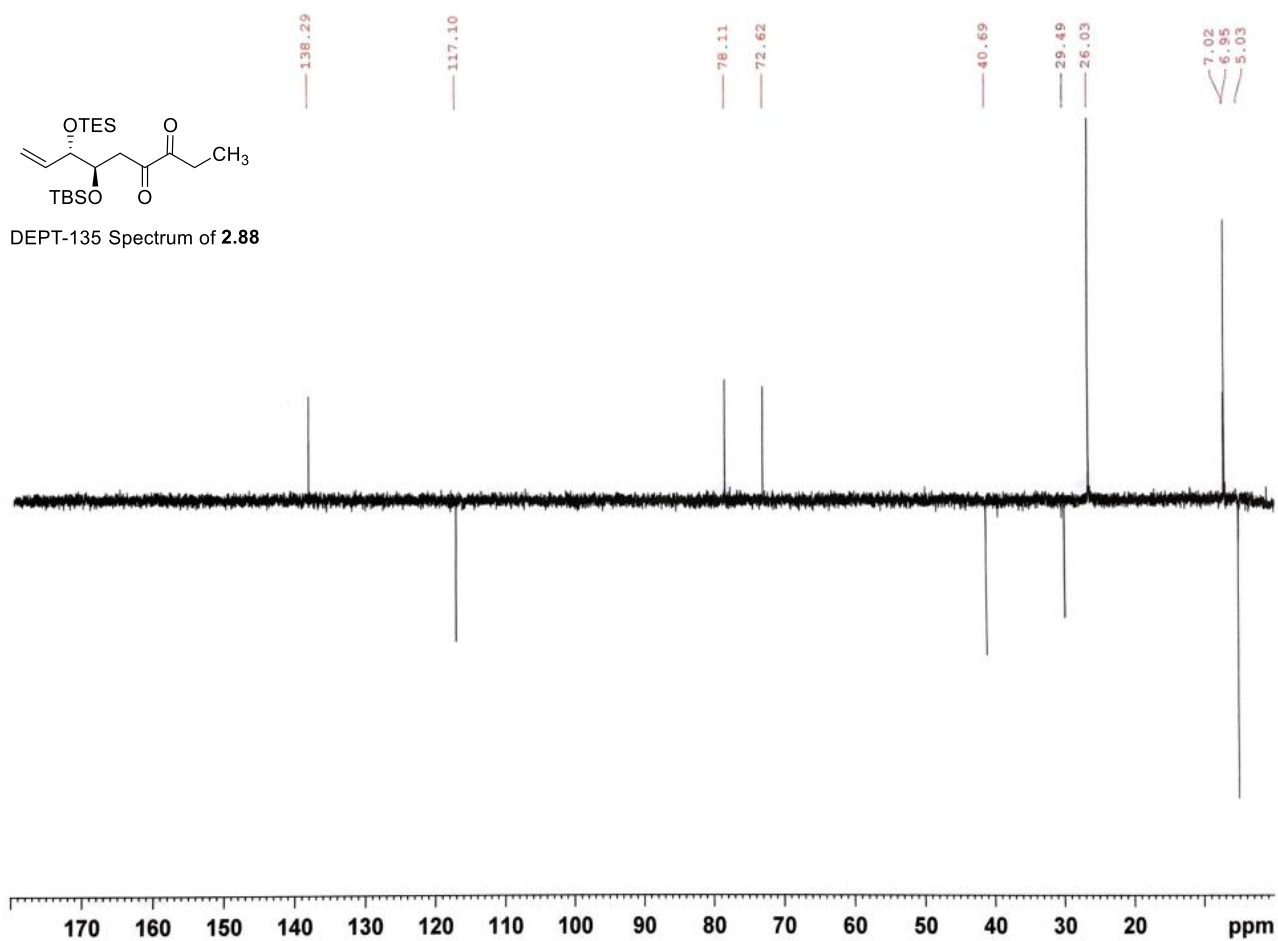


Figure A.2.23. DEPT-135 (150 MHz, CDCl_3) of **2.88**.

Mixture of enone and dicarbonyl isomers

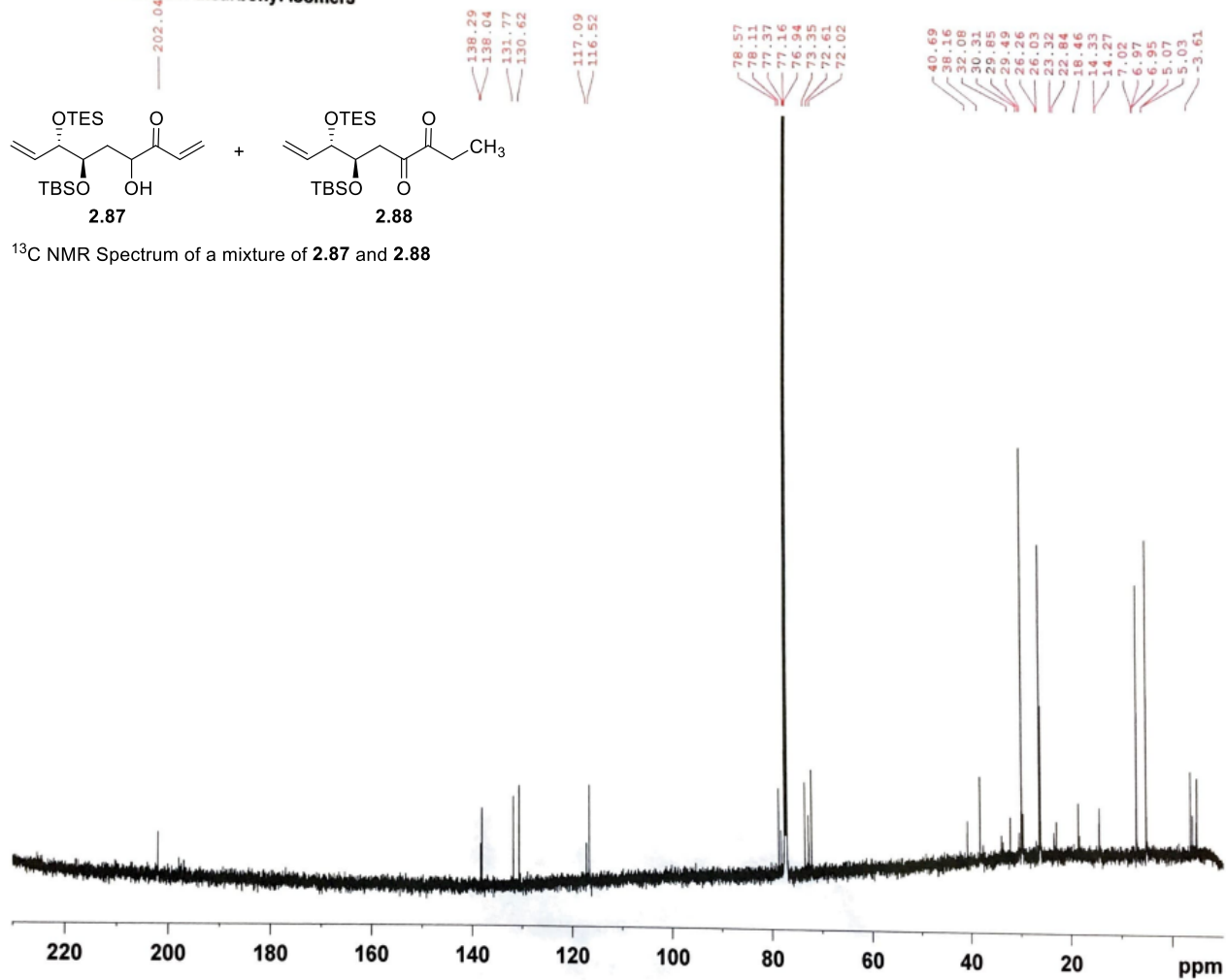


Figure A.2.25. ¹³C NMR (150 MHz, CDCl₃) of **2.87** and **2.88**.

Mixture of enone and dicarbonyl isomers

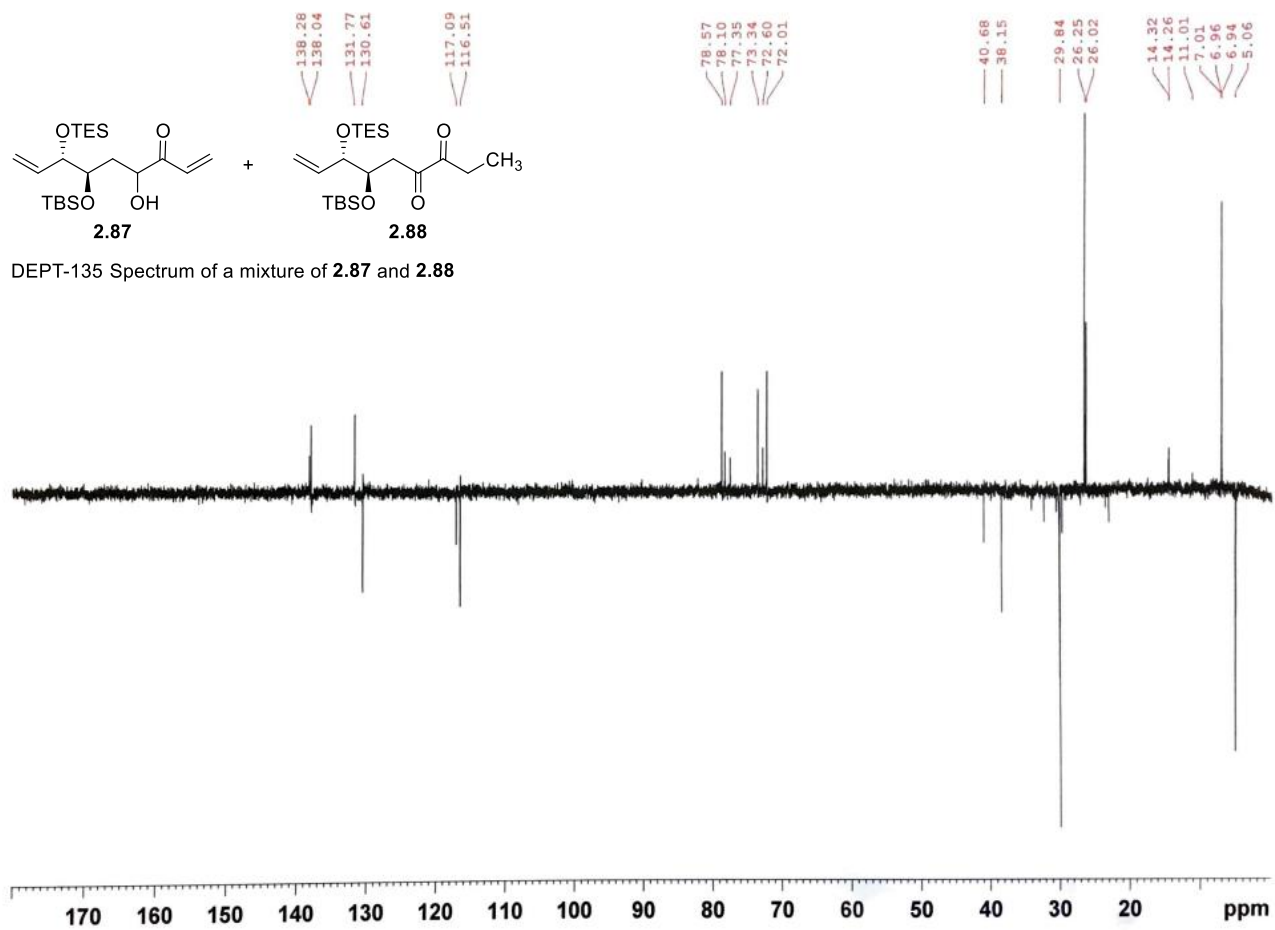


Figure A.2.26. DEPT-135 (150 MHz, CDCl₃) of **2.87** and **2.88**.

CHAPTER 3

GAINING MOLECULAR INSIGHT ON THE SYNTHESIS OF NANOPARTICLES

On the Comparison of How Organic and Nanomaterial Chemists Understand Catalysis

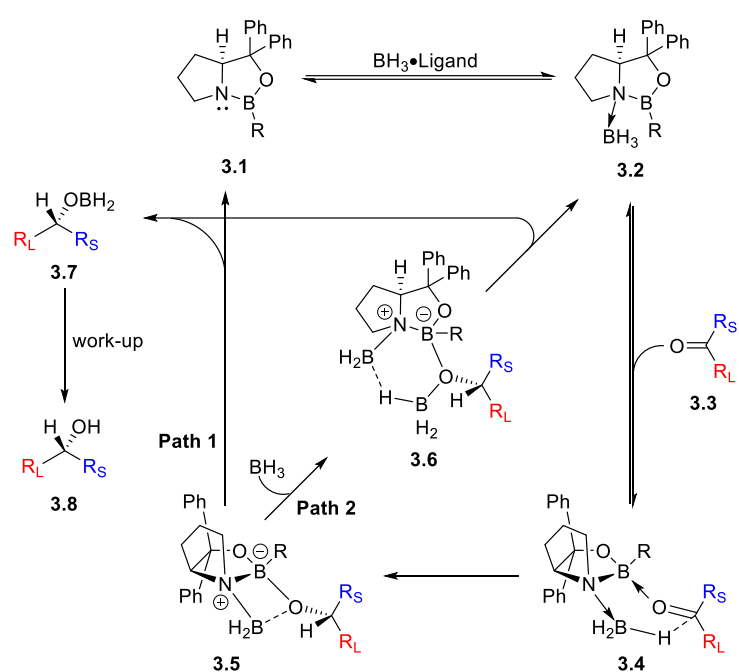
The fundamental understanding of catalysis amongst organic and nanomaterial chemists differs substantially. This perspective will demonstrate how these two fields comprehend catalysis using specific examples from the literature and discuss how these fields may be able to merge these ideas to potentially solve novel problems. This includes critiquing nanoparticle experiments to explain how an organic chemist would approach or seek to further explore ideas originating from the nanoparticle community. The benefits of understanding how different fields approach similar goals can be paramount to advancing technology further to benefit society. To begin, it is necessary to provide a brief synopsis of various differences between the field of organic chemistry and nanomaterials.

Organic chemists have a profound grasp of how to predict and manipulate carbon-containing molecules. Organic synthesis groups have this capability simply because the origin of this field can be dated back to the 1800s where the first synthesis of urea was disclosed.¹ Today in order to access novel targets for drug discovery, it is generally well-known which reagents are necessary to conduct reductions to alcohols, hydrogenations of alkynes, and oxidations of alcohols to carboxylic acids to give a few examples. Furthermore, if a particular oxidation is not successful, a plethora of options are available to attempt until the desired outcome is achieved. For example, if a Swern oxidation is unsuccessful, the Parikh Von Doering, IBX, TEMPO and other oxidations can be tried.^{2,3,4,5} Hundreds of named reactions exist.⁶ This field also has the advantage of databases that organize these reactions, so patterns are easily recognizable, like the electronic Encyclopedia of Reagents for Organic Synthesis (*e-EROS*).

In contrast, due to the fact that nanotechnology is still in its infancy, this field does not have the same advantages that organic chemists have to predict patterns in the synthesis of nanoparticles and by extension catalysis. The nano field uses their knowledge of surfaces and specific facets of nanoparticles to understand catalytic behavior. However, mechanistic understanding of what is occurring in the round bottom flask is still lacking. Although there are scientists in the nano field who are doing amazing work towards this end. Dempsey's impressive endeavors report three separate ligand-based mechanisms between oleate-capped PdS nanocrystals and undec-10-ene-1-thiol.⁷ For example, the author demonstrates that Z-type displacement, L-type binding, and X-type exchange of ligands depends on the surface or facet that the ligand interacts with which is an important aspect to consider in catalysis if ligands are involved. With the main differences between the two fields

established, the next section will discuss how organic chemists approach enantioselective transformations of carbon-based molecules using catalysts.

Enantioselective Catalysis: from the Perspective of Organic Chemists



Scheme 3.1. Mechanism of the CBS reduction, where R_S = small R group and R_L = large R group. *J. Am. Chem. Soc.* **1987**, *109*, 5551–5553.

Organic chemists use their understanding of sterics, electronics, and stereoelectronics to develop catalysts. For example, the clever design of the Corey-Bakshi-Shibata (CBS) catalyst takes advantage of these three aspects for the enantioselective reduction of a carbonyl.^{8,9} As shown in **Scheme 3.1**, the initial step is the coordination of BH_3 to the Lewis basic nitrogen in chiral oxazaborolidine catalyst **3.2**. The effect of this coordination primes the BH_3 to act as a hydride donor, while simultaneously increasing the Lewis acidity of the endocyclic boron atom. CBS catalyst-borane complex **3.4** binds with carbonyl **3.3** in a manner that minimizes steric interactions with the R group attached to the endocyclic boron. From an

electronic standpoint, this is favorable for two reasons; one reason is because the electronically deficient carbon of carbonyl **3.3** aligns with the coordinated BH_3 in a boat-like transition state. Secondly, the oxygen of carbonyl **3.3** coordinates with the Lewis acidic endocyclic boron. With these aspects in mind also consider that complex **3.5** demonstrates the ease in which the stereoelectronic, intramolecular hydride transfer can enantioselectively reduce carbonyl **3.3** to obtain chiral alcohol **3.8**.

Another catalyst organic chemists utilize for enantioselective reductions of carbonyls is the organoborane reagents developed by M. Mark Midland. A chemical review from 1989 showcases a proposed boat-like transition state to explain the enantioselectivity (**Figure 3.1**).¹⁰ It was found that a syn-planar relationship of the B-C-C-H bonds allowed for a faster rate in reduction. As shown from the transition state model, favored transition state **3.9** places the largest R group of the carbonyl substrate in the equatorial position to minimize steric strain with the axial

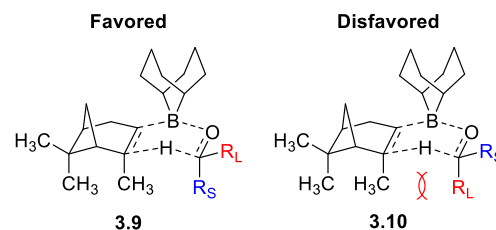
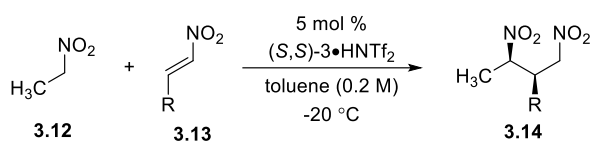
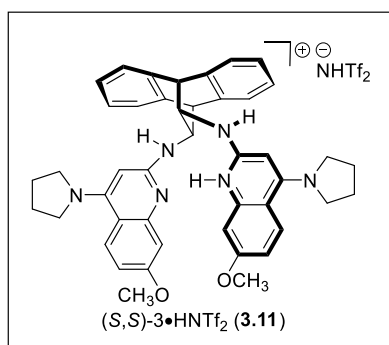


Figure 3.1. Key transition state to explain selectivity for the Midland reduction. *Chem. Rev.* **1989**, *89*, 1553–1561.

methyl group in the alpine borane; while the smaller R group is found in the axial position of boat-like transition state **3.10**. Electronically, transition state **3.9** is favorable because the oxygen from the carbonyl orients itself with the electron deficient boron. This allows for selective hydride delivery into the carbonyl which results in the enantioselective reduction of a desired carbonyl. Typically for Midland reductions, carbonyl substrates containing



Scheme 3.2. Jeffery Johnston's (S,S) -**3•HNTf₂** catalyst, developed for the synthesis of $\beta^{2,3}$ -amino amides from this chiral proton-catalyzed Michael addition of nitroalkanes. *Chem. Sci.* **2019**, *10*, 1138–1143.

amides through umpolung chemistry. Natural products or drugs contain these β -amino amide motifs, and this methodology is even desired by industrial companies.

While not every catalyst utilized in the field will be mentioned herein, it should be said that hydroxyl-directed hydrogenations like Wilkinson's catalyst, in addition to Brown and Crabtree's catalysts, have established importance in the field of organometallic chemistry.^{13,14} Through the development of the CBS, Midland and BAM catalysts, organic chemists have mechanistic clarity of how the enantioselectivity or diastereoselectivity of substrates is achieved.

The last example to be discussed is Lindlar's catalyst, as this mechanism is largely unknown among organic chemists, yet is widely used. With normal palladium catalysts subjected under hydrogen gas, alkenes are reduced to fully saturated alkanes.^{15,16} However, Lindlar's catalyst is used for the semi-hydrogenations of alkynes to *cis*-alkenes.¹⁷ Lindlar's catalyst is a palladium catalyst poisoned with lead and calcium carbonate to reduce its reactivity to allow the semi-hydrogenation to occur. When organic chemistry professors teach the "mechanism", the catalyst is assumed to be a perfectly flat surface in which an alkyne aligns itself, and there is no mention of the potential edges of the catalyst surface or that it is comprised of atoms. A focus on nanocatalyst surface is where nanoparticle chemists particularly shine, which is what the next section will discuss and critique in several different case studies.

alkyne groups provide good selectivity, due to the alkyne's small A-value.¹¹ A-values are numerical values assigned to different substrates to provide a representation of steric bulk. Because smaller A values correspond with decreased steric strain, this allows an alkyne, for example, to lock into the axial position to minimize the overall energy of the transition state; however, the Midland reduction can succeed with other types of R groups as well.

A more recent catalyst developed by Johnston and coworkers in the early 2000's are the Bis(AMidine) (BAM) catalysts for enantioselective catalysis and peptide synthesis.¹²

Scheme 3.2 showcases (S,S) -**3•HNTf₂** (**3.11**), specifically developed for the synthesis of enantioselective $\beta^{2,3}$ -amino

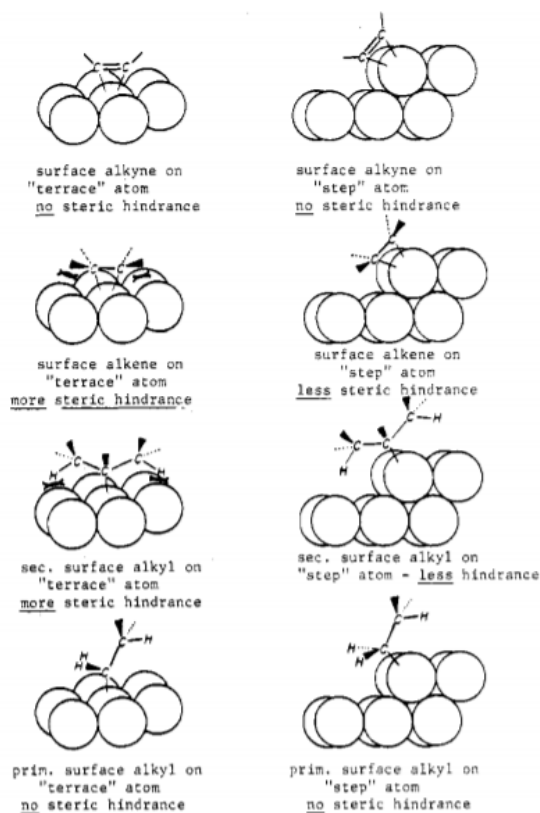


Figure 3.2. Sterics associated with terraces and steps. Reprinted with permission from Ulan, J.; Maier, W.; Smith, D. J. *Org. Chem.* **1987**, 52, 3132–3142. Copyright 2022 American Chemical Society.

Maier *et al.* explain the selectivity of hydrogenation catalysts using arguments of sterics and how the atomic arrangement on the surface of the catalyst may influence the selectivity of hydrogenations. Depending on the substrate chosen for hydrogenation, it may feel more or less strain at the terraces vs. steps pictured in **Figure 3.2**.¹⁸ This plays a role in whether the substrate is semi- or fully hydrogenated. Using this theory, alkynes would experience very little steric hindrance on both terraces and stepped surfaces due to their low A values. Alkenes would undergo more steric hindrance on terraces rather than steps, due to the angle the alkene could orient itself on the steps. And finally, while alkanes would not be hydrogenated further, alkanes would experience even more steric hindrance at the terrace than the stepped surface compared to alkenes and alkynes. This nice visualization portrays how catalyst surfaces *may not*, in fact, be perfectly flat as many organic chemists believe, but may have kinks and edges that are present which may even direct synthesis.

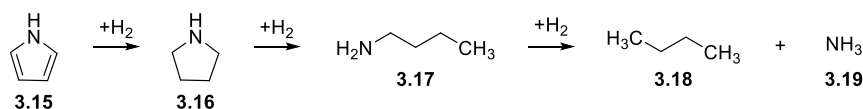
Additionally, it provides a basis for how an alternative semihydrogenation catalyst may be designed. Using this knowledge, the authors of this paper sought to create nanosized Pd particles which selectively semihydrogenate alkynes to *cis*-alkenes by using a catalyst with more terraces.

These authors found a Pd/W film to be a good candidate for the *cis*-selectivity of alkenes and was directly contrasted with Lindlar's catalyst. However, improvements could have been made in the experimental process, as no constant molar or weight percent of the catalysts were used. Their claim that the Pd/W catalyst 'outperforms' Lindlar's catalyst is questionable because without keeping the catalyst loading similar, the reported percent conversions of either catalyst have very little meaning. Additionally, the authors provided a minimal number of external alkynes to screen in this methodology. Including substrates with R groups that are electronically diverse is important to fully understand the grasp how the catalyst is affected by differing electronic environments. The authors choose very similar electron withdrawing and electron donating groups which hinders the ability to form any meaningful patterns. Increasing the sterics of the R groups within these alkynes would also be beneficial to this study. Finally, due the sputtering technique used to make the Pd/W film, carbon impurities were present. The

authors admitted that these impurities limited the longevity of the catalyst at scales bigger than 1-10 mmol. All of these critiques demonstrate how an organic chemist would have reshaped this experiment to better understand the limits of the catalyst.

In the next case study, Somorjai and coworkers researched the reduction of pyrrole **3.15** with dendrimer-templated Pt nanoparticles of 5 nm or less.¹⁹ The reduction of pyrrole **3.15** was investigated, as it is a common agent in fuel. The authors utilized fourth generation hydroxyl-terminated polyamidoamine (PAMAM) dendrimers, polymers with many tree-like branching points, for templating and capping to achieve Pt nanoparticle size control. It was found that the reduction of pyrrole **3.15** to pyrrolidine **3.16** was not sensitive to the varying sizes of the Pt nanoparticles, because the turnover frequencies of pyrrolidine **3.16** ($\text{TOF}_{\text{pyrrolidine}}$) changed negligibly, as shown from **Table 3.1**. However, the TOFs of the transformations from pyrrole **3.15** to *n*-butylamine **3.18** ($\text{TOF}_{n\text{-butylamine}}$) increased with increasing sizes of Pt nanoparticles.

Table 3.1. Turn over frequencies based on pyrrole, pyrrolidine, and *n*-butylamine conversions. Adapted with permission from Kuhn, J.; Huang, W.; Tsung, C.; Zhang, Y.; Somorjai, G. *J. Am. Chem. Soc.* **2008**, *130*, 14026–14027. Copyright 2022 American Chemical Society.



Catalysts ^(a)	$\text{TOF}_{\text{pyrrolidine}} \text{ (ks}^{-1}\text{)}^{(b)}$	$\text{TOF}_{n\text{-butylamine}} \text{ (ks}^{-1}\text{)}^{(c)}$	$\text{TOF}_{\text{butane}} \text{ (ks}^{-1}\text{)}^{(d)}$
0.6% Pt (0.8 nm)/SBA-15	53.4	36.3	0.6
0.6% Pt (1.0 nm)/SBA-15	76.2	57.4	1.2
0.2% Pt (1.5 nm)/SBA-15	73.7	57.0	2.6
0.6% Pt (2.0 nm)/SBA-15	69.7	65.8	2.5
0.3% Pt (2.9 nm)/SBA-15	73.1	71.0	5.0
0.3% Pt (5.0 nm)/SBA-15	76.8	76.8	5.8

Investigating the idea that ultrasmall nanoparticles may have a selection for certain types of molecules with differing amounts of hydrogens is interesting. I admire the authors' decision to look at the reaction conversion rates of *all* the possible side products. One aspect not addressed is how the successive hydrogenations interact on such a complex surface like a dendrimer. Afterall, unlike the Pd/W catalyst in the previous study discussed, a dendrimer would have much fewer flat terraces due to the winding and coil-like nature of the polymer. It would be interesting to explore the mechanism of how the interaction of the polymer and Pt interact with the incoming hydrogenated substrates. Is there an optimal angle at which substrates are hydrogenated on this surface? Organic chemists learn that the Bürgi–Dunitz angle is the optimal angle at which an incoming nucleophile comes in to attack sp^2 hybridized carbonyls. Surely there are optimal angles at which incoming substrates may need to approach different surfaces? Additionally, does the polymer play a role in guiding or repelling incoming substrates? Ultimately, it would be interesting to determine if there is a way to direct the substrates through steric or electronic interactions to guide or repel certain molecules to the dendrimer surface.

In the third case study, Zheng and coworkers explored the hydrogenation of styrene and *trans*-stilbene over palladium nanocrystals.²⁰ The authors noted that different crystals can expose various facets or surfaces on the catalyst, and the facet exposed under hydrogenation conditions determines how effective the hydrogenation takes place. Additionally, there is no guarantee that hydrogen gas saturates every facet of the Pd catalyst equally. This may lead to more reactive surfaces within the catalyst. It was found that both hexagon-shaped Pd nanosheets and Pd nanotetrahedra containing the Pd{111} as their major exposure surfaces provided good catalytic activity for the reduction of styrene, but no activity for *trans*-stilbene. In comparison, Pd nanocubes containing six{100} facets gave high catalytic activity for both substrates. As shown in **Figure 3.3**, the authors use the

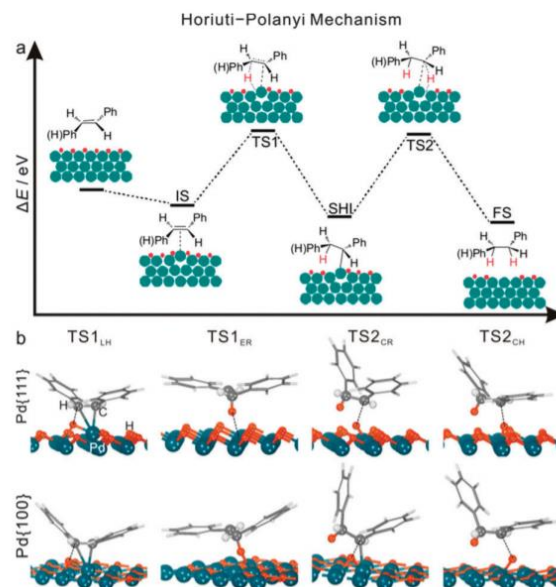


Figure 3.3. Transition states calculated using the Horiuti-Polanyi Mechanism. Used with permission of Royal Society of Chemistry, from Zhao, X.; Zhao, Y.; Fu, G.; Zheng, N. Origin of the Facet Dependence in the Hydrogenation Catalysis of Olefins: Experiment and Theory. *Chem. Commun.* **2015**, *51*, 12016–12019; permission conveyed through Copyright Clearance Center, Inc.

Horiuti-Polanyi mechanism and provide exact calculations of different transition states to explain these experimental results.

While it is interesting to suggest that one hydrogenated face is more reactive than another, this experiment could be improved by providing substrates that are at least similar to compare. Styrene is a monosubstituted alkene, whereas *trans*-stilbene is disubstituted. Due to the drastic difference in sterics of these two alkenes, they should not be compared. An organic chemist would easily predict that the more sterically hindered alkene would prove more difficult to hydrogenate with *any* catalyst. So the result that the Pd{111} provided good catalytic activity for the reduction of styrene, and no activity for *trans*-stilbene is not that surprising at all. More monosubstituted and disubstituted alkenes should be hydrogenated with the chosen nanocrystals to test to see if the facets actually do play a significant role in the transition states. Additionally, the experimentalist should also be consistent with the E or Z configuration of the alkene when comparing the stability of transition states, as there is an energy difference. Finally, the authors only chose two facets to explore. It would be interesting to see if other facets demonstrate special activity. Only after these considerations are established would making a trend about the selectivity of different facets be appropriate. Controlling and keeping these types of variables constant, like how organic chemists optimize methodologies for new reactions, may help nanomaterial chemists learn to predict patterns associated with catalysis.

In the last case study, Wang and coworkers utilize electrochemistry to synthesize tetrahedral Pt nanoparticles using a square-wave potential. It was found that the tetrahedral facets containing high-index planes like {730} and {210} provided the highest catalytic activity.²¹ This paper claims that these facets demonstrate higher catalytic activity than {111} and {100} faces. Interestingly, previous case studies highlighted herein researched the catalytic activities of these more common stable planes. Because high-index planes have more atomic steps, ledges, and kinks, it makes sense why the {730} and {210} facets would exhibit high catalytic behavior considering more interactions with molecules can occur. However, the question remains if these high-index surfaces can provide any selectivity for the desired oxidations. The authors focus on using this catalyst to oxidize formic acid and ethanol, as these two small organic molecules have promise as alternative fuels sources. Two types of catalysts were used as controls: Pt nanospheres and commercially available Pt/C for comparison.

As shown in **Figure 3.4**, the ability of the Pt tetrahedral nanoparticles to oxidize formic acid and ethanol clearly outperforms the other two catalysts. However, details regarding the oxidation states of the products after oxidation are not reported. No information is given regarding if only one oxidized product obtained from formic acid and ethanol or if there are multiple side products. This information would be incredibly useful. Additionally, the particle sizes of all three catalysts differ: Pt tetrahedra ($d = 81$ nm), Pt nanospheres ($d = 115$ nm), and commercial Pt/C ($d = 3.2$ nm). Ideally the experimentalist should choose catalysts similar in size for a proper comparison to gain a better understanding of the catalyst's surface area.

To conclude, it is apparent based on the studies chosen in this perspective that organic chemists and nanomaterial chemists think very differently about catalysis and experimental design. However, both of these types of knowledge should complement each other, not clash. Each field offers a slightly different perspective which may prove beneficial for the advancements of both fields. Organic chemists manipulate carbon-containing molecules based on their knowledge of sterics, electronics, stereoelectronics and intermolecular bonding. Nanoparticle chemists use their knowledge of facets and atomic arrangements to understand how molecules may interact at these surfaces. Collaborations between these two fields could prove quite fruitful. By combining both perspectives from both fields, perhaps newer and more efficient catalysts could be developed to access enantioselective transformations that currently cannot be achieved using our current toolset.

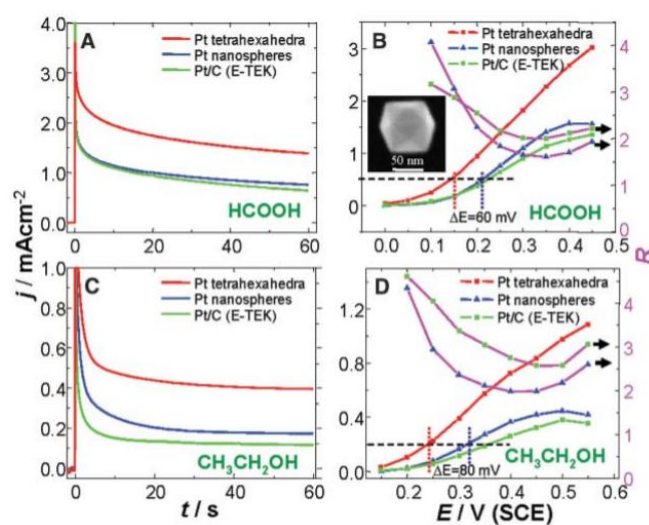


Figure 3.4. Comparison of catalytic activities for Pt tetrahedral, Pt nanospheres, and Pt/C. From Tian, N.; Zhou, Z.; Sun, S.; Ding, Y.; Wang, Z. *Science* (1979) **2007**, 316, 732–735 / Reprinted with permission from AAAS.

Areas where organic and nanomaterial chemists might be able to solve novel transformations in the field of organic chemistry include discovering catalysts that reduce alkynes to *trans*-alkenes. Currently no robust method exists to achieve this transformation using catalysts that are readily available. As seen from this perspective, both fields have thoroughly studied the alkyne to *cis*-alkene hydrogenation with numerous catalysts, but not to *trans*-alkenes. Incorporating ideas of how small drug molecules interact with enzyme pockets and nanosurfaces might be a way in which alkynes could be guided to a surface to produce *trans*-alkenes.

Another void in the organic literature, mentioned previously in Chapter 2 (**Figure 2.1**), is the ability to form unsymmetric 1,2-dicarbonyls. Dechert-Schmitt, Blackmond, and coworkers cleverly designed a one-pot four component Pd-catalyzed coupling *via* a double isocyanide insertion without the use of CO.²² The reaction scope, however, is restricted to aryl halides and alkyl zinc reagents which presents limitations to access natural products containing keto-hemiketal moieties. While this work is a good start to allow the synthesis community access to unsymmetric 1,2-dicarbonyls, more methodologies must be developed to tolerate this coupling directly with alkyl halides.

The development of chiral nanocatalysts is another interest to both fields. The synthesis of chiral nickel sulfide catalysts was attempted in the Macdonald laboratory, but unfortunately failed. One possible reason for the observed failure was that only chiral ligands were utilized. Recently, Hubley *et al.* found that solely chiral ligands are insufficient to create a chiral catalyst.²³ The presence and ratios of *both* achiral and chiral ligands is very important to create a chiral environment which was confirmed by circular dichroism. This work was performed with methylammonium lead bromide perovskite nanoplatelets. To a similar end chiral, plasmonic gold nanocrystals were synthesized *via* the enantioselective adsorption of chiral molecules onto gold seed surfaces.²⁴ Then, upon seeded overgrowth the molecular chirality, introduced from L-glutathione, is then transferred to the nanocrystals. While neither of these works performed any enantioselective or diastereoselective organic transformations, it is a step towards developing very novel transformations in organic chemistry as well as providing interesting chiroptical devices.

Other hot topics in organic chemistry currently include C-H activation and photocatalysis, both of which could potentially benefit from collaborations with nanomaterial chemists.^{25,26,27} In summary, these topics are possible areas in which both organic and nanomaterial chemists could enjoy the mutual benefits of each other's expertise to further the field of chemistry.

References

- (1) Wöhler, F. Ueber Künstliche Bildung Des Harnstoffs. *Ann. Phys. Chem.* **1828**, *87*, 253–256.
- (2) Omura, K.; Swern, D. Oxidation of Alcohols by “Activated” Dimethyl Sulfoxide. a Preparative, Steric and Mechanistic Study. *Tetrahedron* **1978**, *34*, 1651–1660.
- (3) Nicolaou, K.; Reddy, K.; Skokotas, G.; Sato, F.; Xiao, X.; Hwang, C. Total Synthesis of Hemibrevetoxin B and (7a.Alpha.)-Epi-Hemibrevetoxin B. *J. Am. Chem. Soc.* **1993**, *115*, 3558–3575.
- (4) Jubault, P.; Quirion, J.; Lemonnier, G.; Lion, C. Preparation of Fluorinated Cyclopropane Analogs of Glutamic Acid as MGLuR4 Modulators Useful in the Treatment of Neurological Diseases. WO2011009947, 2011.
- (5) Anelli, P.; Montanari, F.; Quici, S. A GENERAL SYNTHETIC METHOD FOR THE OXIDATION OF PRIMARY ALCOHOLS TO ALDEHYDES: (S)-(+)-2-METHYLBUTANAL. *Org. Syn.* **1990**, *69*, 212.
- (6) Kürti, L.; Czakó, B. *Strategic Applications of Named Reactions in Organic Synthesis*; Elsevier Inc., 2005.
- (7) Kessler, M.; Kelm, J.; Starr, H.; Cook, E.; Miller, J.; Rivera, N.; Hsu-Kim, H.; Dempsey, J. Unraveling Changes to PbS Nanocrystal Surfaces Induced by Thiols. *Chem. Mater.* **2022**, *34*, 1710–1721.
- (8) Corey, E.; Bakshi, R.; Shibata, S. Highly Enantioselective Borane Reduction of Ketones Catalyzed by Chiral Oxazaborolidines. Mechanism and Synthetic Implications. *J. Am. Chem. Soc.* **1987**, *109*, 5551–5553.
- (9) Corey, E.; Helal, C. Reduction of Carbonyl Compounds with Chiral Oxazaborolidine Catalysts: A New Paradigm for Enantioselective Catalysis and a Powerful New Synthetic Method. *Angew. Chem. Int. Ed.* **1998**, *37*, 1986–2012.
- (10) Midland, M. Asymmetric Reductions with Organoborane Reagents. *Chem. Rev.* **1989**, *89*, 1553–1561.
- (11) Solel, E.; Ruth, M.; Schreiner, P. London Dispersion Helps Refine Steric A-Values: Dispersion Energy Donor Scales. *J. Am. Chem. Soc.* **2021**, *143*, 20837–20848.
- (12) Vishe, M.; Johnston, J. The Inverted Ketene Synthone: A Double Umpolung to Enantioselective Beta2,3-Amino Amide. *Chem. Sci.* **2019**, *10*, 1138–1143.
- (13) Hoveyda, A.; Evans, D.; Fu, G. Substrate-Directable Chemical Reactions. *Chem. Rev.* **1993**, *93*, 1307–1370.
- (14) Evans, D.; Morrissey, M. Rhodium(1)-Catalyzed Hydrogenation of Olefins. The Documentation of Hydroxyl-Directed Stereochemical Control in Cyclic and Acyclic Systems. *J. Am. Chem. Soc.* **1984**, *106*, 3866–3868.
- (15) Brown, H.; Rangaishenvi, M. A Simple Procedure for the Synthesis of Three-Carbon Homologated Boronate Esters and Terminal Alkenes via Nucleophilic Displacement in α -Haloallylboronate Ester. *Tetrahedron Lett.* **1990**, *31*, 7115–7118.
- (16) Brown, H.; Brown, C. A Simple Preparation of Highly Active Platinum Metal Catalysts for Catalytic Hydrogenation. *J. Am. Chem. Soc.* **1962**, *84*, 1494–1495.

- (17) Penk, D.; Robinson, N.; Hill, H.; Turlington, M. No Title. *Tetrahedron Lett.* **2017**, *58*, 470–473.
- (18) Ulan, J.; Maier, W.; Smith, D. Rational Design of a Heterogeneous Palladium Catalyst for the Selective Hydrogenation of Alkynes. *J. Org. Chem.* **1987**, *52*, 3132–3142.
- (19) Kuhn, J.; Huang, W.; Tsung, C.; Zhang, Y.; Somorjai, G. Structure Sensitivity of Carbon–Nitrogen Ring Opening: Impact of Platinum Particle Size from below 1 to 5 Nm upon Pyrrole Hydrogenation Product Selectivity over Monodisperse Platinum Nanoparticles Loaded onto Mesoporous Silica. *J. Am. Chem. Soc.* **2008**, *130*, 14026–14027.
- (20) Zhao, X.; Zhao, Y.; Fu, G.; Zheng, N. Origin of the Facet Dependence in the Hydrogenation Catalysis of Olefins: Experiment and Theory. *Chem. Commun.* **2015**, *51*, 12016–12019.
- (21) Tian, N.; Zhou, Z.; Sun, S.; Ding, Y.; Wang, Z. Synthesis of Tetrahedral Platinum Nanocrystals with High-Index Facets and High Electro-Oxidation Activity. *Science (1979)* **2007**, *316*, 732–735.
- (22) Dechert-Schmitt, A.; Garnsey, M.; Wisniewska, H.; Murray, J.; Lee, T.; Kung, D.; Sach, N.; Blackmond, D. Highly Modular Synthesis of 1,2-Diketones via Multicomponent Coupling Reactions of Isocyanides as CO Equivalents. *ACS Catal.* **2019**, *9*, 4508–4515.
- (23) Hubley, A.; Bensalah-Ledoux, A.; Baguenard, B.; Guy, S.; Abécassis, B.; Mahler, B. Surface Chemistry of Perovskite Nanoplatelets Exhibiting Circularly Polarized Luminescence. *ChemRxiv. Cambridge: Cambridge Open Engage.* 2022, pp 1–9.
- (24) Googasian, J.; Lewis, G.; Woessner, Z.; Ringe, E.; Skrabalak, S. Seed-Directed Synthesis of Chiroptically Active Au Nanocrystals of Varied Symmetries. *Chem. Commun.* **2022**, *58*, 11575–11578.
- (25) Leibler, I.; Tekle-Smith, M.; Doyle, A. A General Strategy for C(Sp³)–H Functionalization with Nucleophiles Using Methyl Radical as a Hydrogen Atom Abstractor. *Nat. Commun.* **2021**, *12*, 1–10.
- (26) Jiang, Y.; Weiss, E. Colloidal Quantum Dots as Photocatalysts for Triplet Excited State Reactions of Organic Molecules. *J. Am. Chem. Soc.* **2020**, *142*, 15219–15229.
- (27) Till, N.; Tian, L.; Dong, Z.; Scholes, G.; MacMillan, D. Mechanistic Analysis of Metallaphotoredox C–N Coupling: Photocatalysis Initiates and Perpetuates Ni(I)/Ni(III) Coupling Activity. *J. Am. Chem. Soc.* **2020**, *142*, 15830–15841.

CHAPTER 4

DEPENDANCE OF TRANSITION METAL TELLURIDE PHASES ON METAL PRECURSOR REACTIVITY AND MECHANISTIC IMPLICATIONS

Abstract

Modern bottom-up synthesis to nanocrystalline solid-state materials often lacks the reasoned product control that molecular chemistry boasts from having over a century of research and development. This systematic study demonstrates how rationally matching the reactivity of metal precursors to that of the main group precursor is necessary for the successful production of metal tellurides. Six transition metals including iron, cobalt, nickel, ruthenium, palladium, and platinum were reacted with the mild reagent didodecyl ditelluride in their acetylacetonate, chloride, bromide, iodide, and triflate salts. The first colloidal syntheses of iron and ruthenium tellurides (FeTe_2 and RuTe_2) are reported. Hard–soft acid-base theory could not explain all the trends, and instead, comparison of the reactivity of the metal halides to the metal triflates were explored which suggests that radical stability is the better predictor of metal salt reactivity in this case.

Introduction

The techniques used for the bottom-up synthesis of metal sulfides and selenides do not easily translate to the metal tellurides. Because of the soft nature of tellurium, and more positive reduction potentials compared to that of sulfur and selenium ($E^\circ_{\text{Te}, \text{Te}_2^-} = -1.143 \text{ V}^\circ$, $E^\circ_{\text{Se}, \text{Se}_2^-} = -0.924 \text{ V}^\circ$, $E^\circ_{\text{S}, \text{S}_2^-} = -0.476 \text{ V}^\circ$ vs SHE),¹ successfully capturing metal tellurides in the high temperature conditions common to nanocrystal synthesis can be challenging. Yet metal tellurides are important materials from an application standpoint. Iron,^{2,3} cobalt,^{4,5} and nickel^{6,7} chalcogenides have a variety of applications as mercury capture materials, superconductors, catalysts, and as electromagnetic wave absorption materials. Additionally, ruthenium,^{8,9} palladium,^{10,11} and platinum,¹² chalcogenides have uses as catalysts, electrocatalysis, and suppressors of magnetoresistance. Metal sulfides and selenides have had more synthetic development than the telluride counterparts in bottom-up synthesis, leaving an area of underexplored potential and applications for these nanomaterials. We seek ways to rationally choose conditions that will be successful in the bottom up-syntheses to metal tellurides, rather than simply attempting (and often failing) the translation of conditions from the preparations of metals sulfides and selenides.

The metal tellurides chosen for this study have a wide variety of functions. For example, among the chosen first-row metals, iron tellurides have attracted attention for their applications in batteries and electrochemical

sensors.^{13,14} FeTe₂ nanoparticles were used as an electrochemical sensor to detect four small molecules simultaneously to facilitate early detection of a variety of diseases.¹⁴ Cobalt tellurides are active electrocatalysts and photocatalysts,^{15,16,17} including the use of CoTe nanoparticles as photocatalysts for the reduction of carbon dioxide into methane.¹⁷ Additionally, researchers have shown an interest in nickel tellurides for their applications in electrocatalysis, electronics, and optoelectronics.^{18,19,20} NiTe₂ was studied for their potential use as electrocatalysts for hydrogen evolution.²⁰ Among the second and third-row metals, palladium tellurides act as catalysts in organic synthesis.^{21,22} For instance, these nanoparticles have been tested as catalysts in a classic organic chemistry reaction, the Suzuki-Miyaura coupling.²² In contrast to the former transition metal tellurides discussed, platinum tellurides remain elusive amidst the literature; however, they have intriguing plasmonic and electrocatalytic properties.^{23,24,25} Similarly, very little is known about the characteristic properties of ruthenium tellurides. The ruthenium tellurides are a particularly underexplored space, but other ruthenium chalcogenides are powerful hydrodesulfurization catalysis and supercapacitor materials.^{26,27} However, from what *is* known, RuTe₂ can perform hydrogen evolution and has semiconducting abilities.^{28,29} Phase diagrams have been reported for iron, cobalt, nickel, ruthenium, palladium, and platinum tellurides;^{30,31} however, very few colloidal syntheses have been reported for any of the known phases.

In aqueous conditions, dissolved tellurite and tellurate anions can be employed as tellurium sources. Yuan *et al.* synthesized FeTe from mixtures of Te nanorods and FeCl₃·6H₂O,³² where hydrazine was used to reduce dissolved TeO₂ to form the Te nanorod precursors. Praminik and coworkers dissolved TeO₂ in highly basic solution, and then used NaBH₄ as a reducing agent in the presence of various metal salts. The authors chose this route to make CoTe, NiTe,³³ and FeTe₂.¹⁴ In contrast, Masikini *et al.* dissolved PdCl₂ in highly basic solution and used H₂Te gas to form PdTe quantum dots.³⁴ Lastly, Feng and coworkers used NaTeO₃ and RuCl₃ to prepare RuTe₂ supported on graphene.²⁸

In addition to aqueous conditions, solid-state synthesis is commonly used to make transition metal tellurides as well. Campos *et al.* utilized ball milling to access the iron-rich phase of Fe₅Te₄.³⁵ Furthermore, the Pumera group accessed CoTe₂ and NiTe₂ by heating their corresponding stoichiometric ratios of cobalt, nickel and tellurium powders to 1000 °C.²⁰ Li and coworkers synthesized NiTe from temperatures of 700 and 800 °C for four hours.³⁶ In a similar fashion, Gusmão *et al.* heated the appropriate amounts of platinum and tellurium powders to 950 °C for 10 days and synthesized PtTe₂ and Pt₃Te₄.²⁴ Finally, Tsay *et al.* synthesized RuTe₂ by heating elemental ruthenium and tellurium powders into a quartz ampoule to 1000 °C for 10 days.²⁹

Other varieties of synthesis have been performed to access metal tellurides as well. Kang and coworkers synthesized yolk-shell structured FeTe@C and FeTe₂@FeTe₂-C nanospheres by reductively tellurizing iron nitrate-C nanospheres with H₂Te gas at 400 or 700 °C.¹³ NiTe₂ was prepared in a similar fashion by Duan *et al.*, except NiCl₂ was reductively tellurized with H₂Te gas from 550-700 °C.¹⁹ In contrast, Fu and coworkers

synthesized PtTe₂ crystals through van der Waals epitaxial growth on mica.²³ The authors chose a salts-assisted evaporation strategy to form a homogeneous PtCl₄/NaCl precursor. Both the precursor and tellurium powder were placed in a quartz tube and heated to 800 °C for 30 min under 10% H₂/Ar gas.

For the noble metals, preparations become tricky because of their propensity to simply form metal(0) particles. Single source precursors are a way to ensure bonding between the metal and tellurium. Singh *et al.* synthesized PdTe nanoparticles from single source precursors decorated with organic frameworks.²¹ Similarly, Kumar and coworkers synthesized PdTe and Pd₉Te₄ nanoparticles through thermolysis.²² Lastly, Afzaal and coworkers synthesized a variety of transition metal tellurides, including FeTe₂, NiTe, PdTe, PtTe and PtTe₂ from ditelluroimidodiphosphinate complexes.²⁵

Still other research groups prefer other synthetic methods to access metal tellurides. Shrestha *et al.* synthesized CoTe thin films through the anion exchange of cobalt hydroxycarbonate with an aqueous tellurium powder solution.¹⁶ Ashiq *et al.* utilized hydrazine as the reducing agent for Te(0) in a hydrothermal approach to synthesize CoTe.¹⁷ Nath *et al.* used a similar hydrothermal reaction except with TeO₂ to give Ni₃Te₂. Alternatively, the same group synthesized Ni₃Te₂ films through reductive electrodeposition from a solution of NiSO₄·6H₂O and TeO₂ onto Au.¹⁸ Lastly, Xie *et al.* used a solvothermal approach with CoCl₂·6H₂O and Te(0) powder at 160 °C to synthesize CoTe₂ nanorods.³⁷

As the aforementioned syntheses demonstrate, the methods for synthesizing transition metal tellurides often involve high temperatures, long reaction times, and specialized equipment. There are only a few examples in the literature where colloidal synthesis is utilized, in part, because there are only three common tellurium reagents that have been employed. The Schaak group used *bis*(trimethylsilyl)telluride or TOP-Te to tellurize metal(0) particles to prepare a plethora of transition metal tellurides including: CoTe₂, NiTe₂, PdTe, PdTe₂, PtTe₂, Ag₂Te, and RhTe₂.³⁸ In the presence of *bis*(trimethylsilyl)telluride, the more-reactive tellurium reagent, generally, the more tellurium rich phases are obtained. Unfortunately, one disadvantage to *bis*(trimethylsilyl)telluride, is that it is volatile and very toxic. The less reactive tellurium reagent, TOP-Te, produced the less tellurium rich phase of PdTe. By altering the tellurium reagent's reactivity, they were able to obtain phase control of PdTe *vs.* PdTe₂. In another solution phase synthesis, Yu and coworkers selectively prepared CoTe or CoTe₂ nanofleeces by reacting Te nanowires with Co(acac)₂ at 200 °C.¹⁵ Phase control was obtained by altering the millimoles of the cobalt precursor present.

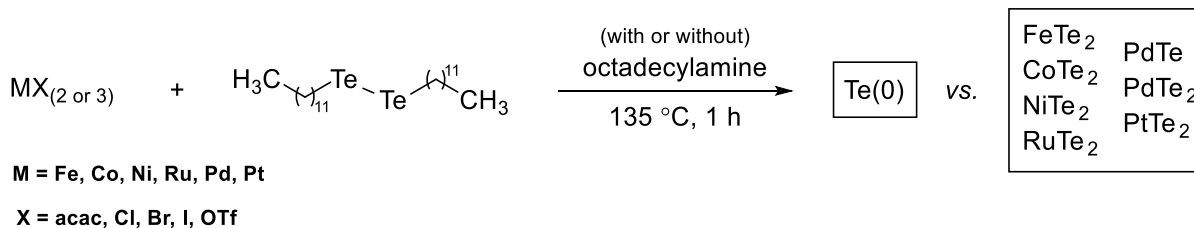
In contrast to the bottom-up preparations, solid-state procedures using stoichiometric mixtures of the metals and tellurium have long produced a larger variety of phases including: Fe₅Te₄, CoTe₂, NiTe, NiTe₂, Pt₃Te₄, PtTe₂, and RuTe₂. Among these phases only CoTe₂, NiTe₂, and PtTe₂ have been accessed *via* colloidal synthesis. Because of this gap of missing phases in the literature from colloidal synthesis, more work must be

done to investigate how to obtain the more exotic phases, typically only observed under solid-state reaction conditions.

Our group has pioneered the use of didodecyl ditelluride as an exceedingly mild reagent for the synthesis of copper tellurides, as it reacts at temperatures that are considered low for colloidal synthesis (< 200 °C). For example, we obtained a metastable phase of Cu_{1.5}Te and CuTe at 135 °C and 155 °C, respectively.³⁹ An added benefit of didodecyl ditelluride is that the red solid has minimal stench, unlike the corresponding selenide. Other than limiting extended light exposure and storage at 0 °C, no special training is required to use or handle this chemical. With the scalability of colloidal synthesis and the mild reaction conditions particularly afforded by this new reagent didodecyl ditelluride, there is potential to readily prepare kinetically trapped phases to allow for a more extensive study and use of metal tellurides in applications. However, as very mild reagent, it is likely that the limiting component will not be the reactivity of the telluride reagent, but rather that of the metal source. Both must be reactive enough at the moderate temperatures to reap the rewards of the mild tellurium source.

Thus, how does one choose a metal source? Toxicity and safety can be a concern, and an infamous example is the early cadmium chalcogenide quantum dot syntheses which used a toxic CdMe₂ reagent, but now CdO is almost exclusively used.⁴⁰ Solubility in heavy organic media is a consideration, and long chain-ligands, such as carboxylates and amines, can be employed either intentionally or serendipitously. For example, recognizing that cadmium oleate binds as a Z-type ligand is important to consider.^{41,42} The counterions from the metal source were also long under examination in their role in surface passivation of the growing crystals.⁴³ To our knowledge, there has not been a systematic study of how the inherent reactivity of the metal precursor can influence the product phase in bottom-up synthesis.

Herein, this work describes a solution phase synthesis of iron, cobalt, nickel, ruthenium palladium, and platinum tellurides under mild reaction temperatures and times, using metal acetylacetonate, chloride, bromide, iodide, triflate salts and didodecyl ditelluride (**Scheme 4.1**). It was found that modulating the reactivity of the chosen transition metal precursor determined whether a metal telluride was achieved and, in the particular case of the palladium tellurides, determined the phase. The results suggest the trends in reactivity are correlated with radical stability of the metal precursor. Of these six transition metal tellurides, the first nanoparticle syntheses of iron and ruthenium tellurides *via* colloidal syntheses are reported.



Scheme 4.1. The reaction of various metal precursors with didodecyl ditelluride gives Tellurium or Transition Metal Tellurides.

Experimental Section

Materials

All reactions were performed in oven-dried 15 mL three neck round-bottomed flasks using standard Schlenk line techniques under an argon atmosphere. Reaction temperatures were controlled using a thermocouple, and stirring rates were set to 1,200 rpm. Reactions without octadecylamine were degassed at 80 °C for 30 min prior to injection; reactions with octadecylamine and/or metal hydrates were degassed at (100 – 135) °C for 1 h to remove water prior to injection.

Cobalt(II) acetylacetonate ($\text{Co}(\text{acac})_2$, 97%), cobalt(II) chloride anhydrous (CoCl_2 , $\geq 98\%$), dioctyl ether (99%), iron(II) acetylacetonate ($\text{Fe}(\text{acac})_2$, 99.95% trace metals basis), iron(II) bromide anhydrous (FeBr_2 , 98%), iron(II) iodide anhydrobeads (FeI_2 , $\geq 99.99\%$ trace metals basis), nickel(II) acetylacetonate ($\text{Ni}(\text{acac})_2$, 95%), nickel(II) chloride hexahydrate ($\text{NiCl}_2 \cdot 6\text{H}_2\text{O}$, 99.9%), octadecylamine (97%), and trifluoromethanesulfonic acid ($\geq 99\%$) were obtained from Sigma Aldrich. Cobalt(II) bromide hydrate ($\text{CoBr}_2 \cdot \text{XH}_2\text{O}$), cobalt(II) iodide anhydrous (CoI_2 , min. 95%), cobalt(II) trifluoromethanesulfonate ($\text{Co}(\text{OTf})_2$, 98%), iron(II) chloride anhydrous (FeCl_2 , 98%), iron(II) trifluoromethanesulfonate ($\text{Fe}(\text{OTf})_2$, 98%), nickel(II) bromide (NiBr_2 anhydrous, 99+%), nickel(II) trifluoromethanesulfonate ($\text{Ni}(\text{OTf})_2$, 98%), palladium(II) acetylacetonate ($\text{Pd}(\text{acac})_2$, 99%), palladium(II) bromide (PdBr_2 , 99%), palladium(II) chloride (PdCl_2 , 99.9%), palladium(II) iodide (PdI_2 , 99%), palladium(II) nitrate hydrate ($\text{Pd}(\text{NO}_3)_2 \cdot \text{XH}_2\text{O}$) (Pd ~40%, 99.9%-Pd), platinum(II) acetylacetonate ($\text{Pt}(\text{acac})_2$, 98%), platinum(II) bromide (PtBr_2 , 98%), platinum(II) chloride (PtCl_2 , 99.9%), platinum(II) iodide (PtI_2 , min. 98%), ruthenium(III) acetylacetonate ($\text{Ru}(\text{acac})_3$, 99%), ruthenium(III) bromide hydrate ($\text{RuBr}_3 \cdot \text{XH}_2\text{O}$), ruthenium(III) chloride anhydrous (RuCl_3), and ruthenium(III) iodide anhydrous (RuI_3 , 98+%) were obtained from Strem Chemicals. XRD analysis of the ruthenium(III) chloride found it to be instead RuOCl_2 .⁴⁴ Nickel(II) iodide (NiI_2 , 98%) was obtained from Ambeed, Inc. All materials were used from the commercial suppliers without further purification.

Synthesis of Transition Metal Telluride (No Ligand)

A solution of metal precursor (0.25 mmol) in dioctyl ether (2.5 mL) was placed in a 15 mL three-neck round bottom flask and was degassed under vacuum at 80 °C for 30 min. A solution of didodecyl ditelluride (0.25 mmol) in dioctyl ether (1.0 mL) was degassed under vacuum at room temperature for 30 min. Both flasks were placed under an argon atmosphere, and then evacuated and refilled with argon three times. The reaction flask containing the metal precursor was heated to 135 °C, and the telluride precursor was injected into the reaction

vessel. The reaction mixture was allowed to stir for 1 h and then cool to room temperature. The post reaction mixture was precipitated in acetone and resuspended in chloroform two to three times (8000 rpm, 8 min).

Synthesis of Transition Metal Telluride (with Octadecylamine)

A solution of metal precursor (0.25 mmol) and octadecylamine (0.50 mmol) in dioctyl ether (2.5 mL) was placed in a 15 mL three-neck round bottom flask and was degassed under vacuum at (100-135) °C for 1 h. A solution of didodecyl ditelluride (0.25 mmol) in dioctyl ether (1.0 mL) was degassed under vacuum at room temperature for 1 h. Both flasks were placed under an argon atmosphere, and then evacuated and refilled with argon three times. The reaction flask containing the metal precursor was heated to 135 °C, and the telluride precursor was injected into the reaction vessel. The reaction mixture was allowed to stir for 1 h and then cool to room temperature. The post reaction mixture was precipitated in warm isopropanol and resuspended in chloroform two to three times (8000 rpm, 8 min).

Synthesis of Palladium Trifluoromethanesulfonate Pd(OTf)₂

To a solution of Pd(NO₃)₂·XH₂O (57.9 mg, 0.25 mmol) in H₂O (8 drops) was added trifluoromethanesulfonic acid (0.88 mL, 10 mmol) dropwise at 0 °C. The resulting purple suspension was allowed to warm to room temperature and stir for 2 h. The post reaction mixture was precipitated with dioctyl ether (8000 rpm, 8 min). The crude material was immediately carried forward into the next reaction with didodecyl ditelluride. This procedure is adapted from the literature.⁴⁵

Characterization

Transmission Electron Microscopy (TEM) was performed on a FEI Technai Osiris 200 kV S/TEM system with EDS mapping capabilities. TEM samples were prepared by dropping a CHCl₃ suspension of the nanoparticles onto a carbon coated Cu or Ni grid. X-ray Diffraction (XRD) measurements were performed using a Rigaku SmartLab powder X-ray diffractometer with a CuKα (λ = 0.154 nm) radiation source set to 40 kV and 44 mA, and a D/teX Ultra 250 1D silicon strip detector. XRD patterns were acquired using a step size of 0.1 ° at 2.5 °/min.

Results and Discussion

In previous works, our lab has established novel syntheses to copper chalcogenides using didodecyl diselenide and didodecyl ditelluride. These syntheses were notable in that the copper chalcogenide products were rare metastable phases such as wurtzite-like $\text{Cu}_{2-x}\text{Se}^{46}$ and $\text{Cu}_{1.5}\text{Te}^{39}$ as well as the first reported colloidal synthesis of vulcanite CuTe . The reagents reacted at moderate temperatures for nanocrystal syntheses: didodecyl diselenide (155 °C) and didodecyl ditelluride (135 and 155 °C). The low synthetic temperatures may partially explain the ability of these reagents to trap the metastable phases and prevent a transformation to more thermodynamically stable phases at higher temperatures.

Control studies indicate that matching the reactivity of the telluride precursor to that of the metal source is important, since the tellurium precursor can decompose on its own at elevated temperatures; didodecyl ditelluride heated to 135 °C for 1 h yields tellurium metal. In both reported syntheses of $\text{Cu}_{1.5}\text{Te}$ and CuTe ,³⁹ $\text{Cu}(\text{acac})_2$ was employed as a copper source; it was reactive at the moderate synthetic temperatures of 135 and 155 °C and able to “capture” the Te precursor before decomposition. This result reinforced the hypothesis that in order to obtain a desired transition metal telluride, the intervention of a metal precursor with comparable reactivity would be needed to form a metal telluride and prevent the decomposition of the didodecyl ditelluride to $\text{Te}(0)$.

Herein, we further the use of didodecyl ditelluride as a useful reagent for the synthesis of a broad range of metal tellurides. However, as one ventures farther from Cu on the periodic table, the bond strength and chemistry of the metal precursors will change the reaction landscape. Poor reactivity of the metal precursor may prevent the formation of metal tellurides. Furthermore, when more than one phase of metal telluride is possible, the reactivity of the metal precursor may also influence the resultant phase. For this reason, a comprehensive and systematic study of a variety of metal precursors was performed to provide rational, predictable trends.

Transition metal tellurides of iron, cobalt, nickel, ruthenium, palladium, and platinum were synthesized from various metal precursors of acetylacetonates, chlorides, bromides, iodides, and triflates with didodecyl ditelluride. For consistency, a 1:1 molar ratio (i.e. 1 metal atom : 2 tellurium atoms) of the reagents were used in dioctyl ether at a constant reaction temperature of 135 °C for 1 h. XRD was used to identify the crystalline products (**Figures 4.1 & 4.2**) and summarized in (**Tables 4.1 & 4.2**). Metal tellurides were identified for all of the metals studied including FeTe_2 (Frohbergite), CoTe_2 (Cobalt Telluride), NiTe_2 (Melonite), RuTe_2 (Ruthenium Telluride), PdTe (Kotulskite), PdTe_2 (Merenskyite) and PtTe_2 (Moncheite). Of particular note, these are the first reported colloidal syntheses of FeTe_2 and RuTe_2 .

FeTe_2 and RuTe_2 have marcasite and pyrite structures, respectively, and were straight forward to identify by XRD. In contrast, CoTe_2 , NiTe_2 , PdTe_2 and PtTe_2 all have layered $\text{Cd}(\text{OH})_2$ structures which sometimes can be challenging to distinguish from the MTe phases by XRD in nanomaterials. EDS was employed to confirm the

MTe₂ stoichiometry (ESI); however, because the differentiation between NiTe vs NiTe₂ and PdTe vs PdTe₂ was very clear by XRD, EDS was not deemed necessary for these metal telluride materials.

It was found that there was a critical dependence of the reaction products on the choice of metal precursor (**Table 4.1** & **Figure 4.1**). Among the first-row transition metals (Fe, Co, and Ni), the acetylacetonates and chlorides only produced tellurium metal, which indicates these precursors were not reactive enough to produce metal tellurides. While NiBr₂ did produce a telluride, only the iodides for all three metals consistently provided a metal telluride product.

Table 4.1. Summary of Phases (no ligand)

Precursor	Fe	Co	Ni	Ru ^a	Pd	Pt
M(acac) ₂	Te	Te	Te	Te	PdTe	PtTe ₂
MCl ₂	Te	Te	Te	Te, RuOCl ₂	PdTe, PdTe ₂	PtTe ₂
MBr ₂	Te	Te	NiTe ₂	Ru	PdTe, PdTe ₂	PtTe ₂
MI ₂	Fe, FeTe ₂	CoTe ₂	NiTe ₂	RuTe ₂	PdTe ₂	PtTe ₂
M(OTf) ₂	Te	Te	Te	—	PdTe ₂	—

^aAll ruthenium precursors utilized were in the +3 oxidation state. The purchased “RuCl₃” precursor was analyzed by XRD and found to be RuOCl₂.

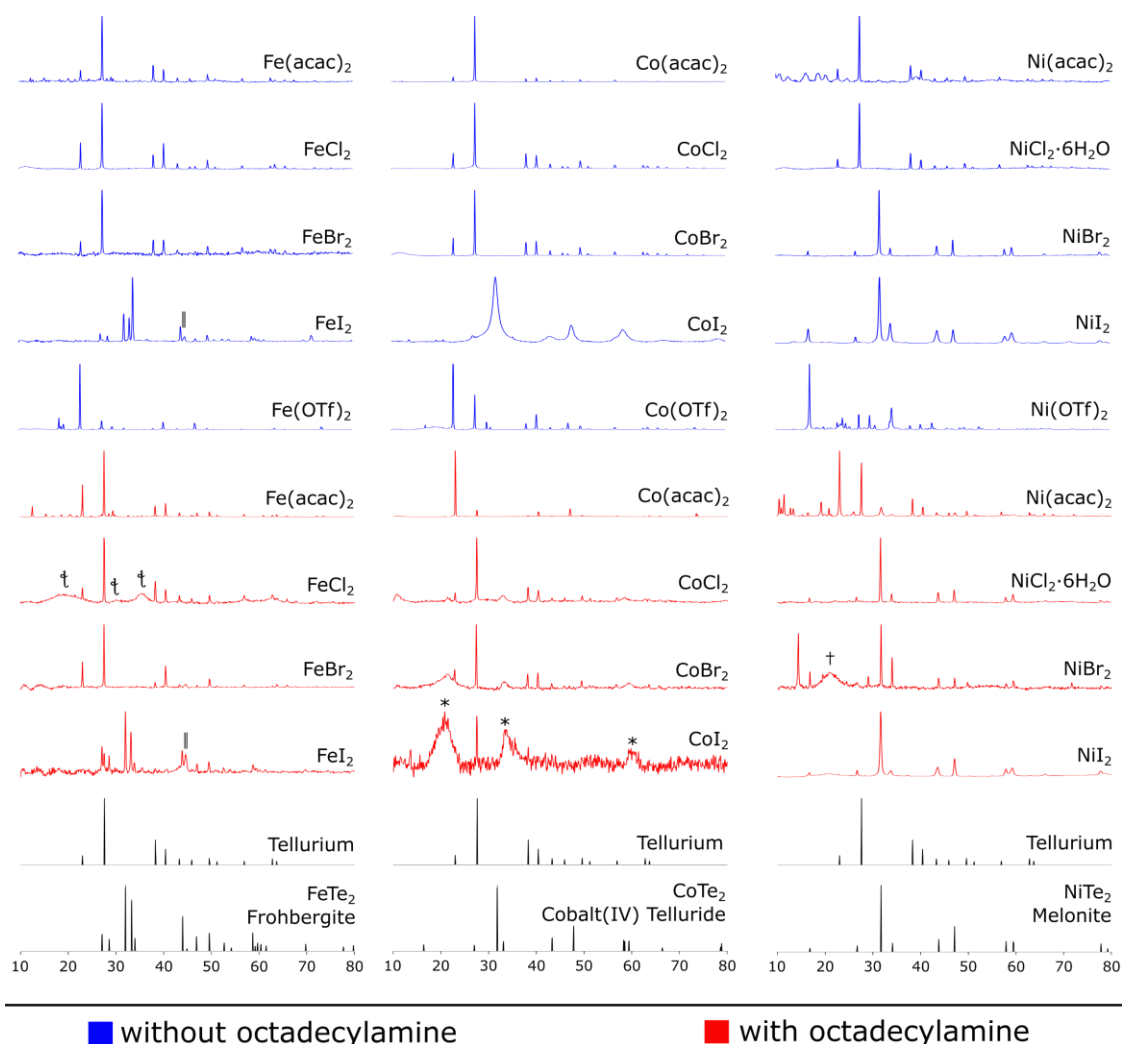


Figure 4.1. XRD of the products of iron, cobalt and nickel salts with didodecyl ditelluride. ICDD: † Fe: #4113931. ‡ Magnetite: #159959. * Different polymorph of CoI_2 confirmed by EDS. † Amorphous octadecylamine (See ESI). Tellurium: #1011098, Frobergite: #77319, Cobalt Telluride: #625401, Melonite: #159382. (For convenience starting metal precursors for every experiment were indicated above each corresponding XRD trace.)

The trend in reactivity of the first-row transition metal precursors appears to match hard–soft acid–base (HSAB) theory. $\text{Fe}(\text{acac})_2$, $\text{Co}(\text{acac})_2$, and $\text{Ni}(\text{acac})_2$ as well as FeCl_2 , CoCl_2 , and NiCl_2 are seemingly the least reactive metal precursors due to the hard–hard interactions and strong–orbital–overlapping characteristics of these reagents. The inability to react with didodecyl ditelluride caused only decomposition to $\text{Te}(0)$ to be observed. Contrastingly, metal iodides were expected to be most reactive due to the hard–soft interactions and poor orbital overlap. Indeed, these were the reagents that gave tellurium-rich phases of FeTe_2 , CoTe_2 and NiTe_2 . (FeTe_2 was particularly prone to oxidation; air-free purification and characterization were needed.) Furthermore, HSAB can explain why of the bromides, NiBr_2 was the only one to provide a metal telluride. The order of hardness of the three metals follows $\text{Fe}^{2+} < \text{Co}^{2+} < \text{Ni}^{2+}$; therefore, hard Ni^{2+} should have the weakest NiX_2 bonds with soft Br^- . However, interestingly, HSAB does not explain the results of the second and third-row metals (*vide infra*).

An alternative hypothesis proposes that the reactivity correlates with the stability of a radical halide, which follows $\text{Cl} \cdot < \text{Br} \cdot < \text{I} \cdot$.⁴⁷ In general, halides can undergo *both* one or two-electron chemistry. A good demonstration of this phenomenon is the Finkelstein reaction in which the $\text{S}_{\text{N}}2$ displacement of a primary alkyl halide is replaced with another halide in a two-electron fashion. However, there are reported instances of sequential cation-free radical mechanisms where dimeric and rearranged products can occur.⁴⁸

To test if one or two-electron chemistry dominates the reactivity of these systems, the products resulting from metal halide and triflate precursors were compared. It is known that metal halides and triflates often have comparable chemistry, but what distinguished the triflates is that they do not easily undergo one-electron chemistry, unlike halides. Triflates are known to be excellent leaving groups in two-electron chemistry such as $\text{S}_{\text{N}}1$ and $\text{S}_{\text{N}}2$ reactions, which follows $\text{Cl}^- < \text{Br}^- < \text{I}^- < \text{OTf}^-$.⁴⁹ Metal triflates similarly are considered "super Lewis Acids".⁵⁰ Thus, a comparison of the reactivity of metal halides with metal triflates can provide evidence for one or two-electron chemistry.

The first-row metal triflates of iron, cobalt, and nickel each reacted with didodecyl ditelluride at 135 °C for 1 h to compare to the metal halides. $\text{Fe}(\text{OTf})_2$, $\text{Co}(\text{OTf})_2$, and $\text{Ni}(\text{OTf})_2$ were all unreactive with the didodecyl ditelluride, and instead only Te metal and polymorphs of the triflate precursors were isolated (identified through control reactions without the presence of didodecyl ditelluride. See ESI.) (**Table 4.1** & **Figure 4.1**). Since the triflates were very unreactive towards the didodecyl ditelluride, yet the iron, cobalt and nickel(II) iodides and nickel(II) bromide were, they must undergo a differing reaction mechanism. It can be cautiously hypothesized that one-electron chemistry dominates this reaction of metal halides with didodecyl ditelluride to form metal tellurides.

The second and third-row metals (Ru, Pd, and Pt) appear to undergo more complex chemistry which further indicates that HSAB theory does not adequately explain the observed phases (**Table 4.1** & **Figure 4.2**). For example, HSAB theory would predict the weakest metal-ligand bonds for $\text{Ru}(\text{acac})_3$ and RuOCl_2 , and so these should be the most reactive, whereas RuI_3 was expected to be least reactive due to the soft-soft interaction. However, $\text{Ru}(\text{acac})_3$ and RuOCl_2 did not yield metal tellurides, only Te(0) metal, and RuI_3 produced RuTe_2 . Thus, HSAB does not explain the results of the ruthenium precursors. Among the palladium series, all reagents were reactive enough to provide a metal telluride phase. $\text{Pd}(\text{acac})_2$ gave PdTe, whereas PdI_2 yielded the more tellurium-rich phase PdTe_2 . PdCl_2 and PdBBr_2 gave mixtures of the two phases, and again, this is contrary to the expected reactivity of HSAB where Pd^{2+} is a soft metal. Similar to the palladium phases, all the platinum precursors successfully produced PtTe_2 . The broad XRD peaks indicate small crystallite sizes due to a burst nucleation event. $\text{Pt}(\text{acac})_2$ gave the sharpest peaks, suggesting the slowest chemistry of the precursors to yield fewer nuclei growing to larger sizes. Once more, the trend in the size of the crystallites of the produced PtTe_2 contrasts with

HSAB. Furthermore, PtCl_2 left a significant amount of starting material, suggesting it was the least reactive of the halides, even though it should have the weakest bonds of the halides, because of the hard-soft interaction.

Efforts were made to synthesize the ruthenium, palladium, and platinum triflates to further probe the radical stability hypothesis of these second and third-row metals, however, our numerous endeavors were not successful for the ruthenium and platinum metals using triflic acid or silver triflate. However, a procedure adapted from literature,⁴⁵ to synthesize palladium triflate from palladium nitrate and triflic acid was successful; this purple material was prone to decomposition even in air-free conditions. Thus, once palladium triflate was synthesized, it was immediately subjected into the next reaction with didodecyl ditelluride at 135 °C without further purification or characterization. $\text{Pd}(\text{OTf})_2$ allowed the formation of PdTe_2 ; in contrast, PdBr_2 produced a mixture of mostly PdTe and PdTe_2 , whereas PdI_2 produced PdTe_2 . (**Table 4.1** & **Figure 4.2**). Since the triflate salt *did* react with the didodecyl ditelluride, two electron chemistry must be possible on palladium with this reagent. Despite the evidence for two-electron chemistry, the reactivity trends of halides still suggest that HSAB theory is a poor predictor of reactivity.

Trends were very difficult to identify for the ruthenium precursors. To begin with, the speciation of ruthenium chlorides is often mislabeled and identified. Indeed, the purchased “ RuCl_3 ” was found to be RuOCl_2 (ESI). The only product of the reactions with $\text{Ru}(\text{acac})_3$ and RuOCl_2 was a very small amount of $\text{Te}(0)$ and precursor. Raising the reaction temperatures from 135°C to 175 °C and 200 °C, saw only more $\text{Te}(0)$ form indicating no reaction with the ruthenium salts.

RuBr_3 was found to be properly labeled (ESI), however, interestingly, the product in this case was $\text{Ru}(0)$. The only other metal salt in this study to provide $\text{M}(0)$ was FeI_2 which was a minor product compared to FeTe_2 . Control experiments for these two precursors without the tellurium source did not give Ru or Fe metal. A simple redox process is possible, yet an examination of reduction potentials shows that the potential of even Te^{2-} is insufficient to act as a reductant from Ru^{3+} or Fe^{2+} to give their metals ($E^\circ_{\text{Te}, \text{Te}^{2-}} = -1.143 \text{ V}^\circ$, $E^\circ_{\text{Ru}^{3+}, \text{Ru}^{2+}} = 0.2487 \text{ V}^\circ$, $E^\circ_{\text{Ru}^{2+}, \text{Ru}} = 0.455 \text{ V}^\circ$, $E^\circ_{\text{Fe}^{2+}, \text{Fe}} = -0.447 \text{ V}^\circ$).¹ Furthermore, it would be expected that the more noble Pd and Pt would be more likely to be reduced yet were not. RuBr_3 will decompose above 400 °C,⁵⁴ and perhaps the didodecyl ditelluride may be catalyzing this process. The chemistry of Ru and Pd is particularly complicated, and it is possible that both one and two-electron mechanisms are active, especially given that these two metals are known to perform varied metal-carbon chemistry.^{55,56}

In contrast to RuBr_3 , RuI_3 provided RuTe_2 as a product, consistent with the other metal iodides studied. It is unclear why RuI_3 “behaved” while RuBr_3 did not, but it is clear that caution and skepticism should be employed when using ruthenium halides as reagents.

It is curious to note that the tellurium rich phases MTe_2 were synthesized almost exclusively, even though MTe are known for many of these metals. Both FeTe_2 and RuTe_2 express Te-Te covalent bonds (formally Te_2^{2-}

units), whereas the Te-Te bonding is through van der Waals interactions in the layered structures of CoTe₂, NiTe₂, PdTe₂ and PtTe₂. Similarly, we achieved the first colloidal synthesis of CuTe (Vulcanite) nanosheets using didodecyl ditelluride, which also features Te-Te van der Waals gaps. It is possible that the proposed one-electron decomposition routes of the didodecyl ditelluride reagent on the metal cations facilitates this type of bonding by selectively breaking the C-Te bonds of the ditellurides. While intermediates from oxidation addition of ditellurides on M(0) complexes have been captured and identified,^{51,52,53} we are unaware of any captured intermediates of reactions of ditellurides onto M(II) and M(III) complexes.

Nanocrystal syntheses are most often conducted in the presence of long chain ligands, which not only provide surface capping to growing crystals, but also are increasingly recognized to their ability to moderate the reactivity of the precursors and influence the resultant phases. For this reason, the formation of metal tellurides was repeated in the presence of octadecylamine (**Figure 4.1**, **Figure 4.2** & **Table 4.2**).

Table 4.2. Summary of Phases (with Octadecylamine)

Precursor	Fe	Co	Ni	Ru ^a	Pd	Pt
M(acac) ₂	Te	Te	Te, NiTe ₂	N/A	PdTe	PtTe ₂
MCl ₂	Te	Te	NiTe ₂	RuOCl ₂	PdTe	PtTe ₂
MBr ₂	Te	Te	NiTe ₂	Ru	PdTe, PdTe ₂	PtTe ₂
MI ₂	Te, FeTe ₂	Te	NiTe ₂	RuTe ₂	PdTe, PdTe ₂	PtTe ₂

^aAll ruthenium precursors utilized were in the +3 oxidation state. The purchased “RuCl₃” precursor was analyzed by XRD and found to be RuOCl₂.

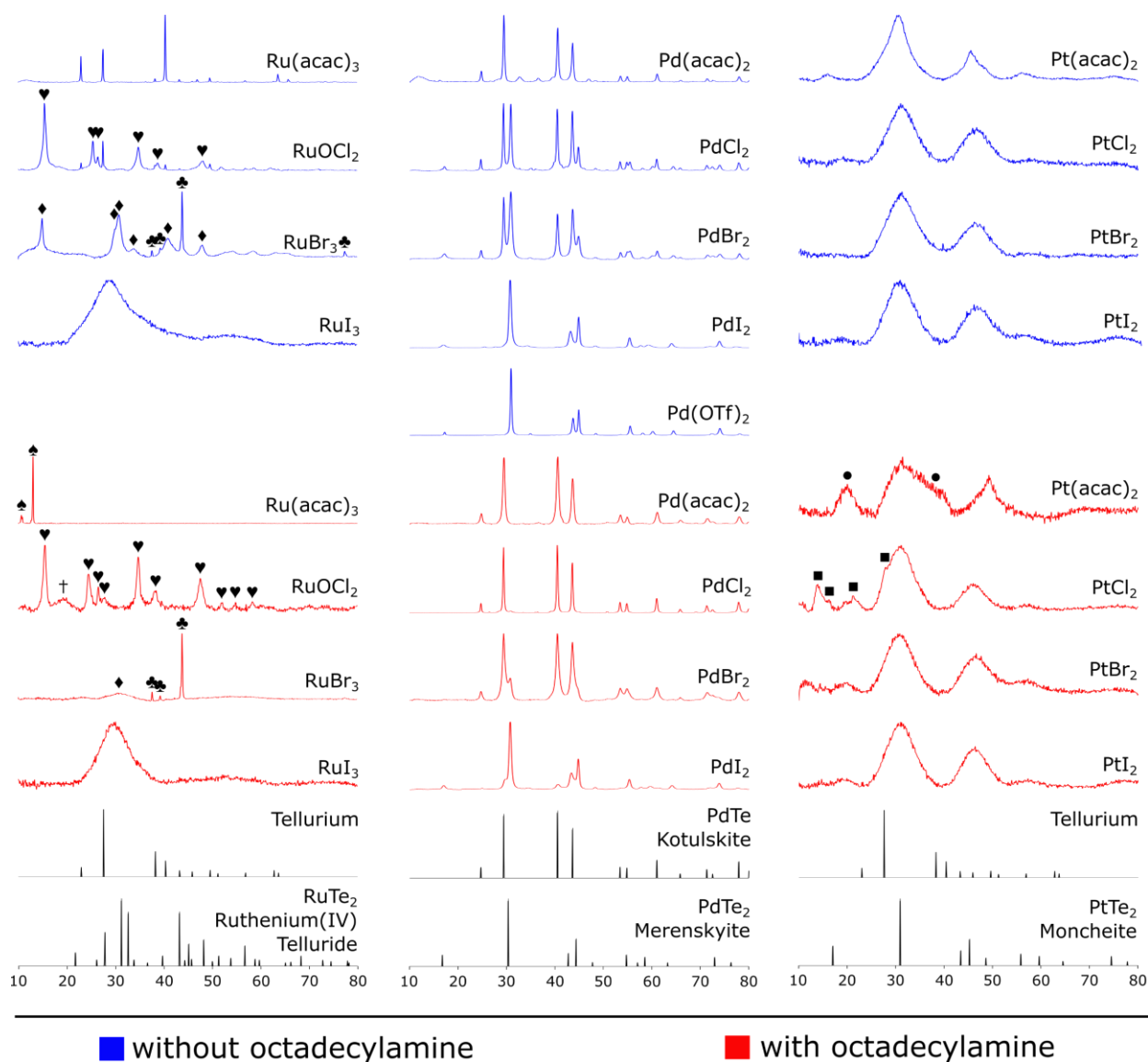


Figure 4.2. XRD of the products of ruthenium, palladium, and platinum with didodecyl ditelluride. ICDD: ♥ unreacted RuOCl_2 - impurity from RuCl_3 starting material (See ESI), ♦ RuBr_3 : #413691, ♣ Ruthenium: #9008513, ♠ $\text{RuC}_{17}\text{H}_{18}\text{O}_3$: #4064886, ● Pt_3O_4 : #27836, ■ PtCl_2 : #28527, Tellurium: #1011098, Ruthenium Telluride: #106001, Kotulskite: #648992, Merenskyite: #648995, Moncheite: #105813.

The comparisons of the reactions with and without octadecylamine highlight the dangers of broadly applying hypothesized mechanisms across metals. For some metals, the presence of the amine does not seem to change product phases (Ru, Pt); in others the amine enhanced the reactivity with the didodecyl ditelluride and the formation of metal tellurides (Ni), and in others, decreased the formation of tellurium rich metal tellurides (Fe, Co, Pd).

The addition of octadecylamine to the reaction with FeI_2 introduced a $\text{Te}(0)$ impurity. Similarly, the amine with CoI_2 prevents CoTe_2 from forming with any of the precursors. Of peculiar interest, the ligand *helps* with the formation of NiTe_2 for all four metal precursors, not just from NiBr_2 and NiI_2 this time. The amine also allowed NiI_2 to produce defined hexagonal platelets (**Figure 4.3**).

Is the reason for the unpredictable behavior of the amine that the metals are less reactive, or that the amine speeds the Te decomposition? The situation is complex, but a control experiment indicated that octadecylamine neither inhibited nor sped up the decomposition of dodecyl ditelluride. The amine in most cases, will be a stronger ligand than the halides, and ligand substitution on the precursor may make precursors more inert or labile, depending on their unique *d* electron counts and coordination geometry. Each of these metals deserves its own independent study to identify the most important factors.

If one compares the results of the second and third-row metals with and without octadecylamine the results are similar, however, exceptions are present in this dataset. One exception is that Ru(acac)₃ with the ligand provided no crystalline product, and only starting material was recovered. Another is with “RuCl₃” where only RuOCl₂, the oxidized impurity from the starting material, is observed, rather than both Te(0) and RuOCl₂. Here the presence of the amine prevented the decomposition of didodecyl ditelluride. The second exception is the trend of the palladium series. The amine appears to improve and promote the formation of PdTe, over PdTe₂, possibly by simply slowing down reactivity, or by selectively inhibiting two-electron processes (**Table 4.1** vs. **Table 4.2**) that we identified were needed for the formation of PdTe₂ from the Pd(OTf)₂ experiment.

No overall trends seem to be present among the transition metals and octadecylamine, and only seem to be metal specific. It is interesting that while the metal precursor is kept constant, different phases are observed with the amine. These results are a good starting point especially for FeTe₂ and RuTe₂, as this is the first colloidal syntheses for these two materials. However, further investigation of ligand effects must be done to see if any shape control can be obtained like with NiI₂.

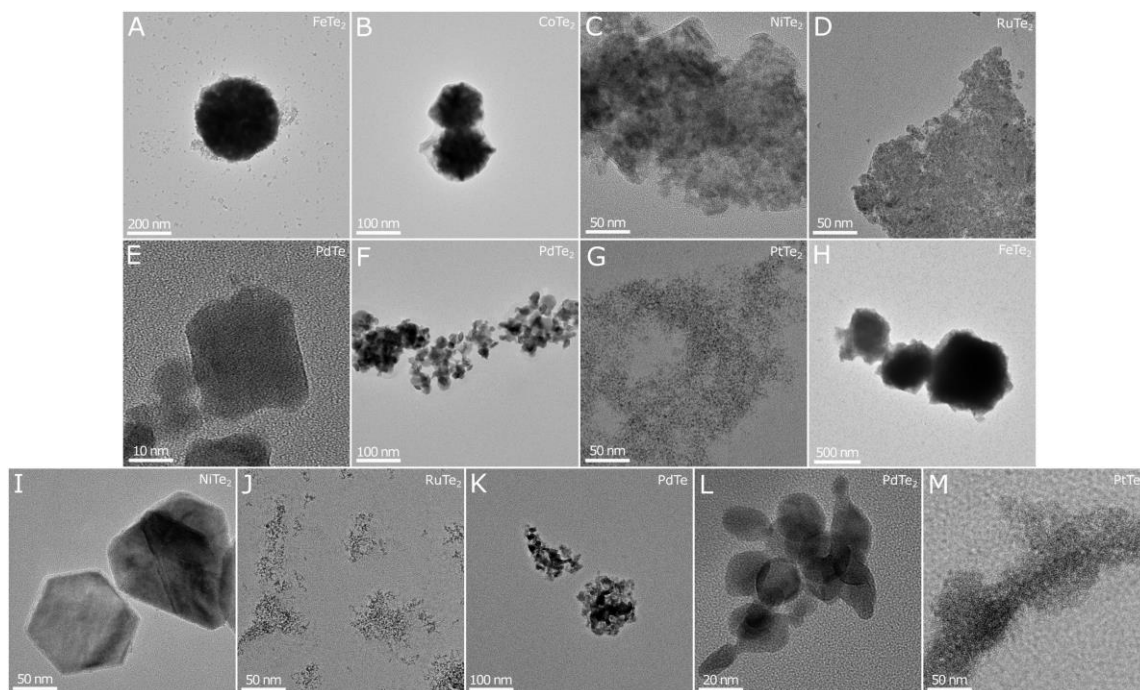


Figure 4.3. Representative TEM images. **A-G:** Without octadecylamine. **A.** from FeI_2 , **B.** from CoI_2 , **C.** from NiI_2 , **D.** from RuI_3 , **E.** $\text{Pd}(\text{acac})_2$, **F.** from PdI_2 , **G.** from PtCl_2 . **H-M:** With octadecylamine. **H.** from FeI_2 , **I.** from NiI_2 , **J.** from RuI_3 , **K.** from $\text{Pd}(\text{acac})_2$, **L.** from PdI_2 , **M.** from PtBr_2 .

Conclusion

Didodecyl ditelluride was used as a reagent in the synthesis of transition metal tellurides at a moderate temperature of 135 °C. FeTe_2 (Frohbergite), CoTe_2 (Cobalt Telluride), NiTe_2 (Melonite), RuTe_2 (Ruthenium Telluride), PdTe (Kotulskite), PdTe_2 (Merenskyite) and PtTe_2 (Moncheite) were synthesized. These represent the first colloidal syntheses to FeTe_2 (Frohbergite) and RuTe_2 (Ruthenium Telluride).

Through an extensive and systematic study of MX_2 (and RuX_3) precursors, it was found that the choice of the coordinating anion, X^- , was instrumental to the success of the reaction. Chosen metal precursors included the acetylacetonates, chlorides, bromides, iodides, and triflates of the six aforementioned-transition metals. When using such a mild tellurium reagent, with a propensity to form $\text{Te}(0)$ side products, it was important for the MX_2 or MX_3 salts to have weak bonds.

Among the first-row transition-metal precursors of Fe, Co, and Ni, only the iodides consistently gave metal telluride phases, while others only provided tellurium metal. Originally, HSAB theory was used to explain these initial results, but application of the same hypothesis to the second and third-row metals failed. Instead, “unsuccessful” reactions with the first-row transition metal triflates, which only undergo two electron chemistry, suggest that the reaction to MTe_2 undergoes a one-electron mechanistic route. Thus, radical stability was instead the better predictor of MX_2 reactivity in this reaction over HSAB. The seeming tendency to form MTe_2 phases

rather than MTe phases suggests that possibly this mechanism involves selective breaking of C-Te bonds in didodecyl ditelluride.

Additionally, attempts were made to synthesize metal triflates of the second and third row metals, but only Pd(OTf)₂ was successful. Reactions with this reagent suggest, in comparison to that of the halides, that a two-electron mechanism furnishes PdTe₂, whereas a one electron route yields PdTe.

The addition of octadecylamine did not provide consistent reaction patterns across the metals studied. Sometimes it promoted the production of the metal telluride, and in others it was a hindrance. While we attempt to identify and interpret trends across the late transition metals, the study with added amine gives us pause; each metal with its unique electron configuration may require individual consideration outside of its neighbors on the periodic table.

This work is just the tip of the iceberg of what the nanomaterial community truly needs to be able to predictably understand how phases form. These types of systematic studies will provide the basis for rational approaches to the syntheses of more complex phases and, by extension, sophisticated technological applications of those materials that we are currently unable to access or foresee with our current toolset. Mechanistic understanding of *how* phases form will become essential in the future to rationally synthesize materials for more elaborate applications.

References

- (1) Electrochemical Series. In *CRC Handbook of Chemistry and Physics*; Lide, D., Frederikse, H., Eds.; CRC Press, Inc., 1994; pp 8.21-8.31.
- (2) Vivanco, H.; Rodriguez, E. The Intercalation Chemistry of Layered Iron Chalcogenide Superconductors. *J. Solid State Chem.* **2016**, *242*, 3–21.
- (3) Liu, Z.; Li, Z.; Xie, X.; Yang, S.; Fei, J.; Li, Y.; Xu, Z.; Liu, H. Development of Recyclable Iron Sulfide/Selenide Microparticles with High Performance for Elemental Mercury Capture from Smelting Flue Gas over a Wide Temperature Range. *Environ. Sci. Technol.* **2020**, *54*, 604–612.
- (4) Maneeprakorn, W.; Malik, M.; O'Brien, P. The Preparation of Cobalt Phosphide and Cobalt Chalcogenide (CoX, X = S, Se) Nanoparticles from Single Source Precursors. *J. Mater. Chem.* **2010**, *20*, 2329–2335.
- (5) Butterfield, A.; McCormick, C.; Veglak, J.; Schaak, R. Morphology-Dependent Phase Selectivity of Cobalt Sulfide during Nanoparticle Cation Exchange Reactions. *J. Am. Chem. Soc.* **2021**, *143*, 7915–7919.
- (6) Ren, H.; Huang, Z.; Yang, Z.; Tang, S.; Kang, F.; Lv, R. Facile Synthesis of Free-Standing Nickel Chalcogenide Electrodes for Overall Water Splitting. *J. Energy Chem.* **2017**, *26*, 1217–1222.
- (7) Li, C.; Li, X.; Yang, S.; Wang, H.; Wang, G. Synthesis of Controllable Nickel Chalcogenide Nano-Hollow Spheres and Their Tunable Absorbing Properties. *ChemistrySelect* **2020**, *5*, 8185–8193.
- (8) Mbese, J.; Ajibade, P. Homonuclear Tris-Dithiocarbamate Ruthenium(III) Complexes as Single-Molecule Precursors for the Synthesis of Ruthenium(III) Sulfide Nanoparticles. *J. Sulfur Chem.* **2016**, *38*, 173–187.
- (9) Zhao, Y.; Cong, H.; Li, P.; Wu, D.; Chen, S.; Luo, W. Hexagonal RuSe₂ Nanosheets for Highly Efficient Hydrogen Evolution Electrocatalysis. *Angew. Chem. Int. Ed.* **2021**, *60*, 7013–7017.
- (10) Kumar, A.; Rao, G.; Kumar, S.; Singh, A. Formation and Role of Palladium Chalcogenide and Other Species in Suzuki-Miyaura and Heck C-C Coupling Reactions Catalyzed with Palladium(II) Complexes of Organochalcogen Ligands: Realities and Speculations. *Organometallics* **2014**, *33*, 2921–2943.
- (11) Musetha, P.; Revaprasadu, N.; Kolawole, G.; Pullabhotla, R.; Ramasamy, K.; O'Brien, P. Homoleptic Single Molecular Precursors for the Deposition of Platinum and Palladium Chalcogenide Thin Films. *Thin Solid Films* **2010**, *519*, 197–202.
- (12) Li, Z.; Zeng, Y.; Zhou, M.; Xie, B.; Zhang, J.; Wu, W. Suppression of Magnetoresistance in PtSe₂ Microflakes with Antidot Arrays. *Nanotechnology* **2018**, *29*, 40LT01.

- (13) Park, G.; Kang, Y. Conversion Reaction Mechanism for Yolk-Shell-Structured Iron Telluride-C Nanospheres and Exploration of Their Electrochemical Performance as an Anode Material for Potassium-Ion Batteries. *Small Methods* **2020**, *4*, 2000556.
- (14) Pradhan, S.; Pramanik, S.; Das, D.; Bhar, R.; Bandyopadhyay, R.; Millner, P.; Pramanik, P. Nanosized Iron Telluride for Simultaneous Nanomolar Voltammetric Determination of Dopamine, Uric Acid, Guanine and Adenine. *New J. Chem.* **2019**, *43*, 10590–10600.
- (15) Gao, Q.; Huang, C.; Ju, Y.; Gao, M.; Liu, J.; An, D.; Cui, C.; Zheng, Y.; Li, W.; Yu, S. Phase-Selective Syntheses of Cobalt Telluride Nanofleeces for Efficient Oxygen Evolution Catalysts. *Angew. Chem. Int. Ed.* **2017**, *56*, 7769–7773.
- (16) Patil, S.; Kim, E.; Shrestha, N.; Chang, J.; Lee, J.; Han, S. Formation of Semimetallic Cobalt Telluride Nanotube Film via Anion Exchange Tellurization Strategy in Aqueous Solution for Electrocatalytic Applications. *ACS Appl. Mater. Interfaces* **2015**, *7*, 25914–25922.
- (17) Khan, M.; Ashiq, M.; Ehsan, M.; He, T.; Ijaz, S. Controlled Synthesis of Cobalt Telluride Superstructures for the Visible Light Photo-Conversion of Carbon Dioxide into Methane. *Appl. Catal. A: Gen.* **2014**, *487*, 202–209.
- (18) Silva, U.; Masud, J.; Zhang, N.; Hong, Y.; Liyanage, W.; Zaeem, M.; Nath, M. Nickel Telluride as a Bifunctional Electrocatalyst for Efficient Water Splitting in Alkaline Medium. *J. Mater. Chem. A* **2018**, *6*, 7608–7622.
- (19) Zhao, B.; Dang, W.; Liu, Y.; Li, B.; Li, J.; Luo, J.; Zhang, Z.; Wu, R.; Ma, H.; Sun, G.; Huang, Y.; Duan, X.; Duan, X. Synthetic Control of Two-Dimensional NiTe₂ Single Crystals with Highly Uniform Thickness Distributions. *J. Am. Chem. Soc.* **2018**, *140*, 14217–14223.
- (20) Chia, X.; Sofer, Z.; Luxa, J.; Pumera, M. Unconventionally Layered CoTe₂ and NiTe₂ as Electrocatalysts for Hydrogen Evolution. *Chem. Eur. J.* **2017**, *23*, 11719–11726.
- (21) Sharma, K.; Joshi, H.; Sharma, A.; Prakash, O.; Singh, A. Single Source Precursor Routes for Synthesis of PdTe Nanorods and Particles: Solvent Dependent Control of Shapes. *Chem. Commun.* **2013**, *49*, 9344–9346.
- (22) Arora, A.; Oswal, P.; Rao, G.; Kumar, S.; Singh, A.; Kumar, A. Catalytically Active Nanosized Pd₉Te₄ (Telluropalladinite) and PdTe (Kotulskite) Alloys: First Precursor-Architecture Controlled Synthesis Using Palladium Complexes of Organotellurium Compounds as Single Source Precursors. *RSC Adv* **2021**, *11*, 7214–7224.
- (23) Fu, L.; Hu, D.; Mendes, R.; Rummeli, M.; Dai, Q.; Wu, B.; Fu, L.; Liu, Y. Highly Organized Epitaxy of Dirac Semimetallic PtTe₂ Crystals with Extrahigh Conductivity and Visible Surface Plasmons at Edges. *ACS Nano* **2018**, *12*, 9405–9411.

- (24) Supriya, S.; Antonatos, N.; Luxa, J.; Gusmão, R.; Sofer, Z. Comparison between Layered Pt₃Te₄ and PtTe₂ for Electrocatalytic Reduction Reactions. *FlatChem* **2021**, *29*, 100280.
- (25) Oyetunde, T.; Afzaal, M.; O'Brien, P. Phenyl Substituted Ditelluro-Imidodiphosphate Complexes of Iron, Nickel, Palladium, Platinum, and Their Pyrolysis Studies Generating Metal Tellurides. *Polyhedron* **2019**, *160*, 157–162.
- (26) de Los Reyes, J. Ruthenium Sulfide Supported on Alumina as Hydrotreating Catalyst. *Appl. Catal. A: Gen.* **2007**, *322*, 106–112.
- (27) Krishnamoorthy, K.; Pazhamalai, P.; Kim, S. Ruthenium Sulfide Nanoparticles as a New Pseudocapacitive Material for Supercapacitor. *Electrochim. Acta* **2017**, *227*, 85–94.
- (28) Gu, X.; Yang, X.; Feng, L. An Efficient RuTe₂/Graphene Catalyst for Electrochemical Hydrogen Evolution Reaction in Acid Electrolyte. *Chem. Asian J.* **2020**, *15*, 2886–2891.
- (29) Tsay, M.; Huang, J.; Chen, C.; Huang, Y. Crystal Growth in Tellurium Flux and Characterization of Ruthenium Dichalcogenides. *Mater. Res. Bull.* **1995**, *30*, 85–92.
- (30) *Binary Alloy Phase Diagrams*, 2nd ed.; Massalski, T., Okamoto, H., Subramanian, P., Kacprzak, L., Eds.; ASM International, 1990; Vol. 2.
- (31) *Binary Alloy Phase Diagrams*, 2nd ed.; Massalski, T., Okamoto, H., Subramanian, P., Kacprzak, L., Eds.; ASM International, 1990; Vol. 3.
- (32) Jiang, L.; Yuan, R.; Chai, Y.; Yuan, Y.; Bai, L.; Wang, Y. An Ultrasensitive Electrochemical Aptasensor for Thrombin Based on the Triplex-Amplification of Hemin/G-Quadruplex Horseradish Peroxidase-Mimicking DNAzyme and Horseradish Peroxidase Decorated FeTe Nanorods. *Analyst* **2013**, *138*, 1497–1503.
- (33) Pradhan, S.; Das, R.; Biswas, S.; Das, D.; Bhar, R.; Bandyopadhyay, R.; Pramanik, P. Chemical Synthesis of Nanoparticles of Nickel Telluride and Cobalt Telluride and Its Electrochemical Applications for Determination of Uric Acid and Adenine. *Electrochim Acta* **2017**, *238*, 185–193.
- (34) Masikini, M.; Ndagili, P.; Ikpo, C.; Feleni, U.; Duoman, S.; Sidwaba, U.; Waryo, T.; Baker, P.; Iwuoha, E. Optoelectronics of Stochiometrically Controlled Palladium Telluride Quantum Dots. *J. Nano Res.* **2016**, *40*, 29–45.
- (35) Ulbrich, K.; Bertolotti, F.; Masciocchi, N.; Cervellino, A.; Guagliardi, A.; Campos, C. A Comprehensive Structural and Microstructural Investigation of a New Iron-Telluride Nano Phase. *J. Mater. Chem. C* **2018**, *6*, 3047–3057.
- (36) Yuan, M.; Li, Q.; Zhang, J.; Wu, J.; Zhao, T.; Liu, Z.; Zhou, L.; He, H.; Li, B.; Zhang, G. Engineering Surface Atomic Architecture of NiTe Nanocrystals Toward Efficient Electrochemical N₂ Fixation. *Adv. Funct. Mater.* **2020**, *30*, 2004208.

- (37) Xie, Yi.; Li, B.; Su, H.; Liu, X.; Qian, Y. Solvothermal Route to CoTe₂ Nanorods. *Nanostructured Materials* **1999**, *11*, 539–544.
- (38) Fenton, J.; Fagan, A.; Schaak, R. General Solution-Phase Synthesis of Nanoscale Transition Metal Tellurides Using Metal Nanoparticle Reagents. *Eur. J. Inorg. Chem.* **2019**, 3490–3493.
- (39) Robinson, E.; Dwyer, K.; Koziel, A.; Nuriye, A.; Macdonald, J. Synthesis of Vulcanite (CuTe) and Metastable Cu_{1.5}Te Nanocrystals Using a Dialkyl Ditelluride Precursor. *Nanoscale* **2020**, *12*, 23036–23041.
- (40) Peng, Z.; Peng, X. Formation of High-Quality CdTe, CdSe, and CdS Nanocrystals Using CdO as Precursor. *J. Am. Chem. Soc.* **2001**, *123*, 183–184.
- (41) Anderson, N.; Hendricks, M.; Choi, J.; Owen, J. Ligand Exchange and the Stoichiometry of Metal Chalcogenide Nanocrystals: Spectroscopic Observation of Facile Metal-Carboxylate Displacement and Binding. *J. Am. Chem. Soc.* **2013**, *135*, 18536–18548.
- (42) Drijvers, E.; de Roo, J.; Martins, J.; Infante, I.; Hens, Z. Ligand Displacement Exposes Binding Site Heterogeneity on CdSe Nanocrystal Surfaces. *Chem. Mater.* **2018**, *30*, 1178–1186.
- (43) Nag, A.; Zhang, H.; Janke, E.; Talapin, D. Inorganic Surface Ligands for Colloidal Nanomaterials. *Z. Phys. Chem.* **2015**, *229*, 85–107.
- (44) Sales, B. Chapter 1: Introduction to the Synthesis of Quantum Materials: Some General Guidelines and A Few Tricks. In *Fundamentals of Quantum Materials: A Practical Guide to Synthesis and Exploration*; 2021; pp 1–17.
- (45) Murata, S.; Ido, Y. Practical Synthesis of Palladium Bis(Trifluoromethanesulfonate) and Its Application to the Synthesis of Palladium Complexes. *Bull. Chem. Soc. Jpn.* **1994**, *67*, 1746–1748.
- (46) Hernández-Pagán, E.; Robinson, E.; la Croix, A.; Macdonald, J. Direct Synthesis of Novel Cu₂-XSe Wurtzite Phase. *Chem. Mater.* **2019**, *31*, 4619–4624.
- (47) Smith, M.; March, J. *March's Advanced Organic Chemistry: Reactions, Mechanisms, and Structure*, 5th ed.; John Wiley & Sons, Inc., 2001.
- (48) Kürti, L.; Czakó, B. *Strategic Applications of Named Reactions in Organic Synthesis*; Elsevier Inc., 2005.
- (49) Smith, M.; March, J. *March's Advanced Organic Chemistry: Reactions, Mechanisms, and Structure*, 5th ed.; John Wiley & Sons, Inc., 2001.
- (50) Kobayashi, S.; Sugiura, M.; Kitagawa, H.; Lam, W. Rare-Earth Metal Triflates in Organic Synthesis. *Chem. Rev.* **2002**, *102*, 2227–2302.
- (51) Jain, V.; Chauhan, R. New Vistas in the Chemistry of Platinum Group Metals with Tellurium Ligands. *Coord. Chem. Rev.* **2016**, *306*, 270–301.

- (52) Karjalainen, M.; Wiegand, T.; Rautiainen, J.; Wagner, A.; Görls, H.; Weigand, W.; Oilunkaniemi, R.; Laitinen, R. Competitive Te-Te and C-Te Bond Cleavage in the Oxidative Addition of Diaryl and Dialkyl Ditellurides to Pt(0) Centers. *J. Organomet. Chem.* **2017**, 836–837, 17–25.
- (53) Polo, A.; Real, J. 39.32.2.1 Synthesis of Product Subclass 2. In *Science of Synthesis*; 2008; Vol. 39, pp 1145–1161.
- (54) Greenwood, N.; Earnshaw, A. Halides and Oxohalides. In *Chemistry of the Elements*; Reed Educational and Professional Publishing Ltd: Great Britain, 1997; pp 1082–1083.
- (55) Xu, Y.; Wong, J.; Samkian, A.; Ko, J.; Chen, S.; Houk, K.; Grubbs, R. Efficient Z-Selective Olefin-Acrylamide Cross-Metathesis Enabled by Sterically Demanding Cyclometalated Ruthenium Catalysts. *J. Am. Chem. Soc.* **2020**, 142, 20987–20993.
- (56) Lee, S.; Lee, W.; Sulikowski, G. An Enantioselective 1,2-Aziridinomitosene Synthesis via a Chemoselective Carbon-Hydrogen Insertion Reaction of a Metal Carbene. *J. Org. Chem.* **1999**, 64, 4224–4225.

Appendix 2
Relevant Data for Chapter 4

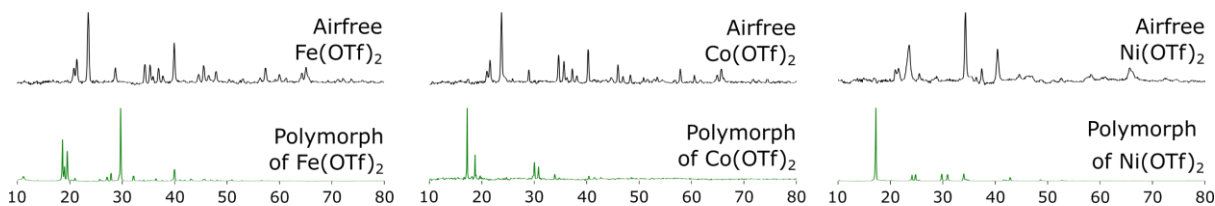


Figure A.4.1. XRD of commercially available $\text{Fe}(\text{OTf})_2$, $\text{Co}(\text{OTf})_2$, and $\text{Ni}(\text{OTf})_2$ in an air-free sample holder (black). The corresponding triflates were heated to $135\text{ }^\circ\text{C}$ in dioctyl ether for 1 h, mimicking a nanocrystal synthesis without the didodecyl ditelluride. Polymorphs of the commercially available starting materials were isolated. (green) These polymorph peaks of the $\text{Fe}(\text{OTf})_2$, $\text{Co}(\text{OTf})_2$, and $\text{Ni}(\text{OTf})_2$ can be observed in **Figure 4.1**.

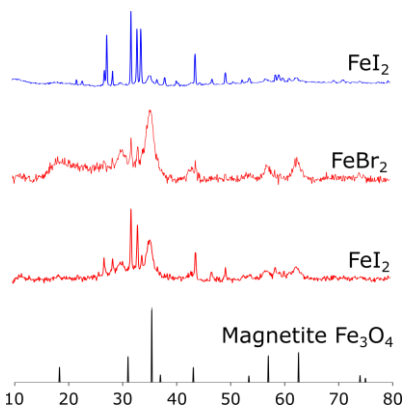


Figure A.4.2. XRD for experiments with FeBr_2 and FeI_2 with (red) and without (blue) the presence of octadecylamine. Unlike the data presented in **Figure 4.1**, these were purified, outside the glovebox in ambient conditions. The presence of iron oxides was observed if the workup was done outside of the glovebox.

ICDD – Magnetite: #159959.

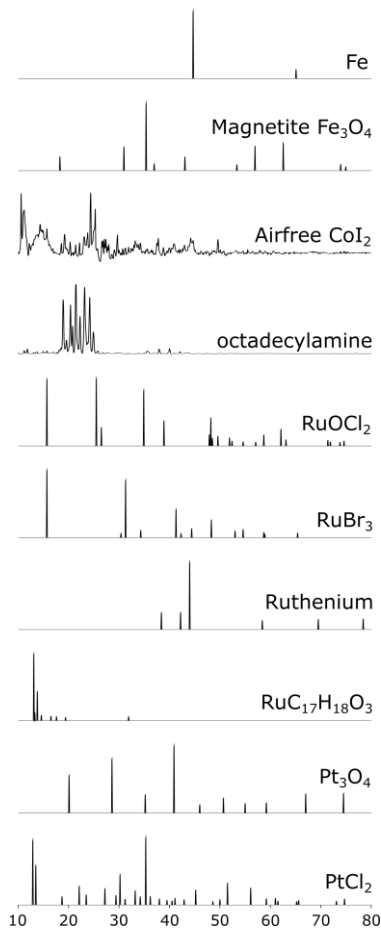


Figure A.4.3. XRD patterns referenced in **Figures 4.1 & 4.2.**

ICDD – Fe: #4113931, Magnetite: #159959, RuOCl₂: #83883, RuBr₃: #413691, Ruthenium: #9008513, RuC₁₇H₁₈O₃: #4064886, Pt₃O₄: #27836, PtCl₂: #28527.

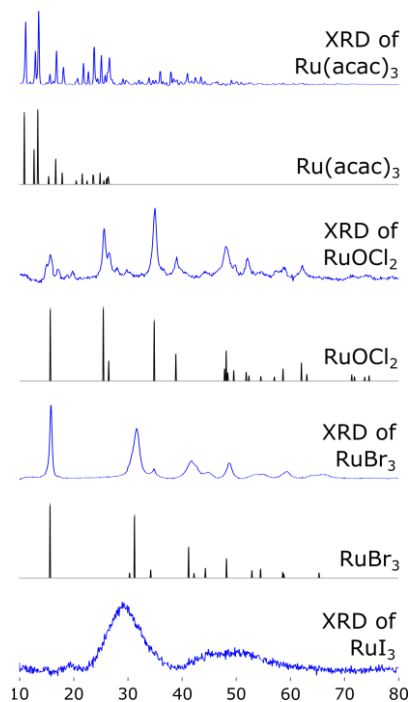


Figure A.4.4. XRD of commercially available ruthenium precursors (blue) and their corresponding literature patterns (black). Commercially available Ru(acac)₃ and RuBr₃ match their XRD traces, however, “RuCl₃” actually was confirmed to be RuOCl₂. The XRD pattern of RuI₃ is not known and for convenience the XRD of this commercially available starting material is presented here. It appears to be, at best, nanocrystalline.

ICDD: – Ru(acac)₃: #7027948,
 RuOCl₂: #83883, and RuBr₃:
 #413691.

Table A.4.1. Stoichiometry of the nanocrystalline products as determined by EDS (no ligand)

Precursor	Co	Ru	Pt
M(acac) ₂	—	—	PtTe _{3.14}
MCl ₂	—	—	PtTe _{1.85}
MBr ₂	—	—	PtTe _{1.96}
MI ₂	CoTe _{1.96}	RuTe _{2.12}	—

Table A.4.2. Stoichiometry of the nanocrystalline products as determined by EDS (with Octadecylamine)

Precursor	Pt
M(acac) ₂	PtTe _{2.06}
MCl ₂	PtTe _{1.96}
MBr ₂	PtTe _{2.00}
MI ₂	PtTe _{1.79}